TECHNISCHE UNIVERSITÄT MÜNCHEN
FAKULTÄT FÜR CHEMIE
PROFESSUR FÜR MOLEKULARE KATALYSE

Dinuclear Au(I) Complexes Bearing Bridge-Functionalized NHC Ligands As Anticancer Agents

BRUNO DOMINELLI

TECHNISCHE UNIVERSITÄT MÜNCHEN
FAKULTÄT FÜR CHEMIE
PROFESSUR FÜR MOLEKULARE KATALYSE

Dinuclear Au(I) Complexes Bearing Bridge-Functionalized NHC Ligands As Anticancer Agents

BRUNO DOMINELLI

Vollständiger Abdruck der von der Fakultät für Chemie der Technischen Universität München zur Erlangung des akademischen Grades eines

Doktors der Naturwissenschaften (Dr. rer. nat.)

genehmigten Dissertation.

Vorsitzende:	Prof. Dr. Angela Casini
Prüfer der Dissertation:	1. Prof. Dr. Fritz E. Kühn
	2. Prof. Dr. João D. G. Correia

Die Dissertation wurde am 09.01.2020 bei der Technischen Universität München eingereicht und durch die Fakultät für Chemie am 04.02.2020 angenommen.

Die vorliegende Arbeit wurde im Zeitraum von November 2016 bis Januar 2020 im Fachgebiet Molekulare Katalyse (Prof. Dr. Fritz E. Kühn) der Technischen Universität München in Zusammenarbeit mit dem Instituto Superior Técnico der Universidade de Lisboa (Prof. Dr. João D. G. Correia) angefertigt.

Mein ganz besonderer Dank gilt meinem Doktorvater

Herrn Prof. Dr. Fritz E. Kühn

für die Aufnahme in seiner Arbeitsgruppe und für die Möglichkeit meinen Doktortitel zu erlangen. Dabei durfte ich mit der richtigen Dosis an Freiheit ein sehr spannendes und anwendungsbezogenes Thema in der medizinischen Chemie ausüben. Zusätzlich ermöglichte mir Herr Prof. Kühn Zugang zu ausländischen und internen Kooperationen, die von besonderer Wichtigkeit für meine Doktorarbeit waren und zusätzlich meinen Horizont erweiterten.

ACKNOWLEDGMENTS

This thesis could have never been completed without the contribute of many of the Technical University of Munich and the Instituto Superior Técnico, Universidade de Lisboa. Therefore, I would like to express all my gratitude to

Prof. Dr. João D. G. Correia, who helped me with very precious suggestions regarding all my syntheses and biological evaluations in skype meetings every month. I am sure that without your expertise this thesis would not have reached all these results, particularly, in the field of anticancer studies. My time in Lisbon and in your group was amazing and educational as well. Hence, thanks to the **Instituto Superior Técnico**, **Universidade de Lisboa**, in the beautiful Bobadela, which gave me the opportunity to collect international experience.

Mrs. Hifinger, who always helped me to deal with the bureaucracy of the TUM.

TUM Graduate School for financial support and to the **ERASMUS** program, which enabled me to collect international experience in the Instituto Superior Técnico, Universidade de Lisboa.

Dr. Alexander Pöthig, who supported this thesis as my mentor and gave me the opportunity to visit his subgroup meetings, which have been very interesting and helpful in terms of gold chemistry.

Dr. Fernanda Marques, who babysitted me during my research stay in Lisbon and teached me in several cytotoxicity assays as well as in internalization and cell distribution studies. All the discussion related to cell biology were very interesting and I could enlarge my knowledge in the field of anticancer studies. Despite your huge number of collaborations, you are still finding the time to evaluate my complexes.

Prof. Dr. Rianne Lord, who was the first person teaching me in MTT assays and helped me to finalize the building of the cell laboratory. Without your precious contributions during your stay in Munich the group of Prof. Kühn could not have published all the reports about gold NHCs with anticancer studies.

Dr. Martin Haslbeck, who provided me a S1 laboratory equipped with a flow bench, incubator and further accessories for building the cell laboratory. Thank you for introducing me in cell culturing and for all the necessary cancer cell lines for my evaluation studies.

Dr. Teresa Pinheiro, who conducted the proton irradiation-based internalization studies of my complexes and thus, helping me to start investigating the mechanism of action of my compounds. You enabled me to combine the physics and chemistry and it was amazing to work with a tandem accelerator.

Dr. Robert Reich, who always made time for me listening to my research and laboratorial problems as well as correcting and submitting all my manuscripts, despite he was very busy with all the international affairs of the TUM.

Dr. Julia Rieb and **Dr. Rui Zhong**, who have been my supervisors for the Master's and Bachelor's theses, respectively. Without your previously performed doctoral theses, my PhD topic would not have exist.

Christian Jakob, who supported my work during his Master's thesis working on esterification studies with anthracene moieties. During your PhD time you continued helping me with HPLC separations and especially with syntheses necessary to conclude manuscripts for submission.

Dr. Pauline Fischer, **Dr. Christian Jandl** and **Eva-Maria Esslinger**, who supported the characterization of my gold complexes via single crystal X-ray diffraction experiments and refinements.

Jens Oberkofler, who enabled the understanding of reactivity of my gold complexes by performing geometry optimization studies.

Han Li, who shared the same laboratory-row for more than 3 years with me and helped me equipping our laboratory. It was my pleasure to let you taste the traditional Bavarian candy.

Dr. Elisabeth Bauer, who helped me in the cell laboratory, who was the best company during the lunch time, coffee breaks and train journeys, but contemporarily annoyed me correcting all the time my German speech defects.

Dr. Pauline Fischer, **Dr. Felix Kaiser**, **Eva-Maria Esslinger** and **Nadine Tappe**, who shared the same laboratory and created an harmonic atmosphere, which for sure was one reason leading to results in this thesis.

Dr. Sebastian Hölzl, **Dr. Lorenz Pardatscher** and **Jens Oberkofler**, who have been very loyal fellow students and during my thesis my coffee, beer and dart buddies.

all my students, **Ardy Tan**, **Lisa Groll**, **Waldemar Schmidt**, **Kathrin Kollmannsberger**, **Andreas Rehpenn**, **Louis Hartmann**, **Fiona Kiefer**, **Franziska Schuderer**, **Nicholas Lim**, **Lucas Stieglitz**, **Lukas Eylert** for experimantal support.

Jarek Marciniszyn, **Marc Kloberg**, **Insu Lee**, **Michael Henkel**, **David Ruseckas** and **Ryan Karongo**, who supported me during my thesis as very good friends.

Dr. Andreas Hinterberger, **Dr. Anja Lindhorst**, **Dr. Pauline Fischer** for inspiring me to participate twice on the Wörthsee triathlon. I always enjoyed training with you.

Marco Bernd, **Alex Böth**, **Daniela Hey**, **Florian Dyckhoff**, **Christiane Egger**, **Alexander Imhof**, **Jonas Schlagintweit** and **Caro Hintermeier** for the precious collegiality and collaboration.

Jürgen Kudermann, **Olaf Ackermann**, **Maria Matthews** und **Burghard Cordes**, who supported me during the application of several analytica methods.

RINGRAZIAMENTO

Il successo al lavoro non sarebbe mai emerso senza il contributo della mia famiglia e per questo voglio esprimere i miei ringraziamenti

a mio padre **Salvatore Dominelli** ed a mia madre **Rosaria Albano**, per avermi supportato durante gli studi. Senza di voi non sarei mai arrivato a raggiungere il titolo del dottore in chimica. Sono fiero di avervi come genitori. Grazie mille di cuore.

ai miei fratelli **Nazzareno Dominelli** e **Luca Dominelli**, per essere cresciuto insieme a voi. Vi auguro tanta fortuna per concludere gli studi.

DANKSAGUNG

Ich möchte mich auch ganz herzlich bei meiner Freundin **Sandra Deiser** bedanken, die mich seit knapp 2 Jahren in meinem Leben begleitet und mir vor Allem gezeigt hat, dass eine gesunde *work-and-life*-Balance der Weg zum Erfolg ist. Du hattest stets ein Ohr für meine Laborfrustrationen und jeder Urlaub mit dir war immer sehr erholsam.

Natürlich danke ich auch **Ingrid**, **Pauli** und **Sara Steinegger** für die nette Aufnahme in eure Familie. Ich genieße jedes Mal meine Freizeit mit euch.

Desweiteren möchte ich meinem Sensei **Werner Bachhuber** danken, der mich seit knapp 21 Jahren das Shorin Ryu Seibukan Karate und seit ca. 8 Jahren das Jinbukan Kobudo lehrt. Ich danke dir für das große Vertrauen, das du mir schenkst. Du ermöglichtest mir meine Assistenztrainerkarriere und meine Tätigkeit als ersten Vorsitzenden der SRSKUD e.V. auszuüben. Ich bin stolz dein Deshi zu sein und hoffe, dass du mir noch mindestens weitere 21 Jahre den Weg weist. ARIGATO GOZAIMASHITA!

Ich danke auch Kyoshi **Jamal Measara**, der mit seinem immensen Karate- und Kobudowissen meinen Sensei ausgebildet hat. Es ist für mich immer eine sehr große Ehre dich und meinem Sensei zusammen zu erleben und von euch beiden zu lernen. ARIGATO GOZAIMASHITA!

Weiteren Karate- und Kobudokollegen, wie **Thomas Gunters** und **Lisa Berchtold** möchte ich auch ganz herzlich danken, die mir während des Trainings mit Rat und Tat zur Seite stehen.

Ganz zum Schluss möchte **Xiaoyu Zhou**, **Florian Gellert** und **Fabian Freire** als guten Freunden danken.

KURZZUSAMMENFASSUNG

Trotz der langfristigen klinischen Anwendung als Chemotherapeutika, führen das DNA-adressierende Cisplatin und dessen Analoga immer noch zu schweren Nebenwirkungen und Resistenzproblemen. Das Element Gold bietet sich als alternatives Metall an, welches stattdessen mit schwefel- und selenhaltigen Enzymen interagiert, die in einigen Krebszelllinien überexprimiert werden. Die fortschrittlichste gold-basierte Verbindung ist Auranofin, welches kürzlich in Phase II der klinischen Studien gegen chronisch-lymphozytäre Leukämie (CLL) getestet wurde. Die starke Affinität zum Schwefel ist jedoch sowohl ein Fluch und als auch ein Segen für diese Gold(I)-Phosphan-Komplexe. Untersuchungen solcher Verbindungen *in vivo* werden aufgrund der Inaktivierung durch thiol-haltiger Transportsysteme im Blut erschwert. *N*-heterozyklische Carbene (NHCs), insbesondere Bisimidazolyliden-Einheiten (bisNHC), wurden als alternatives Ligandensystem eingeführt. Diese bieten verschiedene Möglichkeiten für die Modifikation der elektronischen und sterischen Parameter, sowie den Grad der Lipo- und Hydrophilie. Die jeweiligen dinuklearen Gold(I)-Komplexe weisen eine moderate bis gute Antikrebsaktivität *in vitro* und *in vivo* auf. Bisimidazolyliden-Liganden können zusätzlich brückenfunktionalisiert werden und die erfolgreiche Umsetzung zu den jeweiligen dinuklearen Gold(I)-Komplexen wurde erst kürzlich berichtet. Dabei zeigten die neuesten Ergebnisse die Bildung von syn- und anti-Isomeren an der Methylenbrücke.

Die vorliegende Doktorarbeit setzt sich weiterhin mit brückenfunktionalisierten bisNHC-Einheiten auseinander, mit dem Schwerpunkt auf die Anwendung der entsprechenden dinuklearen Gold(I)-Komplexe als Antikrebsmittel. Erste Ergebnisse an den Gold(I)-Komplexen **14a**-**d** mit 2-Hydroxyethan-1,1-diyl-verbrückten Bisimidazolyliden-Liganden zeigten, dass die Bildung der syn- und anti-Isomeren in Abhängigkeit von den *N*-Substituenten variieren kann. Der Komplex mit Mesityl-*N*-Substituenten **14d** lieferte eine moderate antiproliferative Aktivität in den beiden humanen Krebszelllinien *HepG2* und *A549*. DFT-Berechnungen ergaben ein Energieprofil für alle sechs möglichen Isomere, das die Zuordnung der Konformeren im Falle eines Isomerengemisches erleichtert. Die energetisch günstigste exo-Konfiguration (vom Metallazyklus wegstehende Methylenbrücken-Funktionalisierung) konnte durch einkristalline Röntgenbeugung bestätigt werden.

In Folgestudien wurden die verschiedenen syn- und anti-Isomere desselben *N*-substituierten Gold(I)-Komplexes getrennt. Dabei konnte das zweite, noch nicht analytisch charakterisierte Isomer des Gemisches als das jeweils andere syn-/anti-exo-Konformer identifiziert werden. Beide isolierten Isomere wurden in *HeLa*- und *HepG2*-Krebszelllinien untersucht und beide Konformationen zeigten keine drastischen Unterschiede in der antiproliferativen Aktivität. Das syn-Konformer besitzt zwar im Vergleich zum Anti-Analogon eine höhere Stabilität in Gegenwart von L-Cystein unter physiologischen Bedingungen, zeigte allerdings eine schlechtere Hemmung des Enzyms Thioredoxin Reduktase. Der

Austausch des Anions $(PF_6)^-$ zu Chlorid erhöhte die Löslichkeit des zytotoxischsten und stabilsten Mesityl-*N*-substituierten Gold(I)-Komplexes **syn-exo-14d** in Wasser und führte zu einer mit Auranofin vergleichbaren antiproliferativen Aktivität. Darüber hinaus überwand dieser Komplex die Cisplatin-Resistenz, da er in beiden *A2780* und *A2780cisR* Eierstockkrebs-Zelllinien gleichermaßen toxisch ist. Zusätzlich zeigte dieser Komplex in der humanen Prostatakrebs-Zelllinie *PC3* sowie in den beiden humanen Brustkrebs-Zelllinien *MDA-MB-231* und *MCF-7* Aktivität. **Syn-exo-14d** wurde in der *V79* Fibroblasten-Zelllinie, die als gesunde Referenz-Zelllinie eingesetzt wurde, als weniger zytotoxisch beobachtet. Unter Berücksichtigung der IC_{50}-Werte von **syn-exo-14d** in *V79* und *MCF-7*, zeigte der resultierende Selektivitätsindex, dass dieser Komplex für eine therapeutische Behandlung der humanen *MCF-7* Brustkrebszelllinie potentiell anwendbar sein könnte. Die Internalisierung von **syn-exo-14d** in der *PC3*-Krebszelllinie wurde durch Analyseverfahren mittels Protonenbestrahlung bestätigt. Dabei führten erste Beobachtungen zu dem Schluss, dass dieser Komplex im Vergleich zu Auranofin tiefer in die Zelle internalisiert. Eine genauere Verteilung in den jeweiligen Zellabteilungen wird mittels ICP-MS sowie durch Elektronenmikroskopie derzeit noch untersucht.

Der nicht zytotoxische Komplex **syn-exo-14b** mit Isopropyl-*N*-Substituenten wurde durch Veresterung beider Hydroxylgruppen mit 9-Anthracenoylchlorid post-modifiziert. Es wurde ein Produktgemisch aus dem Monoester **16** und dem Diester **17** erhalten, das erfolgreich getrennt und charakterisiert werden konnte. Der Komplex **16** ist deutlich zytotoxischer als **14b** und zeigt eine attraktive antiproliferative Aktivität in *HeLa*- und *MCF-7*-Krebszelllinien. Allerdings erweist sich Komplex **syn-exo-14d** mit Mesityl-*N*-Substituenten in dieser Arbeit immer noch als die aktivste Verbindung. Der Diester **17** fällt im Kulturmedium bei 37 °C aus und der Austausch des Anions zu Chlorid führt anstatt einer Erhöhung der Löslichkeit in Wasser zu einer Zersetzung durch Hydrolyse. **16** und **17** zeigten Lumineszenz mit maximalen Quantenausbeuten bei 365 nm in Höhe von 20% bzw. 8%. Im Fall von **17**, führte eine Photodimerisierung zwischen den benachbarten Anthracen-Molekülen zu einer teilweisen Lumineszenzlöschung. Das daraus resultierende Produkt zeigte jedoch eine thermoinduzierte Reversibilität bei 37°C. Diese Eigenschaften könnten Komplex **17** als metallbasierten Photo-Lichtschalter attraktiv machen.

Die beiden Gold(I)-Komplexe **15a** und **15b** mit 2,2-Acetat-verbrückten Bisimidazolyliden-Liganden wurden synthetisiert und vollständig charakterisiert. Beide Komplexe wiesen dabei das gleiche Strukturmotiv und die gleiche Isomerisierung wie **14a**-**d** auf. Die Variation der funktionellen Gruppe der Brücke von Hydroxyl- zu Carboxylatgruppen führte zu zwitterionischen Komplexen, die in Wasser zwar löslich sind, aber in den *HeLa*- und *HepG2*-Krebszelllinien keine Zytotoxizität zeigten. Die Erweiterung der *N*-Substituenten auf lipophilere Systeme (z.B. Mesityl) war wegen des Verlustes der Brückenfunktionalität durch thermoinduzierte Decarboxylierung nicht möglich. Dieses Phänomen wurde in Zusammenhang mit der Nähe der Carboxylatgruppen zu den Imidazolium/Imidazolyliden-

Systemen gebracht. Darüber hinaus waren die Carboxylatgruppen nicht reaktiv in Veresterungs- oder Amidierungs-Post-Modifikationen. Protonierungsexperimente mit Tetrachlorogoldsäure lieferten einen tetranuklearen Au(I)/Au(III)-Komplex.

Die Verlängerung der Brücke von C1 nach C3 ermöglichte die erfolgreiche Kombination von Mesityl-*N*-Substituenten und Carboxylgruppen als Brückenfunktionalität. Der entsprechende Gold(I)-Komplex **18** wurde erfolgreich synthetisiert und vollständig charakterisiert. Erste Konjugationsversuche ermöglichten die Kopplung von **18** an einen bifunktionellen DOTA-Chelator zur möglichen Radiometallierung. Das entstandene Zwischenprodukt **19** bietet nun zusätzlich zur bereits vorhanden zytotoxischen Einheit für die Therapie (Thera-) einen Chelator für die radioaktive Diagnostik (-nostik). Das resultierende Theranostikum könnte weiterhin mit einer kurzen Peptidsequenz zur Adressierung überexprimierter Membranrezeptoren erweitert werden und somit eine Erhöhung der Selektivität ermöglichen.

ABSTRACT

Despite their long-term applications, the nowadays clinically applied DNA-targeting cisplatin and analogues still suffer on severe side effects and resistance issues. Alternatively, gold emerged as a possible candidate acting differently by targeting sulfur- and selenium-containing enzymes, which are overexpressed in some cancer cell lines. The most advanced gold metallodrug is auranofin, which was recently tested in phase II clinical trials against chronic lymphocytic leukemia (CLL). However, the strong thiophilicity represents a curse and blessing for gold(I) phosphine complexes hampering their evaluation *in vivo* due to inactivation by thiol-containing molecules of the blood. *N*-heterocyclic carbenes (NHCs), in particular bisimidazolylidene moieties (bisNHC), have been alternatively introduced offering different positions for fine-tuning electronic, steric, lipo- and hydrophilic parameters and the respective dinuclear gold(I) complexes exhibit moderate to good anticancer activity *in vitro* and *in vivo*. Recently, bisimidazolylidene ligands have been additionally bridge-functionalized and the synthesis of the respective dinuclear gold(I) complexes was reported. Thereby, latest developments showed the formation of syn- and anti-isomers at the methylene bridge.

This thesis continues exploring bridge-functionalized bisNHC moieties, focusing on the application of the respective dinuclear gold(I) complexes as anticancer agents. Preliminary results on the gold(I) complexes **14a**-**d** bearing 2-hydroxyethane-1,1-diyl-bridged bisimidazolylidenes showed that the formation of syn- and anti-isomers alters in dependency on the *N*-substituents. The complex with mesityl-wingtips **14d** delivered moderate antiproliferative activity in both human cancer cell lines *HepG2* and *A549*. DFT calculations revealed an energy profile for all six possible isomers, which facilitates the assignment of conformers in case of an isomeric mixture. The energetically most favoured exo-configuration (methylene-bridge functionalization pointing away from the metallacycle) could be confirmed by single crystal X-ray diffraction.

In follow-up studies, the different syn- and anti-isomers of the same *N*-substituted gold(I) complex were separated and the second not yet analytically characterized isomer of the mixture could be identified as the respective other syn-/anti-exo-conformer. Both isolated isomers were evaluated in *HeLa* and *HepG2* cancer cell lines showing no drastic differences in antiproliferative activity. The syn-conformer was more stable in the presence of L-cysteine under physiological conditions, but a weaker inhibitor of the enzyme thioredoxin reductases (Trx) than the anti-analogue. Counter-anion exchange from $(PF_6)^-$ to chloride enhanced the solubility in water of the most cytotoxic and most stable mesityl *N*-substituted gold(I) complex **syn-exo-14d**, which allowed to improve its antiproliferative activity in *HepG2* cancer cell line to a range comparable to auranofin. Furthermore, this complex overcame cisplatin-resistance, being equally toxic in both ovarian cancer cell lines *A2780* and *A2780cisR* and showed also activity in human prostate cancer cell line *PC3* as well as in both human breast cancer cell

lines *MDA-MB-231* and *MCF-7*. **Syn-exo-14d** was observed to be less cytotoxic in the fibroblast cell line *V79,* which was applied as healthy reference cell line. Considering the IC_{50}-values of *V79* and *MCF-7*, the resulting selectivity index revealed that this complex could be attractive for a therapeutic treatment of this human breast cancer cell line. The internalization of **syn-exo-14d** in *PC3* cancer cell line was confirmed by proton irradiation-based analytical techniques. Thereby, first observations led to the conclusion that this complex internalizes deeper into the cell when compared to auranofin. A more specific cell distribution via cell compartment separation and subsequent ICP-MS as well as via electron microscopy are ongoing.

The non-cytotoxic complex **syn-exo-14b** with isopropyl wingtips was post-modified via esterification of both hydroxyl groups with 9-anthracenoyl chloride. A product mixture containing the mono-ester **16** and di-ester **17** was obtained, which could be successfully separated and characterized. Complex **16** is remarkably more cytotoxic than **14b**, showing attractive antiproliferative activity in *HeLa* and *MCF-7* cancer cell lines, however, the mesityl-*N*-substituted complex **syn-exo-14d** still appeared as the most cytotoxic compound in this thesis. The di-ester **17** precipitated in the culture-medium at 37 °C and counter-anion exchange reactions to chloride led to decomposition via hydrolysis instead of an increase of water-solubility. **16** and **17** showed luminescence with maximal quantum yields at 365 nm amounting to 20% and 8%, respectively. In case of **17**, a photodimerization between the vicinal anthracene molecules led to a partial quenching of the luminescence. However, the obtained product showed a thermo-induced reversibility at 37°C, which could make this system attractive as metal-based photo-switcher.

Two gold(I) complexes **15a** and **15b** with 2,2-acetate bridged bisimidazolylidene ligands have been synthesized and fully characterized showing the same structure motive and isomerization as **14a**-**d**. The variation of the functional group of the bridge from hydroxyl to carboxylate groups led to zwitterionic complexes soluble in water, but not cytotoxic in the *HeLa* and *HepG2* cancer cell lines. The extension of *N*-substituents to more lipophilic systems (e.g. mesityl) was unfeasible due to a loss of bridge-functionality via thermo-induced decarboxylation. This phenomenon was related to the proximity of the carboxylate groups to the imidazolium/imidazolylidene moiety. In addition, both carboxylate groups resulted to be unreactive towards esterification or amidation post-modifications. Protonation experiments with tetrachloroauric acid delivered a tetranuclear Au(I)/Au(III) complex.

Elongation of the bridge from C_1 to C_3 allowed the successful combination of mesityl *N*-substituents and carboxylic groups as bridge-functionality. The respective gold(I) complex **18** was successfully synthesized, fully characterized and first conjugation attempts enabled the coupling to a DOTA analogue as a bifunctional chelator for radiometalation. The resulting intermediate **19** consists of a cytotoxic moiety for therapy (thera-) and a chelator for radioactive diagnostics (-nostic). The resulting

theranostic agent could be further extended with a short peptide sequence to address overexpressed membrane receptors and consequently to enable an increase in selectivity.

List of Abbreviations

ASK1	mitogen-activated protein kinase p38
ATP	adenosintriphosphat
bisNHC	bisimidazolylidene
CLL	chronic lymphocytic leukemia
CTBS	cathepsin B
CTR	copper transporter
CTSL	cathepsin L
DFT	density functional theory
DMSO	dimethyl sulfoxide
DOSY	diffusion-ordered spectroscopy
DOTA	1,4,7,10-tetraazacyclodo-decane-1,4,7,10-tetraacetic acid
DTNB	5,5'-disulfanediylbis(2-nitro-benzoic acid)
EA	elemental analysis
endo	pointing towards a system
EPR	enhanced permeability and retention
ESI-MS	electron-spray-ionization-mass spectrometry
exo	pointing away from a system
FDA	US Food and Drug Administration
FG	functional group
HK	hexokinases
HX	general formula for Brønsted acids
HBr	hydrobromic acid
HOTf	trifluoroacetic acid
IC_{50}	half maximal inhibitory concentration
ICP-MS	inductive coupled plasma-mass spectrometry
iPr	isopropyl
IR	infrared
Me	methyl
MeCN	acetonitrile
Mes	mesityl
meso	mixture of exo and endo
MOF	metalorganic framework
MOMP	mitochondrial outer membrane permeabilization
MPTP	mitochondrial permeability transition pores
MTT	3-(4,5-dimetylthiazol-2-yl)-2,5-diphenyltetrazolium bromide
NADP	nicotinamide adenine dinucleotide phosphate
NCI	National Cancer Institute
NHC	*N*-heterocyclic carbene
NMR	nuclear magnetic resonance
OCT	organic cation transporter
p38-MAPK	mitogen-activated protein kinase p38
PARP-1	poly(adenosine diphosphate (ADP)ribose) polymerases 1
Ph	phenyl
PIXE	proton induced X-ray emission
PLL	prolymphocytic lymphoma
Prx	peroxidases
Py	pyridyl
RBS	Rutherford backscattering
RCC	renal-cell carcinoma
Ref.	reference
ROS	reactive oxygen species
RP-HPLC	reverse phase high performance liquid chromatography
SC-XRD	single crystal X-ray diffraction
SEM	scanning electron microscopy
SI	selectivity index
SLL	small lymphocytic lymphoma

STIM	scanning transmission ion microscopy
TEM	transmission electron microscopy
TF	transcription factor
THT	tetrahydrothiophene
Trx	thioredoxin
TrxR	thioredoxin reductases
VT	varied temperature
WHO	World Health Organization

List of Cell lines

A549	human *breast* epitheloid carcinoma
HepG2	human *liver* hepatocellular carcinoma
HeLa	human *cervix* epitheloid carcinoma
PC3	human *prostate* epitheloid carcinoma
MCF-7	human *breast* epitheloid carcinoma
MDA-MB-231	human triple negative *breast* epitheloid carcinoma
A2780	human *ovarian* epitheloid carcinoma
A2780cisR	human cisplatin-resistant *ovarian* epitheloid carcinoma
V79	hamster lung fibroblast cell

TABLE OF CONTENTS

1 INTRODUCTION

1.1 Statistics and Hallmarks of Cancer

The World Health Organization (WHO) revealed that cancer is the first or second leading cause of death worldwide predicting 18.1 million incidences and 9.6 million deaths by cancer disease for 2018.[1] Until 2030, the above-mentioned numbers are expected to increase up to 27 million new cases of cancer diseases and thereof 17 million deaths.[2] Comparing both sexes, the most common type of cancer besides lung are prostate for men and breast for women. Although these numbers and statistics are appalling, the nearly fifty years old field of chemotherapy still fails in overcoming selectivity issues. Nowadays, in case of a cancer disease, several clinical treatments exist such as surgery, radio-, chemo-, hormonal and immuno-therapy.[3] Since this thesis is reporting gold-based organometallic complexes and assessment of their anticancer properties, the whole introduction is subsequently focusing on the development of metal-based chemotherapeutics. In order to enhance the selectivity towards cancer cells, it became very evident that outlining the differences between healthy cells and respective malignant clones (cancer cell) plays a decisive role in finding safer strategies to take measures against cancer. Indeed, cancer cells revealed to have several different characteristics (highlighted in the following in *italic style*) when compared to healthy cells, which have been reviewed in a very interesting article entitled "hallmarks of cancer" of Hanahan and Weinberg in 2011.[4] The tumorigenesis (process forming cancer cells) can be attributed to *genome instability and random mutation*, which can lead to chromosomal rearrangements and thus, affect for example proto-oncogenes or tumor suppressor genes responsible for cell number maintenance.[4-5] The production and release of *growth-promoting signals* is increased in cancer cells resulting in disruption of the homeostasis and causing unstoppable cell proliferation. In addition, *growth suppressors* are evaded consequently supporting the limitless growth of number of malignant cells. These properties can lead to *replicative immortality,* which finally causes macroscopic tumor masses. Major reasons for genetic mutation are for instance the population growth and ageing, exposures to chemicals, nutrition or smoking. In particular the ageing increases the risk of neoplasia (formation of cancer cells), since genes start to become "older" and more delicate to gene mutation. Other minor risks are for example sun exposure, pollution or distraction.[6] Another neoplastic risk is an increased number of inflammatory cells generated by the immune system after injuries which can promote the formation of cancer cells.[7] Tumor cells are more *resistant against cell death processes* when compared to healthy cells. There are more or less 13 known different intrinsic and extrinsic cell death mechanisms.[8] Considering the application of metalloagents, the two most-occurring mechanisms are apoptosis or necrosis, which take place inside the cell. The first one is a programmed mechanism, in which the activation of several enzymes leads to cell death. Thereby, a symptom is for instance a shrinkage of the cell. In contrast, necrosis leads to a swelling of the cell

releasing the cellular offal to the extracellular environment. Platinum- or gold-based metallodrugs have been reported to mainly induce apoptosis. These processes and all involved enzymes will be discussed more detailed in the following chapters. One more hallmark of cancer cells is the higher rate of *angiogenesis*, which leads to changes in the morphology of blood vessels (sprouting) and thus, supporting the expanding of tumor cells. Additional malignant properties of cancer cells are the activated abilities of *tissue invasion and metastasis* to other parts of the body. A recently observed characteristic of cancer cells is the *evasion of immunological destruction* starting to be resistant against T- and B-lymphocytes or natural cell killers. Another not yet fully validated hallmark is the *reprogrammation of the cellular metabolism* influencing the energy production. This effect was firstly discovered by Warburg in 1924, confirming that some cancer cell lines exhibit increased glycolysis under high oxygen tension conditions producing consequently more lactate.[9-10] The higher glucose uptake evidently enhances ATP production in cancer cells benefiting their growth and almost all above-mentioned hallmarks. Kroemer and coworker reported that the cell metabolism should be considered as the "cancer's achilles' heel" and thus as possible target for a more selective cancer therapy.[11] The mitochondrion plays therefore a decisive role, since it regulates approximately 80% of the total energy production in cell. In addition, it controls apoptotic processes and maintains the redox state in equilibrium.[12-13] Indeed, some compounds based on transition metals (e.g. gold) have been categorized as antimitochondrial compounds.[14] The drug delivery plays also an indispensable role in enhancing the selectivity and drugs should be designed for potential chemotherapy with high affinity to the microenvironment of cancer cells, which remarkably differs from that of healthy cells. Besides for example the lower pH-value or lower concentration of oxygen (hypoxia), the leakiness of tumor vasculature caused by angiogenesis enhances the permeability of sprouted blood vessels in tumors. This allows the delivery and retention of for example high molecular weight macromolecules in tumorigenic cells, which usually do not penetrate through normal tissues. This phenomenon is called enhanced permeability and retention effect (EPR). Another approach is to find suitable extra- or intracellular targets like receptors or enzymes, respectively, which are overexpressed in cancer cells and increases the selectivity.[15] Especially, the thioredoxin reductase (TrxR) is a very druggable target for gold-based complexes, which was observed to be overexpressed in some cancer cells and will be discussed more detailed in the following chapters of the introduction.[16]

1.2 Platinum-Based Treatment of Cancer

Cisplatin (cis-diamminedichloroplatinum(II), Scheme 1) is nowadays indicated, for instance, to treat testicular and ovarian cancer.[17] The synthesis and structural characterization of cisplatin - known as Peyrone's chloride - was first published by Peyrone in 1845.[18] Almost one century later, Rosenberg discovered by accident the cell growth inhibition potential of cisplatin during cell division experiments

in *Escherichia coli* using a platinum electrode.[19] Cisplatin was a decomposition product of the electrode. In 1968, first *in vivo* studies of this drug in mice confirmed a remarkable tumor regression.[20] Consequently, clinical studies were conducted by the US National Cancer Institute (NCI) and the first patients were treated with cisplatin in 1971. In 1978, cisplatin was approved by the US Food and Drug Administration (FDA).[21] Interestingly, transplatin is noticeable less active when compared to cisplatin.[22]

The most known mechanism of action of cisplatin is the interaction with DNA in the nucleus.[23] A generalized mechanism including cellular uptake, activation, DNA interaction and cell death inducing processes as well as the detoxifying release is depicted in Scheme 1.

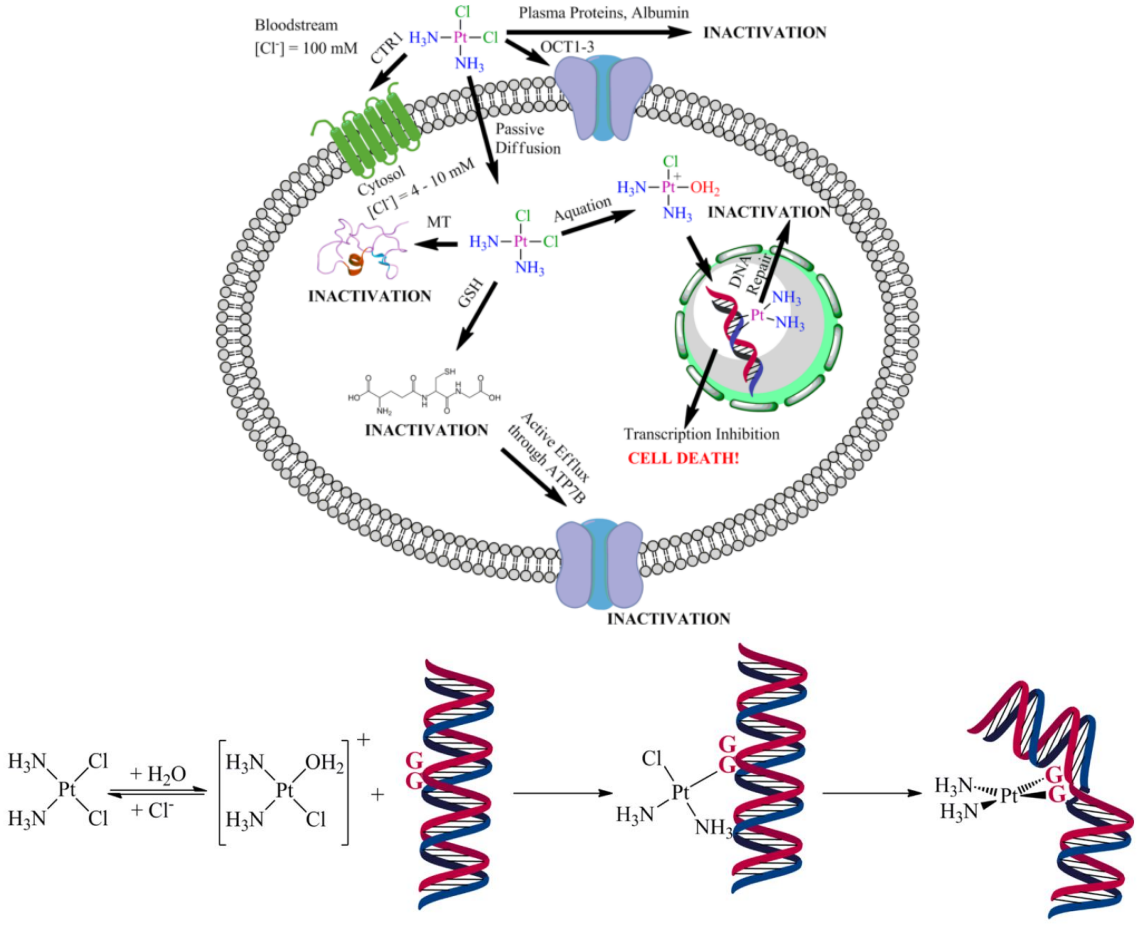

Scheme 1: General depiction of the mode of action of cisplatin in cancer cells (top) and interaction steps with the DNA (bottom). Reprinted with permission of Ref [24].

Considering the square planar geometry, cisplatin is internalized by passive diffusion or by active transport through membrane proteins such as for example copper transporters (CTR1) or by organic cationic transporters (OCT1-3).[24-27] Before forming the DNA adduct cisplatin is intracellularly activated by hydrolysis exchanging one chloride ligand with one water molecule leading to the cationic mono-aqua complex as highly active species. Therefore, the lower intracellular chloride concentration (external 100 mM and internal 20 mM) was considered as the driving force for the aquation of cisplatin, which occurs within 2 h.[28] The mono-aqua complex is able to enter the nucleus and the

negatively charged DNA attracts the cationic activated cisplatin species. Thereby, the leaving ligands (water or chloride) can be substituted by the nucleophilic nitrogen atoms of DNA guanine residues.[22] These interactions lead to a DNA bending, which causes a disruption of transcription processes.[29] In addition, cisplatin damages, for example, proteins responsible for DNA-damage recognition and repair, which finally leads to apoptosis. Cisplatin can be inactivated by sulfur-containing delivery systems in the blood such as human serum albumin. The internalized cisplatin can be inactivated by metallothioneins such as glutathione, and the resulting xenobiotics are exported from the cell by pumping systems like ATP7A/B.[30]

Despite its long-term clinical application, cisplatin still causes severe side effects, namely a nephrotoxicity, ototoxicity, neurotoxicity and toxicity to gastrointestinal tract.[21, 30] In addition, cisplatin showed acquired or intrinsic resistance issues. These disadvantages motivated researchers worldwide to develop better alternatives towards overcoming the above-mentioned side effects and to ensure a safer chemotherapy for patients. As a result, less toxic derivatives such as carboplatin or oxaliplatin entered in global clinical application in 1989 and 2002, respectively, showing improvements in treatment but still bearing resistance issues due to the same mode of action as cisplatin (Figure **1**).[22, 31]

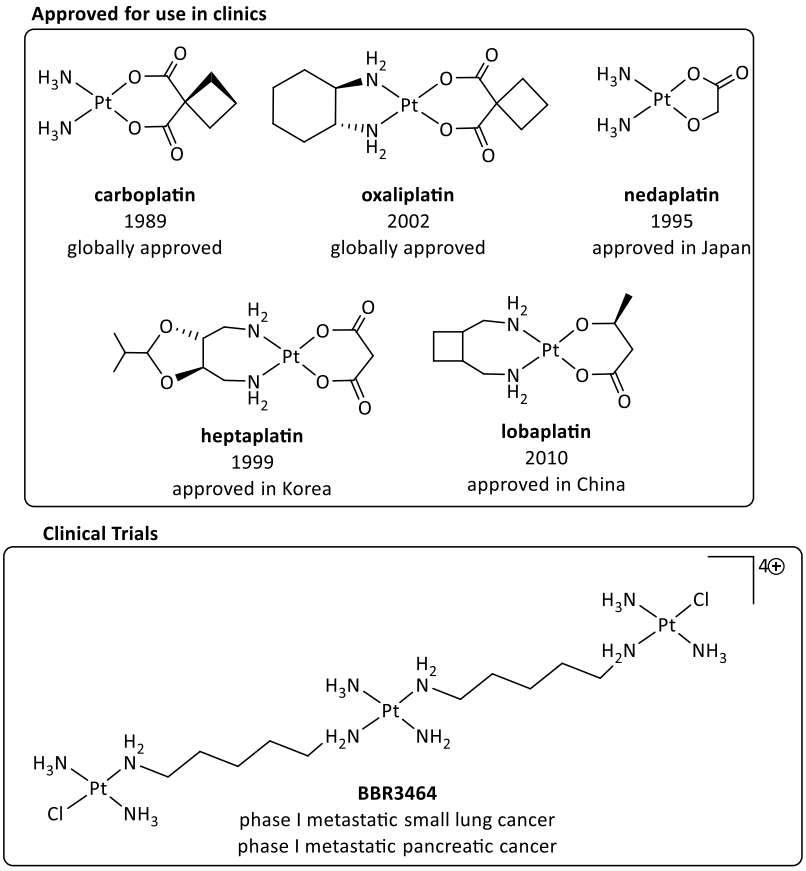

Figure 1: Structures of clinically approved carboplatin, oxaliplatin, nedaplatin, heptaplatin and lobaplatin as well as first example of multinuclear anticancer agent in cationic form reaching clinical trials.

Furthermore examples of platinum-based clinically approved chemotherapeutics are nedaplatin, heptaplatin or lobaplatin, which are used in Asia.[22] Alternatively, the non-leaving amino-ligands were extended with substrates, which allow the access to more selective cisplatin analogues adressing as above-mentioned receptors overexpressed on cancer cell surfaces.[22] This includes targeting molecules like for example glucose, estrogen or folic acid.[32-34] For taking advantage of the EPR effect, the size of cisplatin was enhanced by conjugating it to polymeric systems or encapsulation in nano-delivery systems like carbon-based nanotubes, metal organic frameworks (MOFs) or in polymeric micelles.[22] Another attractive strategy to overcome the above-mentioned cisplatin issues includes the synthesis of multinuclear platinum-based complexes like BBR3464 (Figure 1).[35] This trinuclear platinum complex represents the first example of a multinuclear homo-metallic anticancer agent and was tested in phase I clinical trials against metastatic small lung cancer or metastatic pancreatic cancer.[36-37] However, it never reached the next phase due to drug decomposition in blood via bridge cleavage leading to inactive mono- or dinuclear metabolites.[38] Nevertheless, BBR3464 allowed the introduction of multinuclear complexes into the field of anticancer studies, which is the main focus of this thesis reporting dinuclear gold(I) complexes.

1.3 Advances of Transition-Metal-Based Anticancer Complexes

The accidental discovery of cisplatin and analogues allow scientists to apply alternative transition metals (e.g. Ti, Fe, Ru, Os, Ir, Pd, Cu, Ag, Au) with success in preclinical anticancer studies.[8] The emergence of non-platinum-based metalloagents has been a focus of interest worldwide, since other

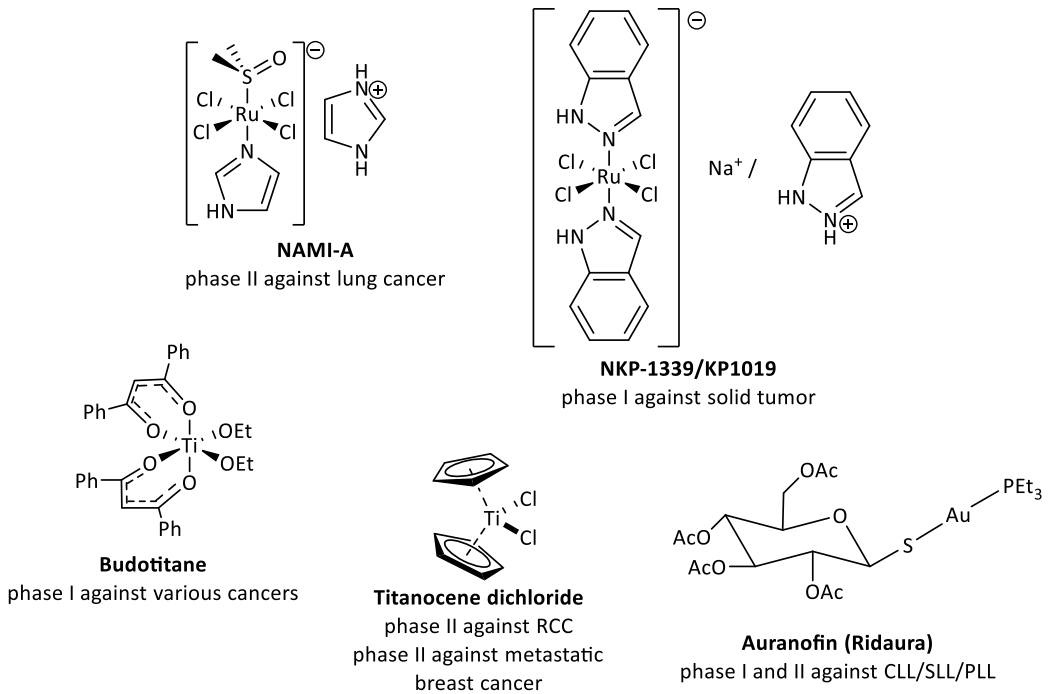

Figure 2: Structures of ruthenium-, titanium- or gold-based metallodrugs being tested in clinical trials against divers cancers.

transition metals are expected to have different mechanisms of action when compared to cisplatin, which could lead to more selective metal-based anticancer agents. The ruthenium-, titanium- or gold-based complexes depicted in Figure 2 have entered phase I and II clinical trials.

Titanium-based complexes were the first non-platinum examples entering in clinical trials after the success of cisplatin.[39] Nowadays, the two most-known drugs are still Budotitane and titanocene dichloride. The first one was tested in a phase I clinical trials against several malignant tumors, which could not be treated with standard clinical procedures.[40] Titanocene dichloride reached phase II clinical studies against both renal-cell carcinoma (RCC) and metastatic breast cancer.[41-43] Unfortunately, these titanium-based complexes displayed insufficient efficacy to toxicity ratio and high instability under physiological conditions.[39]

Alternatively, ruthenium complexes such as NAMI-A have been tested in phase II clinical trials for lung cancer treatment.[44] Despite being well tolerated by the patients, this ruthenium complex could not pass into the next step due to its poor toxicity profile and insufficient efficacy. Later on, the analogues KP1019 and the respective water-soluble complex NKP-1339 have shown promising results in phase I clinical trials against solid tumors.[45-46] Additionally, NAMI-A and KP1019 showed anti-metastatic properties rendering this transition metal very attractive for chemotherapy.[47] The redox activity of ruthenium in the reductive microenvironment of cancer cells was proposed to be the major mode of action leading to cell cycle arrest, disruption of DNA synthesis and finally to apoptosis.

Auranofin (Ridaura®, [(tetra-O-acetyl-β-D-glucopyranosyl)thio](triethylphosphine)-gold(I), Figure 2) is a gold(I) phosphine complex that was tested in phase II clinical trials against chronic lymphocytic leukemia (CLL), small lymphocytic lymphoma (SLL) and prolymphocytic lymphoma (PLL). It still represents the most advanced gold-based complex applied in chrysotherapy, which is the umbrella term for the application of gold in medicine.[48 14, 49] In addition, auranofin showed to overcome cisplatin-resistance in for example ovarian cancer cell lines in preclinical studies.[13, 50-51] This agent profits from the strong thio- and selenophilicity of gold allowing the targeting of enzymes, which is considered to be a more selective alternative mode of action when compared to cisplatin as DNA targeting drug.

1.4 Gold(I) Phosphine Complexes as Anticancer Agents

Auranofin is the gold-standard in the research field of gold-based anticancer agents (Figure 2). Before focusing on current progresses and mechanistic insights of auranofin as anticancer agent, it is worth to give a short historic flashback about gold as therapeutic element.

Interestingly, the element gold has a very long history of development, since its therapeutic application was found to have origins dated back to 2500 BC in China.[13] In the medieval period, physicians like Paracelsus used colloidal gold mixtures against ulcerative skin and rheumatism as well.[52] In 1890, Koch

delivered the very first pioneering laboratorial evidences for the use of gold in medicinal purposes testing a gold cyanide solution against tuberculosis.[52] However, Koch was not able to confirm the antitubercular activity of gold in animals and interrupted his studies. A few years later, some gold-based salts like potassium tetrachloroaurate were found active against lupus vulgaris (one example of tuberculosis) and syphilis.[52] The "flourishing" decade of gold was between 1925 and 1935, in which gold-based solutions were used intravenously against tubercular diseases. During this period, however, it became very evident, that no real antitubercular activity was observed, but rather serious side effects.

Forestier was the first to discover the benefits of gold against rheumatoid arthritis.[53] Gold thiolates (e.g. Myocrisin and Solganol, Figure 3) were approved as drugs for treating rheumatoid arthritis.[13] After observing severe side effects of these intravenously injected gold thiolates, Sutton and colleagues introduced auranofin (early 1980s), which was approved as an orally active anti-rheumatic drug in 1985.[52]

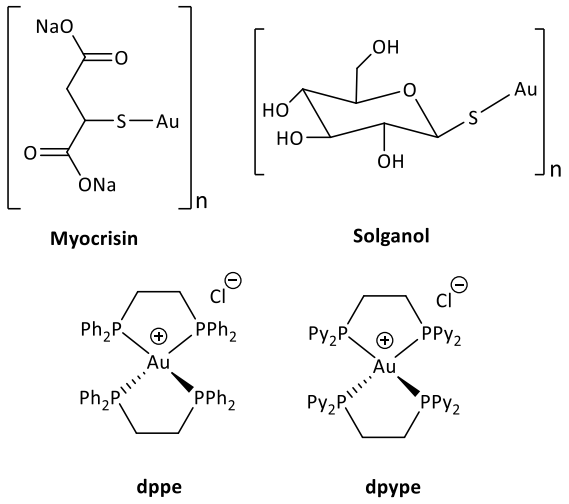

Figure 3: Molecular structures of Myocrysin and Solganol as well as gold(I) complexes with tetrahedral geometry bearing dppe (1,2-bis(diphenyl-phosphino)ethane) or dpype (1,2-bis(dipyridylphosphino)ethane) ligands.

In the same year, inspired by its success in the field of rheumatoid arthritis, Mirabelli reported auranofin as a potent anticancer agent highlighting the antiproliferative activity in various cancer cell lines and observing a regression of the tumor mass *in vivo*.[54] This studies gave the "green light" to gold in the research field of cancer, and the number of gold complexes with various ligand types reported with anticancer properties exponentially rose.[55-57]

Auranofin and mononuclear analogues bearing phosphine-type ligands were discovered to cause mainly mitochondrial-induced apoptosis and therefore gold complexes in general were classified as antimitochondrial agents.[58-59] The key reactivity of gold inside the cell is based on its high affinity to sulfur and selenium. However, this affinity was observed to be a crucial weakness of gold compounds as well, limiting their application for *in vivo* studies.[54] The irreversible binding to thiol-containing blood

transporters (e.g. serum albumin) are hampering the process to surpass preclinical studies.[57] As a result of the early studies on auranofin, it quickly became obvious that ligand system tuning is crucial to moderate the reactivity towards sulfur and selenium.[13, 60] Thus, chelating diphosphine-type ligands (1,2-bis(diphenylphosphino)ethane and analogues) have been introduced leading to very stable mononuclear gold(I) complexes with tetrahedral geometry (Figure **3**).[61] The change from mono- to bidentate ligand moieties drastically hampered ligand exchange reactions without affecting the antimitochondrial activity.[62] Once the high reactivity towards (selenol-)cysteine was alleviated, new selectivity issues appeared for this family of tetrahedral gold complexes due to the very high lipophilicity degree .[63] Preclinical studies in dogs and rabbits have shown severe side effects to heart, liver and lung resulting from mitochondrial dysfunction.[64-65] Alternatively, the pendant groups of the phosphine-type bidentate ligands were altered (e.g. from phenyl to pyridyl) for counter-balancing the lipo-/hydrophilicity ratio and to overcome selectivity issues.[66-67] Thus, synthetically, the design of a suitable ligand system to ensure highly selective cellular uptake without inactivation during the transport is still a never-ending challenge.

The most investigated (and understood) mode of action of gold-based complexes is the inhibition of mitochondrial thioredoxin reductases (TrxR, family of pyridine nucleotide-disulfide oxidoreductases), which is involved actively and passively in a various number of intracellular processes.[59] This enzyme was observed to be overexpressed in some cancer cell lines.[16] TrxR is responsible for the regulation of reactive oxygen species (ROS, e.g. H_2O_2) by recovering the redox equivalent $NADPH/H^+$ in cell.[68-69] The recycling of $NADP^+$ and the reduction of ROS, respectively, is performed by a cooperative enzymatic process in which thioredoxin reductases (TrxR), thioredoxin (Trx) and peroxidoredoxin (Prx) are involved.[59] Considering that the mitochondrion is indispensable for the cell, this enzyme resulted to be a very attractive druggable target.[12-13] Mitochondrial uptake of gold complexes is ensured by the delocalized lipophilic cationic (DLC) character.[62] Thereby, driving force for the internalization of cationic compounds in mitochondria is the mitochondrial membrane potential, which is higher in some examples of carcinoma cells when compared to healthy cells.[70] Once inside this organelle, gold complexes are expected to undergo ligand exchange reactions with TrxR replacing their ligands by cysteine and/or selenocysteine units, which defines the active centrum of this enzyme. Thus, this element interrupts dithiol-disulfide switching redox cycles in the gold(I) enzyme adduct, which disrupts the whole enzymatic cascade, leading to a redox de-equilibration and finally inducing various mitochondrial apoptotic pathways.[71-73] A detailed investigation on the mode of action of auronofin over the past decades allowed to get an intracellular reactivity profile, which might be useful towards the design of the next gold(I) complexes generation. Scheme 2 summarizes the mechanisms of action of auranofin, including all cellular organelles and the main reactions involved in apoptosis.

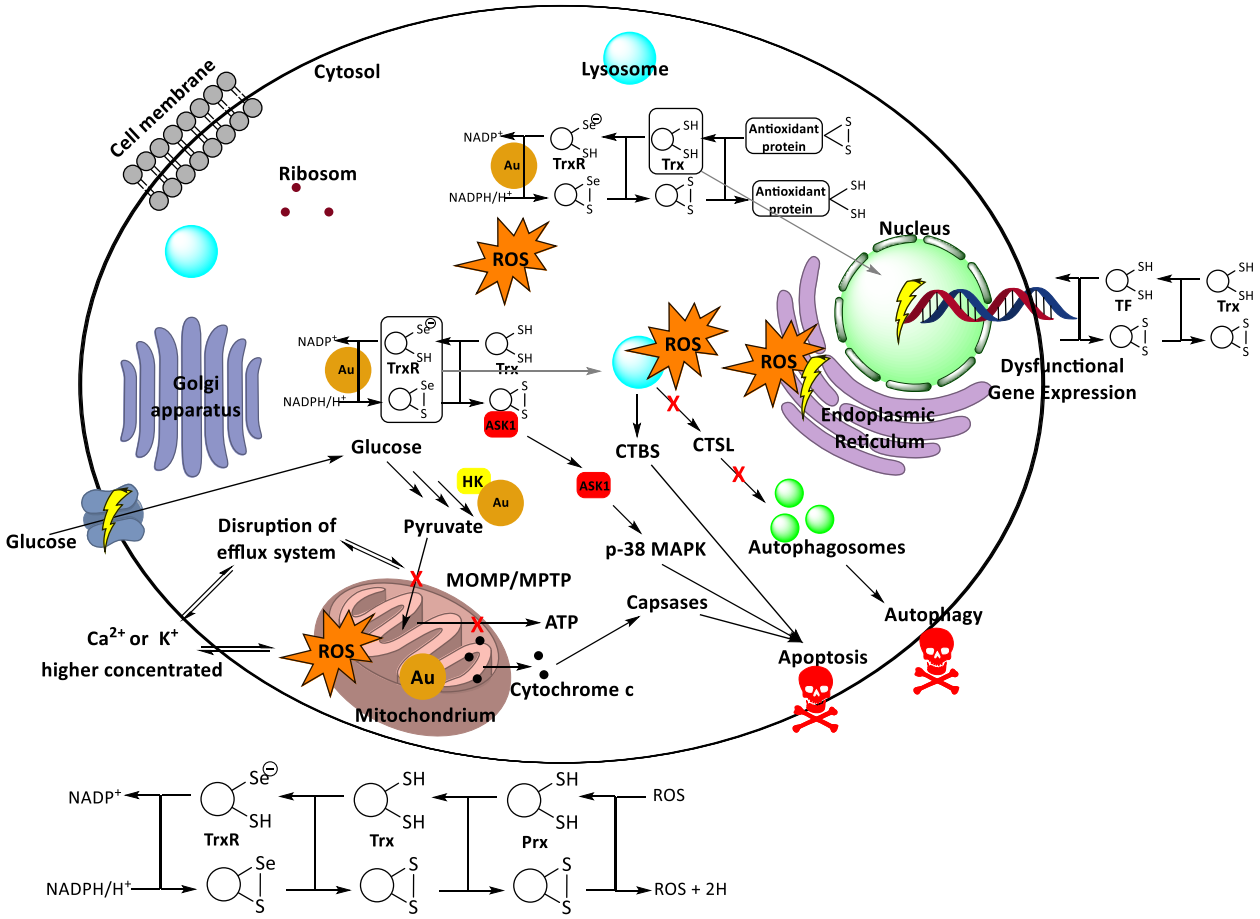

Scheme 2: Summary of mitochondrial induced apoptotic pathways as a consequence of TrxR inhibition by gold(I). TrxR = thioredoxin reductases; Trx = thioredoxin; Prx = peroxidases; TF = transcription factors; HK = hexokinases; CTBS = cathepsin B; CTSL = cathepsin L; p-38 MAPK = mitogen-activated protein kinase p38; ASK1 = mitogen-activated protein kinase p38; MOMP = mitochondrial outer membrane permeabilization; MPTP = mitochondrial permeability transition pores. One should take into consideration that cells normally are not well spherically shaped.

Increasing concentration of ROS in cell was reported to induce the opening of mitochondrial permeability transition pores (MPTP), to increase the mitochondrial outer membrane permeabilization (MOMP) and to enhance the efflux of substrates in- and outside the mitochondria.[73-74] The effect of MOMP initiates for example the release of several pro-apoptotic proteins (e.g. cytochrome c), which trigger a caspases cascade (cysteine aspartyl-specific proteases) known to activate apoptosis.[75] Typical symptoms of a dysfunction is a mitochondrial swelling, which is caused by the entering of small molecules (e.g. H^+, K^+, Ca^{2+}, H_2O). Indeed, a calcium-overload was experimentally confirmed to be in correlation with an increase of H_2O_2.[76-77] Furthermore, auranofin was observed to inhibit the hexokinases, which is the first enzyme of glycolysis involved in the conversion of glucose to pyruvate.[78] Once the formation of pyruvate is limited, the mitochondrion does not produce the required ATP amount, which is in particular for cancer cells crucial, since this organelle is responsible for approximately 80% of energy production. In addition, glucose uptake was hampered as well.

The cytosolic TrxR is isoform to the mitochondrial analogue and can be targeted also by gold.[59] This inhibition and the resulting high concentration of ROS were reported to affect the lysosomes. Thereby,

a lysosomal-mediated autophagy is induced, since lysosomal cathepsins like the pro-autophagy proteases CTSL is inhibited. This inhibition consequently blocks the formation of autolysosomes, which are responsible for the degradation and recycling of undesired cytoplasmic materials or organelles.[8, 79] In addition, the inhibition of TrxR enhances the activity of lysosomal pro-apoptotic CTSB, which finally leads to apoptosis. Another pre-apoptotic effect of a high cellular ROS content is the oxidation of Trx, which consequently activates ASK1 (apoptosis signal-reglation kinase 1) and furthermore the p38-MAPK (mitogen-activated protein kinase p38). Both kinases are involved in apoptotic cell death mechanisms.[80-82] Additionally, the presence of gold and the highly concentrated ROS were observed to cause endoplasmic reticulum stress and to affect DNA transcription processes in the nucleus as well. [13, 83-84] By inhibiting the cytosolic TrxR, the Trx cannot be reduced and as a consequence DNA transcription factors (TF) cannot be recycled leading to a dysfunction of the gene expression.

Despite their more or less well-investigated cytotoxic properties and intracellular modes of action, the lability of phosphine-type ligands against exchange reactions with extra- and intracellular thiol-based nucleophiles rendered these moieties less attractive for the design of gold(I) based complexes with anticancer properties. Additionally, phosphines were reported to be cytotoxic, since they can be involved in redox reactions being oxidized under physiological conditions.[85] Thus, as already mentioned before, one of the main goals in this field is to establish a more suitable ligand system, which enables the formation of more stable gold(I) complexes and offers a high versatility in terms of tuning steric and electronic parameters as well as the lipo- and hydrophilic ratio. In addition, the ligand should not show cytotoxicity. Recently, NHCs emerged as promising alternatives to phosphines in the new millennium showing attractive results as ligands for gold(I)-based anticancer molecules. First positive effects of the replacement of phosphines by NHCs were observed in the field of catalysis.[86-87] NHCs resulted to be stronger σ-donating ligands than phosphines allowing the access to more stable complexes able to overcome decomposition processes in homogeneous catalysis.[88] The higher stability of the complexes caused by NHCs led to the exploitation of novel gold(I)-based complexes in the biomedical field as anticancer, antibacterial, antifungal, antiparasitic and antiviral agents [55, 85, 89] as well as in the field of photochemistry with for example photo-switchable properties.[90]

1.5 NHCs as Alternative Ligands Anticancer Studies

Carbenes are per definition carbon-containing species having a six-electron valence shell and thus, result in very reactive and unstable species due to an electron deficiency.[91] One example is the family of NHCs, which are defined as carbenes in a cyclic systems containing at least one nitrogen as stabilizing heteroatom.

N-containing carbenes owe first pioneering results to Tschugajeff in 1925, who prepared two first examples of these carbenes deriving from a hydrazine analogue (Scheme 3).[92]

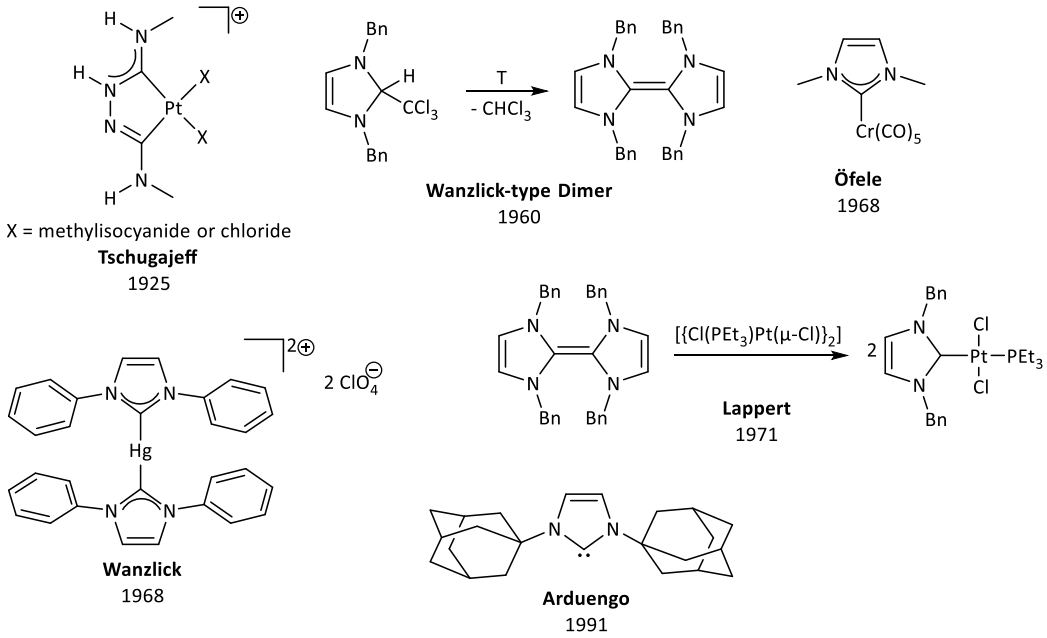

Scheme 3: Structures and reactions of the first discovered NHC-type compounds.

Curiously, in this period the structures were still not understood and took up to 1970, when the Tschugajeff's salts were recognized as diamino-carbene platinum complexes.[93] In 1960, Wanzlick tried to isolate a free NHC via an α-elimination of chloroform (Scheme **3**).[94-96] However, the free carbene was observed to form a Wanzlick-type dimer. In 1968, the pioneering works of Wanzlick and Öfele delivered isolated mercury and chromium NHC complexes, respectively (Scheme **3**).[97-98] Both scientists used metal precursors with basic ligands ($Hg(OAc)_2$ or $[HCr(CO)_5]^-$, respectively) observing the deprotonation of the imidazolium salts and the formed carbene could be stabilized by the presence of a coordinative unsaturated transition metal. A few years later, Lappert was successful in preparing platinum NHC complexes after inserting a metal precursor into the double bond of the Wanzlick-type dimer.[99-100] The definitive successful isolation of a "bottleable" NHC was delivered by Arduengo in 1991, who reported the isolation of 1,3-di(adamantyl)imidazol-2-ylidene, characterizing it as free carbene via single crystal X-ray diffraction (SC-XRD).[101] This discovery opened a new era in the field of carbenes and an explosive number of reports related to NHCs have been published.[91]

Nowadays, considering the five-membered ring system, different NHCs moieties, with varying number of nitrogen, were reported, and some examples are depicted in Figure **4**.[91, 102-105] The pyrrolidinylidene species is an example of NHCs bearing only one nitrogen atom. More common are the imidazol-2-ylidene or the analogue with saturated backbones (C4 and C5) imidazolin-2-ylidene with two nitrogen atoms. Extending the backbone-positions with benzyl or derivatives delivers the benzimidazol-2-

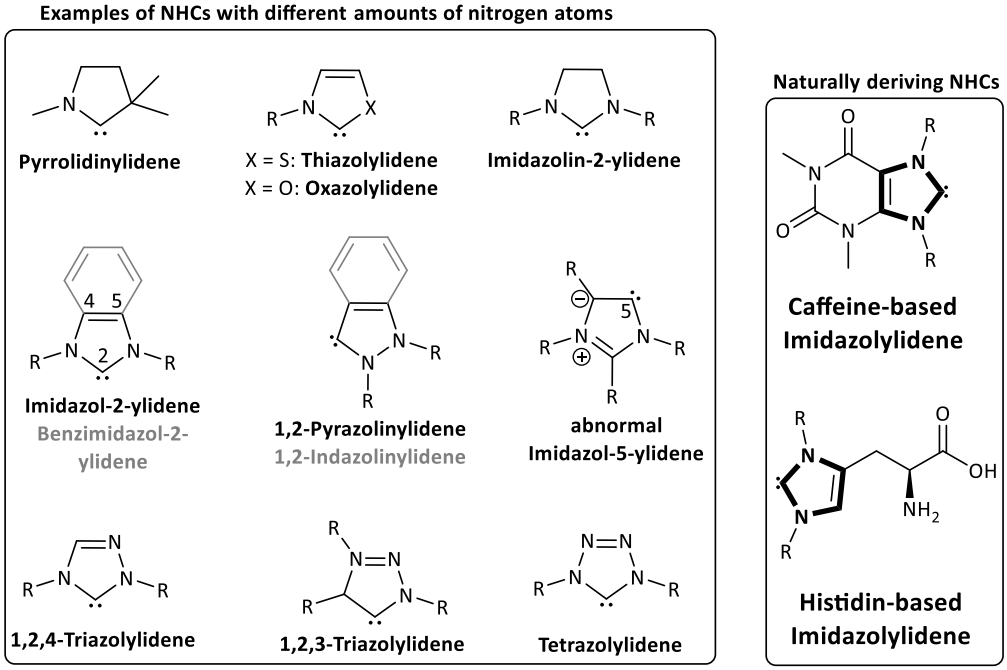

Figure 4: Different examples of five-membered NHCs moieties varying in the number of nitrogen atom or being naturally deriving.

ylidene. Further systems known with two nitrogen atoms are 1,2-pyrazolin-and 1,2-indazolinylidenes. In case of an alkylated C2 position in imidazolylidene moieties, the carbene can be generated at the C5 position known as an abnormal imidazole-5-ylidene system. Extending the number of nitrogen atoms to three gives the 1,2,4- or the click-derived 1,2,3-triazolylidene system. Four N-atoms allow the synthesis of tetrazolylidenes.[106] Replacing one nitrogen atom by an oxygen or sulfur in imidazolylidene systems enables the synthesis of oxazolylidenes or thiazolylidenes, respectively.

Going into more detail in the imidazole-2-ylidene system, most of the imidazole-based precursors are commercially available. In addition, there also exist some naturally derived compounds like caffeine[107] or histidine[108], which have imidazole-type rests as possible NHC precursors (Figure 4). As above-mentioned, NHCs are generated by deprotonating the respective imidazolium salts. These NHC precursors can be synthesized in different pathways as are summarized in Scheme **4**. Segmenting an imidazolium ring retro-synthetically, the cycle can be formed directly via a ring closure condensation reaction between glyoxal, two amines bearing *N*-substituents and formaldehyde.[103] Alternatively, this synthesis can be performed with an intermediate step isolating the diimine moiety, which can be converted in a second step with formaldehyde under acidic conditions to the desired imidazolium salt. Both pathways allow the synthesis of symmetrically *N*-substituted imidazolium salts. Replacing one substituted amine with an ammonium salt ends up with the formation of a *N*-monosubstituted imidazole, which is required for the synthesis of commercially non-available imidazole derivatives.[109] These monosubstituted imidazoles can be further converted to an asymmetrical or symmetrical imidazolium salt via alkylation or arylation under basic conditions. Alternatively, using a bridging

material bearing to leaving groups (e.g. halides) can lead to the formation of bisimidazolium systems (Scheme **4**).[102, 110]

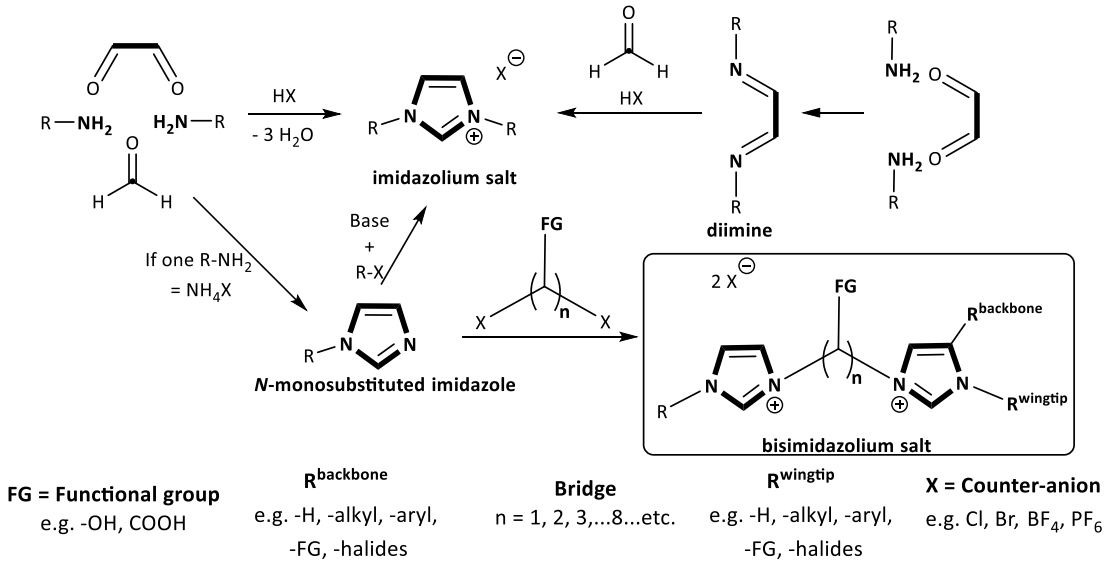

Scheme 4: Different synthetic pathways for the synthesis of imidazole moieties as well as of imidazolium or bridged bisimidazolium salts.

The bisimidazolium scaffold can offer up to five different modification possibilities allowing the tuning of various parameters aimed at for anticancer properties.[110] The first three tuning sites, namely the backbones, the wingtips and the counter-anion, are already known to influence steric and electronic parameters as well as the solubility properties of an imidazolium salt and the respective metal NHC complexes.[91]

In contrast to phosphine-type ligands, these properties of NHCs can be modified faster and the high versatility of these three different modification positions allow a more specific and individual variation.[91] A highly cited review of Glorius *et al.* (2014) gives very specific insights about the tuning effects as well as methods to quantify these parameters.[91] Two more modification strategies are related to the bridging unit, which can be elongated as well as it gives access to a new position for introducing functional groups.[102, 110] The variation of the bridge length gives more flexibility to complexes, whereas the functionalization open new strategies for balancing the degree of lipo- and hydrophilicity. The effect of these two tuning possibilities on dinuclear gold(I) complexes will be discussed in the following chapter. Nowadays, only a few example of alkylene-bridge-functionalized bisimidazolium moieties have been reported and are summarized in Figure 5.[111-119] The first bridge-functionalized bisimidazolium salts **L1**-**L3** were introduced and patented by Kühl in 1995.[111] Further examples of bisimidazolium salts were reported by Peris (**L4**-**L6**, 2004/2005)[112-114], Kang (**L7**, 2005)[115], Kühn (**L8**-**L11**, 2014-2017)[110, 116-118] and Hölscher (**L10**, 2018)[119]. The bisimidazolium salt **L8** was originally designed for the immobilization of catalytically active palladium or iron complexes on supporter materials.[110, 120] Recently, the same ligand system allowed the synthesis of dinuclear gold(I)

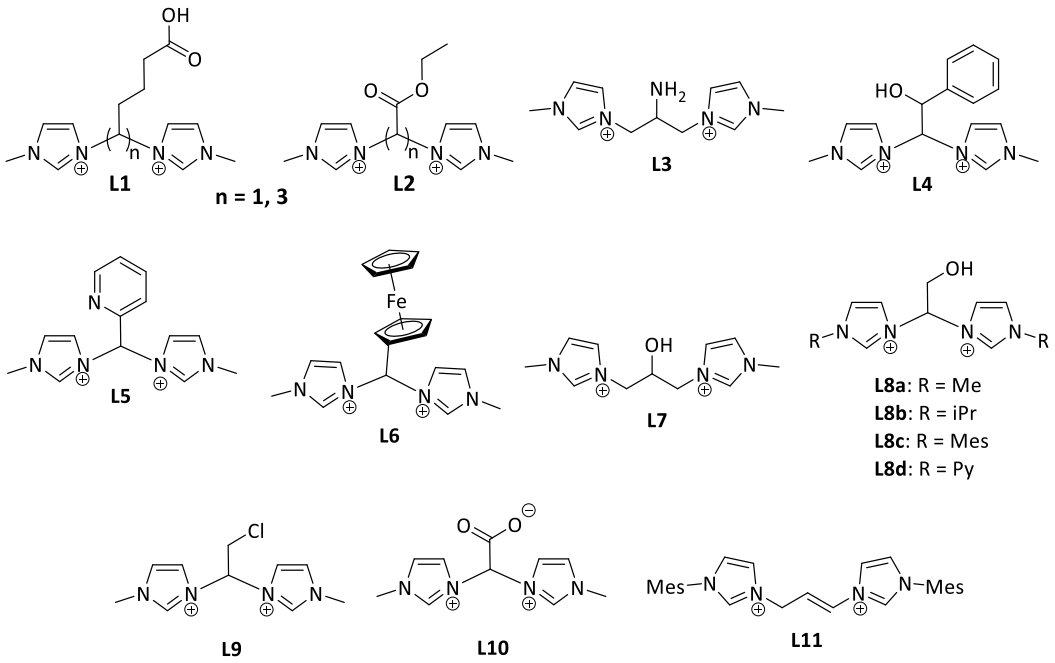

Figure 5: Examples of bridge-functionalized bisimidazolium salts.

complexes bearing bridge-functionalized bisimidazolyliedene ligands. Subsequently, the water-soluble **L10** with an acetate-bridge as well as the asymmetrical **L11** with a *N*,*N*'-allyl-bridge have been introduced as new bridge-functionalized bisimidazolium salts. The respective gold complexes including their anticancer properties will be discussed more detailed in the next chapter.

1.6 Au(I) NHC Complexes with Anticancer Properties

The first gold(I)-NHC complexes **1a-b** has been reported by Burini and coworker in 1989 (Figure **6**).[121]

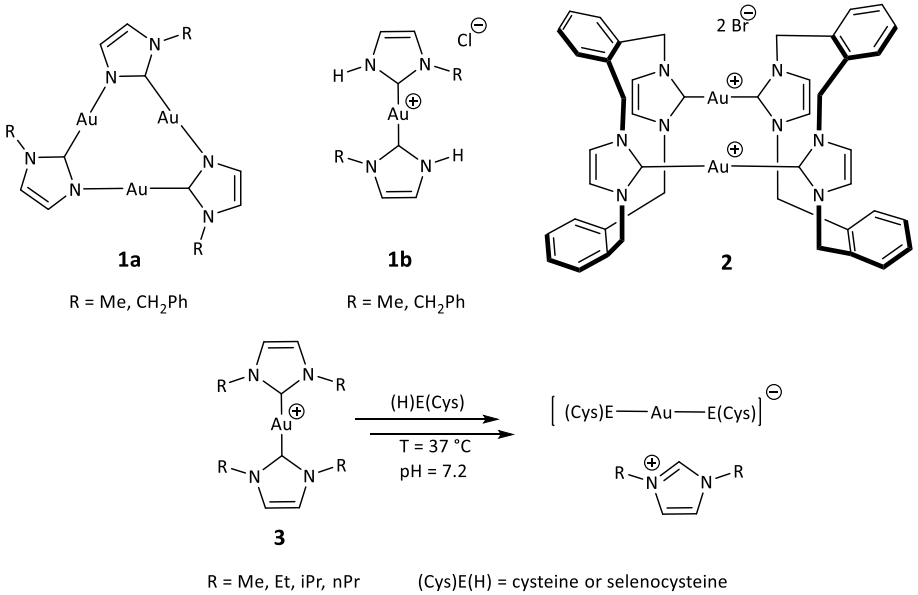

Figure 6: First reported synthesis of gold NHC complexes (**1a-b**) and first gold NHC complexes (**2** and **3**) tested as anticancer agents.

The synthesis of gold(I)-based NHC complexes are straightforward and two very common procedures are applied nowadays. The respective bisimidazolium salt can be treated with silver(I) oxide and the resulting isostructural Ag(I) complex is subsequently transmetallated to the gold(I) precursor of the type L-Au-Cl (L = Me_2S, tetrahydrothiophene = THT, PPh_3). Alternatively, the NHC precursor can be directly converted to the gold(I) complex by using a mixture of a moderate base (e.g. inorganic carbonates) and gold(I) precursor.[121-123]

First pioneering results in the application of gold(I) NHC complexes as anticancer agents were made by Berner's Price and coworker in 2004, who published dinuclear cationic gold(I) cyclophane-NHC complexes of the type **2** exhibiting antimitochondrial activity (Figure 6).[124] Four years later, the same group reported a two-step ligand exchange of mononuclear NHC complexes **3** with L-cysteine and L-selenocysteine under physiological conditions.[16] Despite their stronger σ-donating properties, this pioneering work showed that mononuclear gold(I) NHC complexes can undergo the same reactivity with TrxR as observed for gold(I) phosphine complexes, possibly involving the nucleus in ligand exchange reactions. In addition, a 20- to 80-fold higher reactivity to selenium was observed when compared to sulfur, since selenocysteine was found to exist in its deprotonated form as selenolate under physiological condition rendering it more attractive for gold. Thus, showing antimitochondrial properties, NHC-based gold(I) complexes were observed to undergo similar modes of action as above-described for auranofin. After this pioneering works, an exponentially rising number of gold NHC complexes have been reported with various ligand types and antiproliferative activity.[125-126] Thereby, the above-mentioned backbones, wingtips or counter-anions as tuning sites of NHCs have been modified with different aliphatic or aromatic groups as well as halides, pseudohalides or functional groups leading to a huge number of mono- or multinuclear (homo- and heterometallic) gold(I) complexes with *in vitro* cytotoxicity in the range of micromolar up to subnanomolar.

A glance at the literature approximately one decade later after the pioneering work of Berner's Price, reveals that only a small number of mononuclear gold(I) NHC complexes (**4**-**9**, Figure 7) have been evaluated in tumor regression studies *in vivo*.

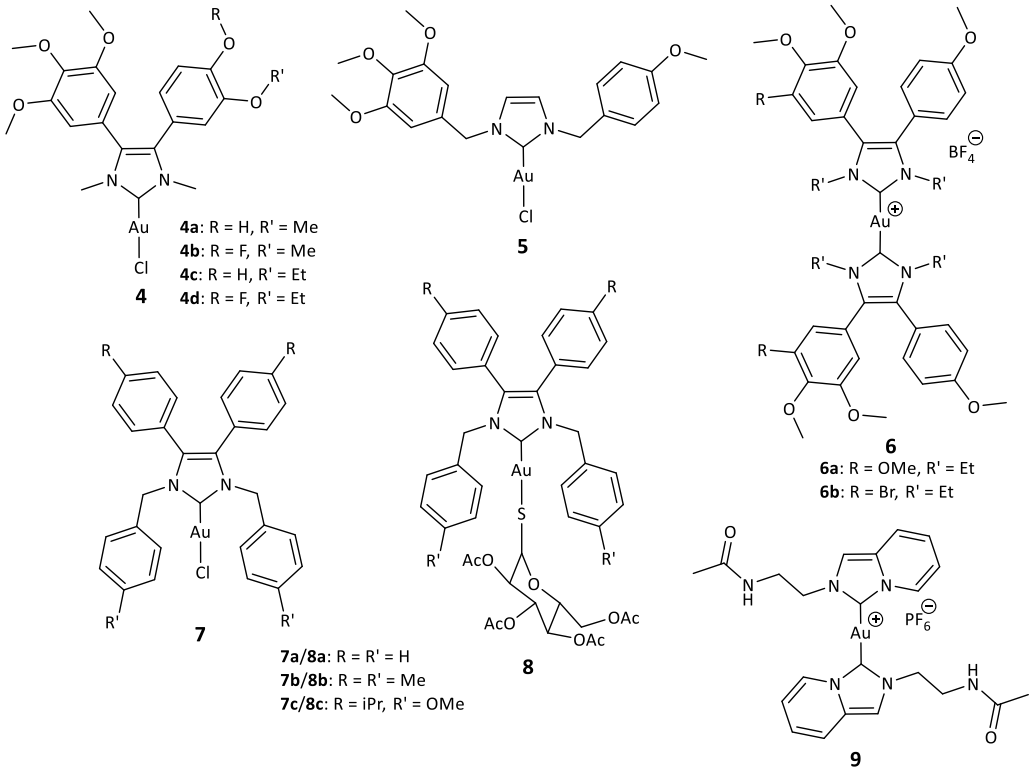

Figure 7: Mononuclear gold(I) complexes **4**-**9** evaluated *in vivo* in mouse models.

Complexes **4a-d** and **5** bearing combretastatin-type backbone-modified or benzylic wingtip substituted NHC ligands, respectively, present antivascular effects *in vitro* and *in vivo* in chicken embryos.[127-128] Based on these results, the respective cationic moieties **6a-b** were applied in treating highly metastatic mouse melanoma cell lines showing a noticeable regression of the tumor mass including antimetastatic and irregular blood vessels-repairing properties.[129] Both, **7** and **8**, reduce tumor mass in *Caki-1* xenografts mouse models following ROS induced apoptotic pathway.[130] Complex **9** showed melanoma tumor growth suppression in *B16F10* mouse melanoma cells inducing mitochondrial death pathways as well.[131] In all cases, no change in animal weight was observed after treatment, indicating no severe side effects. Despite the first promising *in vivo* evaluations, the application of stronger σ-donating NHC moieties as substitute of phosphine-type ligands could not solve the thiol-lability issues of a large number of gold NHC complexes reported as anticancer agents. Thus, only a handful of complexes were evaluated *in vivo* yet.[57] Inspecting the structural composition of the above-mentioned complexes (Figure **7**), it was immediately evident that all mononuclear complexes (**4**-**9**) bear bulky aromatic backbone- or wingtip-substituents mostly functionalized with ether-groups for balancing the hydro- / lipophilicity ratio. Higher sterical hindrance was reported to hamper the accessibility of the gold nuclei for nucleophilic thiol groups.[132] As described for gold phosphine complexes, the degree of lipophilicity should not be exaggerated in order not to reduce the selectivity towards tumorigenic cells.[66-67]

Another attractive strategy to design ligands for thiol-stable gold complexes are bidentate bisimidazolylidene moieties similarly to what was described for chelating phosphines. A prominent example is complex **10**, which bears a methylene-bridged bisimidazolylidene and a diphosphine ligand forming a dinuclear gold(I) complexes in parallely-shaped metallacycle (Figure 8).[133]

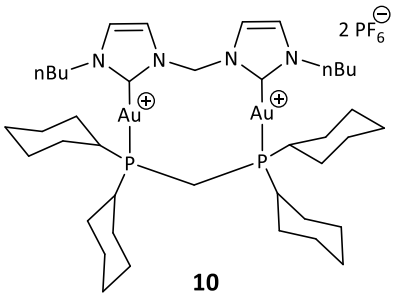

10

Figure 8: Dinuclear gold(I) bisimidazolylidene complex **10** evaluated in vivo in mouse models.

This complex is very stable in presence of blood thiols and act as a potent TrxR inhibitor and antimitochondrial agent. *In vivo* evaluations of **10** in mice bearing *HeLa* xenografts or with *B16F10* mouse melanoma have shown very promising tumor mass regressions. Nowadays, a plethora of dinuclear gold(I) complexes bearing bisimidazolylidene ligands have been reported, showing promising *in vitro* activity in a various number of human cancer cell lines.[102, 125]

Besides the tuning of electronic and steric parameters of NHCs on the backbone- and wingtip-positions, another attractive criterion of bisimidazolylidene moieties are the above-mentioned additional tuning sites of the bridging unit. The most important effects of elongating or functionalizing the bridge of bisimidazolylidene ligands on the structure of dinuclear complexes are depicted in Figure **9**. The elongation of the alkylene-bridge affects the structure of the dinuclear gold(I) complexes. A methylene unit (n = 1) gives the dinuclear complex **11** as metallacycle in a parallel form as described for **10**.[133] The same structure motif is also present for longer alkylene-chains (n ≥ 3) except for a ethylene-bridge (n = 2), which leads to complexes **12** with a twisted form causing an approximation of both gold(I) nuclei in a range for aurophilic interactions (≥ 3.32 Å).[134-135] These d_{10}-d_{10}-interactions introduce luminescence properties offering an additional advantageous criterion applicable for example in cell imaging studies.[136] Enhancing the bridge to octylene (n = 8) the dinuclear complex **13a** started to be in equilibrium with the mononuclear moiety **13b**, since the bisimidazolylidene moiety is long enough for binding as a bidentate ligand around one nucleus.[137]

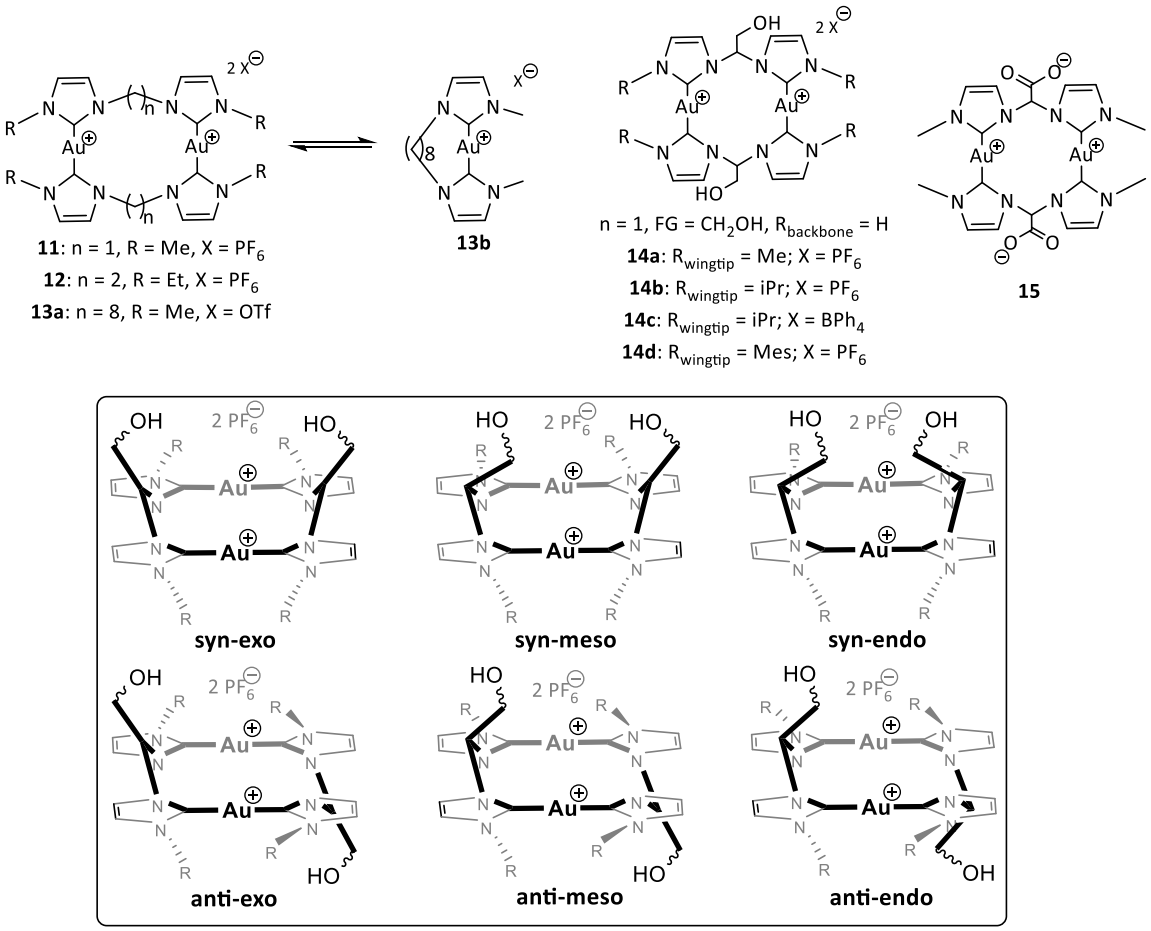

Figure 9: Influence of elongation of the bridging unit **11**-**13** or functionalization of the methylene bridge **14** and **15** on the structure of dinuclear gold(I) complex bearing two bisimidazolylidene ligands. Additionally, all six possible isomers of bridge-functionalized Au(I) complexes with bridge-functionalized bisNHCs are depicted.

The first dinuclear gold(I) complex bearing two 2-hydroxyethane-1,1-diyl-bridged bisimidazolylidene ligands (**14a**) was published in 2015.[116] This complex is isostructural to **10**, forming a similar parallel-shaped 12-membered metallacycle, but the presence of functional groups led to constitutional syn- and anti-isomers (Figure **9**)[116] Syn/anti-isomerization processes have been already observed for dinuclear gold(I) complexes with for example diisocyano-, dithiophosphonates- or bisNHC-based bidentate ligands.[138-148] DFT-calculations revealed three different species for each, the syn- and anti-isomers, resulting to a total number of six configurations (Figure 9). Thereby, the hydroxymethyl-units on both methylene bridges are involved in the isomerization, since they can point both away (exo) or toward (endo) the metallacycle as well as in a mixed form (meso).

In follow-up studies of previously reported doctoral theses in the group of Kühn, the *N*-substituents of this ligand system were extended to more bulky isopropyl and mesityl groups and the respective gold(I) complexes **14b**/**c** and **14d** were reported.[118] Thereby, the wingtips resulted to have an influence on the final most-favoured configuration of the gold(I) complexes and the most lipophilic complex **14d** showed moderate antiproliferative activity in both human cancer cell lines *A549* and *HepG2* after 48 h. Meanwhile, the bridge-functionality was altered from a hydroxyl group to a carboxylate group and first

indications for the successful formation of complex **15** in zwitterionic form were reported.[117] Considering these preliminary synthetic works, the main goal of this thesis is to apply dinuclear gold(I) complexes with bridge-functionalized bisNHC ligands as anticancer agents. More details about the objectives of this thesis are summarized in the next chapter.

2 OBJECTIVES

Considering the first promising *in vivo* studies of complex **10** bearing one bisimidazolylidene moiety (Figure 8) and the various number of possible modification positions of NHCs, in particular the bridging unit, this thesis continues exploring dinuclear gold(I) complexes bearing divers bridge-functionalized bisNHC ligands and their evaluation as anticancer agents.

Firstly, the previously reported **14a**-**d** and **15** (Figure 9) are evaluated in human cancer cell lines to verify whether these gold(I) complexes are cytotoxic and to have an insight into the right ratio between hydrophilic functional groups of the bridge and lipophilic *N*-substituents. Another fact to be examined is the influence of syn- and anti-isomerization on the antiproliferative properties. Therefore, a suitable separation method for the isomer mixtures should be explored and the isolated isomers should be evaluated and compared in human cancer cell lines. The influence of bridge-functionalization and the geometry of the different isomers on the stability of these complexes in presence of L-cysteine is investigated. These first evaluation studies should allow to gather information on the most appropriate strategies towards the design of further gold(I) complexes of this type.

Once the most active and most stable complex is found, a screening of its cytotoxicity in more cancer cell lines allows to analyze for example cisplatin resistance phenomena or the application in more common cancer types like breast and prostate. The evaluation of this complex in a healthy cell line enable to have an insight into the selectivity towards tumorigenic cell lines and to proof whether it could have therapeutic potential by calculating selectivity indices with the respective cancer cell line.

Another goal of this thesis is to analyze the mode of action of this family of complexes and to compare with the intracellular reactivity profile of auranofin (Scheme 2). Strategies should be developed to investigate whether the complex is internalized and where it is located in the cell in order to get an idea of which possible systems are targeted by this compound. Nevertheless, the very first enzymatic studies are performed with TrxR to proof the inhibition properties of the most active complex, since this enzyme is known to be the most investigated target for gold(I) compounds.

Furthermore, the elaboration of suitable synthetic strategies for the post-modification of the functional groups of the bridging unit of these gold(I) complexes is of high interest. Thereby, the main goal is to start developing a theranostic system consisting of a gold(I) based cytotoxic framework extended with a chelator for radioactive labeling as well as a peptide sequence for ensuring highly selective cellular uptake in cancer cell lines.

3 Results – Publication Summaries

3.1 Publication Summaries

This chapter gives a summary of the most important publications originated from this thesis and their printed versions can be found in the appendix.

3.1.1 Influence of Wing-tip Substituents and Reaction Conditions on the Structure, Properties and Cytotoxicity of Ag(I)- and Au(I)-bis(NHC) Complexes

Julia Rieb, Bruno Dominelli, David Mayer, Christian Jandl, Jonas Drechsel, Wolfgang Heydenreuter,

Stephan A. Sieber and Fritz E. Kühn

Dalton Trans. **2017**, *46,* 2722-2735

Based on previously reported coinage metal complexes bearing two 2-hydroxyethane-1,1-diyl-bridged bisimidazolylidene moieties, this publication focused on the same ligand system extending the wingtip substituents from methyl to isopropyl and mesityl groups (Scheme 5).[149]

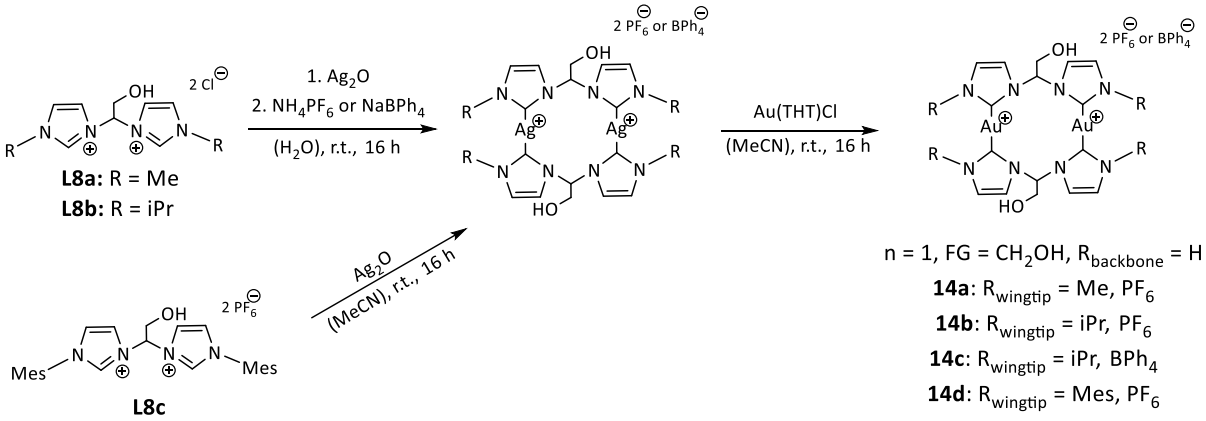

Scheme 5: Summary of all synthetic procedures for the dinuclear gold(I) complexes bearing two 2-hydroxyethane-1,1-diyl-bridged bisimidazolylidene moieties. Adapted from Ref. [149] with permission of The Royal Society of Chemistry.

The Ag(I) and Au(I) complexes **14a-d** have been synthesized according to the literature following the Ag_2O-route and consequent transmetallation step, respectively. A counter-anion exchange of the chloride complexes to $(PF_6)^-$ or $(BPh_4)^-$ was performed by adding NH_4PF_6 or $NaBPh_4$ in aqueous solution, respectively. This work demonstrated that the different syn- and anti-isomers can vary by altering the *N*-substituents and indeed, methyl and mesityl groups led to the formation of syn- whereas isopropyl to anti-conformers. According to the NMR spectrum in deuterated acetonitrile, the Ag(I) complex with isopropyl wingtips was obtained isomerically pure, but measuring the same complex in deuterated dimethyl sulfoxide showed an additional resonance pattern assigned to another isomer. DMSO seems

to slow dynamic processes between the carbene and the nucleus. The previously calculated six different isomers (syn/anti-exo, -meso or -endo) could be classified for the isopropyl-*N*-substituted Ag(I) complex in an energy profile and the anti-exo-fashion (bridge-functionalization pointing away from the metallacycle) resulted to be the energetically most favoured conformer followed by syn-meso. Nevertheless, these calculations should be treated with caution, since until now, only the exo-isomers could be characterized by SC-XRD. After transmetallation in acetonitrile, **14a** and **14c** have been obtained isomerically pure whereas **14b** was obtained as an isomer mixture. This mixture shows thermo-neutrality once it is formed, however, variation of the transmetallation temperature affects the isomer ratio. Nevertheless, isomerically pure **14b** was not possible to be isolated. Several crystallization attempts of the isomer mixture delivered single crystals, which could be always identified as **anti-exo-14b** via SC-XRD. The second species could not be crystallized in a suitable form for SC-XRD and it was theoretically assigned to have the syn-meso conformation when considering the above-mentioned energy profile. The mesityl-*N*-substituted Ag(I) complex showed argentophilic interactions. However, these d_{10}-d_{10} interactions where lost after transmetallation to gold(I), since no aurophilic interactions were observed.

The cytotoxic activities of **14a-d** were determined on the human lung epitheloid carcinoma (*A549*) cell line and on the human liver hepatocellular carcinoma (*HepG2*) cell line by a colorimetric method (3-(4,5-dimethylthiazol-2-yl)-2,5-diphenyltetrazolium bromide, MTT assay). Using an appropriate range of concentrations, dose-response curves after 48 h of incubation time were obtained and the corresponding IC_{50}-values for all compounds are depicted in Figure 10.

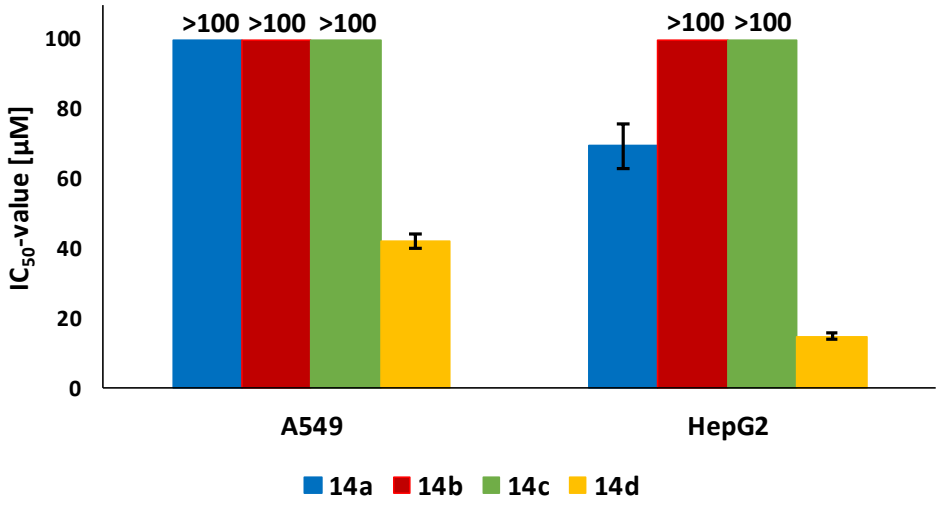

Figure 10: Antiproliferative activity of **14a**, **14b**, **14c** and of **14d** in *A549* and *HepG2* after 48 h of incubation expressed as IC_{50}-values.

Complex **14d** showed the highest cytotoxicity in *A549* (IC_{50} = 42.2±2.2 µM) and *HepG2* cancer cell lines (IC_{50} = 14.9±0.9 µM). Thereby, the moderate antiproliferative activity was related to its poor solubility

in water. **14b** was tested as an isomer mixture and the isopropyl wingtips resulted to deliver not enough lipophilicity for activity. The change of counter-anion to $(BPh_4)^-$ showed no difference in cytotoxicity.

3.1.2 Medicinal Applications of Gold(I/III)-Based Complexes Bearing *N*-Heterocyclic Carbene and Phosphine Ligands

Bruno Dominelli

João D. G. Correia and Fritz E. Kühn

J. Organomet. Chem. **2018**, *866*, 153-164

"Special Issue dedicated to Prof. Wolfgang Herrmann's 70th birthday"

This review updates information (until 2017) on gold(I/III) phosphine and NHC complexes and their application as anticancer, antibacterial, antiparasitic (malaria, leishmaniasis or tyrpanosomasis) and antiviral (HIV-1) agents.[85] Thereby, the main focus was set on depicting different phosphine- or NHC-type ligands applied to stabilize gold complexes and organize them in tables with the corresponding IC_{50}-values. All tables included information on incubation times and type of cell line. Additionally, mechanistic insights or luminescence properties as well as biological evaluation have been provided. All results were compared with cisplatin and auranofin as reference compounds. The main goal of this review was to find trends in ligand design for medicinal purposes, in particular for the preparation of complexes with antiproliferative properties. Issues such as the balance between lipo- and hydrophilicity, the presence of functional groups, the utilization of multinuclear complexes (homo-metallic vs. hetero-metallic) and the comparison of neutral versus cationic complexes were addressed.

The comparison among the different ligand moieties used in gold complexes could help recognizing some trends from repeated observations, which might be applicable for both ligand systems presented in this review. Considering the focus of this thesis, namely the study of the antiproliferative properties of gold complexes in cancer cell lines, the following main conclusions could be drawn:

1. A certain balance between hydro- and lipophilic character is demanded and the lipophilicity is more pivotal than the presence of functional groups. Aromatic *N*- or backbone substituents of NHC ligands like phenyl, mesityl, pyridine-groups or analogues or as additional ligands in the first coordination sphere of gold are very attractive. However, the degree of lipophilicity is limited, otherwise the ligand itself exhibits cytotoxicity. Amide bonds are more adequate, since ester bonds are for example hydrolyzed by esterases present in biological systems.
2. Multidentate ligands have shown promising results after evaluation of the cytotoxicity *in vitro* and *in vivo*. Chelating ligand moieties can deliver stable metallacycles with high cytotoxicity and even more interesting with higher selectivity towards cancer cells. These mono- or multinuclear complexes appear to be more stable in presence of thiol-based nucleophiles showing in some cases a different coordination of these substrates without dissociating the

ligand. The elongation of the bridging alkyl-chain improves the activity of gold phosphine complexes.

3. The number of gold nuclei seems to have a small effect on the cytotoxicity and a higher number of gold atoms is found to be more favorable. However, it should be considered that the activity is not proportionally rising with the increasing number of gold nuclei.
4. Both neutral or cationic complexes are equally active and no trend can be pointed out so far.
5. The synthesis of hetero-metallic complexes is extremely advantageous, since a synergism between both anticancer metals leads to multiple targeting metallodrugs with very low drug resistance. Additionally, some examples of hetero-metallic complexes have shown to be much more cytotoxic in human cancer cells compared to their homo-metallic analogues reaching IC_{50}-values in the nanomolar range.

3.1.3 Dinuclear zwitterionic silver(I) and gold(I) complexes bearing 2,2-acetate-bridged bisimidazolylidene ligands

Bruno Dominelli, Gerri M. Roberts, Christian Jandl,
Pauline J. Fischer, Robert M. Reich, Alexander Pöthig,
João D. G. Correia and Fritz E. Kühn

Dalton Trans., **2019***, 48,* 14036-14043

Two novel Au(I) complexes, **15a** and **15b,** bearing 2,2-acetate-bridged bisimidazolylidene ligands (methyl and isopropyl *N*-substituents, respectively) were synthesized and fully characterized by NMR, ESI-MS and IR spectroscopy as well as elemental analysis and single-crystal X-ray diffraction analysis (Scheme 6).[150] The new bridge-functionalization (carboxylate) led to dimerization in solution and in the solid state. Co-crystallized water molecules formed five-membered rings by hydrogen bond interactions and connected two bisimidazolium molecules in the solid state. The same phenomenon of pseudo-dimerization was observed in solution, since the hydrodynamic radii were in the range of the corresponding complexes (DOSY NMR). The respective Ag(I) and Au(I) complexes were characterized showing the same metallacyclic structure motif and the same formation of syn- and anti-isomers as previously reported for complexes **14a**-**d** (Figure **9** and Scheme **5**).[116, 149]

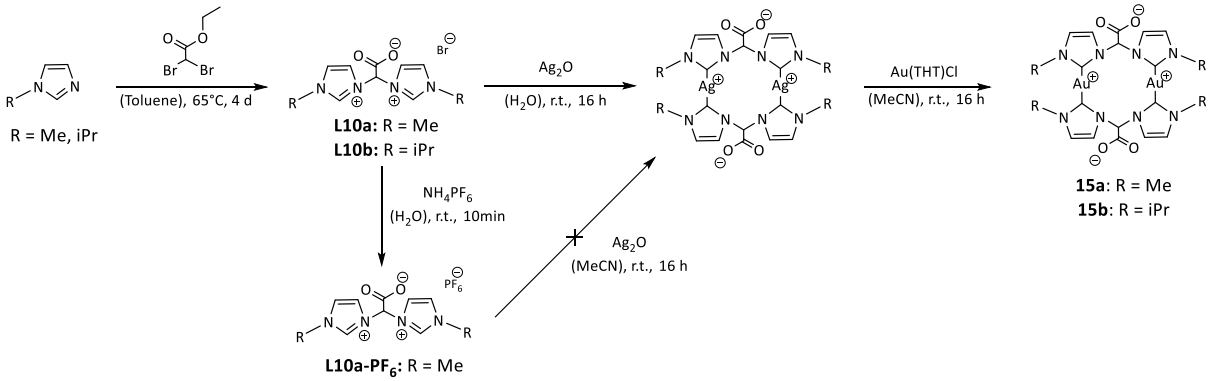

Scheme 6: Synthesis procedure for the 2,2-acetate-bridged bisimidazolium salts **L10a** and **L10b** as well as the repective silver(I) and Au(I) complexes **15a** and **15b**. Adapted from Ref. [150] with permission of The Royal Society of Chemistry.

The replacement of the hydroxyl group with a carboxylate moiety led to water-soluble coinage-metal complexes in zwitterionic form. All distances between both Ag(I) or Au(I) nuclei were too long and not in the range of argento- or aurophilic interactions. In the case of the Ag(I)-complex in syn-form, intermolecular interactions were observed between the carboxylate group and the silver nucleus in a T-shaped coordination geometry. Antiproliferative studies of the Au(I) complexes in human cancer cell lines (*HepG2* and *A549*) resulted in no cytotoxicity properties for this family of complexes. Probably, these complexes were not lipophilic enough for a possible cellular uptake. Unfortunately, the variation of *N*-substituents to more bulky (more lipophilic) groups such as benzyl, mesityl or pyridyl was

unsuccessful due to thermal-induced decarboxylation side reaction of the resulting bisimidazolium salt. The C_α (methylene bridge) bears additionally to the carboxylate group two electron-withdrawing imidazolium/imidazolylidene rings leading to a *Krapcho*-type decarboxylation. The formation of the bridge-unmodified side products was observed during a variable temperature NMR experiment (VT-NMR) in deuterated DMSO. The same experiment in water showed no decarboxylation, however, protic solvents are not suitable for nucleophilic substitution reactions (i.e. the synthesis of bisimidazolium salts). Likewise, the synthesis of the Ag(I) complexes under water-free conditions gave a dinuclear complex with two bridge-unmodified NHC ligands. The presence of water during the synthesis steps is crucial to stabilize this system and to avoid oxidative *Hunsdiecker*-type decarboxylation. The proximity of the carboxyl unit to the NHC rings affects the reactivity towards esterification and/or amidation post-modifications as well. Different methods (activation of the carboxylic acid or the use of coupling reagents) failed in order to stabilize the bridge and to increase the degree of lipophilicity. Only protonation experiments with different acids (HBr, HOTf ad $HAuCl_4$) successfully yielded the respective complexes with carboxyl groups and the corresponding counter-anions. Thereby, a tetranuclear Au(I)/A(III) complex was obtained and the $[AuCl_4]^-$ counter-anion showed interaction with the carboxylate changing the resonance pattern in NMR spectrum when compared to the zwitterionic structure. No change of the chemical shifts was observed after treatment with HBr and HOTf. Interestingly, only the syn-isomer was stable under acidic conditions, whereas the same experiment performed on the anti-species resulted in decomposition.

3.2 Unpublished Results

This chapter summarizes very briefly the most important unpublished results, which were obtained in follow-up studies after the above-summarized publications. Supporting NMR and ESI-MS spectra are attached in the appendix.

3.2.1 Antiproliferative properties of gold(I) complexes bearing 2-hydroxy-ethane-1,1-diyl-bridged bisimidazolylidene ligands

Aimed at comparing the *in vitro* antiproliferative activity in specific cancer cell lines of isolated isomers, the isomer mixtures of **14b** and **14d** were separated via reverse phase high performance liquid chromatography (RP-HPLC).[151] In case of **14b**, the second isomer was identified as syn-exo conformer and not in syn-meso configuration as predicted in the DFT calculations in the above-summarized publication (Figure 11).

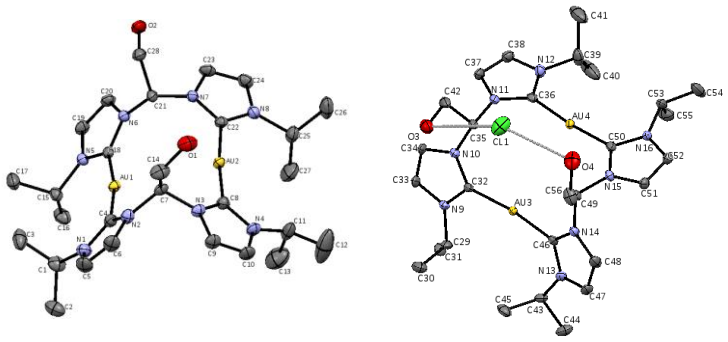

syn-exo-14b **syn-exo-14b(Cl)**

Figure 11: ORTEP-style view of the cationic fragment of **syn-exo-14b**. All atoms are shown using ellipsoids at a probability level of 50%. Hydrogen atoms and counter-anion are omitted for clarity. Relevant bond lengths [Å] and angles [°] of **syn-exo-14b**: Au1–C4 2.015, Au1–C18 2.021, Au2–C8 2.022, Au2–C22 2.024, C21–N6 1.467, C21–N7 1.463, C7–N2 1.463, C7–N3 1.462; Au1 Au2 3.607; C4–Au1–C18 170.32, C8–Au2–C22 174.17, N2–C7–N3 108.63, N6–C21–N7 110.43. Relevant bond lengths [Å] and angles [°] of **syn-exo-14b(Cl)**: Au3–C32 2.021, Au3–C46 2.024, Au4–C36 2.026, Au4–C50 2.026, C35–N10 1.457, C35–N11 1.455, C49–N14 1.454, C49–N15 1.451; Au3 Au4 3.758; C32–Au3 C46 172.08, C36–Au4–C50 174.66, N10–C35–N11 111.13, N14–C49–N15 111.43; O3 Cl1 distances 3.211 Å and O4 Cl1 3.084 Å.

Nevertheless, the refinement of the crystal structure of this isomer revealed the additional presence of co-crystallized chloride as counter-anion, which could have affected the isomerization process. No differences in bond lengths and angles were found between the syn-exo configured **14b** (**syn-exo-14b**) and the previously reported anti-exo isomer of **14b** (**anti-exo-14b**), which was cyrstallized and analyzed via SC-XRD as well.[149]

Sterically more demanding wingtips were observed to lead to isomer mixtures with more than two conformers. The isomer mixture of **14d** was separated analogously leading to the isolation of the syn-exo isomer (**syn-exo-14d**) with high purity and a second fraction containing one main isomer and traces of other species, which are assigned to further constitutional isomers. In accordance with the above-described DFT calculations and previously reported SC-XRD results, the second main isomer was

considered to have the anti-exo configuration (**anti-exo-14d**). Antiproliferative activities of syn-exo and anti-exo isomers of **14b** and **14d** were evaluated in human cervix epitheloid carcinoma (*HeLa*) cell line and in the human liver hepatocellular carcinoma (*HepG2*) cell line by a colorimetric method (3-(4,5-dimethylthiazol-2-yl)-2,5-diphenyltetrazolium bromide, MTT assay). Thereby, appropriate ranges of concentrations were injected into the culture-medium and dose-response curves were collected after 48 h incubation time. The corresponding IC_{50}-values for all compounds were depicted in Figure **12**.

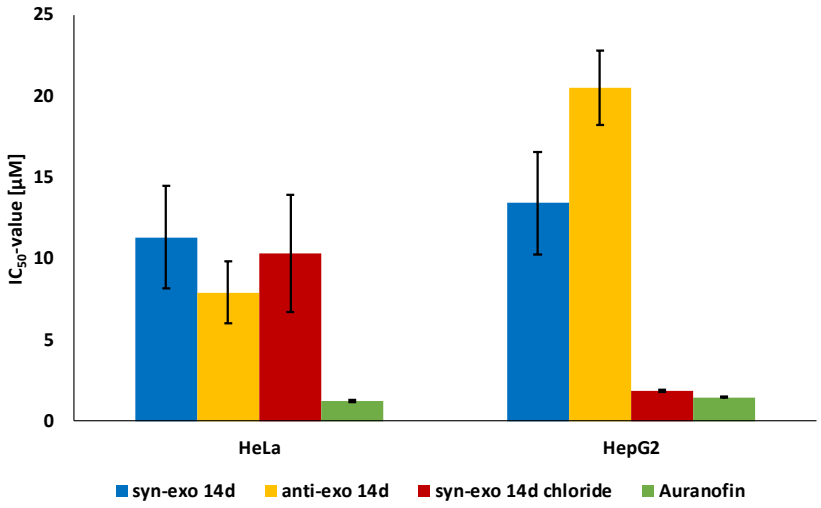

Figure 12: Antiproliferative activity of syn-exo and anti-exo of complexes **14d** as well as auranofin and cisplatin as reference.

Both isomers of **14b** showed no differences in cytotoxicity and resulted to be not active (IC_{50} > 100 µM). In the case of **14d**, both, syn-exo and anti-exo-isomers, present a comparable antiproliferative activity with IC_{50}-values amounting to 11.3±3.17 µM and 7.9±1.9 µM for HeLa, respectively, and 13.4±3.17 µM and 20.5±2.31 µM for HepG2, respectively. The above-mentioned worse solubility of **14d** in water in syn-exo form was overcome by exchanging the counter-anion from $(PF_6)^-$ to chloride. The resulting antiproliferative activity in HepG2 (IC_{50} = 1.85±0.05 µM) was improved into a range comparable to auranofin (IC_{50} = 1.47±0.02 µM).

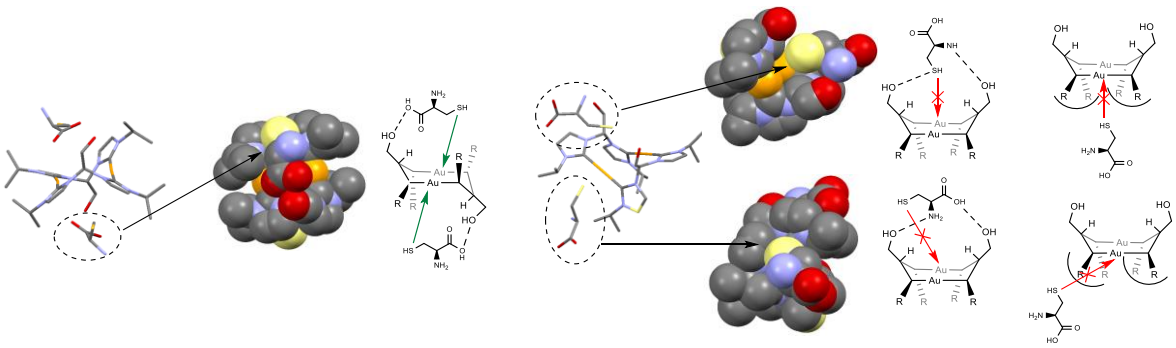

Scheme 7: Density functional: ωB97x-D; basis set: double zeta split valence basis set 6-31G* for non-metals and LANL2DZ for Au.

Independent on the wingtip groups, the syn-isomer resulted to be more stable in presence of L-cysteine under physiological conditions. In contrast, the anti-exo isomer of **14b** showed

decomposition in presence of L-cysteine undergoing the exchange of one bisimidazolylidene ligand by thiolates. Geometry optimization calculations have shown that the gold(I) nuclei of the anti-conformation are more accessed to nucleophiles (Scheme **7**).

TrxR inhibition studies were performed for **syn-exo-14d**, **anti-exo-14d** and auranofin following a DTNB-based (5,5'-Disulfanediylbis(2-nitrobenzoic acid)) colorimetric assay and the respective IC_{50}-values are summarized in Figure **13**.

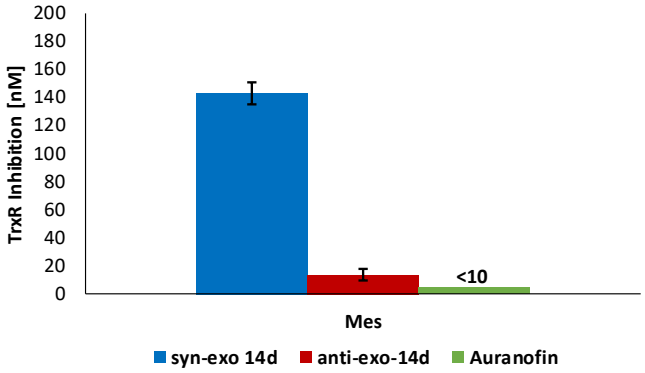

Figure 13: TrxR inhibition studies of syn-exo and anti-exo of **14d** compared with auranofin.

The higher reactivity of the anti-exo configuration resulted in stronger inhibition properties of TrxR (IC_{50} = 14±4 nM) when compared to the syn-analogue (IC_{50} = 143±8 nM).

Considering the similar antiproliferative activity as the anti-analogue, but higher stability towards nucleophiles and nonetheless TrxR inhibition properties, **syn-exo-14d** was found to be the most cytotoxic and the most stable complex in this thesis. Thus, this complex was further screened in more cell lines and all respective IC50-values are depicted in Figure **14**.

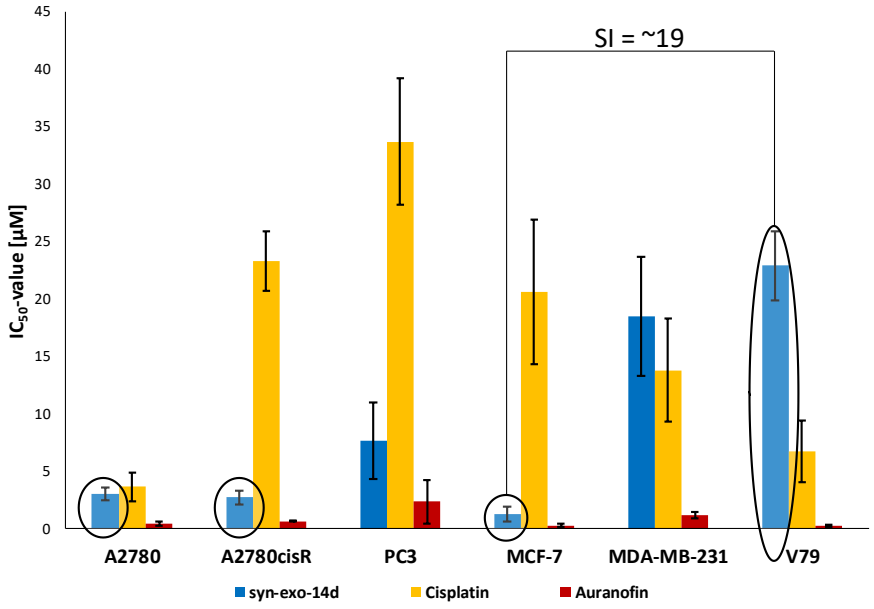

Figure 14: Antiproliferative activity of **syn-exo-14d**, cisplatin and of auranofin in divers cancer cell lines and in healthy fibroblast cells *V79* after 48 h of incubation expressed as IC_{50}-values.

Syn-exo-14d was similarly cytotoxic in the human ovarian epitheloid carcinoma (*A2780*) cell line (IC_{50} = 3.00±0.56 µM) and in the corresponding cisplatin-resistant line (*A2780cisR*, 2.76±0.61 µM) showing to overcome cisplatine resistance. It was more active (IC_{50} = 7.66±3.3 µM) than cisplatin (IC_{50} = 33.7±5.5 µM) in the human prostate epitheloid carcinoma (*PC3*) cell line. Interestingly, it has also shown antiproliferative activity in triple negative breast cancer cells (*MDA-MB-231*, 18.5±5.2 µM). In addition, this complex showed the best antiproliferative activity in the human breast epitheloid carcinoma (*MCF-7*) cell line with an IC_{50}-value amounting to 1.22±0.65 µM. Evaluation in the healthy fibroblast cell line *V79* (IC_{50} = 22.9±3.0 µM) revealed that **syn-exo-14d** was less toxic when compared to cisplatin and, particularly to auranofin. Considering the low antiproliferative activity in *V79* and the high cytotoxicity in *MCF-7*, the resulting selectivity index (SI) of approximately 19 shows that **syn-exo-14d** might be potentially useful for the treatment of breast carcinoma *in vivo*.

First preliminary internalization studies were conducted via proton induced X-ray emission (PIXE) in combination with Rutherford backscattering (RBS) and scanning transmission ion microscopy (STIM) techniques. After an incubation time of approximately 1 h in PC3 cells, both auranofin and **syn-exo-14d** were irradiated with a proton beam and the emitted X-rays, the proton-backscattering as well as the proton transmission were detected and processed in images (Figure **15**).

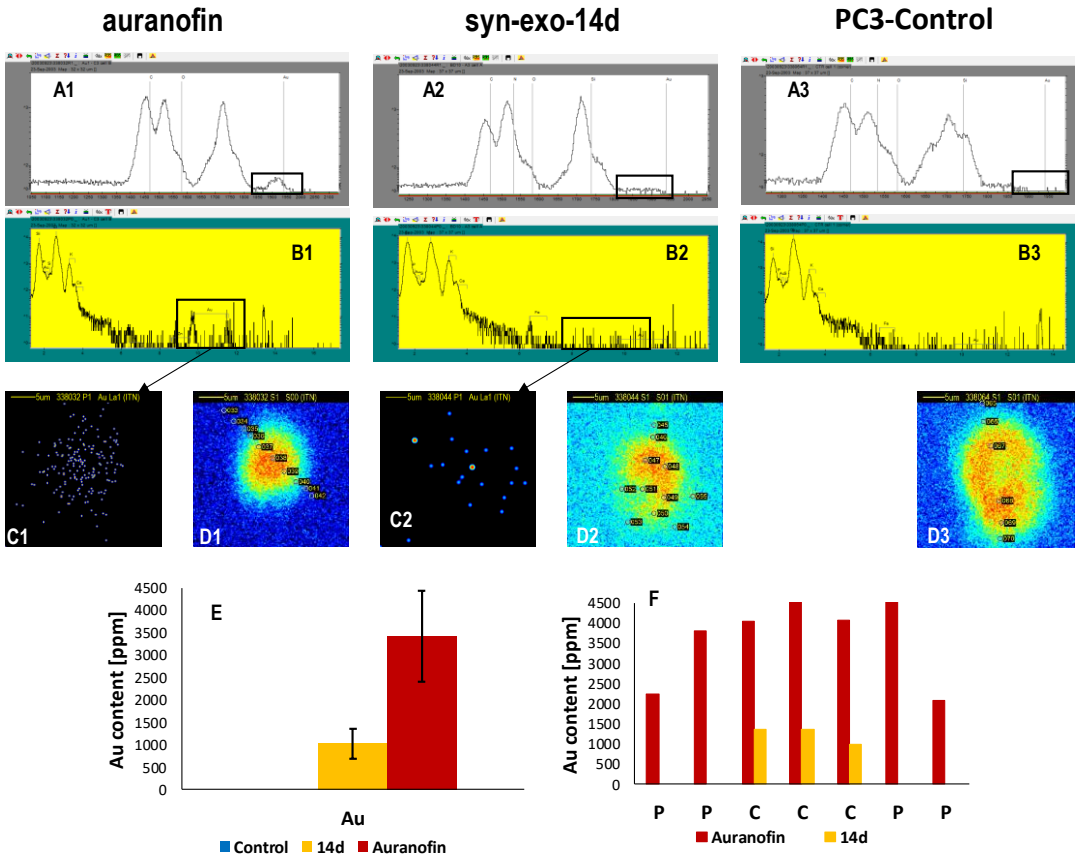

Figure 15: RBS spectrum (A), PIXE spectrum (B), PIXE image (C) and STIM image with selected points (D) for Auranofin, **syn-exo-14d** and a non-treated *PC3* cell. In addition, the calculated gold uptake (E) and distribution of gold content based on points selected in STIM image (F).

The presence of gold inside the *PC3* cell treated with auranofin and **syn-exo-14d** was confirmed by the detection of Lα, Lβ and Lγ emission lines in the respective PIXE spectra. The very broad barrier-type RBS-signal of **syn-exo-14d** in the range of gold shows a deeper internalization of this complex when compared to auranofin with a sharper signal. The RBS spectrum of the non-treated PC3 cell has no signals in the range of gold. According to the selected points in periphery (turquois area) or in the centrum of the cell (yellow-orange area) in the STIM, the overall cellular amount of gold could be quantified. Auranofin internalizes three times higher than the complex after an incubation time of approximately 1 h. However, while auranofin seems to be distributed in the whole cell, **syn-exo-14d** was only detected in the selected points of the STIM image in the centrum. This observation could strengthen the assumption that **syn-exo-14d** internalizes deeper than auranofin. Further studies regarding the cell distribution are ongoing in which four cell compartments (nucleus, cytosol, cell membrane and cell skeleton) have been extracted and the amount of gold will be subsequently quantified via ICP-MS. In addition, electron microscopy techniques (SEM and TEM) are also planned in the near future in order to observe changes of the cell surface or cell organelle morphology after treatment with auranofin or **syn-exo-14d**.

3.2.2 Post-modification of gold(I) complexes bearing 2-hydroxyethane-1,1-diyl-bridged bisimidazolylidene ligand

The non-cytotoxic complex **syn-exo-14b** was post-modified via esterification of both hydroxyl groups with 9-anthracenoyl chloride (Scheme 8).

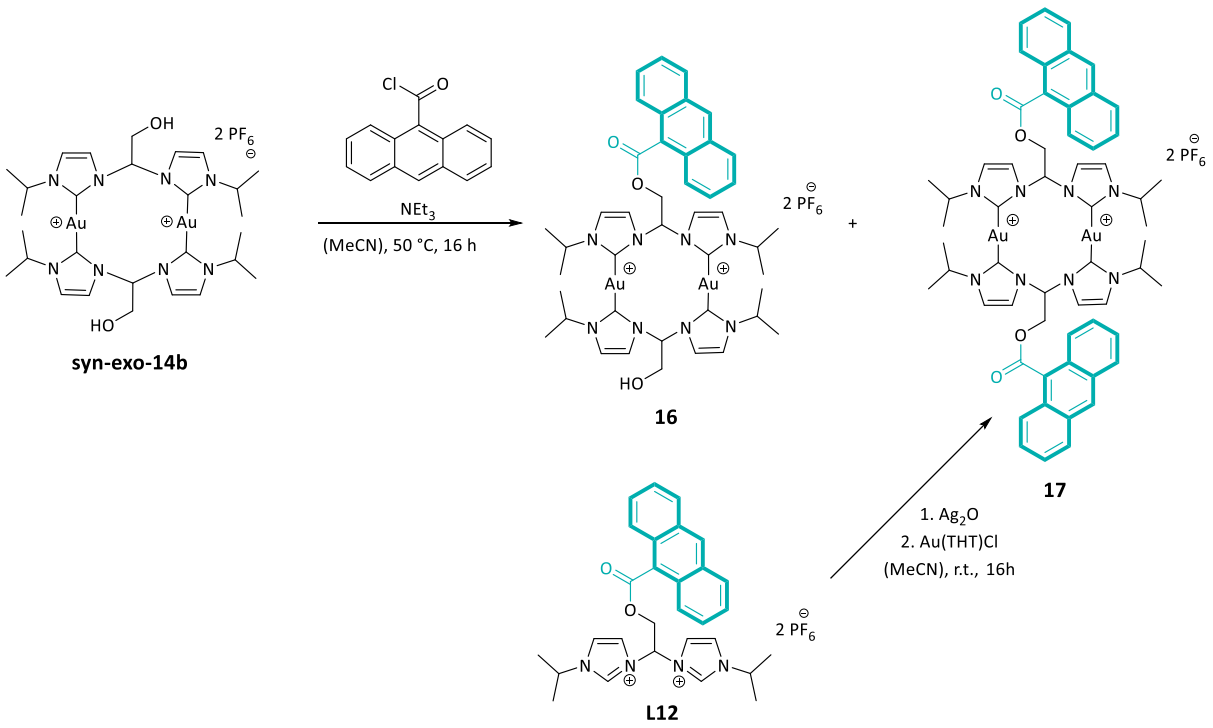

Scheme 8: Post-modification of **syn-exo-14b** via esterification leading to the mono-esterified **16** and di-esterified **17**.

Previously, the bisimidazolium salt **L8b** was esterified with 9-antracenoyl chloride and the resulting product **L12** was treated with Ag_2O and transmetallated to Au(THT)Cl. Unfortunately, the extension of the hydroxyethyl-unit increased the number of isomers.[152] Thus, the syn-exo isomer of complex **14b** was tried to be directly post-modified and indeed, a product mixture of the mono-ester **16** and di-ester **17** could be obtained. Both complexes could be separated by RP-HPLC technique and after isolation fully characterized. The complex **16** showed luminescence properties with a maximum quantum yield of 20% at 365 nm. First *in vitro* evaluations were performed following the above-mentioned colorimetric assay (MTT) and all calculated IC_{50}-values of **16** are summarized in Figure **16** and compared to **syn-exo-14b** and **syn-exo-14d**.

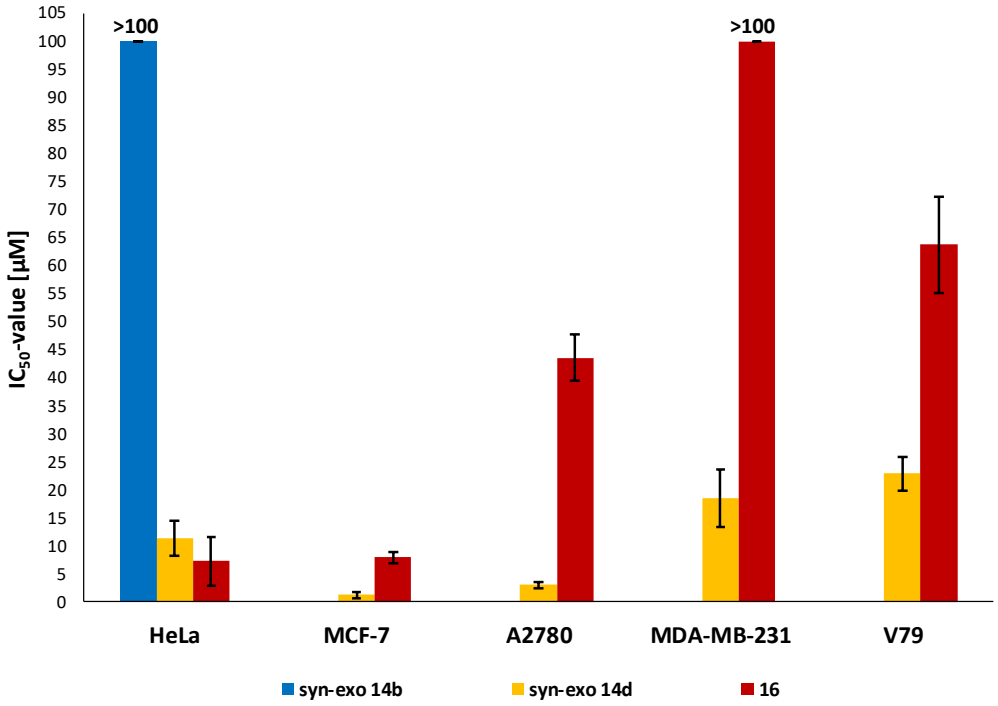

Figure 16: Antiproliferative activity of **syn-exo-14b**, **syn-exo-14d** and of **16** in divers cancer cell lines and in healthy fibroblast cells *V79* after 48 h of incubation expressed as IC_{50}-values.

The antiproliferative activity of **16** in *HeLa* (IC_{50} = 7.26±4.33 µM) remarkably increased when compared to the non-toxic **syn-exo-14b** (IC_{50} > 100 µM). Furthermore, **16** shows good activity in *MCF-7* (IC_{50} = 7.92±0.96 µM). Nevertheless, **16** resulted to be less cytotoxic compared to **syn-exo-14d**, particularly in *A2780* (IC_{50} = 43.6±4.1 µM) and *MDA-MB-231* (IC_{50} = > 100 µM). Despite **16** has a negligible cytotoxicity in the healthy fibroblast cell line *V79* (IC_{50} = 63.7±8.6 µM), it is still not attractive for a potential *in vivo* evaluation, since the selectivity index is not in a range for therapeutic treatment (SI > 10).

TrxR inhibition studies were also performed for **16** following the same above-mentioned colorimetric assay and the respective IC_{50}-values are summarized in Figure **17** and compared with the respective bisimidazolium salt **L12** as well as **syn-exo-14d** and auranofin.

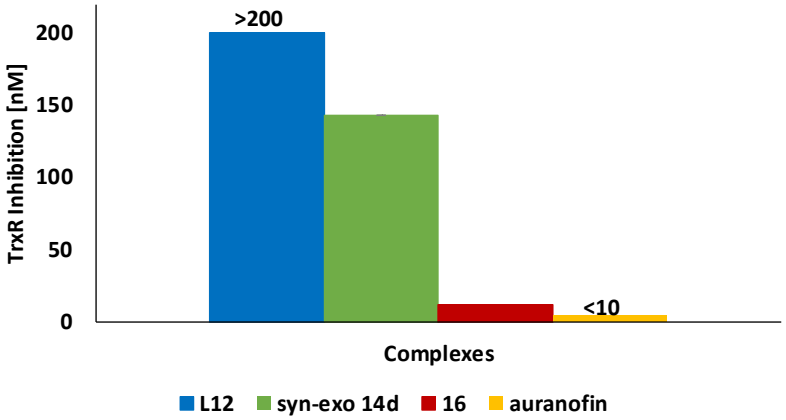

Figure 17: TrxR inhibition studies of **L12**, syn-exo **14d**, syn-exo **16** and auranofin.

16 (IC_{50} = 12±0.003 nM) is approximately 10 times stronger as TrxR inhibitor than **syn-exo-14d** (IC_{50} = 143±8 nM), whereas the inhibition ability of the bisimidazolium salt **L12** can be neglected (IC_{50} > 200 nM). These results lead to the tentative conclusion that probably a synergism between the gold nuclei and the aromatic systems improves the inhibition of TrxR. A similar phenomenon was observed for literature-known square-planar gold(III) complexes inhibiting aquaporin by forming π-π-interactions with the enzyme.[153]

The di-esterified complex **17** resulted to be not suitable for *in vitro* studies, since it precipitates in the culture-medium. The same above-mentioned counter-anion exchange route to obtain the di-ester complex as chloride or even as acetate salt was unsuccessful, since this complex showed to hydrolyze to the mono-esterified **16**. Complex **17** shows luminescence properties as well, however, has only a maximum quantum yield of 8% at 366 nm. Irradiation NMR-scale experiments at 365 nm for 2 h in degassed deuterated acetonitrile showed the formation of at least two new species (Figure 18). The new formed species were tentatively assigned to products resulting from a photodimerization of both vicinal anthracene molecules at 366 nm, which is literature-known for organic anthracene moieties[154] and for dinuclear gold(I) complexes having four example coumarin-based *N*-substituents.[138] Especially, the new formed chemical shifts around 5 ppm could indicate the formation of a saturated cyclic system. A more confirming observation for the photocycloaddition is the thermo-reversibility of these cyclic products. Indeed, heating the product mixture to 37°C for 2 h in the same solution, the new resulting resonance pattern formed back to the lonely chemical shifts of **17**. Thus, this complex seems to be very attractive for further investigations in the field of metal-based photo-switcher, however, the yield should be optimized, since **17** is not fully converted after irradiation at 365 nm for 2 h and longer, since its resonance pattern is still present in the NMR spectrum.

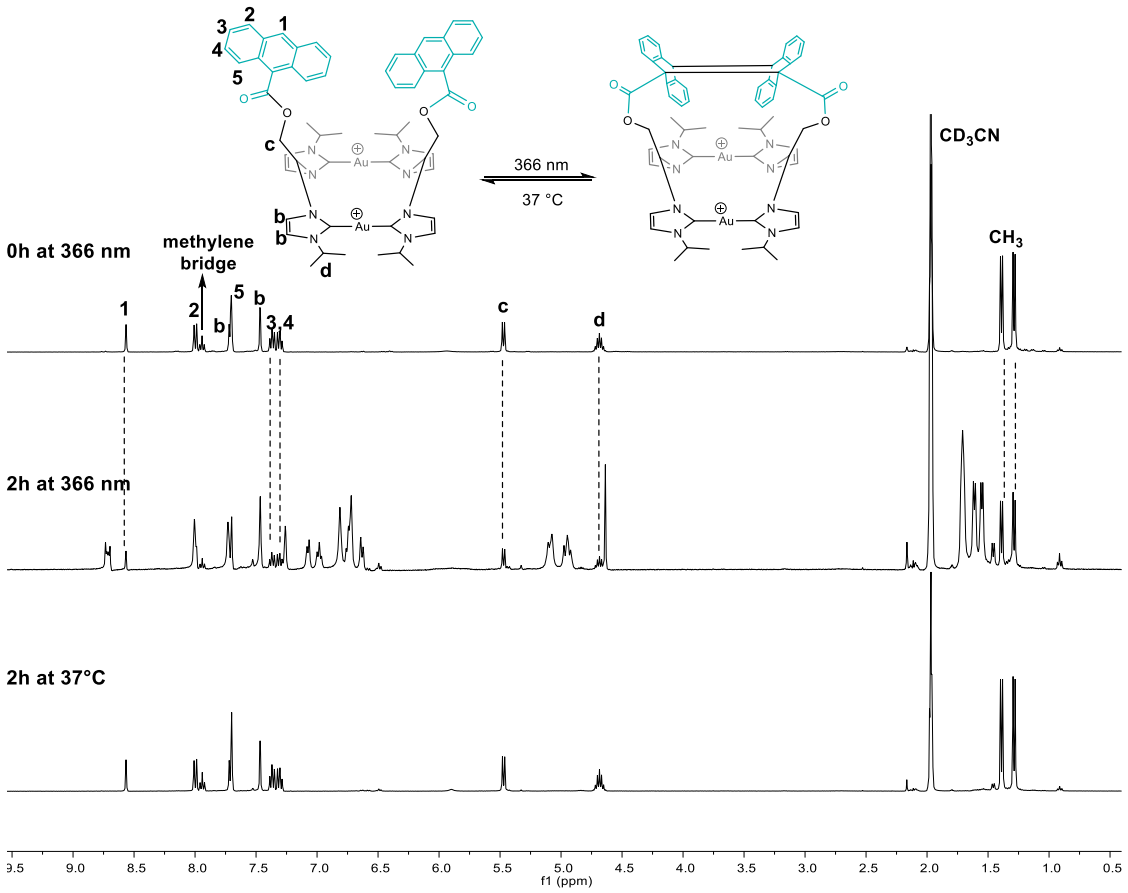

Figure 18: Stacked ^{1}H NMR spectra of **17** before (top), after irradiation at 366 nm for 2 h (middle) and after heating the irradiated solution at 37 °C for 2 h (bottom). The spectra are shown in a range between 8.0 ppm and 4.2 ppm in degassed CD_3CN at room temperature.

The same strategy of esterification was applied for complex **14d** and the same product mixture of mono- and di-esterified complex was observed. This showed that both hydroxyl groups are accessible for post-modification routes despite the presence of the sterically more demanding mesityl wingtips. However, these complexes have been neglected, since **17** revealed that the limit of lipophilicity was already reached.

3.2.3 Synthesis of a gold(I)-based complexes for theranostic applications

As above-mentioned in the summary of publications, the amide bond is preferred to avoid hydrolysis-based decomposition as observed for example for complex **17**. Unfortunately, all amidation attempts on the 2,2-acetate-bridged complex **15** failed due to inactivation of the carboxylate group caused by the proximity of the imidazolium/ imidazolylidene rings. Additionally, several reactions performed to transform the hydroxyl group of the most cytotoxic complex **14d** into azide or amine groups failed as well.

Considering these results, a new carboxyl bridge-functionalized bisimidazolylidene ligand was synthesized bearing an elongated bridging unit from methylene (C_1) to propylene (C_3). The synthesis

of the respective dinuclear gold(I) complex **18** was straightforward following the same procedure as described for **syn-exo-14d** (Scheme 9).

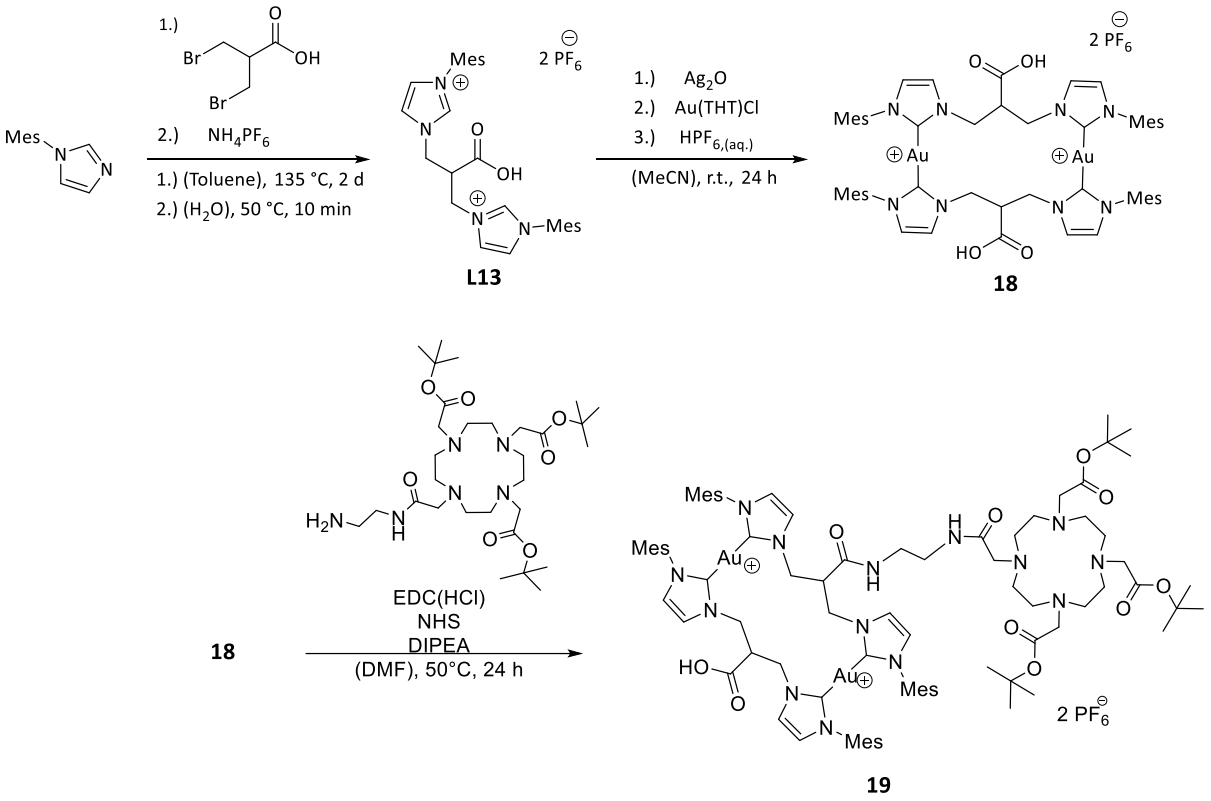

Scheme 9: Synthesis of bisimidazolium salt **L13**, the respective gold(I) complex **18** and the conjugation of a DOTA derivative leadinf to complex **19**.

This complex was conjugated to a 1,4,7,10-Tetraazacyclododecane-1,4,7,10-tetraacetic acid (DOTA) analogue to give complex **19**. The successful amidation of **18** was confirmed by analytical RP-HPLC coupled to ESI-MS. This is the first step for the synthesis of a gold(I)-based theranostic agent. The free carboxyl group of **19** could be further conjugated to a regulator peptide sequence, which allows to increase the selectivity towards certain cancer cell lines by possessing contemporarily a cytotoxic gold(I)-based framework for therapy and a chelator for radioactive metals for diagnostic.

4 CONCLUSIONS AND OUTLOOK

The differently *N*-substituted 2-hydroxyethane-1,1-diyl-bridged bisimidazolium salts **L8a-c** (Figure 5) allowed the preparation of the dinuclear gold(I) complex **14a-d** (Figure 9). The formation of syn- and anti-isomers alters in dependency on the *N*-substituents and more sterically demanding wingtips leads to isomer mixtures. According to an energy profile obtained by DFT calculations as well as the characterization of all isomers presented herein by SC-XRD, the anti- and syn-exo structure motif resulted to be the energetically most favored configurations. First evaluations in both human cancer cell lines *A549* (lung) and *HepG2* (liver) have shown **syn-exo-14d** with mesityl *N*-substituents to have moderate to good antiproliferative activity. The respective **anti-exo-14d** complex, which could be isolated by RP-HPLC technique, showed no different cytotoxicity in *HeLa* (cervix) and *HepG2*. However, independent on the *N*-substituents, the anti-isomer was observed to be less stable in the presence of L-cysteine as nucleophile showing an exchange of one bisimidazolylidene ligand by two thiolates. Geometry optimization calculations have been performed to understand the different reactivity between the syn-exo-and anti-exo-isomers of **14d** with L-cysteine, which revealed that the gold nuclei are more accessible to nucleophiles in the case of the anti-conformation. Thus, after these preliminary studies on the cytotoxicity and stability of the different isomers, the complex **syn-exo-14d** was found as the most cytotoxic and most stable compound presented in this thesis.

Syn-exo-14d was screened in more cancer cell lines showing attractive antiproliferative activity in both human cancer cell lines *PC3* (prostate) and *MDA-MB-231* (breast). This complex overcame cisplatin-resistance in both ovarian cancer cell lines *A2780* and *A2780cisR* and the highest cytotoxicity was found in the breast cancer cell line *MCF-7*. The evaluation in the healthy fibroblast cell line *V79* showed a lower toxicity of **syn-exo-14d** when compared to some of the above-mentioned cancer cell lines and the selectivity index for *MCF-7* amounts to a range being attractive for a potential *in vivo* evaluation in breast carcinoma.

First observations during the studies of the antiproliferative properties of **syn-exo-14d** revealed that its poor solubility in water could have a limiting effect on its cytotoxicity. The exchange of the counter-anion $(PF_6)^-$ to chloride enhanced the water solubility of **syn-exo-14d**, leading also to cytotoxicity enhancement in preliminary cytotoxicity assays in *HepG2* cell line, having an IC_{50}-value in the same range of that of auranofin.

The internalization of **syn-exo-14d** in *PC3* cells was confirmed by proton irradiation-based experiments (PIXE, RBS and STIM), and preliminary results have shown a deeper internalization of this complex when compared with auranofin. ICP-MS studies of extracted cell compartments to determine the gold content (nucleus, cytosol, membrane and cytoskeleton) as well as electron microscopy (SEM and TEM) to observe the morphology of intracellular organelles on *PC3* cells treated with **syn-exo-14d** are

ongoing in order to obtain a more specific localization. A first enzymatic assay revealed that **syn-exo-14d** was still able to inhibit the TrxR in the nanomolar range (IC_{50} = 143±8 nM), despite its stability towards nucleophiles. Once the cell distribution of this complex is characterized, different enzymatic studies specific for the gold-containing cell organelles are of high interests with the goal to depict an intracellular mechanism of action profile as summarized for auranofin in Scheme 2 in the introduction. In the case of localization in the cell nucleus, for example, the inhibition of the enzyme PARP-1 (poly(adenosine diphosphate (ADP)ribose) polymerases 1) or interactions with DNA can be investigated.[155] Furthermore, the influence of **syn-exo-14d** on the glycolysis rate could be studied.

First esterification attempts of the hydroxyethane-unit of the non-cytotoxic **14b** with an anthracene moiety gave the mono-ester complex **16** and the di-ester **17**. Complex **16** was cytotoxic against *HeLa* and *MCF-7* cell lines, however, not as active as **syn-exo-14d**. Complex **17** fully precipitates in the culture-medium, being sensitive to hydrolysis after diverse counter-anion exchange attempts. **16** and **17** showed luminescence properties with maximum quantum yields amounting to 20% and 8% (365 nm), respectively. The lower quantum yield of **17** was related to a quenching photocycloaddition between both anthracene molecules, which showed thermo-reversibility at 37 °C and indicates a possible application of this complex as metal-based photo-switcher. The analogue post-modification of complex **14d** delivered the same product mixture showing that the hydroxyl group is accessible despite the presence of the sterically demanding mesityl *N*-substituents.

Considering the lability of ester-bonds under physiological conditions, complexes **15a** and **15b** bearing 2,2-acetate-bridged bisimidazolylidene ligands have been introduced. The change of functionality from hydroxyl to carboxylate increased the solubility in water, however, evaluation in the cancer cell lines *HeLa* and *HepG2* have shown no cytotoxicity properties. The proximity of the functional group to the imidazolium/imidazolylidene moiety turns the carboxylate group prone to decarboxylation, impeding the extension of *N*-substituents to more lipophilic systems. In addition, the carboxylate is unreactive towards esterification or amidation post-modifications. Protonation experiments with tetrachloroauric acid delivered a tetranuclear mix-valent Au(I)/Au(III) complex.

Elongation of the bridge from C_1 to C_3 allowed the successful combination of mesityl *N*-substituents and carboxylic groups as bridge-functionality. The respective gold(I) complex **18** was successfully synthesized, fully characterized and first conjugation attempts in form of an amidation reaction enabled the coupling of a bifunctional DOTA derivative as chelator for radiolabeling. The resulting intermediate product **19** is planned to be further converted into a theranostic agent bearing a gold cytotoxic complex for therapy (**thera**), a DOTA-stabilized radiometal for diagnostic (**nostic**) imaging and a peptide sequence for specific receptor targeting on cancer cells.

5 Reprint Permissions

Permission of American Chemical Society

Scheme 1 was composed from two figures of Ref. [24] and was reproduced with permissions of the American Chemical Society.

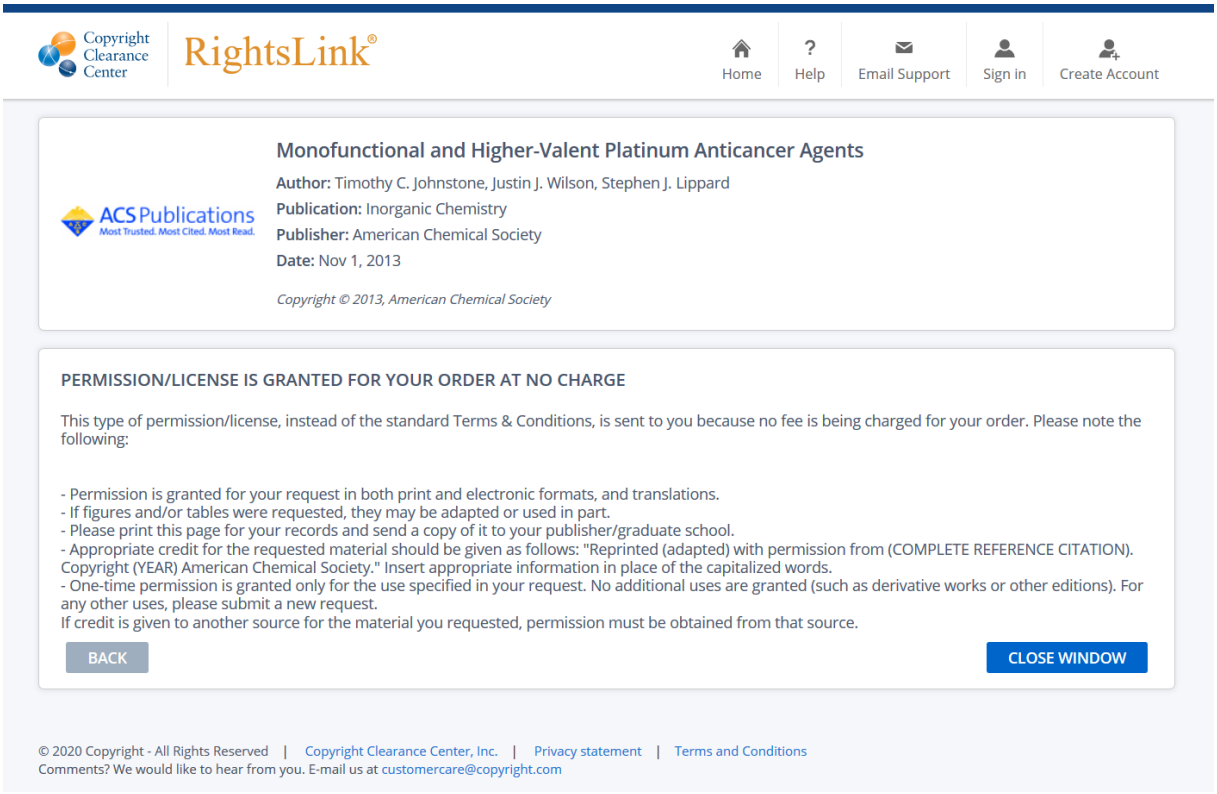

Figure 19: Reprint permission of the American Chemical Society for Scheme 1.

Permission of The Royal Society of Chemistry

Both publications “Influence of Wing-tip Substituents and Reaction Conditions on the Structure, Properties and Cytotoxicity of Ag(I)- and Au(I)-bis(NHC) Complexes” (Ref. [149]) as well as “Dinuclear zwitterionic silver(I) and gold(I) complexes bearing 2,2-acetate-bridged bisimidazolylidene ligands” (Ref. [150]) were reproduced with permission of The Royal Society of Chemistry. The required guidelines are summarized in Figure 20 can be consulted using following link:

https://www.rsc.org/journals-books-databases/journal-authors-reviewers/licences-copyright-permissions/#deposition-sharing (02.01.2020).

Author reusing their own work published by the Royal Society of Chemistry

You do not need to request permission to reuse your own figures, diagrams, etc, that were originally published in a Royal Society of Chemistry publication. However, permission should be requested for use of the whole article or chapter except if reusing it in a thesis. If you are including an article or book chapter published by us in your thesis please ensure that your co-authors are aware of this.

Reuse of material that was published originally by the Royal Society of Chemistry must be accompanied by the appropriate acknowledgement of the publication. The form of the acknowledgement is dependent on the journal in which it was published originally, as detailed in 'Acknowledgements'.

Figure 20: Reprint permission of The Royal Society of Chemistry.

PERMISSION OF ELSEVIER

The publication "Medicinal Applications of Gold(I/III)-Based Complexes Bearing *N*-Heterocyclic Carbene and Phosphine Ligands" (Ref. [85]) was reproduced with permission of Elsevier.

Figure 21: Reprint permission of Elsevier.

6 BIBLIOGRAPHIC DATA OF COMPLETE PUBLICATIONS

6.1 Influence of Wing-tip Substituents and Reaction Conditions on the Structure, Properties and Cytotoxicity of Ag(I)- and Au(I)-bis(NHC) Complexes

Julia Rieb,[a] Bruno Dominelli,[a] David Mayer,[a] Christian Jandl,[b] Jonas Drechsel,[c] Wolfgang Heydenreuter,[c] Stephan A. Sieber[c] and Fritz E. Kühn*[a]

[a] Department of Chemistry and Catalysis Research Center, Molecular Catalysis,Technische Universität München, Lichtenbergstr. 4, D-85747 Garching bei München, Germany.

[b] Catalysis Research Center, Technische Universität München, Ernst-Otto-Fischer-Straße 1, D-85747 Garching bei München, Germany.

[c] Chair of Organic Chemistry II, Department of Chemistry, Technische Universität München, Lichtenbergstraße 4, D-85747 Garching bei München, Germany.

Dalton Trans. **2017***, 46,* 2722-2735.

Direct Link (DOI): 10.1039/C6DT04559F

6.2 Medicinal Applications of Gold(I/III)-Based Complexes Bearing N-Heterocyclic Carbene and Phosphine Ligands

Bruno Dominelli[a], João D. G. Correia[b, **], Fritz E. Kühn[a,*]

[a] Molecular Catalysis, Catalysis Research Center and Department of Chemistry, Technische Universität München, Lichtenbergstr. 4, 85747 Garching bei München, Germany.

[b] Centro de Ciências e Tecnologias Nucleares, Instituto Superior Técnico, Universidade de Lisboa, Campus Tecnológico e Nuclear, Estrada Nacional 10 (km 139,7), 2695-066 Bobadela LRS, Portugal

J. Organomet. Chem. **2018**, *866*, 153-164.

"Special Issue dedicated to Prof. Wolfgang Herrmann's 70th birthday"

Direct Link (DOI): 10.1016/j.jorganchem.2018.04.023

6.3 Dinuclear zwitterionic silver(I) and gold(I) complexes bearing 2,2-acetate-bridged bisimidazolylidene ligands

Bruno Dominelli,[a] Gerri M. Roberts,[a] Christian Jandl,[a] Pauline J. Fischer,[a] Robert M. Reich,[a] Alexander Pöthig,[a] João D. G. Correia,[b] and Fritz E. Kühn*[a]

[a] Molecular Catalysis, Catalysis Research Center, Technische Universität München, Ernst-Otto-Fischer-Straße 1, D-85748 Garching bei München, Germany.

[b] Centro de Ciências e Tecnologias Nucleares, Instituto Superior Técnico, Universidade de Lisboa, Campus Tecnológico e Nuclear, Estrada Nacional 10 (km 139,7), 2695-066 Bobadela LRS, Portugal

Dalton Trans., **2019***, 48,* 14036-14043.

Direct Link (DOI): 10.1039/c9dt03035b

7 REFERENCES

1. F. Bray; J. Ferlay; I. Soerjomataram; R. L. Siegel; L. A. Torre; A. Jemal *CA-CANCER J CLIN* **2018,** *68*, 394-424.
2. S. B. Sutcliffe *Curr. Oncol.* **2012,** *19*, 12-15.
3. A. B. Miller; B. Hoogstraten; M. Staquet; A. Winkler *Cancer* **1981,** *47*, 207-214.
4. D. Hanahan; R. A. Weinberg *Cell* **2011,** *144*, 646-674.
5. D. Hanahan; R. A. Weinberg *Cell* **2000,** *100*, 57-70.
6. B. N. Ames; L. S. Gold; W. C. Willett *Proc. Natl. Acad. Sci.* **1995,** *92*, 5258.
7. L. M. Coussens; Z. Werb *Nature* **2002,** *420*, 860-867.
8. C. P. Tan; Y. Y. Lu; L. N. Ji; Z. W. Mao *Metallomics* **2014,** *6*, 978-995.
9. O. Warburg *Science* **1956,** *123*, 309-314.
10. O. Warburg; K. Posener; E. Negelein *Biochem. Z.* **1924,** *152*, 319–344.
11. G. Kroemer; J. Pouyssegur *Cancer Cell* **2008,** *13*, 472-482.
12. P. J. Barnard; S. J. Berners-Price *Coord. Chem. Rev.* **2007,** *251*, 1889-1902.
13. S. J. Berners-Price; A. Filipovska *Metallomics* **2011,** *3*, 863-873.
14. I. Ott *Coord. Chem. Rev.* **2009,** *253*, 1670-1681.
15. M. J. Akhtar; M. Ahamed; H. A. Alhadlaq; S. A. Alrokayan; S. Kumar *Clin. Chim. Acta* **2014,** *436*, 78-92.
16. J. L. Hickey; R. A. Ruhayel; P. J. Barnard; M. V. Baker; S. J. Berners-Price; A. Filipovska *J. Am. Chem. Soc.* **2008,** *130*, 12570-12571.
17. L. Kelland *Nat. Rev. Cancer* **2007,** *7*, 573-584.
18. G. B. Kauffman; R. Pentimalli; S. Doldi; M. D. Hall *Platinum Met. Rev.* **2010,** *54*, 250-256.
19. B. Rosenberg; L. Van Camp; T. Krigas *Nature* **1965,** *205*, 698-699.
20. B. Rosenberg; L. VanCamp; J. E. Trosko; V. H. Mansour *Nature* **1969,** *222*, 385-386.
21. C. Bergamini; G. Dolci; S. Truong; L. Zanolla; G. Benfari; E. Fiorio; A. Rossi; F. L. Ribichini *Cardiovasc. Toxicol.* **2019,** *19*, 485-492.
22. T. C. Johnstone; K. Suntharalingam; S. J. Lippard *Chem. Rev.* **2016,** *116*, 3436-3486.
23. Z. H. Siddik *Oncogene* **2003,** *22*, 7265-7279.
24. D. P. Gately; S. B. Howell *Br. J. Cancer* **1993,** *67*, 1171-1176.
25. S. B. Howell; R. Safaei; C. A. Larson; M. J. Sailor *Mol. Pharmacol.* **2010,** *77*, 887-894.
26. P. Abada; S. B. Howell *Met. Based Drugs* **2010,** *2010*, 317581.
27. S. Zhang; K. S. Lovejoy; J. E. Shima; L. L. Lagpacan; Y. Shu; A. Lapuk; Y. Chen; T. Komori; J. W. Gray; X. Chen; S. J. Lippard; K. M. Giacomini *Cancer Res.* **2006,** *66*, 8847.
28. J. W. Reishus; D. S. Martin *J. Am. Chem. Soc.* **1961,** *83*, 2457-2462.
29. G. L. Cohen; W. R. Bauer; J. K. Barton; S. J. Lippard *Science* **1979,** *203*, 1014-1016.
30. C. A. Rabik; M. E. Dolan *Cancer Treat Rev* **2007,** *33*, 9-23.
31. B. W. Harper; A. M. Krause-Heuer; M. P. Grant; M. Manohar; K. B. Garbutcheon-Singh; J. R. Aldrich-Wright *Chem. Eur. J.* **2010,** *16*, 7064-7077.
32. S. P. Vyas; A. Singh; V. Sihorkar *Crit Rev Ther Drug Carrier Syst* **2001,** *18*, 1-76.
33. J. Carlsson; H. Nordgren; J. Sjöström; K. Wester; K. Villman; N. O. Bengtsson; B. Ostenstad; H. Lundqvist; C. Blomqvist *Br. J. Cancer* **2004,** *90*, 2344-2348.
34. S. D. Weitman; R. H. Lark; L. R. Coney; D. W. Fort; V. Frasca; V. R. Zurawski, Jr.; B. A. Kamen *Cancer Res.* **1992,** *52*, 3396-3401.
35. M. B. G. Kloster; J. C. Hannis; D. C. Muddiman; N. Farrell *Biochemistry* **1999,** *38*, 14731-14737.
36. https://clinicaltrials.gov/ct2/show/NCT00014547?term=BBR3464&draw=2&rank=1, accessed: 12.12.2019.
37. https://clinicaltrials.gov/ct2/show/NCT00024362?term=BBR3464&draw=2&rank=2, accessed 12.12.19.
38. N. P. Farrell *Chem. Soc. Rev.* **2015,** *44*, 8773-8785.
39. E. Y. Tshuva; M. Miller *Coordination Complexes of Titanium(IV) for Anticancer Therapy* in *Metallo-Drugs: Development and Action of Anticancer Agents*Walter De Gruyter Gmbh, Berlin, **2018**; *18*, 219-250.

40. T. Schilling; K. B. Keppler; M. E. Heim; G. Niebch; H. Dietzfelbinger; J. Rastetter; A. R. Hanauske *Invest. New Drugs* **1995,** *13*, 327-332.
41. G. Lümmen; H. Sperling; H. Luboldt; T. Otto; H. Rübben *Cancer Chemother. Pharmacol.* **1998,** *42*, 415-417.
42. N. Kröger; U. R. Kleeberg; K. Mross; L. Edler; D. K. Hossfeld *Oncol. Res. Treat.* **2000,** *23*, 60-62.
43. K. Strohfeldt; M. Tacke *Chem. Soc. Rev.* **2008,** *37*, 1174-1187.
44. S. Leijen; S. A. Burgers; P. Baas; D. Pluim; M. Tibben; E. van Werkhoven; E. Alessio; G. Sava; J. H. Beijnen; J. H. Schellens *Invest. New Drugs* **2015,** *33*, 201-214.
45. R. Trondl; P. Heffeter; C. R. Kowol; M. A. Jakupec; W. Berger; B. K. Keppler *Chem. Sci.* **2014,** *5*, 2925-2932.
46. https://clinicaltrials.gov/ct2/show/study/NCT01415297?term=ruthenium&draw=2&rank=2, accessed 12.12.2019.
47. A. van Niekerk; P. Chellan; S. F. Mapolie *Eur. J. Inorg. Chem.* **2019,** *2019*, 3432-3455.
48. X. Chen; X. Shi; C. Zhao; X. Li; X. Lan; S. Liu; H. Huang; N. Liu; S. Liao; D. Zang; W. Song; Q. Liu; B. Z. Carter; P. Q. Dou; X. Wang; J. Liu *Oncotarget* **2014,** *5*, 9118-9132.
49. https://clinicaltrials.gov/ct2/show/NCT01419691?term=Auranofin&draw=2&rank=4, accessed 12.12.19
50. G. Moreno-Alcantar; G. Romo-Islas; M. Flores-Alamo; H. Torrens *New J. Chem.* **2018,** *42*, 7845-7852.
51. C. X. Zhang; S. J. Lippard *Curr. Opin. Chem. Biol.* **2003,** *7*, 481-489.
52. B. M. Sutton *Gold Bull.* **1986,** *19*, 15-16.
53. W. F. Kean; F. Forestier; Y. Kassam; W. W. Buchanan; P. J. Rooney *SEMIN. ARTHRITIS RHEU.* **1985,** *14*, 180-186.
54. C. K. Mirabelli; R. K. Johnson; C. M. Sung; L. Faucette; K. Muirhead; S. T. Crooke *Cancer Res.* **1985,** *45*, 32-39.
55. B. Đ. Glišić; M. I. Djuran *Dalton Trans.* **2014,** *43*, 5950-5969.
56. B. Bertrand; A. de Almeida; E. P. M. van der Burgt; M. Picquet; A. Citta; A. Folda; M. P. Rigobello; P. Le Gendre; E. Bodio; A. Casini *Eur. J. Inorg. Chem.* **2014,** *2014*, 4532-4536.
57. T. T. Zou; C. N. Lok; P. K. Wan; Z. F. Zhang; S. K. Fung; C. M. Che *Curr. Opin. Chem. Biol.* **2018,** *43*, 30-36.
58. M. J. McKeage; L. Maharaj; S. J. Berners-Price *Coord. Chem. Rev.* **2002,** *232*, 127-135.
59. A. Bindoli; M. P. Rigobello; G. Scutari; C. Gabbiani; A. Casini; L. Messori *Coord. Chem. Rev.* **2009,** *253*, 1692-1707.
60. E. R. T. Tiekink *Crit. Rev. Oncol. Hematol.* **2002,** *42*, 225-248.
61. S. J. Berners-Price; C. K. Mirabelli; R. K. Johnson; M. R. Mattern; F. L. McCabe; L. F. Faucette; C.-M. Sung; S.-M. Mong; P. J. Sadler; S. T. Crooke *Cancer Res.* **1986,** *46*, 5486.
62. J. S. Modica-Napolitano; J. R. Aprille *Adv. Drug Deliv. Rev.* **2001,** *49*, 63-70.
63. G. D. Hoke; G. F. Rush; G. F. Bossard; J. V. McArdle; B. D. Jensen; C. K. Mirabelli *J. Biol. Chem.* **1988,** *263*, 11203-11210.
64. P. F. Smith; G. D. Hoke; D. W. Alberts; P. J. Bugelski; S. Lupo; C. K. Mirabelli; G. F. Rush *J. Pharmacol. Exp. Ther.* **1989,** *249*, 944.
65. G. D. Hoke; R. A. Macia; P. C. Meunier; P. J. Bugelski; C. K. Mirabelli; G. F. Rush; W. D. Matthews *Toxicol. Appl. Pharmacol.* **1989,** *100*, 293-306.
66. M. J. McKeage; S. J. Berners-Price; P. Galettis; R. J. Bowen; W. Brouwer; L. Ding; L. Zhuang; B. C. Baguley *Cancer Chemother. Pharmacol.* **2000,** *46*, 343-350.
67. J. J. Liu; P. Galettis; A. Farr; L. Maharaj; H. Samarasinha; A. C. McGechan; B. C. Baguley; R. J. Bowen; S. J. Berners-Price; M. J. McKeage *J. Inorg. Biochem.* **2008,** *102*, 303-310.
68. S. Gromer; L. D. Arscott; C. H. Williams; R. H. Schirmer; K. Becker *J. Biol. Chem.* **1998,** *273*, 20096-20101.
69. S. Gromer; S. Urig; K. Becker *Med. Res. Rev.* **2004,** *24*, 40-89.
70. L. B. Chen *Annu. Rev. Cell Biol.* **1988,** *4*, 155-181.
71. K. John; V. Alla; C. Meier; B. M. Pützer *Cell Death Differ.* **2011,** *18*, 874-886.

72. L. Kong; X. Zhou; Y. Wu; Y. Wang; L. Chen; P. Li; S. Liu; S. Sun; Y. Ren; M. Mei; X. Wang; L. Zhang *Curr. Mol. Med.* **2015,** *15*, 952-960.
73. B. Yu; L. Ma; J. Jin; F. Jiang; G. Zhou; K. Yan; Y. Liu *Toxicol. Res.* **2018,** *7*, 1081-1090.
74. A. A. Gerencser; J. Doczi; B. Töröcsik; E. Bossy-Wetzel; V. Adam-Vizi *Biophys. J.* **2008,** *95*, 2583-2598.
75. D. R. Green; G. Kroemer *Science* **2004,** *305*, 626.
76. E. Varghese; D. Büsselberg *Cancers* **2014,** *6*, 2243-2258.
77. M. T. Harper *Platelets* **2019,** *30*, 98-104.
78. G. X. Hou; P. P. Liu; S. Y. Zhang; M. Q. Yang; J. W. Liao; J. Yang; Y. M. Hu; W. Q. Jiang; S. J. Wen; P. Huang *Cell Death Dis.* **2018,** *9*, 15.
79. P. Nagakannan; E. Eftekharpour *Free Radical Biol. Med.* **2017,** *108*, 819-831.
80. G. Fujino; T. Noguchi; A. Matsuzawa; S. Yamauchi; M. Saitoh; K. Takeda; H. Ichijo *Nat. Rev. Mol. Cell Biol.* **2007,** *27*, 8152.
81. M. Saitoh; H. Nishitoh; M. Fujii; K. Takeda; K. Tobiume; Y. Sawada; M. Kawabata; K. Miyazono; H. Ichijo *EMBO J.* **1998,** *17*, 2596-2606.
82. X. L. Cheng; P. Holenya; S. Can; H. Alborzinia; R. Rubbiani; I. Ott; S. Wolfl *Mol. Cancer* **2014,** *13*.
83. W. Fiskus; N. Saba; M. Shen; M. Ghias; J. Liu; S. D. Gupta; L. Chauhan; R. Rao; S. Gunewardena; K. Schorno; C. P. Austin; K. Maddocks; J. Byrd; A. Melnick; P. Huang; A. Wiestner; K. N. Bhalla *Cancer Res.* **2014,** *74*, 2520-2532.
84. P. Zou; M. X. Chen; J. S. Ji; W. Q. Chen; X. Chen; S. L. Ying; J. R. Zhang; Z. H. Zhang; Z. G. Liu; S. L. Yang; G. Liang *Oncotarget* **2015,** *6*, 36505-36521.
85. B. Dominelli; J. D. G. Correia; F. E. Kühn *J. Organomet. Chem.* **2018,** *866*, 153-164.
86. W. A. Herrmann *Angew. Chem., Int. Ed.* **2002,** *41*, 1290-1309.
87. M. S. Sanford; J. A. Love; R. H. Grubbs *J. Am. Chem. Soc.* **2001,** *123*, 6543-6554.
88. C. M. Crudden; D. P. Allen *Coord. Chem. Rev.* **2004,** *248*, 2247-2273.
89. W. K. Liu; R. Gust *Coord. Chem. Rev.* **2016,** *329*, 191-213.
90. E. Peris *Chem. Rev.* **2018,** *118*, 9988-10031.
91. M. N. Hopkinson; C. Richter; M. Schedler; F. Glorius *Nature* **2014,** *510*, 485-496.
92. L. Tschugajeff; M. Skanawy-Grigorjewa; A. Posnjak; M. Skanawy-Grigorjewa *Z. Anorg. Allg. Chem.* **1925,** *148*, 37-42.
93. A. Burke; A. L. Balch; J. H. Enemark *J. Am. Chem. Soc.* **1970,** *92*, 2555-2557.
94. H. W. Wanzlick *Angew. Chem., Int. Ed.* **1962,** *1*, 75-80.
95. H. W. Wanzlick; H. J. Kleiner *Angew. Chem.* **1961,** *73*, 493-493.
96. H. W. Wanzlick; E. Schikora *Angew. Chem.* **1960,** *72*, 494-494.
97. K. Öfele *J. Organomet. Chem.* **1968,** *12*, P42-P43.
98. H.-W. Wanzlick; H.-J. Schönherr *Angew. Chem., Int. Ed.* **1968,** *7*, 141-142.
99. D. J. Cardin; B. Cetinkaya; E. Cetinkaya; M. F. Lappert; L. J. Manojlović-Muir; K. W. Muir *J. Organomet. Chem.* **1972,** *44*, C59-C62.
100. M. F. Lappert *J. Organomet. Chem.* **2005,** *690*, 5467-5473.
101. A. J. Arduengo; R. L. Harlow; M. Kline *J. Am. Chem. Soc.* **1991,** *113*, 361-363.
102. M.-M. Gan; J.-Q. Liu; L. Zhang; Y.-Y. Wang; F. E. Hahn; Y.-F. Han *Chem. Rev.* **2018,** *118*, 9587-9641.
103. F. E. Hahn; M. C. Jahnke *Angew. Chem., Int. Ed.* **2008,** *47*, 3122-3172.
104. H. V. Huynh *Chem. Rev.* **2018,** *118*, 9457-9492.
105. Q. Q. Teng; H. V. Huynh *Dalton Trans.* **2017,** *46*, 614-627.
106. W. F. Gabrielli; S. D. Nogai; J. M. McKenzie; S. Cronje; H. G. Raubenheimer *New J. Chem.* **2009,** *33*, 2208-2218.
107. B. Bertrand; L. Stefan; M. Pirrotta; D. Monchaud; E. Bodio; P. Richard; P. Le Gendre; E. Warmerdam; M. H. de Jager; G. M. M. Groothuis; M. Picquet; A. Casini *Inorg. Chem.* **2014,** *53*, 2296-2303.
108. F. Schmitt; K. Donnelly; J. K. Muenzner; T. Rehm; V. Novohradsky; V. Brabec; J. Kasparkova; M. Albrecht; R. Schobert; T. Mueller *J. Inorg. Biochem.* **2016,** *163*, 221-228.

109. G. Occhipinti; V. R. Jensen; K. W. Törnroos; N. Å. Frøystein; H.-R. Bjørsvik *Tetrahedron* **2009,** *65*, 7186-7194.
110. R. Zhong; A. Pöthig; S. Haslinger; B. Hofmann; G. Raudaschl-Sieber; E. Herdtweck; W. A. Herrmann; F. E. Kühn *ChemPlusChem* **2014,** *79*, 1294-1303.
111. O. Kühl *Germany Pat* **2012,** *WO2012034880A1*.
112. E. Mas-Marzá; M. Poyatos; M. Sanaú; E. Peris *Organometallics* **2004,** *23*, 323-325.
113. E. Mas-Marzá; M. Sanaú; E. Peris *J. Organomet. Chem.* **2005,** *690*, 5576-5580.
114. M. Viciano; E. Mas-Marzá; M. Poyatos; M. Sanaú; R. H. Crabtree; E. Peris *Angew. Chem., Int. Ed.* **2005,** *44*, 444-447.
115. T. Kang; Q. Feng; M. Luo *Synlett* **2005,** *2005*, 2305-2308.
116. R. Zhong; A. Pöthig; D. C. Mayer; C. Jandl; P. J. Altmann; W. A. Herrmann; F. E. Kühn *Organometallics* **2015,** *34*, 2573-2579.
117. R. Zhong; F. E. Kühn *Doctoral thesis* **2015**.
118. J. Rieb; F. E. Kühn *Doctoral thesis* **2017**.
119. R. Puerta-Oteo; M. Hölscher; M. V. Jiménez; W. Leitner; V. Passarelli; J. J. Pérez-Torrente *Organometallics* **2018,** *37*, 684-696.
120. A. C. Lindhorst; M. Kaspar; P. J. Altmann; A. Pöthig; F. E. Kühn *Dalton Trans.* **2018,** *47*, 1857-1867.
121. F. Bonati; A. Burini; B. R. Pietroni; B. Bovio *J. Organomet. Chem.* **1989,** *375*, 147-160.
122. S. Y. Hussaini; R. A. Haque; M. R. Razali *J. Organomet. Chem.* **2019,** *882*, 96-111.
123. S. P. Nolan *Acc. Chem. Res.* **2011,** *44*, 91-100.
124. P. J. Barnard; M. V. Baker; S. J. Berners-Price; D. A. Day *J. Inorg. Biochem.* **2004,** *98*, 1642-1647.
125. M. Porchia; M. Pellei; M. Marinelli; F. Tisato; F. Del Bello; C. Santini *Eur. J. Med. Chem.* **2018,** *146*, 709-746.
126. M. Mora; M. C. Gimeno; R. Visbal *Chem. Soc. Rev.* **2019,** *48*, 447-462.
127. L. Kaps; B. Biersack; H. Müller-Bunz; K. Mahal; J. Münzner; M. Tacke; T. Mueller; R. Schobert *J. Inorg. Biochem.* **2012,** *106*, 52-58.
128. J. Muenzner; B. Biersack; L. Kaps; R. Schobert; F. Sasse *Int. J. Clin. Pharmacol. Ther.* **2013** *51* 44-46.
129. J. K. Muenzner; B. Biersack; H. Kalie; I. C. Andronache; L. Kaps; D. Schuppan; F. Sasse; R. Schobert *ChemMedChem* **2014,** *9*, 1195-1204.
130. W. Walther; O. Dadac; O; C. Beirnec; I. Ott; G. Sanchez-Sanz; C. Schmidt; C. Werner; X. Zhu; M. Tacke *Lett Drug. Des. Discov.* **2017,** *14*, 125-134.
131. A. Nandy; S. K. Dey; S. Das; R. N. Munda; J. Dinda; K. D. Saha *Mol. Cancer* **2014,** *13*, 57.
132. H. F. Dos Santos; M. A. Vieira; G. Y. Sánchez Delgado; D. Paschoal *J. Phys. Chem. A* **2016,** *120*, 2250-2259.
133. T. Zou; C. T. Lum; C.-N. Lok; W.-P. To; K.-H. Low; C.-M. Che *Angew. Chem., Int. Ed.* **2014,** *53*, 5810-5814.
134. S. Kobialka; C. Müller-Tautges; M. T. S. Schmidt; G. Schnakenburg; O. Hollóczki; B. Kirchner; M. Engeser *Inorg. Chem.* **2015,** *54*, 6100-6111.
135. A. Bondi *J. Phys. Chem.* **1964,** *68*, 441-451.
136. F. L. Thorp-Greenwood; R. G. Balasingham; M. P. Coogan *J. Organomet. Chem.* **2012,** *714*, 12-21.
137. J. Gil-Rubio; V. Cámara; D. Bautista; J. Vicente *Inorg. Chem.* **2013,** *52*, 4071-4083.
138. Y.-F. Han; G.-X. Jin; C. G. Daniliuc; F. E. Hahn *Angew. Chem., Int. Ed.* **2015,** *54*, 4958-4962.
139. L. E. Wedlock; P. J. Barnard; A. Filipovska; B. W. Skelton; S. J. Berners-Price; M. V. Baker *Dalton Trans.* **2016,** *45*, 12221-12236.
140. Z. Chen; Z. Li; L. Yang; J. Liang; J. Yin; G.-A. Yu; S. H. Liu *Dyes Pigment.* **2015,** *121*, 170-177.
141. R. M. Almotawa; G. Aljomaih; D. V. Trujillo; V. N. Nesterov; M. A. Rawashdeh-Omary *Inorg. Chem.* **2018,** *57*, 9962-9976.
142. A. Maspero; I. Kani; A. A. Mohamed; M. A. Omary; R. J. Staples; J. P. Fackler *Inorg. Chem.* **2003,** *42*, 5311-5319.
143. M. Preisenberger; P. Pyykkö; A. Schier; H. Schmidbaur *Inorg. Chem.* **1999,** *38*, 5870-5875.

144. W. E. van Zyl; J. M. López-de-Luzuriaga; A. A. Mohamed; R. J. Staples; J. P. Fackler *Inorg. Chem.* **2002,** *41*, 4579-4589.
145. J. B. Foley; A. Herring; B. Li; E. V. Dikarev *Inorg. Chim. Acta* **2012,** *392*, 300-310.
146. M. A. Rawashdeh-Omary; M. A. Omary; J. P. Fackler *Inorg. Chim. Acta* **2002,** *334*, 376-384.
147. A. Biffis; M. Cipani; C. Tubaro; M. Basato; M. Costante; E. Bressan; A. Venzo; C. Graiff *New J. Chem.* **2013,** *37*, 4176-4184.
148. R. Gericke; M. A. Bennet; S. H. Priver; S. K. Bhargav *Organometallics* **2017,** *36*, 3178-3188.
149. J. Rieb; B. Dominelli; D. Mayer; C. Jandl; J. Drechsel; W. Heydenreuter; S. A. Sieber; F. E. Kühn *Dalton Trans.* **2017,** *46*, 2722-2735.
150. B. Dominelli; G. M. Roberts; C. Jandl; P. J. Fischer; R. M. Reich; A. Pöthig; J. D. G. Correia; F. E. Kühn *Dalton Trans.* **2019**, 14036-14043.
151. B. Dominelli; C. H. G. Jakob; J. Oberkofler; P. J. Fischer; E.-M. Esslinger; R. M. Reich; F. Marques; J. D. G. Correia; F. E. Kühn *Inorg. Chem.* **2019**, submitted.
152. C. H. G. Jakob; F. E. Kühn *Master's thesis* **2017**.
153. M. N. Wenzel; A. F. Mósca; V. Graziani; B. Aikman; S. R. Thomas; A. de Almeida; J. A. Platts; N. Re; C. Coletti; A. Marrone; G. Soveral; A. Casini *Inorg. Chem.* **2019,** *58*, 2140-2148.
154. J. Manchester; D. M. Bassani; J.-L. H. A. Duprey; L. Giordano; J. S. Vyle; Z.-y. Zhao; J. H. R. Tucker *J. Am. Chem. Soc.* **2012,** *134*, 10791-10794.
155. F. Mendes; M. Groessl; A. A. Nazarov; Y. O. Tsybin; G. Sava; I. Santos; P. J. Dyson; A. Casini *J. Med. Chem.* **2011,** *54*, 2196-2206.

8 Complete List of Publications

8.1 Journal Articles

Influence of wing-tip substituents and reaction conditions on the structure, properties and cytotoxicity of Ag(I)– and Au(I)–bis(NHC) complexes
Julia Rieb, **Bruno Dominelli**, David Mayer, Christian Jandl, Jonas Drechsel, Wolfgang Heydenreuter, Stephan A. Sieber and Fritz E. Kühn
Dalton Transaction, **2017**, *46*, 2722-2735

Medicinal Applications of Gold(I/III)-Based Complexes Bearing N-Heterocyclic Carbene and Phosphine Ligands
Bruno Dominelli, João D.G. Correia, Fritz E. Kühn
Journal of Organometallic Chemistry, **2018**, *866*, 153-164

Dinuclear zwitterionic silver(I) and gold(I) complexes bearing 2,2-acetate-bridged bisimidazolylidene ligands
Bruno Dominelli, Gerri M. Roberts, Christian Jandl, Pauline J. Fischer, Robert M. Reich, Alexander Pöthig, João D. G. Correia and Fritz E. Kühn
Dalton Transaction, **2019**, *48*, 14036-14043

8.2 Other Articles

C-H Bond Oxidation with Transition-Metal-Based Carbene Complexes
Bruno Dominelli, Anja C. Lindhorst, Fritz E. Kühn
Book Chapter (5) in *Alkane Functionalization* (ISBN 9781119378808), John Wiley & Sons Ltd, Armando J. L. Pombeiro, M. Fátima C. Guedes da Silva, USA, **2019**, 105-112.

Bridge-functionalized bisimidazolium bromides as catalysts for the conversion of epoxides to cyclic carbonates with CO_2
Yuanhui Li, **Bruno Dominelli**, Robert M. Reich, Boping Liu, Fritz E. Kühn
Catalysis Communications, **2019**, *124*, 118–122

‡ These authors have equally contributed to this work.

8.3 Conference Contributions

Inorganic Chemistry meets Medicine

Bruno Dominelli, Christian H. G. Jakob, Jonas Drechsel, Stephan A. Sieber, Fritz E. Kühn

Poster, TUM-IAS & University of Birmingham-IAS Workshop, München, Deutschland, **2017**

9 APPENDIX

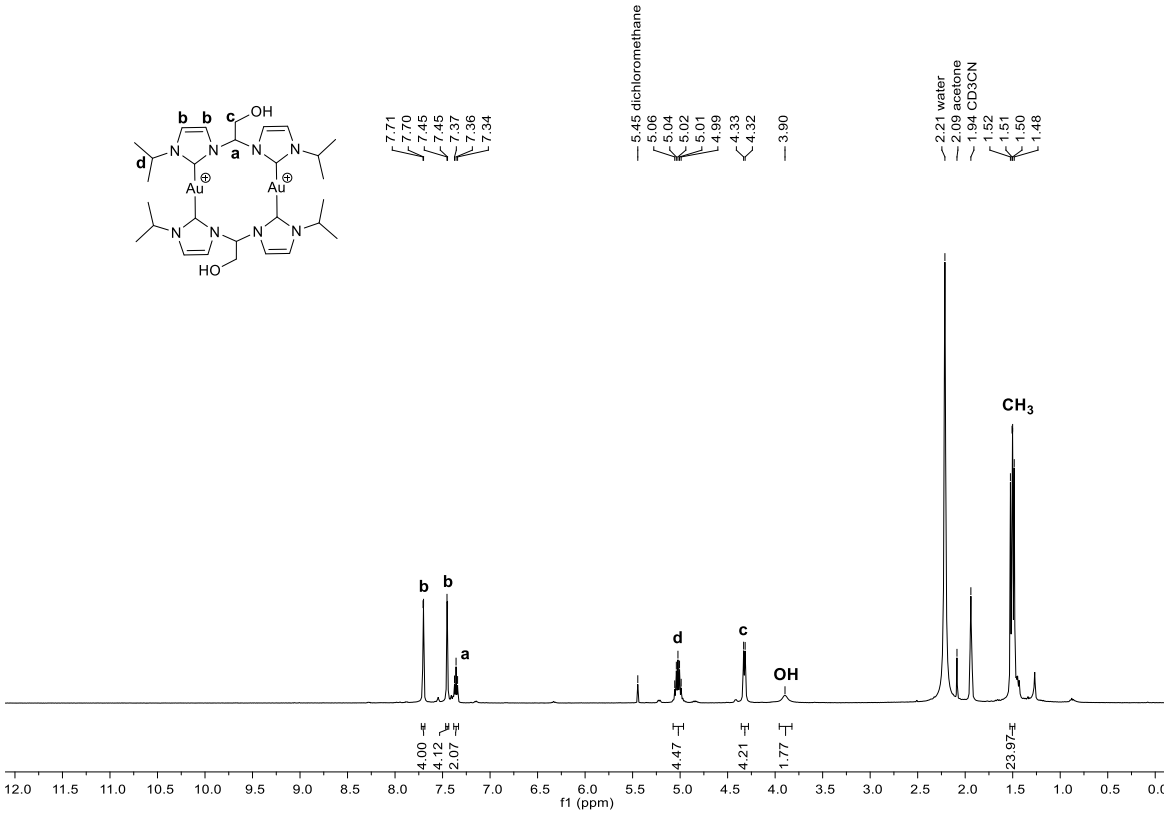

Figure 22: ^{1}H NMR spectrum of **anti-exo-14b** in CD_3CN at room temperature.

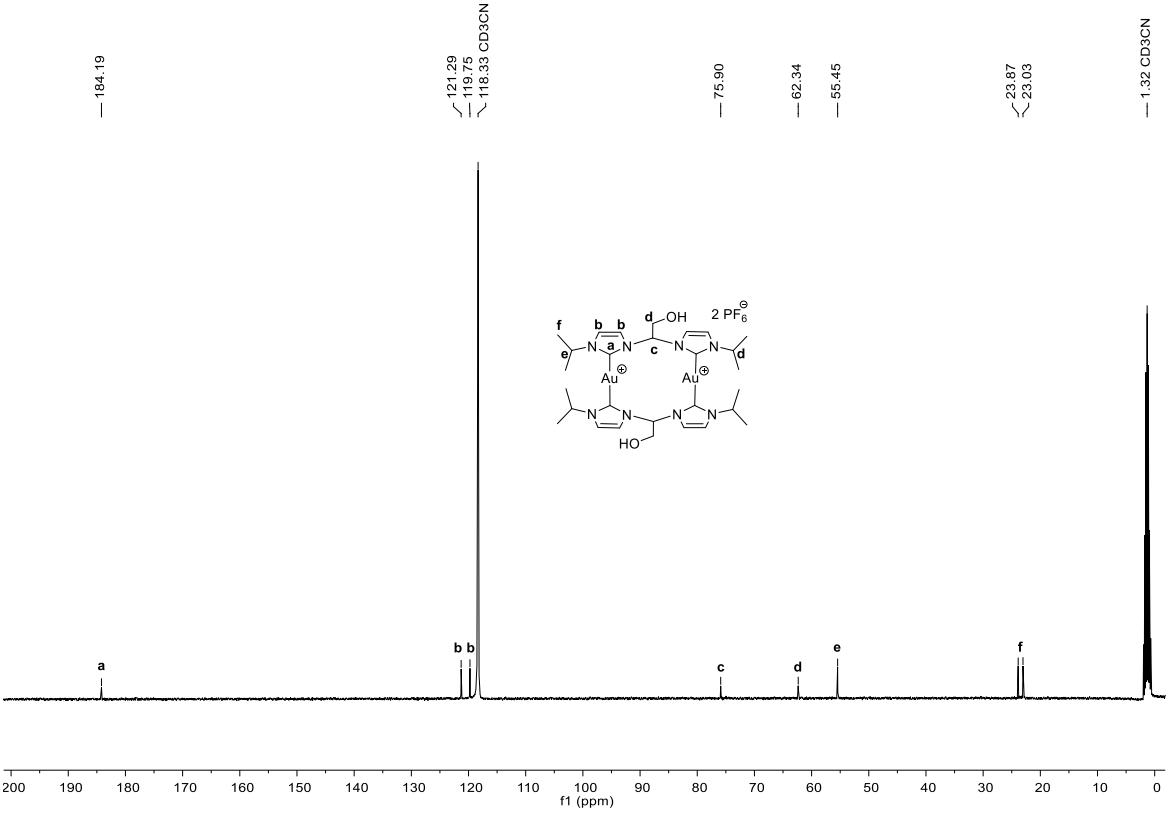

Figure 23: $^{13}C\{^{1}H\}$ NMR spectrum of **anti-exo-14b** in CD_3CN at room temperature.

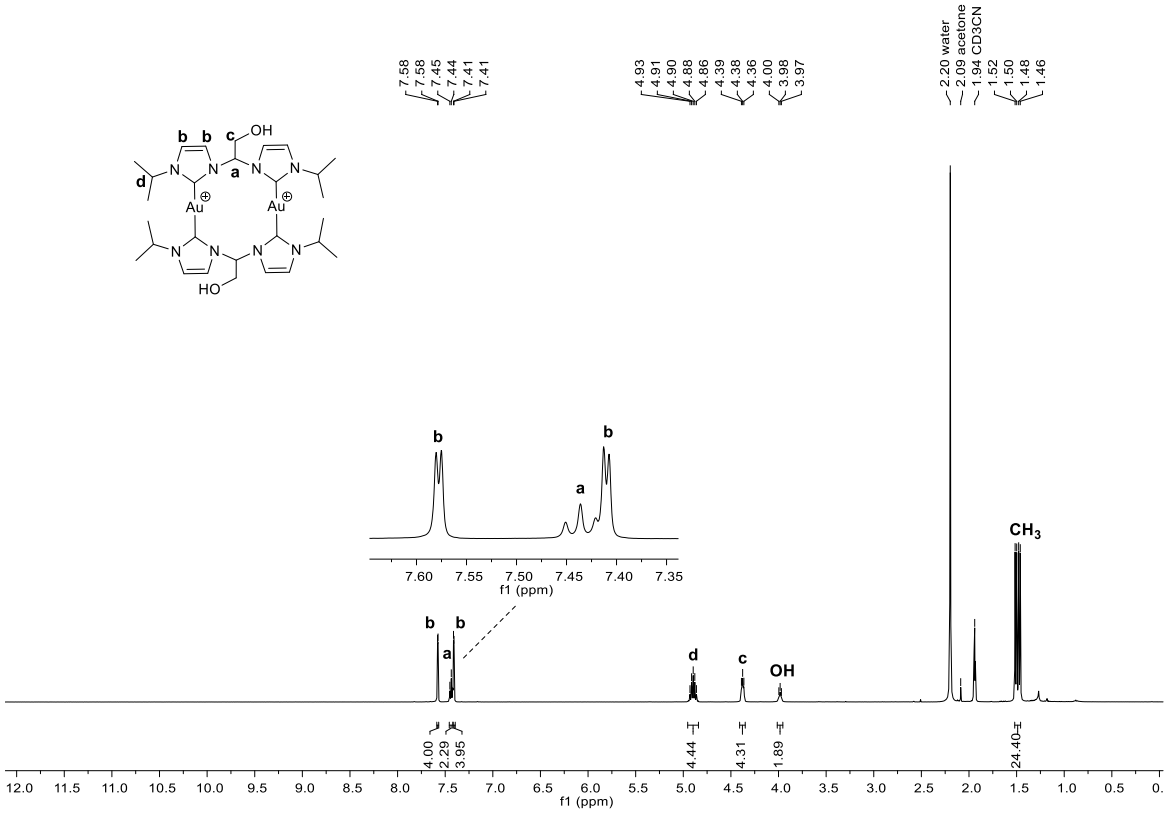

Figure 24: ^{1}H NMR spectrum of **syn-exo-14b** in CD_3CN at room temperature.

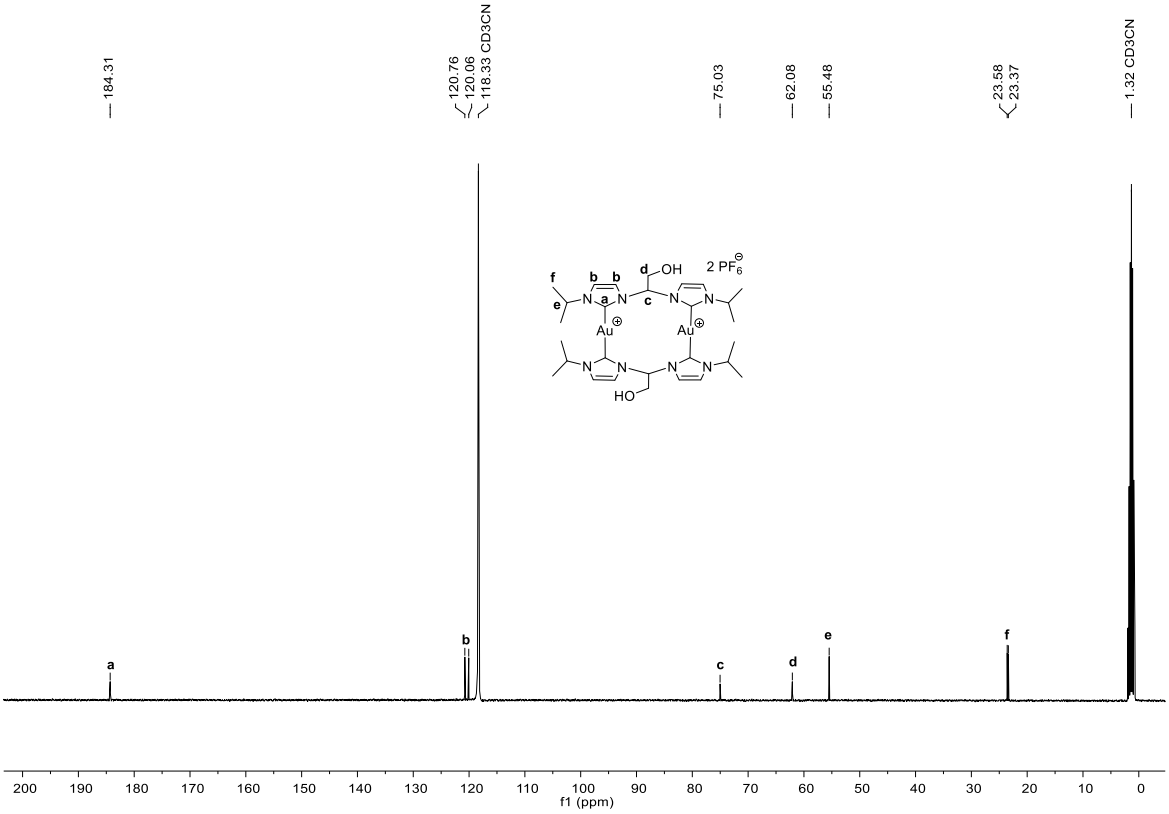

Figure 25: $^{13}C\{^{1}H\}$ NMR spectrum of **syn-exo-14b** in CD_3CN at room temperature.

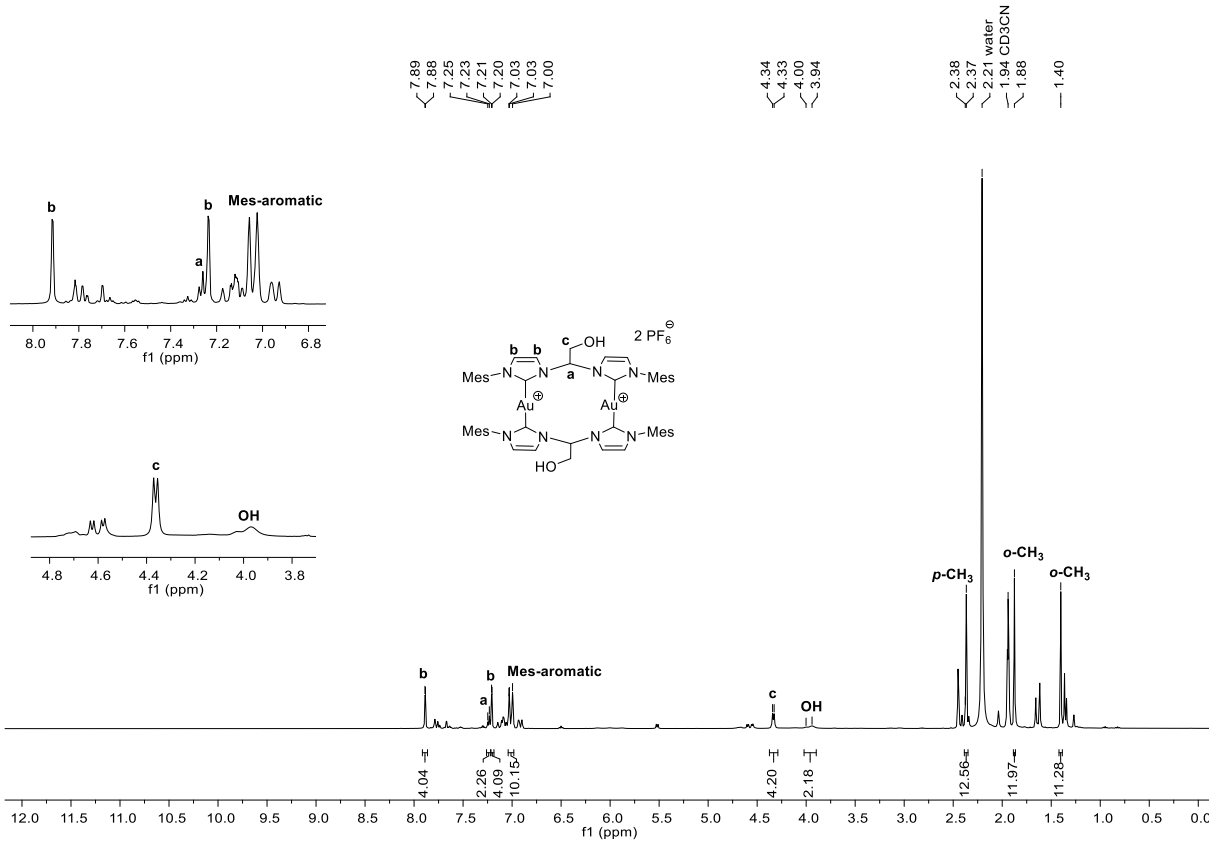

Figure 26: ^{1}H NMR spectrum of **anti-exo-14d** in CD_3CN at room temperature.

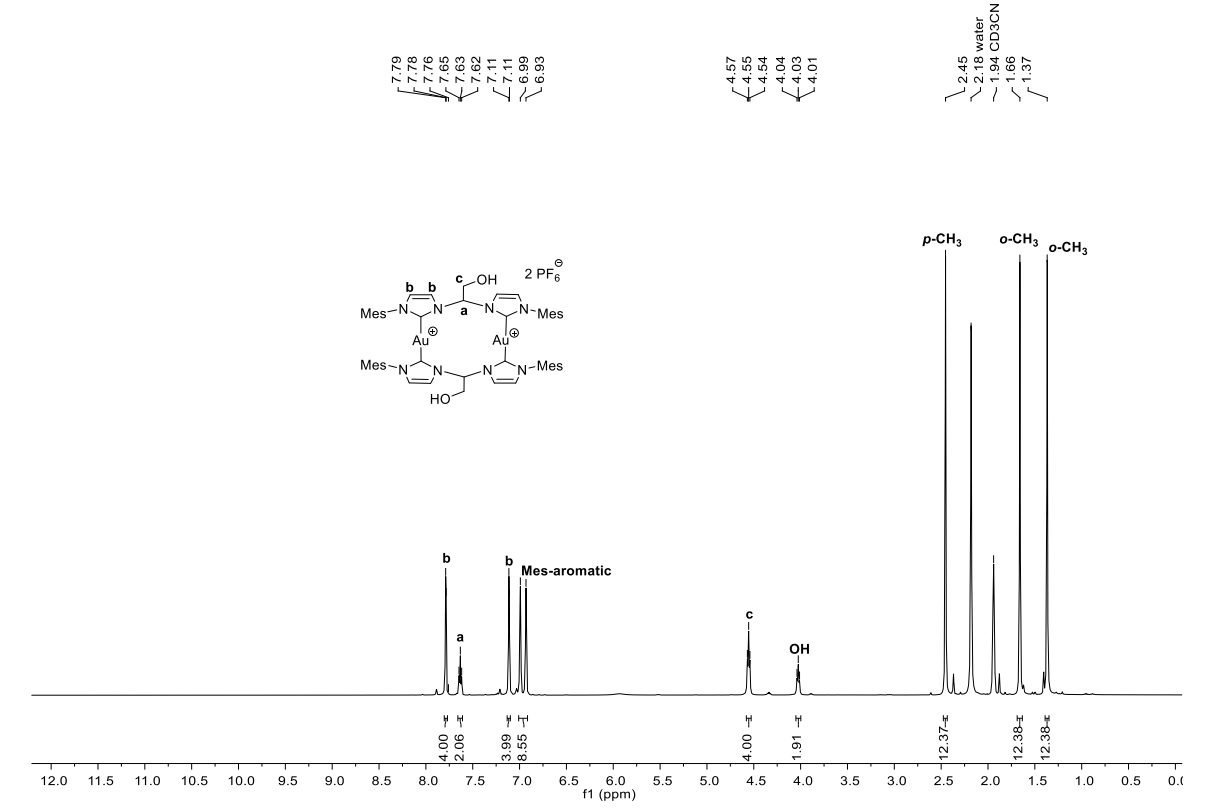

Figure 27: ^{1}H NMR spectrum of **syn-exo-14d** in CD_3CN at room temperature.

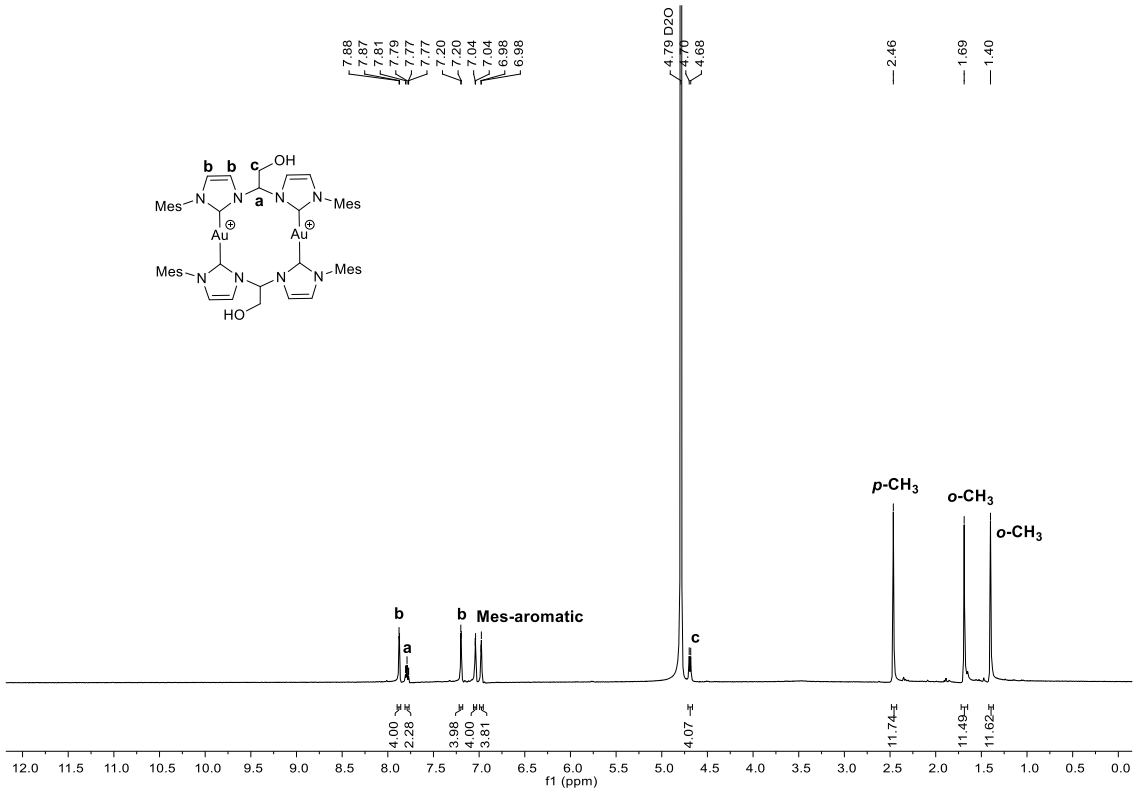

Figure 28: ^{1}H NMR spectrum of **syn-exo-14d** after counter-anion exchange to chloride in D_2O at room temperature.

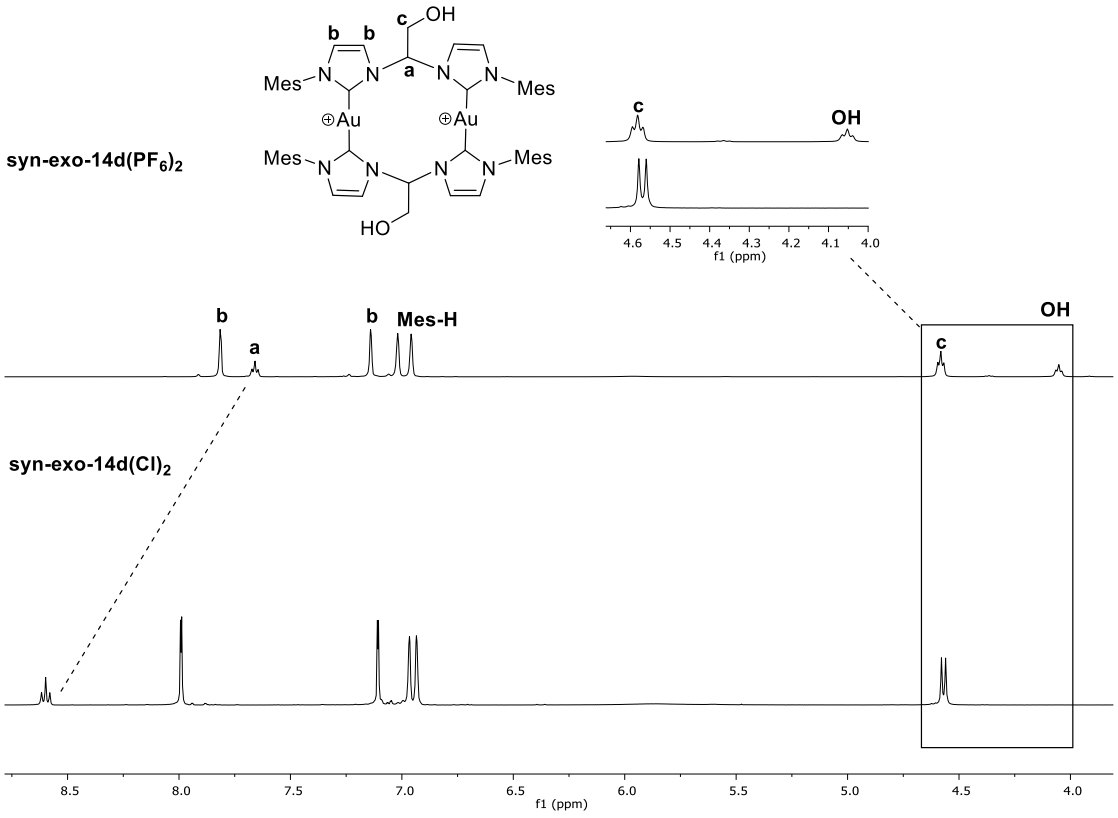

Figure 29: ^{1}H NMR spectra of **syn-exo-14d(PF$_6$)$_2$** (top) and **syn-exo-14d(Cl)$_2$** (bottom) between 8.75 ppm and 4.25 ppm in CD_3CN at room temperature.

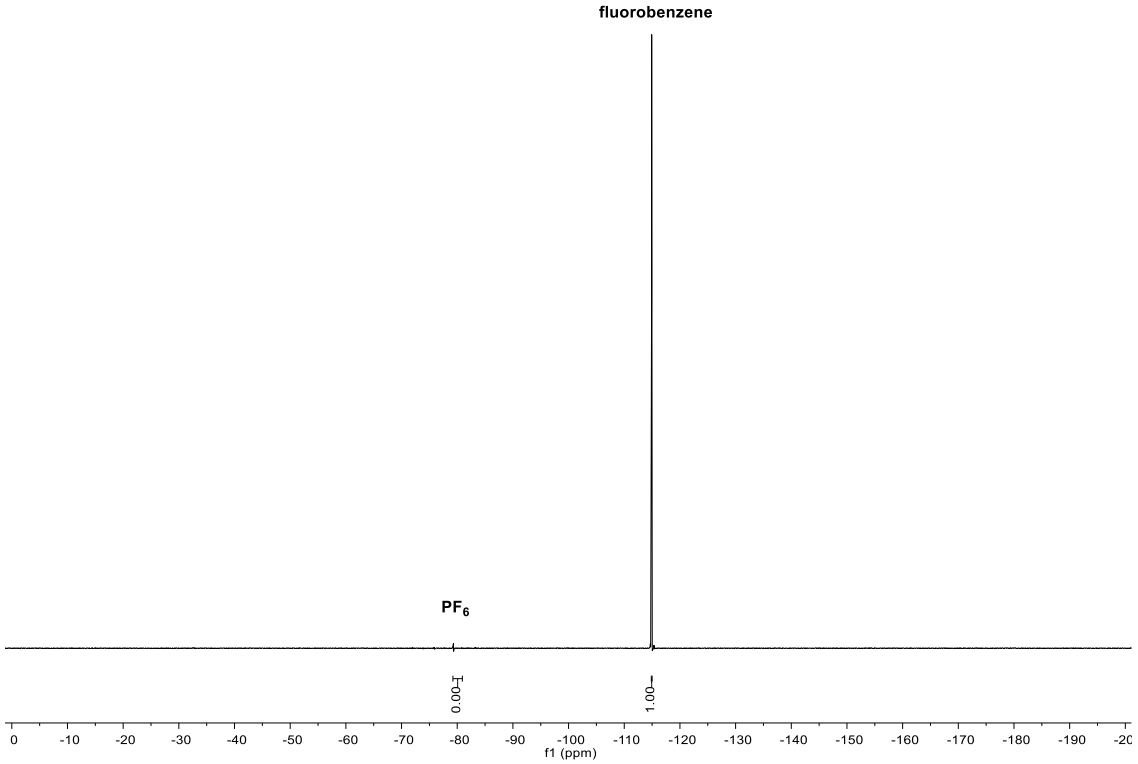

Figure 30: ^{19}F NMR spectrum of **syn-exo-14d** after counter-anion exchange to chloride with fluorobenzene (reference) in CD_3CN at room temperature.

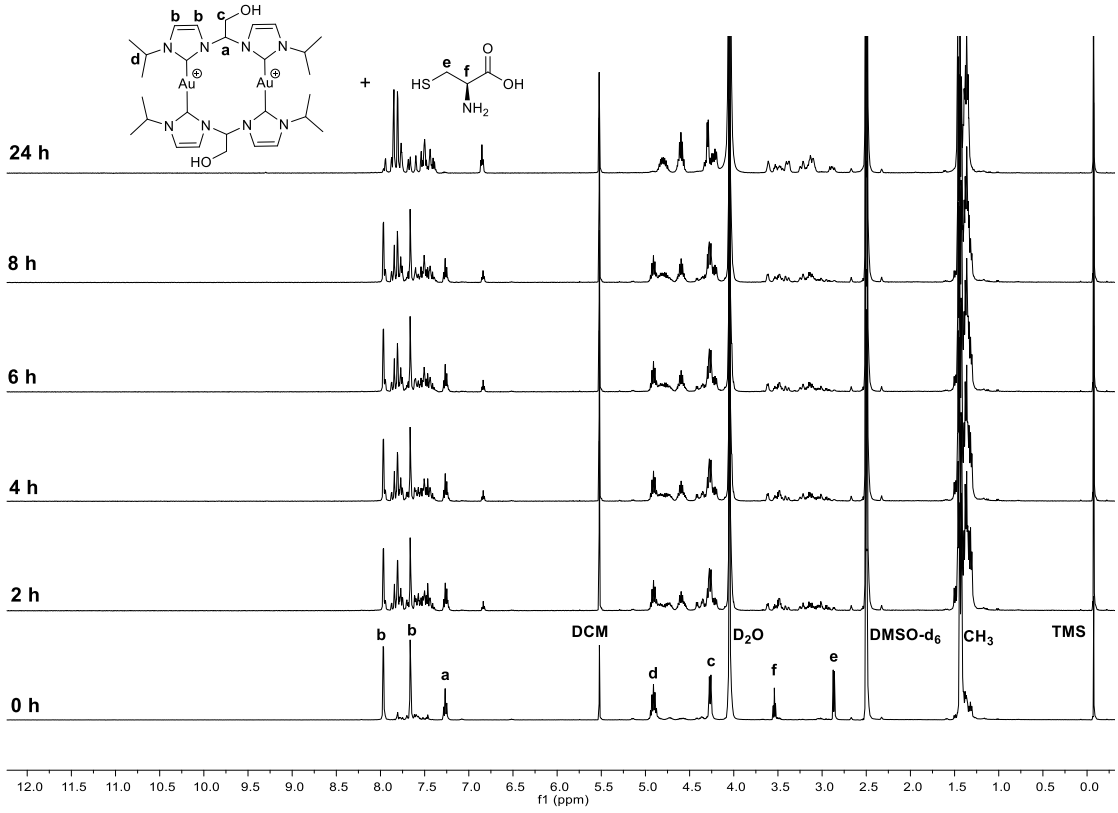

Figure 31: Stacked ^1H NMR spectra of **anti-exo-14b** and 4.5 eq. L-cysteine in DMSO/D2O (0.35 mL/0.1 mL) at 37°C.

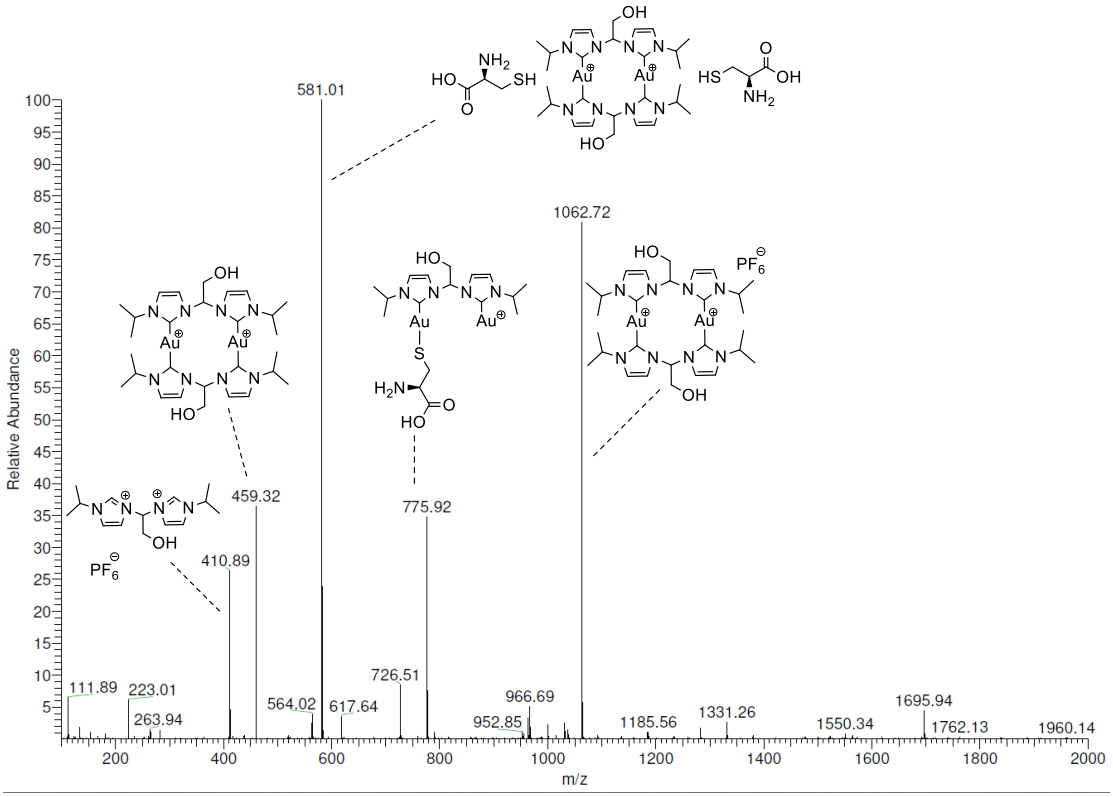

Figure 32: ESI MS spectrum of **anti-exo-14b** and 4.5 eq. L-cysteine in DMSO/D2O (0.35 mL/0.1 mL) at 37°C.

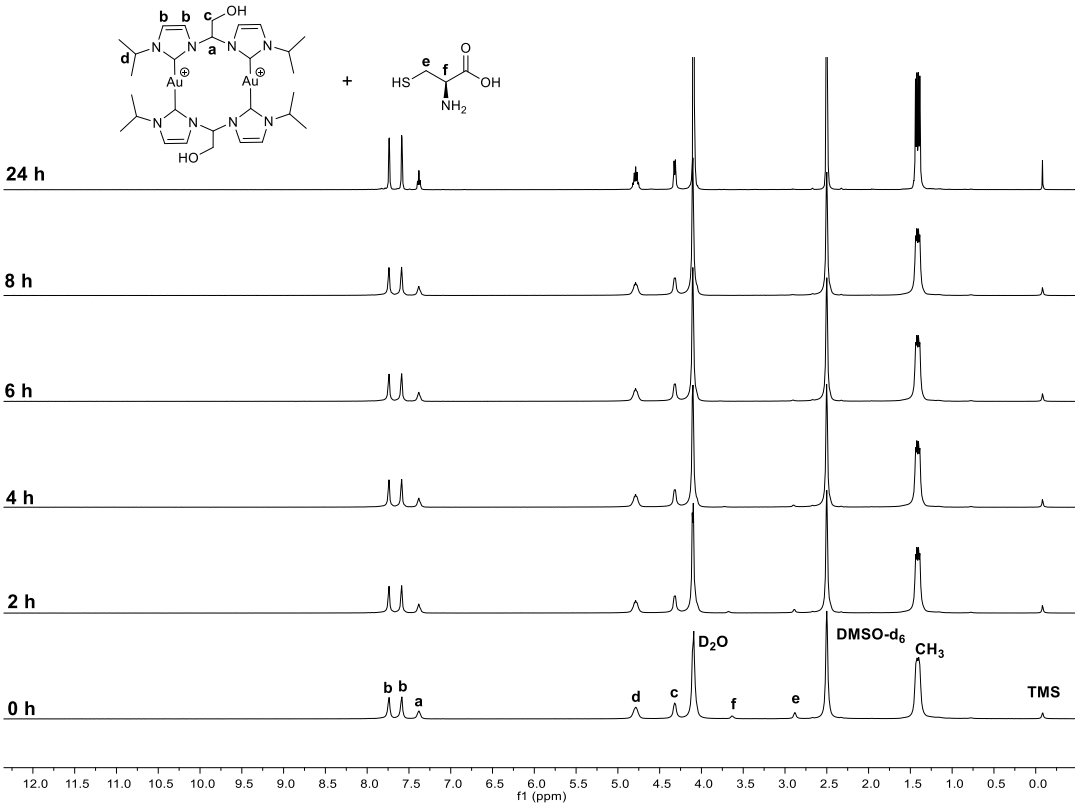

Figure 33: Stacked ^{1}H NMR spectra of **syn-exo-14b** and 4.5 eq. L-cysteine in DMSO/D2O (0.35 mL/0.1 mL) at 37°C.

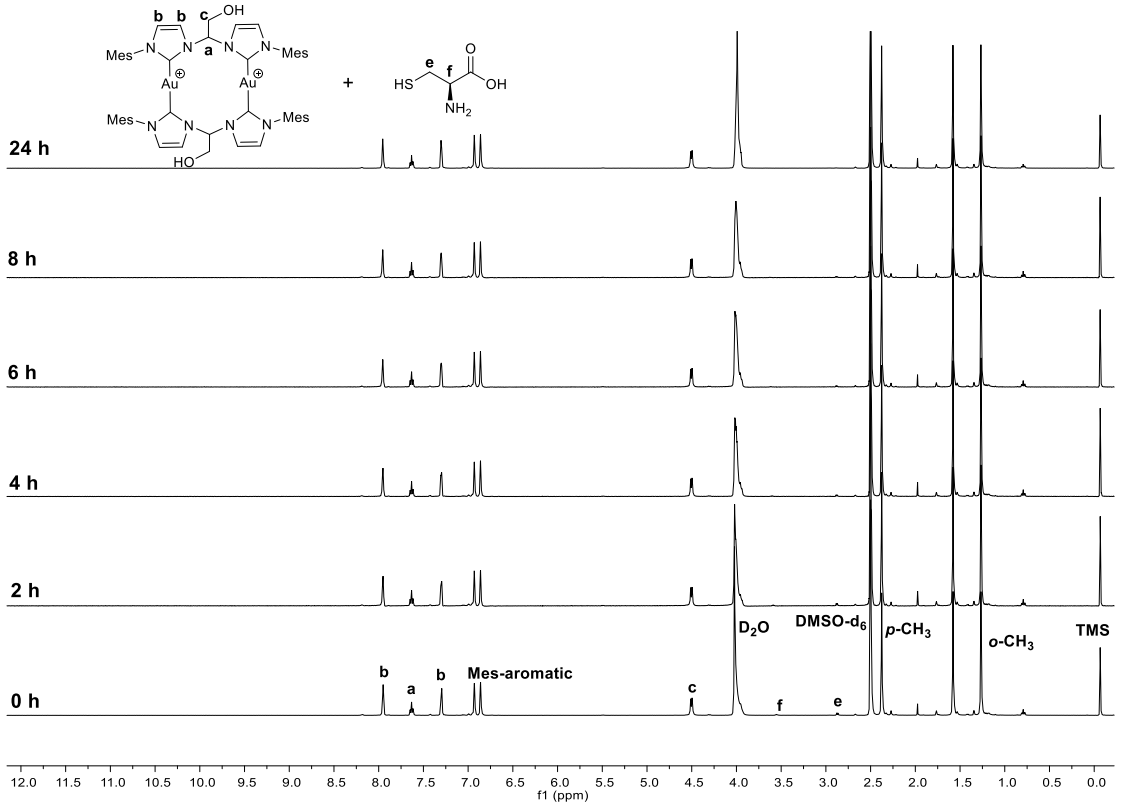

Figure 34: Stacked ^{1}H NMR spectra of **syn-exo-14d** and 4.5 eq. L-cysteine in DMSO/D2O (0.35 mL/0.1 mL) at 37°C.

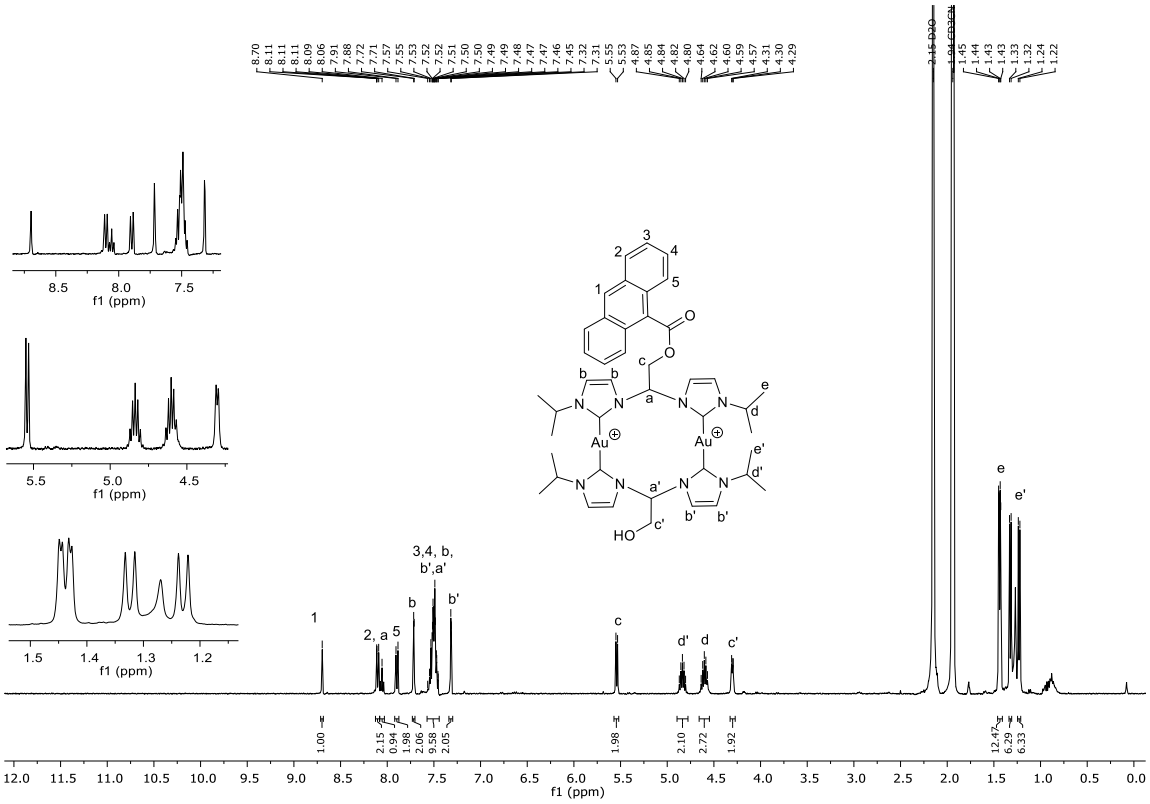

Figure 35: ^{1}H NMR spectrum of **16** in CD_3CN at room temperature.

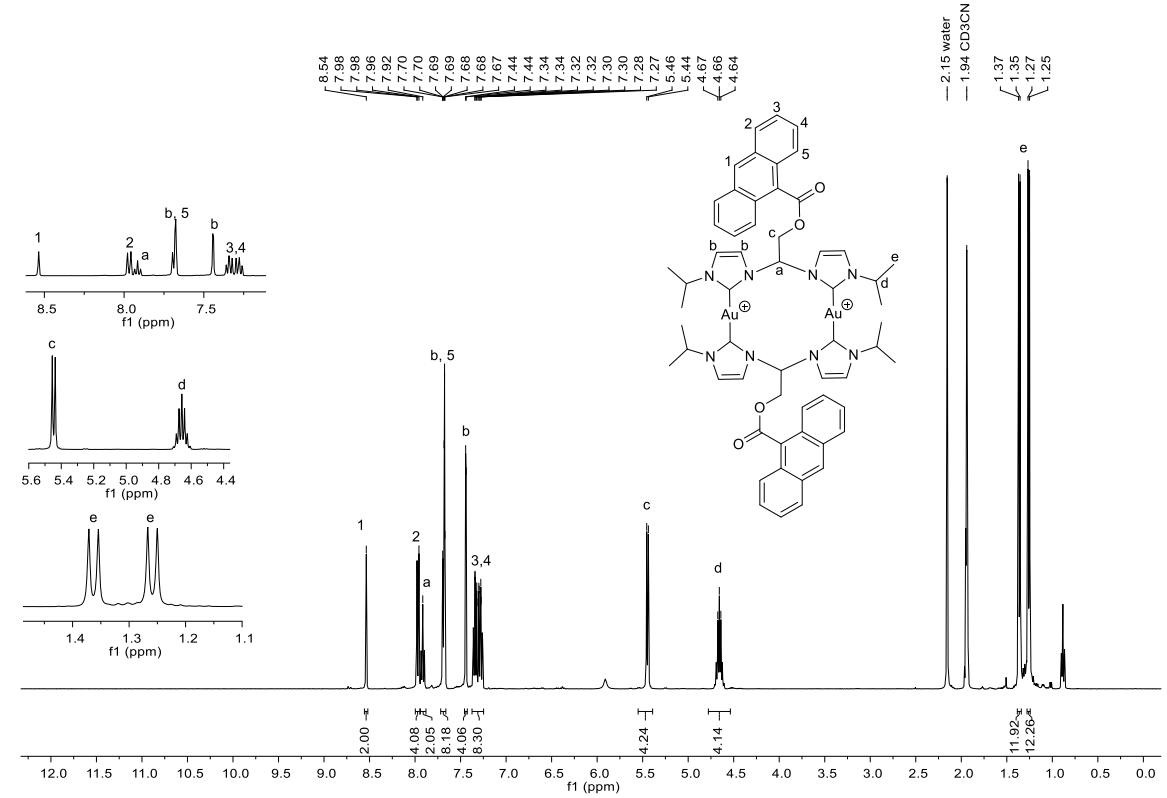

Figure 36: ^{1}H NMR spectrum of **17** in CD_3CN at room temperature.

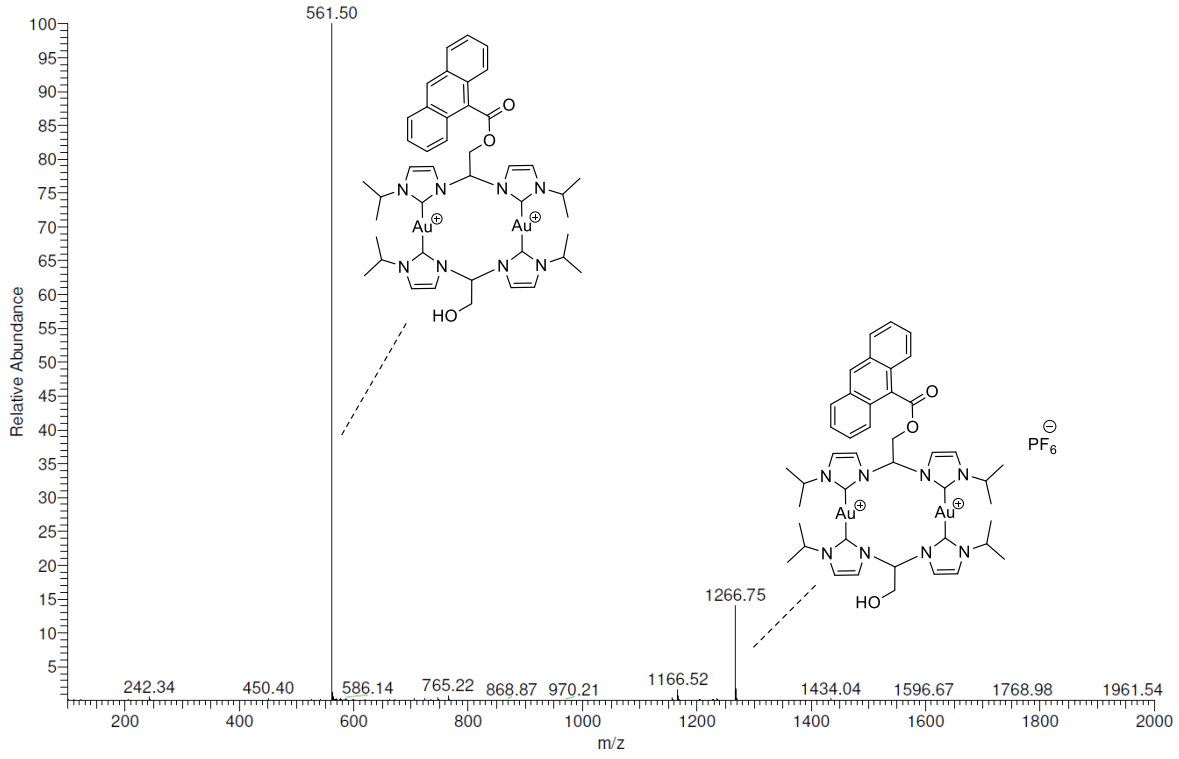

Figure 37: ESI MS spectrum of **16**.

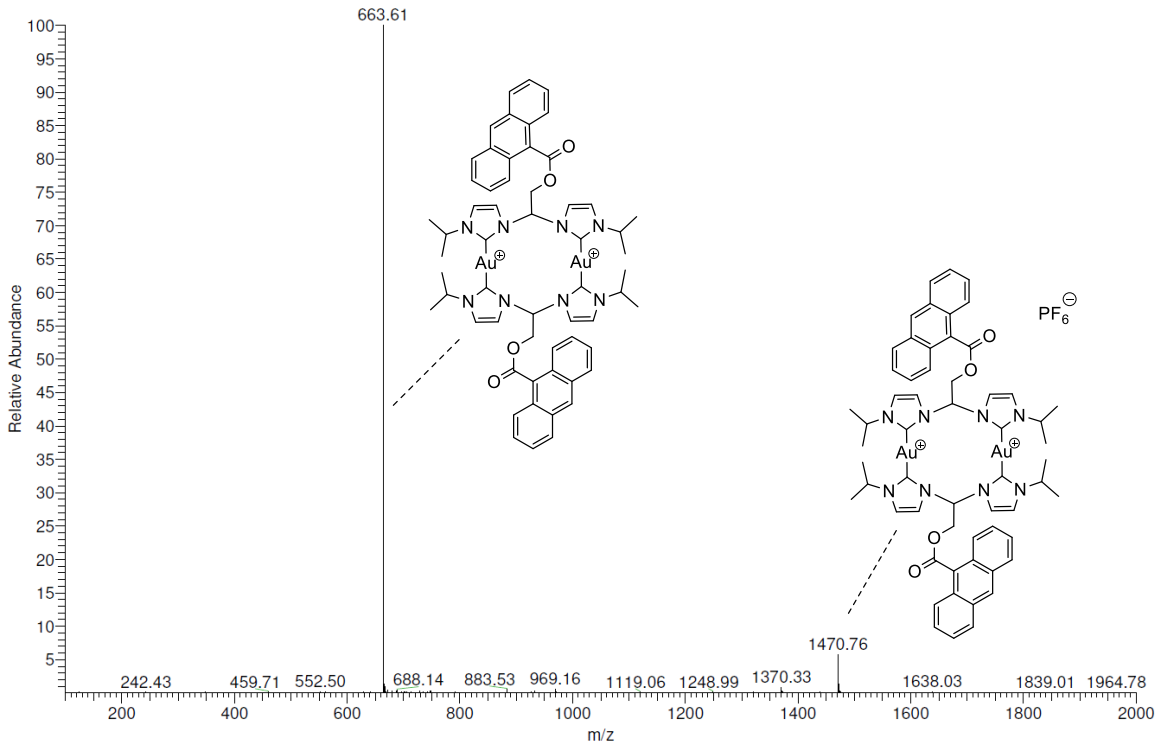

Figure 38: ESI MS spectrum of **17**.

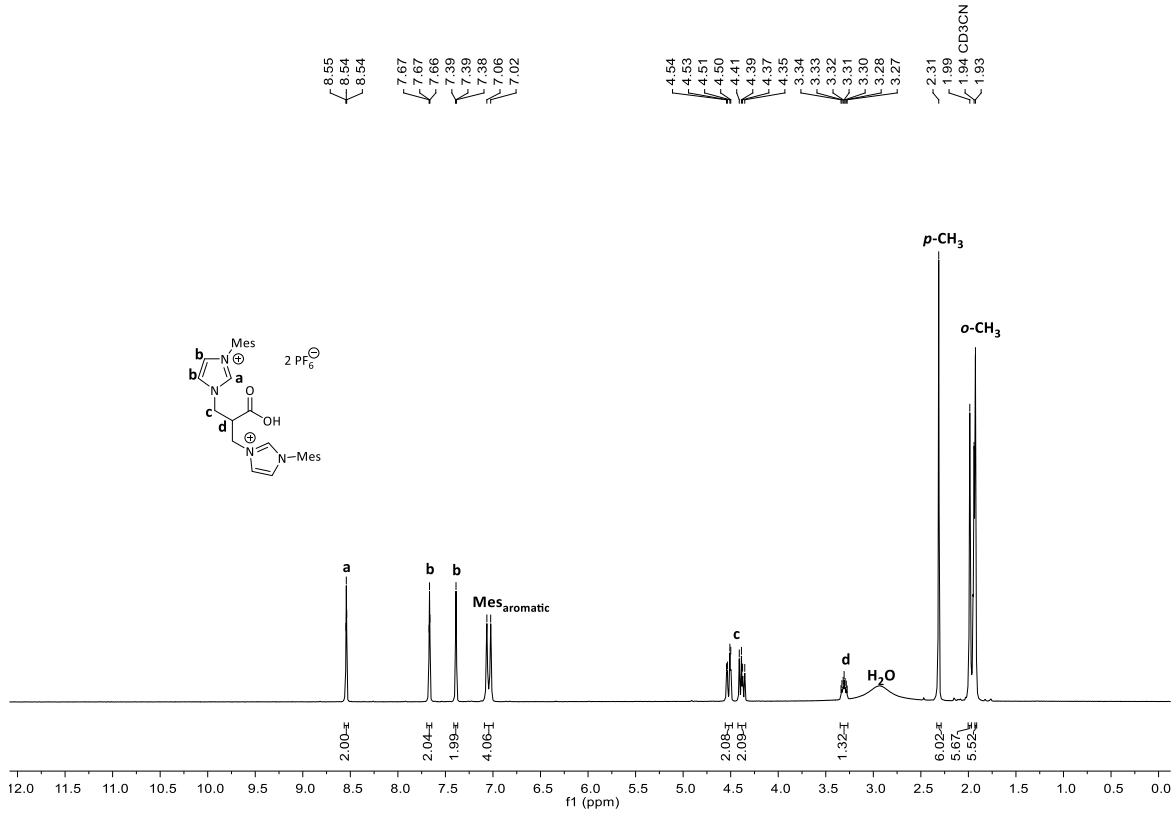

Figure 39: ^{1}H NMR spectrum of **L13** in CD_3CN at room temperature.

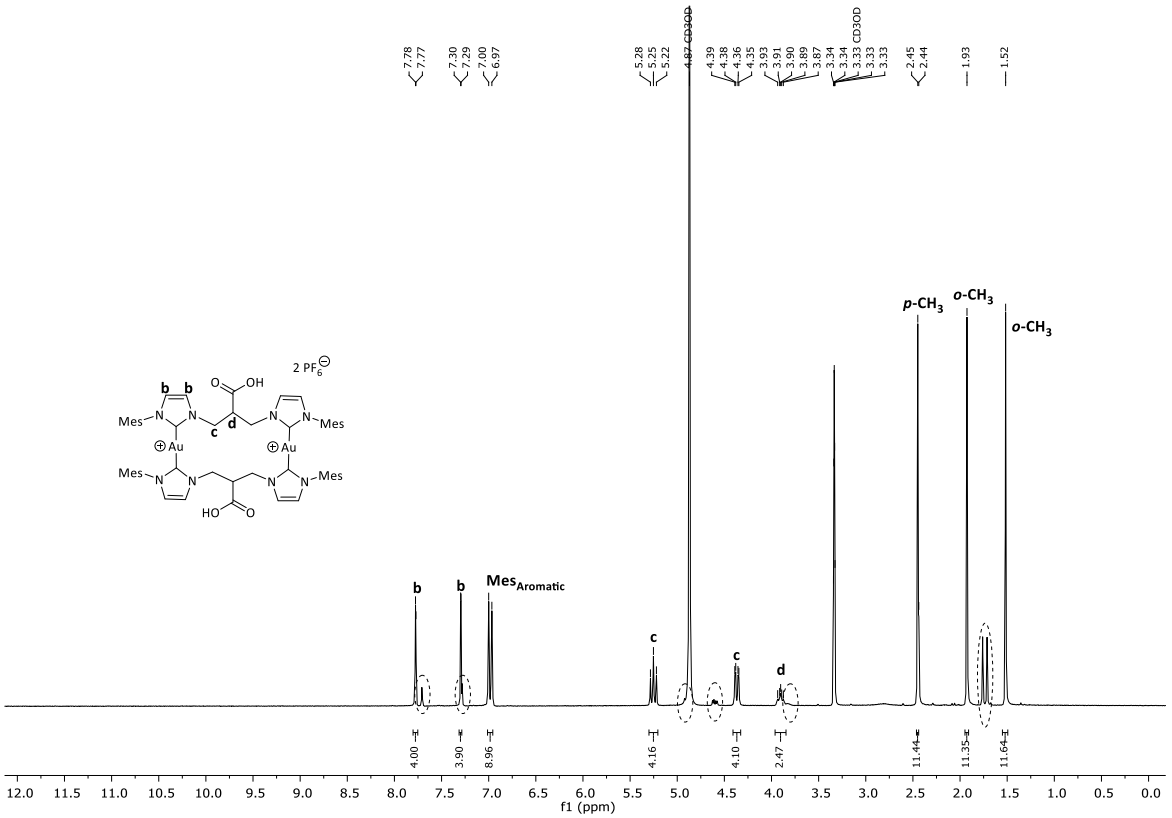

Figure 40: ^{1}H NMR spectrum of **18** in CD_3OD at room temperature. Second species labelled with dotted circle tentatively assigned to isomer.

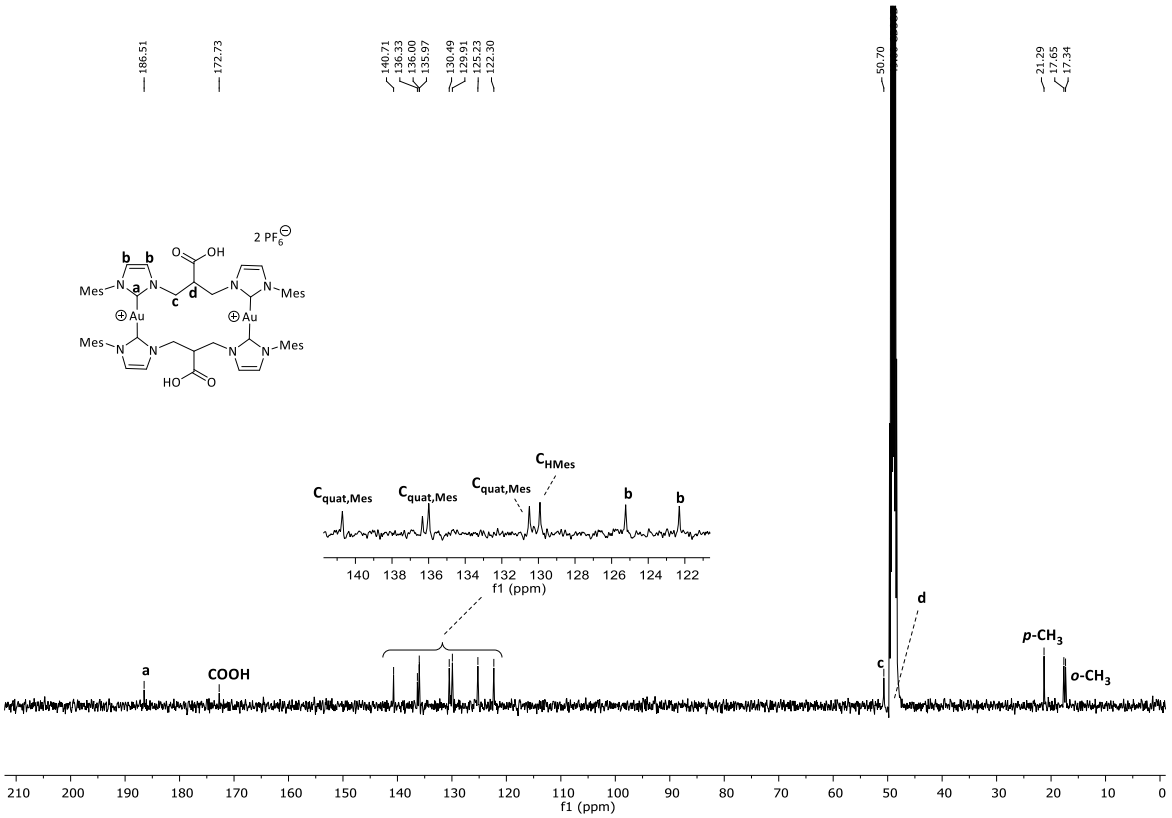

Figure 41: $^{13}C\{^{1}H\}$ NMR spectrum of **18** in CD_3OD at room temperature.

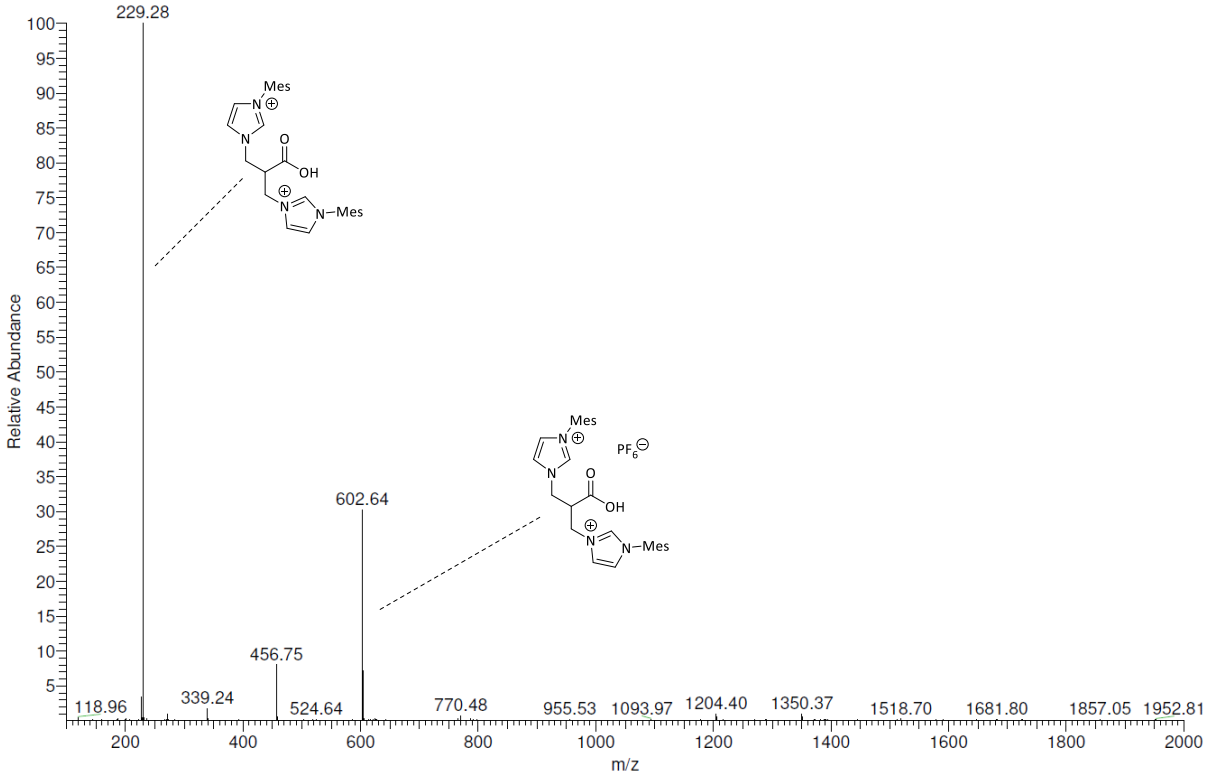

Figure 42: ESI MS spectrum of **L13**.

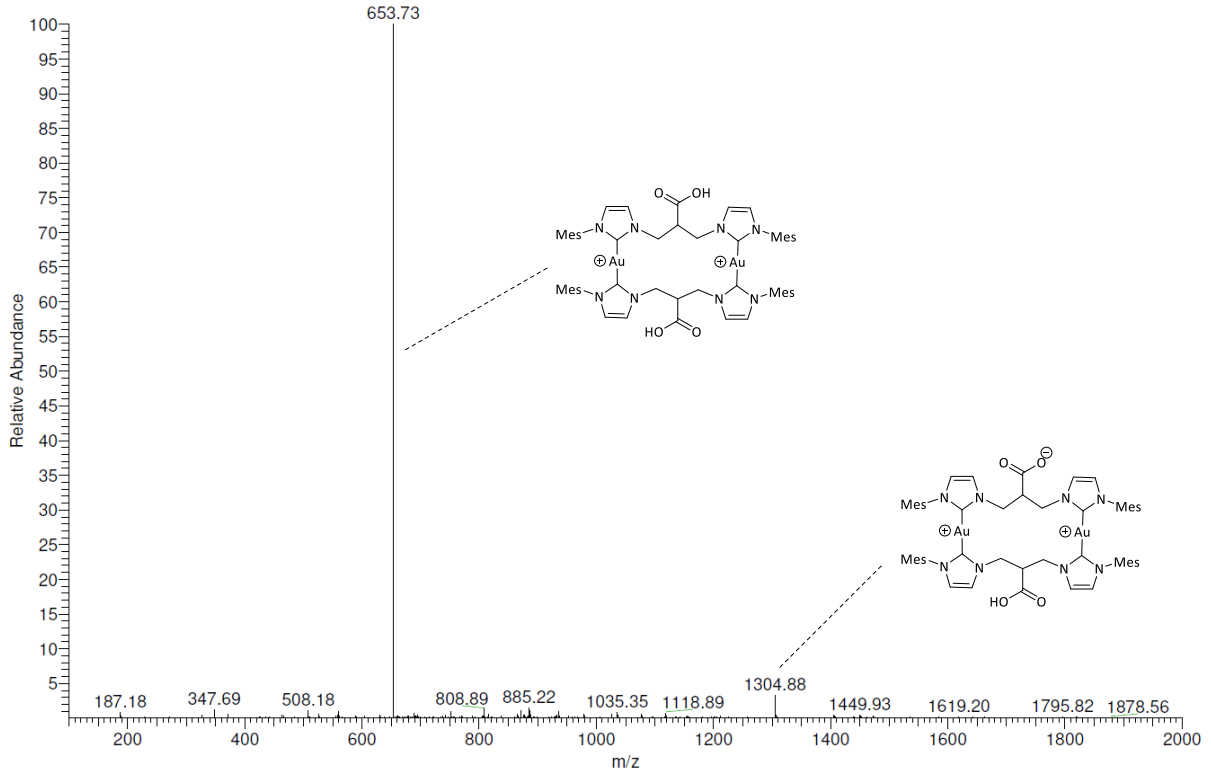

Figure 43: ESI MS spectrum of **18**.

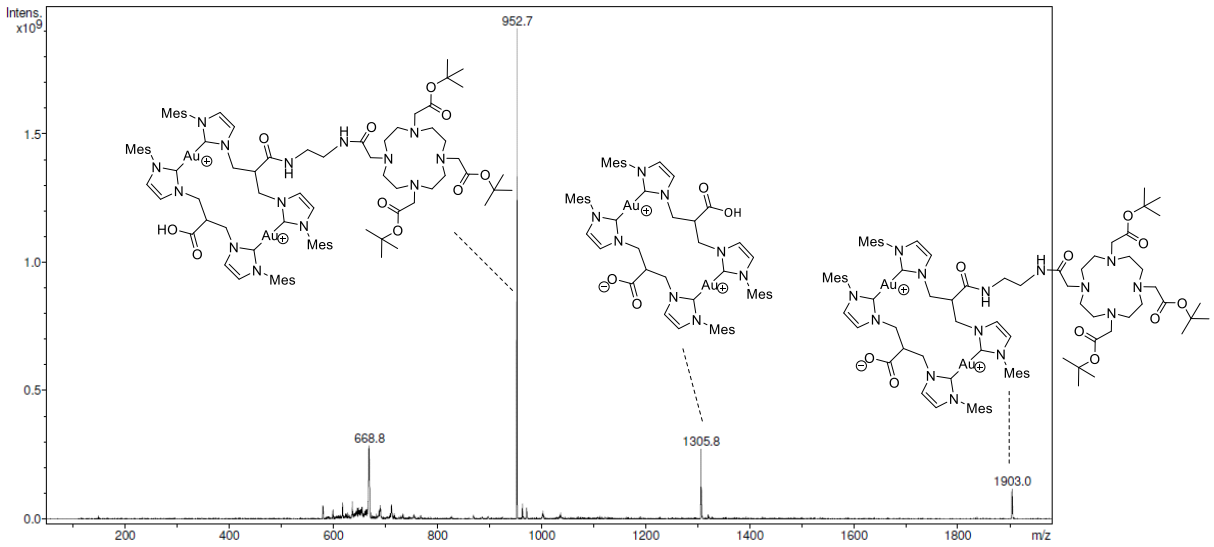

Figure 44: ESI MS spectrum of **19.**

Dalton Transactions

PAPER

View Article Online
View Journal | View Issue

Cite this: *Dalton Trans.*, 2017, **46**, 2722

Influence of wing-tip substituents and reaction conditions on the structure, properties and cytotoxicity of Ag(I)– and Au(I)–bis(NHC) complexes†

Julia Rieb,[a] Bruno Dominelli,[a] David Mayer,[a] Christian Jandl,[b] Jonas Drechsel,[c] Wolfgang Heydenreuter,[c] Stephan A. Sieber[c] and Fritz E. Kühn*[a]

Received 2nd December 2016,
Accepted 21st January 2017

DOI: 10.1039/c6dt04559f

rsc.li/dalton

The formation of different conformers of dinuclear silver(I) and gold(I) 1,1′-(2-hydroxyethane-1,1-diyl) bridge-functionalized bis(NHC) complexes with various wing-tip substituents (R = methyl, isopropyl and mesityl) has been investigated using multinuclear NMR spectroscopy and SC-XRD as well as DFT calculations. The ratio of *anti*/*syn* isomers strongly depends both on wing-tip substituents and the metal. Moreover, the reaction temperature plays a significant role during the transmetallation process for the ratio of gold(I) conformers, which is further affected by purification procedures. All obtained Au(I)–bis(NHC) complexes have been applied in a standard MTT assay performed for screening the antiproliferative activity against human lung and liver cancer cells. Strong evidence for a significant influence of both wing-tip substituents and conformation on the cytotoxic properties of the applied complexes has been found.

Introduction

The application of N-heterocyclic carbenes (NHCs) in coordination chemistry has been a rapidly expanding field since the isolation of the first thermally stable NHC.[1] During the last 25 years the number of reported NHC complexes for a plethora of elements has grown rapidly and many of the compounds show very promising behaviour for a variety of applications (*e.g.* catalysis, materials science, the design of new metal-based drugs *etc.*).[2–6] Among others, dinuclear coinage metal complexes, supported by bis(NHC) ligands with various substituents and linkers, have been intensively investigated.[7–12] Silver–NHCs are mainly used as transmetallation agents but have also gained importance in their own right as photoluminescent materials[13,14] as well as antimicrobial and antitumor agents.[14–17] In particular, Au(I)–NHCs exhibit very interesting luminescent properties,[18–20] and show high potential for applications in catalysis[21,22] and medicinal chemistry.[23–25]

Numerous gold compounds have been reported to display antiproliferative activity in various cancer cell lines by targeting selectively mitochondria.[23,26] By inhibiting thioredoxin reductase these compounds induce severe oxidative stress inside the mitochondria causing ultimately apoptotic cell death.[23,27] Generally, gold complexes are not particularly selective against cancer cells and also show significant toxicity in healthy cells. However, charged cationic Au–NHC species accumulate in cancer cells due to the overexpression of organic cation transporters (COTs) in the cell membrane, showing remarkable selectivity,[28] *e.g.* for breast cancer cell lines.[29] Therefore and because of the high complexity of biological media, the fine-tuning of the steric and electronic properties of Au(I)–NHCs is crucial to the selective cytotoxic properties of Au–NHCs. The efficient and fast optimization of NHCs as well as the high stability of complexes bearing these ligands make them suitable candidates for rapid screening as potential metal-based drugs.[30]

Recently, our group reported the synthesis and characterization of 1,1′-(2-hydroxyethane-1,1-diyl)-functionalized bis(NHC) coinage metal complexes showing interesting conformational behaviour and offering a wide range of possibilities for further modification of the bridge between two NHC moieties.[31] This further-reaching, comparative study focuses on the influence of wing-tip modification on the structure and properties of the

[a]*Department of Chemistry and Catalysis Research Center, Molecular Catalysis, Technische Universität München, Lichtenbergstr. 4, D-85747 Garching bei München, Germany. E-mail: fritz.kuehn@ch.tum.de; Fax: +49 89 289 13473; Tel: +49 89 289 13096*

[b]*Catalysis Research Center, Technische Universität München, Ernst-Otto-Fischer Straße 1, D-85747 Garching bei München, Germany*

[c]*Chair of Organic Chemistry II, Department of Chemistry, Technische Universität München, Lichtenbergstraße 4, D-85747 Garching bei München, Germany*

† Electronic supplementary information (ESI) available: NMR and UV-vis spectra for all compounds, further details of crystallographic characterization, cytotoxicity studies and DFT calculations (PDF), and CIF files (CIF). CCDC 1511526–1511533. For ESI and crystallographic data in CIF or other electronic format see DOI: 10.1039/c6dt04559f

respective dinuclear 1,1′-(2-hydroxyethane-1,1-diyl)-functionalized silver and gold complexes and tentatively explores the implications on the antiproliferative activity of the reported Au(I)–bis(NHC) complexes in cancer cells.

Results and discussion

Synthesis and characterization of ligand precursors

The preparation of the 1,1′-(2-hydroxyethane-1,1-diyl)-bridged bis(NHC) pro-ligand with methyl groups as wing-tip substituents has been published by our group.[31,32] To investigate the implication of different wing-tip substituents on the characteristics of Ag(I)- and Au(I)–bis(NHC) complexes, this ligand class has been expanded to isopropyl and mesityl modified compounds. Using differently substituted imidazoles as precursors an appropriately modified synthetic method has been applied (Scheme 1).[32]

In comparison with $\mathbf{H_2L^{Me}Cl_2}$, its i-Pr and Mes analogues, $\mathbf{H_2L^{IPr}Cl_2}$ and $\mathbf{H_2L^{Mes}Cl_2}$, were obtained in quite low yields (48% and 26% respectively). Due to a poor leaving group, high temperature and long reactions times are required in the case of more sterically demanding substituents. Despite these drawbacks, the procedure is straightforward and all imidazolium chlorides can be obtained in high purity as they precipitate out of toluene. Subsequently, if necessary, the anion exchange to PF_6^- or BPh_4^- ions for i-Pr and Mes analogues can be conveniently performed in water using 2.5 equiv. of NH_4PF_6 or $NaBPh_4$. For $\mathbf{H_2L^{Me}Cl_2}$ an anion exchange is carried out with stoichiometric amounts of $AgPF_6$ in acetonitrile due to partial solubility of $\mathbf{H_2L^{Me}(PF_6)_2}$ in water. In comparison with $\mathbf{H_2L^{Me}X_2}$, the modified congeners $\mathbf{H_2L^{IPr}X_2}$ and $\mathbf{H_2L^{Mes}X_2}$ are not hygroscopic (X = Cl or PF_6). The i-Pr and mesityl substituted analogues with non-coordinating anions show good solubility in methanol, polar non-protic solvents and DCM. All the obtained imidazolium salts have been characterized by multinuclear NMR spectroscopy, ESI or FAB-MS and elemental analysis.

Single crystals of $\mathbf{H_2L^{IPr}(BPh_4)_2}$ could be obtained by crystallization from an acetone/pentane mixture and were characterized by SC-XRD. The molecular structure of $\mathbf{H_2L^{IPr}(BPh_4)_2}$, which crystallizes in the triclinic space group $P\bar{1}$, is shown in ESI Fig. S32.† The observed bond distances and angles are similar to $\mathbf{H_2L^{Me}Cl_2}$, whose molecular structure was previously published by Zhong *et al.*[32]

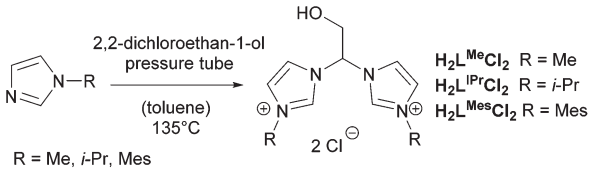

Scheme 1 Synthesis of 1,1′-(2-hydroxyethane-1,1-diyl)-functionalized bis(imidazolium)chlorides.

Synthesis and characterization of silver(I)–bis(NHC) complexes

The synthesis of transition metal complexes with NHC ligands *via* transmetallation though the corresponding Ag(I)–NHC compounds is well established.[15,33] In fact, this method is very attractive in comparison with other procedures, which often require inert or harsher conditions. In particular, polynuclear Ag(I)–(NHC) complexes with non-coordinating anions proved to be valuable reagents due to their extraordinary moisture and light stability and are often successfully applied due to the rather simple transfer procedure.[31,34,35]

Ag–NHC complexes reported in this study can be obtained under mild conditions *via* the silver base route, the most widely applied protocol (Scheme 2).[15,33,36] The deprotonation and metalation of $\mathbf{H_2L^{Me}Cl_2}$ and $\mathbf{H_2L^{IPr}Cl_2}$ using 2.5 equiv. of Ag_2O can be performed in water at room temperature. A subsequent addition of a saturated solution of either NH_4PF_6 or $NaBPh_4$ to the raw product yields the desired complexes $\mathbf{Ag_2(L^{Me})_2(PF_6)_2}$, $\mathbf{Ag_2(L^{IPr})_2(PF_6)_2}$ and $\mathbf{Ag_2(L^{IPr})_2(BPh_4)_2}$. For the mesityl-modified ligand-precursor a direct reaction of $\mathbf{H_2L^{Mes}(PF_6)_2}$ with 2.5 equiv. of Ag_2O in acetonitrile was found to produce better results. The yields are reasonable, particularly since the priority of this work was set on high purity. Multinuclear NMR spectroscopy, SC-XRD, elemental analysis and mass spectrometry proved the successful synthesis of the complexes. All compounds can be isolated as white solids and are stable for many weeks under aerobic conditions and exposure to light. They show good solubility in DMSO, acetonitrile and acetone. $\mathbf{Ag_2(L^{Mes})_2(PF_6)_2}$ is also soluble in DCM.

As expected, ^{1}H-NMR spectra of Ag(I) complexes in acetonitrile-d_3 confirm the successful deprotonation of imidazolium

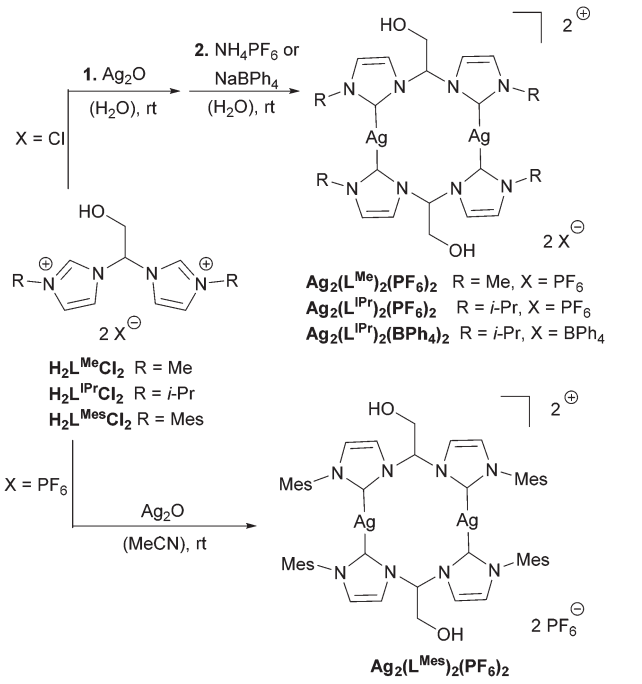

Scheme 2 Synthesis of 1,1′-(2-hydroxyethane-1,1-diyl)-functionalized bis(NHC) complexes of silver(I).

moieties indicating a symmetrical coordination of the ligand to the Ag(I) centre. Ultimately, ^{13}C-NMR resonances at 181.35 ppm (br d, $^{1}J_{AgC}$ = 182.60 Hz) for $\mathbf{Ag_2(L^{IPr})_2(PF_6)_2}$, 181.34 (br d, $^{1}J_{AgC}$ = 205.80 Hz) for $\mathbf{Ag_2(L^{IPr})_2(BPh_4)_2}$ and 183.23 ppm (dd, $^{1}J_{^{107}AgC}$ = 181.9 Hz, $^{1}J_{^{109}AgC}$ = 211.1 Hz) for $\mathbf{Ag_2(L^{Mes})_2(PF_6)_2}$ clearly prove the successful synthesis of all target compounds. The obtained values lie within the range reported in the literature.[15,33] No NCN resonance was observable in the ^{13}C-NMR spectrum of $\mathbf{Ag_2(L^{Me})_2(PF_6)_2}$ in acetonitrile-d_3, which is not unusual, since there are reports of a significant number of Ag(I)–NHC complexes with the same bahaviour.[15] Despite the presence of two naturally abundant NMR-active silver isotopes, most compounds described in the literature show no coupling of carbene carbon atoms to Ag(I) centres. Lin and others speculated that a fast fluxional behaviour on the NMR time scale is responsible for this observation.[37–39] The reason for the complete absence of carbene signals is, however, still unclear, but a fast dynamic behaviour combined with the poor relaxation of quaternary NCN carbon could account for it.[15] In summary, in the series of bis(NHC) compounds examined in this study, the fluxionality in acetonitrile is apparently correlated to the steric demand of wing-tip substituents (Me ≫ i-Pr > Mes).

The ^{1}H-NMR spectra of $\mathbf{Ag_2(L^{Me})_2(PF_6)_2}$, $\mathbf{Ag_2(L^{IPr})_2(PF_6)_2}$ and $\mathbf{Ag_2(L^{IPr})_2(BPh_4)_2}$ change if recorded in acetone-d_6 or DMSO-d_6. In this case, additional sets of signals with lower intensity appear (*e.g.* in the ratio of 0.4 : 1.0 for the minor : major species of $\mathbf{Ag_2(L^{IPr})_2(PF_6)_2}$; Fig. 1, for other spectra see the ESI†). Also, in the ^{13}C-NMR spectra in DMSO, minor products are visible. Moreover, the carbene resonances of the main species exhibit now a coupling to both silver isotopes and appear as a doublet of doublets, thereby suggesting lesser dynamic behaviour at room temperature (Fig. S5, ESI†) The mesityl-substituted analogue, however, shows no splitting of the signals either in ^{1}H-NMR or in ^{13}C-NMR spectra recorded in DMSO (Fig. S8 and 9, ESI†).

To shed more light on thermal behaviour and possible interconversion between the two species, a variable temperature NMR study on $\mathbf{Ag_2(L^{IPr})_2(BPh_4)_2}$ was carried out in acetonitrile and DMSO. Neither in acetonitrile nor in DMSO a significant influence of temperature on the ^{1}H-NMR spectra is observed (ESI Fig. S10 and 11†). Furthermore, ^{1}H diffusion ordered spectroscopy (DOSY) NMR experiments for $\mathbf{Ag_2(L^{IPr})_2(PF_6)_2}$ and $\mathbf{Ag_2(L^{IPr})_2(BPh_4)_2}$ in DMSO show that there is no difference in diffusion coefficients for the major and the minor set of ligand signals, indicating that the two species have the same or a very similar hydrodynamic radius. These observations suggest that the new set of signals in DMSO could be another isomer, whose existence is not observed in acetonitrile, possibly due to dynamic processes.

Coinage metal bis(NHC) complexes have been previously reported to exhibit either *syn* or *anti* isomerism, which corresponds to a boat or chair-like conformation of cyclohexane (Fig. 2).[18,20,31,40,41] For methylene bridged Ag–bis(NHC) cations a fast interconversion, depending on temperature and concentration, which increases intermolecular argentophilic interactions, was recently investigated by NMR studies and small angle X-ray scattering.[11,12] The implication of a 1,1′-(2-hydroxyethane-1,1-diyl)-functionalized bridge, which breaks the C_{2v} symmetry to C_s, was previously addressed by our group for methyl-substituted 1,1′-(2-hydroxyethane-1,1-diyl)-functionalized coinage metal–bis(NHC) complexes $\mathbf{M_2(L^{Me})_2(PF_6)_2}$ (M = Ag, Au, Cu).[31] In this case the number of possible isomers is increased in comparison with methylene bridged analogues: additionally to *syn*- and *anti*-conformation, the hydroxymethyl substituents can point away from the metal centres (*exo*), towards them (*endo*) or in opposite directions (*meso*) (Fig. 2). By comparing gas phase free energies, the theoretical calculations predict the *syn*, *exo* conformation to be the most favourable for methyl-substituted gold and silver complexes.[31] These results are consistent with the single crystal structure of

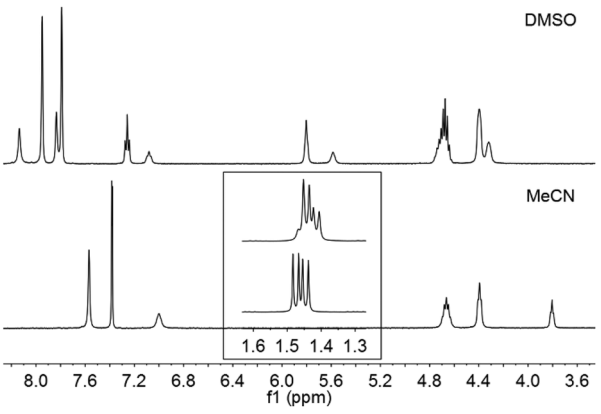

Fig. 1 ^{1}H-NMR spectra of $\mathbf{Ag_2(L^{IPr})_2(PF_6)_2}$ in acetonitrile-d_3 (bottom) and DMSO-d_6 (top) at room temperature.

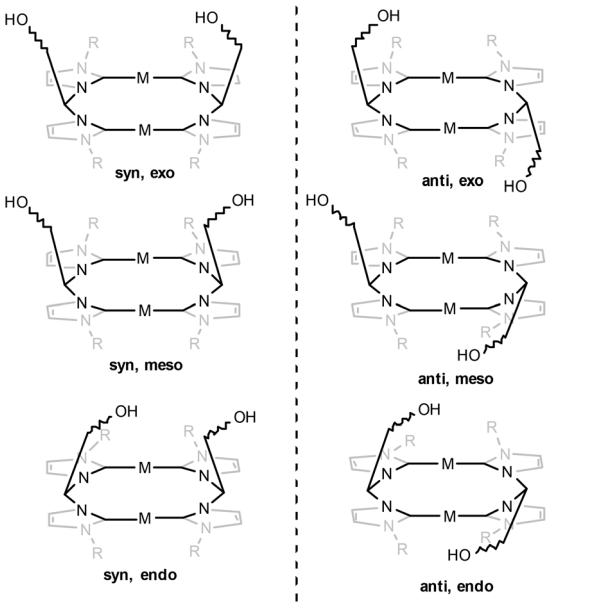

Fig. 2 Possible stereoisomers of dinuclear 1,1′-(2-hydroxyethane-1,1-diyl)-functionalized bis(NHC) complexes of Ag(I) and Au(I).

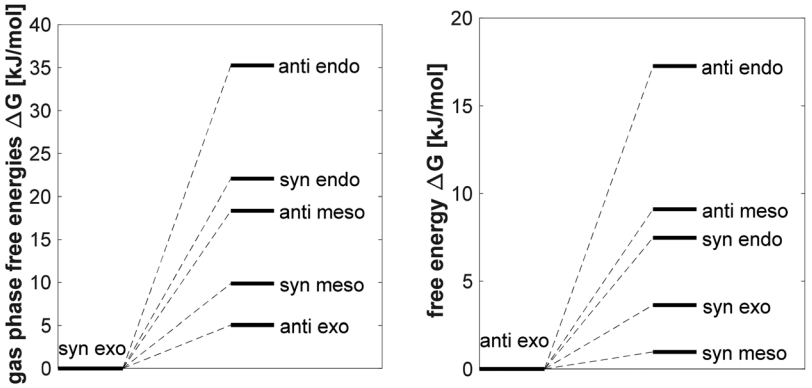

Fig. 3 Calculated gas free energies ΔG (left) and free energies in acetonitrile (right) of $[Ag_2(L^{IPr})_2]^{2+}$ for the different isomers referenced to the particular lowest energy species.

$Au_2(L^{Me})_2(PF_6)_2$, which co-crystallized with a water molecule hydrogen-bonded to both OH groups of the ligand, reducing the energy gap to the *anti* isomer. Further calculations, considering the presence of water and acetonitrile, show that the *anti*, *exo* species is more favourable for the silver complex. This fact was also experimentally confirmed by X-ray diffraction.[31] However, in the previous study the influence of different solvents and wing-tip substituents on conformation has not been investigated. Thus, to gain better insight into the correlation between different conformers and solvents as well as wing-tip substituents, DFT calculations on the isopropyl functionalized Ag(I)- and Au(I)–bis(NHC) complexes both in MeCN and DMSO have been carried out.

Since the ωB97X-D functional has already been applied successfully for the methylene substituted gold and silver complexes, this functional was used again to ensure comparability to the former calculations.[31] In terms of C–C, C–N and C–M bond lengths the results show excellent accordance with the obtained crystal structures (ESI, Table S3†). The free energies were calculated for all optimized structures both in gas phase and with an implicit solvent model. The gas phase calculations predict the *syn*, *exo* conformation to be the lowest energy species and, as expected, the *meso* and *endo* conformations are calculated to be significantly higher in energy, as already found for the methylene substituted silver complexes.[31] However, by changing to a more precise description in favour of real experimental conditions using a SMD solvent model, the order of the free energies of the isomers changes entirely. In agreement with the crystal structure of $Ag_2(L^{IPr})_2(PF_6)_2$, the *anti*, *exo* isomer now is calculated to be the lowest energy species, showing an endergonic gap to the *syn*, *meso* isomer of just ΔG = 0.97 kJ mol^{-1}, indicating two thermoneutral species (Fig. 3).

Based on these results, the free energies for the *anti*, *exo* as well as the *syn*, *meso* conformations have been calculated for the silver and gold complexes in acetonitrile as well as dimethylsulfoxide (Table 1).

Therefore, within the accuracy of the calculations, the *anti*, *exo*/*syn*, *meso* isomer pairs can be regarded as thermodynamically equally stable species. The most important feature, in comparison with the calculation results, of the methyl-substituted isomers is the distortion of the assumed geometry in the case of more sterically demanding substituents, as also found experimentally by SC-XRD experiments (see Fig. 4 and 5). As expected, by changing to a more sterically demanding wing-tip, the influence of the CH_2OH group decreases. For every isomer form, the calculations predict a stronger deviation from the *anti* or *syn* isomerism towards a torsion of the NHC planes out of the metal carbene plane, a behaviour that was not found for the methyl-substituted

Table 1 Free energy values (kJ mol^{-1}) of the calculated *syn*, *meso* complexes of gold(I) and silver(I) in acetonitrile and dimethylsulfoxide referenced to the *anti*, *exo* species

Complex	MeCN (*syn*, *meso*) [kJ mol^{-1}]	DMSO (*syn*, *meso*) [kJ mol^{-1}]
$[Ag_2(L^{IPr})_2]^{2+}$	+0.97	+0.13
$[Au_2(L^{IPr})_2]^{2+}$	+1.1	+0.11

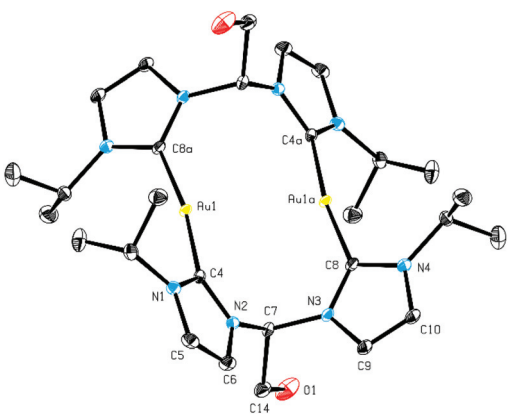

Fig. 4 ORTEP style representation of the cation of $Ag_2(L^{IPr})_2(PF_6)_2$ with ellipsoids at 50% probability. Hydrogen atoms, PF_6^- and co-crystallized diethyl ether molecules are omitted for clarity.

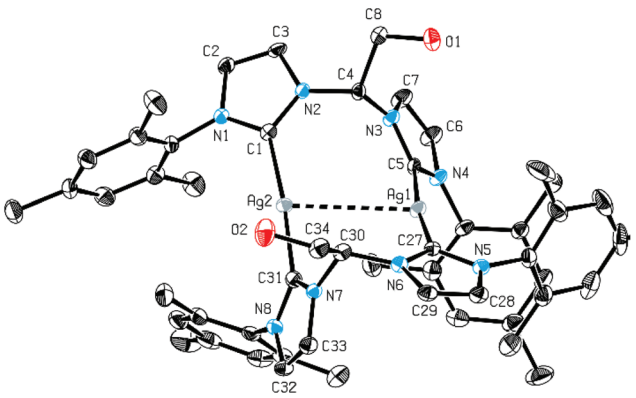

Fig. 5 ORTEP style representation of the cation of $Ag_2(L^{Mes})_2(PF_6)_2$ with ellipsoids at 50% probability. Hydrogen atoms, PF_6^- and co-crystallized acetonitrile molecules are omitted for clarity.

complexes. This might give an answer to the differences in energies, as the *syn* configuration was found to be higher in energy for the $Ag_2(L^{Me})_2(PF_6)_2$ than for the isopropyl-substituted complex.

To confirm DFT calculations a H,H-NOESY spectrum of $Ag_2(L^{IPr})_2(PF_6)_2$ was recorded in DMSO-d_6 (see ESI Fig. S12 and 13†). According to these data a spatial proximity of the NCHN-bridge proton to the backbone protons of imidazol-2-ylidenes is suggested for the major species. As such a correlation is only possible for the *meso* or *endo* isomers, these observations confirm DFT calculations by supporting the assumption of the formation of the *syn*, *meso* species of $Ag_2(L^{IPr})_2(PF_6)_2$. For the minor species visible in DMSO such a spatial proximity was not observed. However, spatial proximity of the CH_2-group of the bridge to the backbone protons of imidazol-2-ylidenes is evident instead. Therefore, the resonances of the minor species can be attributed to the *anti*, *exo* isomer, as due to distortion of the ligand these protons are forced in quite close proximity (see the XRD studies presented below). Interestingly, the H,H-NOESY spectrum of $Ag_2(L^{IPr})_2(PF_6)_2$ also suggests the presence of *syn–anti* aggregates. The formation of molecular dimers as a result of intermolecular argentophilic interactions was previously suggested for similar methylene bridged Ag–bis(NHC) complexes.[12] In the case described here the existence of dynamic dimer systems is conceivable as the hydrodynamic radius of $[Ag_2(L^{IPr})_2]^{2+}$ (calculated on the basis of ^{1}H-DOSY NMR experiments ($r_H = k{\cdot}T/[6\pi{\cdot}\eta{\cdot}D]$)[42,43]) increases in DMSO (7.7 Å in MeCN *vs.* 8.6 Å DMSO for $Ag_2(L^{IPr})_2(PF_6)_2$).

To confirm the results described above, single crystals suitable for SC-XRD have been grown through slow diffusion of diethyl ether into a saturated solution of the respective Ag(I) complexes in acetonitrile. The obtained data unambiguously prove the successful synthesis of dinuclear bis(NHC) complexes. For a comparison of all the obtained Ag(I)–bis(NHC) complexes the relevant bond distances and angles are given in Table 2.

The molecular structure of $Ag_2(L^{IPr})_2(PF_6)_2$, crystallizing in the monoclinic space group $P2_1/c$, is shown in Fig. 4. It exhibits a similar spatial arrangement to the $Ag_2(L^{IPr})_2(BPh_4)_2$ (Fig. S33, ESI†) and to previously reported $Ag_2(L^{Me})_2(PF_6)_2$.[31] $Ag_2(L^{Mes})_2(PF_6)_2$, however, shows significant structural differences from its less sterically hindered analogues (Fig. 5). It crystallizes in the monoclinic space group $P2_1/c$ as the *syn*, *exo* isomer, whereas for methyl and isopropyl the *anti*, *exo* isomers were obtained. Since the Ag···Ag distances for $Ag_2(L^{Me})_2(PF_6)_2$ and $Ag_2(L^{IPr})_2X_2$ (X = PF_6, BPh_4) are longer than the sum of the van der Waals radii of two Ag(0) atoms (3.44 Å),[44] intramolecular argentophilic interactions in the solid state can be excluded for these compounds. On the other hand, as a consequence of the different conformations and bulky substituents, the silver cations in $Ag_2(L^{Mes})_2(PF_6)_2$ come much closer to each other, resulting in an Ag···Ag distance of 3.3314(5) Å thereby suggesting weak argentophilic interactions in the solid state. Regardless of the conformation, the Ag–C_c bonds for all complexes lie within the same range, with $Ag_2(L^{Mes})_2(PF_6)_2$ showing on average slightly shorter distances, probably due to packing effects. The C_c–Ag–C_c angles slightly deviate from linearity as a consequence of the linker and wing-tip substituents. All the values for bond distances and bond angles are comparable to the literature values.[15,31]

Interestingly, X-ray characterization of single crystals obtained by slow diffusion of diethyl ether into a solution of $Ag_2(L^{IPr})_2(BPh_4)_2$ in a mixture of DMSO and methanol reveals the *anti*, *exo* isomer with DMSO molecules coordinated to the Ag(I) cations (Ag–O = 2.763(2) Å) (Fig. S34, ESI†). Additionally, two other DMSO molecules are interacting with the metal centres at the longer distance of 3.372(2) Å (Ag–O) on the respective opposite side. The steric repulsion of the nearby

Table 2 Selected bond lengths (Å) and angles (°) for the reported Ag(I)–bis(NHC) complexes

	$Ag_2(L^{Me})_2(PF_6)_2$[b,a]	$Ag_2(L^{IPr})_2(PF_6)_2$[c]	$Ag_2(L^{IPr})_2(BPh_4)_2$[c]	$Ag_2(L^{IPr})_2(BPh_4)_2{\cdot}$DMSO[c]	$Ag_2(L^{Mes})_2(PF_6)_2$
M···M	3.4556(9)–3.8964(8)	3.4600(6)	3.6474(4)	3.6029(8)	3.3314(5)
M–C_c	2.065(5)–2.100(5)	2.087(2)–2.090(2)	2.086(2)–2.094(2)	2.099(2)–2.102(2)	2.071(2)–2.088(3)
N–C_c	1.334(6)–1.370(6)	1.344(2)–1.360(2)	1.347(3)–1.357(3)	1.345(3)–1.358(3)	1.348(3)–1.361(3)
N–C_b	1.446(6)–1.466(6)	1.452(2)–1.464(2)	1.457(3)–1.461(3)	1.458(3)–1.459(2)	1.456(3)–1.461(3)
N–C_c–N	102.8(4)–105.0(4)	104.2(1)–104.5(2)	104.4(2)–104.6(2)	104.1(2)–104.3(2)	103.8(2)–104.1(2)
N–C_b–N	110.1(4)–111.5(4)	110.3(1)	110.6(2)	110.3(2)	109.48(2)–109.8(2)
C_c–Ag–C_c	168.5(2)–175.8(2)	169.3(7)	171.74(8)	165.65(8)	172.3(1)–175.4(1)

[a] Reported previously.[31] [b] Contains two molecules in the asymmetric unit. [c] Contains an intramolecular inversion centre; C_c = carbene, C_b = bridge CH.

located hydroxymethyl group of the ligand could account for the elongation of the Ag–O distances in this case. This observation suggests that the coordinating ability of DMSO could in fact be responsible for the prominent high-field shift of the respective *anti*, *exo* isomer in the ^{1}H-NMR spectrum in DMSO in comparison with MeCN. A hypothetical *syn* isomer is probably unaffected by acetone or DMSO and would therefore exhibit different resonances for the main species. This would also explain why no second set of signals for $\mathbf{Ag_2(L^{Mes})_2(PF_6)_2}$ in DMSO is observed. For a *syn* isomer the steric repulsion from hydroxymethyl substituents on the one side and wing-tip substituents on the other side of the C–Ag–C plane could prevent DMSO molecules from coordination. This assumption would also imply that in comparison with methyl and isopropyl analogues $\mathbf{Ag_2(L^{Mes})_2(PF_6)_2}$ was obtained as an isomeric pure material. However, the interaction with DMSO is probably very dynamic on the NMR scale, since no additional signal for DMSO was observed. Also then H,H-NOESY NMR experiments showed no evidence of spatial proximity of DMSO to any protons of the ligand framework. Solely as expected, the hydrogen bonded residual water shows close proximity to the OH-group.

It should be noted that an interconversion between the *syn*- and *anti*-isomers is conceivable either by folding of the 12-membered metallacycle or *via* M–C bond cleavage, which leads to a contemporary ligand dissociation and re-association forming the other isomer species. Both mechanisms have been previously suggested for Ag(I)–bis(NHC) complexes.[11,12,45,46] However, the second possibility is more likely, as a conformational change by folding would break symmetry and therefore should have a substantial activation barrier. Since the VT-^{1}H-NMR study mentioned above shows no dependence of the isomer ratios on the temperature, there is also a possibility that interconversion between two species does not happen at room temperature at least in DMSO.

Transmetallation to gold(I)

Using Ag(I)–bis(NHC) complexes as transfer reagents and AuCl(SMe$_2$) or AuCl(THT) (THT = tetrahydrothiophene) as gold precursors, the corresponding Au(I)–bis(NHC) complexes can be obtained in good yields and high purity (Scheme 3). Similar

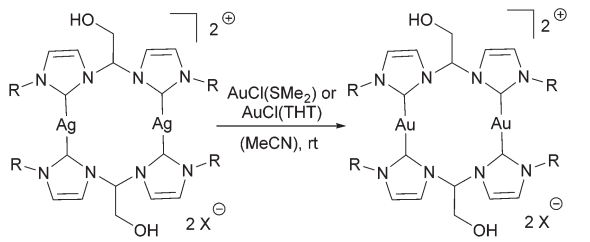

$\mathbf{Ag_2(L^{Me})_2(PF_6)_2}$	R = Me, X = PF_6	$\mathbf{Au_2(L^{Me})_2(PF_6)_2}$	R = Me, X = PF_6
$\mathbf{Ag_2(L^{IPr})_2(PF_6)_2}$	R = *i*-Pr, X = PF_6	$\mathbf{Au_2(L^{IPr})_2(PF_6)_2}$	R = *i*-Pr, X = PF_6
$\mathbf{Ag_2(L^{IPr})_2(BPh_4)_2}$	R = *i*-Pr, X = BPh_4	$\mathbf{Au_2(L^{IPr})_2(BPh_4)_2}$	R = *i*-Pr, X = BPh_4
$\mathbf{Ag_2(L^{Mes})_2(PF_6)_2}$	R = Mes, X = PF_6	$\mathbf{Au_2(L^{Mes})_2(PF_6)_2}$	R = Mes, X = PF_6

Scheme 3 Transmetallation of Ag(I)–bis(NHC) complexes to the respective Au(I) compounds.

to Ag(I) complexes, the use of PF_6^- as a counteranion results in better yields and an easier synthetic procedure than BPh_4^- analogues. All bulk materials have been characterized by multinuclear NMR spectroscopy, ESI-MS and elemental analysis, confirming the successful isolation. The Au(I)–bis(NHC) complexes show the same solubility behaviour as their silver counterparts.

NMR spectra of all Au–bis(NHC) compounds show higher resolutions than the spectra of the silver congeners. Moreover, no differences in signal pattern were visible in the ^{1}H-NMR spectra of the complexes in DMSO-d_6 in comparison with MeCN-d_3. These observations suggest a less fluxional nature of the corresponding gold compounds, which is in accordance with the general agreement that an Au–C_c bond is stronger than the corresponding Ag–C_c bond.[33,47] Generally, all ^{1}H resonances of gold complexes are slightly downfield shifted in comparison with the silver analogues, indicating a stronger deshielding effect of Au nuclei. There is also a slight downfield shift of the carbene signals in ^{13}C-NMR spectra, being in the range of those in previously published reports.[31,33]

The solid state structure of $\mathbf{Au_2(L^{Me})_2(PF_6)_2}$ has been previously reported by our group. This compound was isolated after the transmetallation at 45 °C as an isomeric pure material, which crystallizes as the *syn*, *exo* isomer in acetonitrile by slow diffusion of diethyl ether.[31] By repeating the reaction at room temperature but otherwise under the same conditions, a mixture of two $\mathbf{Au_2(L^{Me})_2(PF_6)_2}$ isomers can be obtained as a crude product. Also, the transmetallation of $\mathbf{Ag_2(L^{IPr})_2(PF_6)_2}$ to $\mathbf{Au_2(L^{IPr})_2(PF_6)_2}$ at room temperature yields two isomers in even higher ratios in contrast to the close relative $\mathbf{Au_2(L^{IPr})_2(BPh_4)_2}$, which is isolated as an almost isomeric pure material after the transmetallation at 50 °C. Since it is unlikely for non-coordinating anions to influence the transfer that much, these unexpected observations lead to a suspicion that the reaction temperature has a significant impact on the formation of different isomers.

To address this question, a series of NMR scale reactions on the transfer of the ligands $\mathbf{L^{IPr}}$ and $\mathbf{L^{Mes}}$ from Ag(I) to Au(I) centres at different temperatures was undertaken. The isomer ratios obtained in these reactions before the purification procedures are collected in Table 3. Assuming that during crystallization there is no interconversion between the two species, based on the crystallographic data previously published[31] and presented below, the downfield shifted minor species can be assigned to an *anti* isomer and the species appearing at lower frequency to the corresponding *syn* isomer. As expected and

Table 3 The ratio of conformational *anti*/*syn* isomers for not purified Au complexes synthesized at different temperatures

Complex	RT	45–50 °C	90 °C
$\mathbf{Au_2(L^{Me})_2(PF_6)_2}$	0.2 : 1.0	0.0 : 1.0[a]	n.d.
$\mathbf{Au_2(L^{IPr})_2(PF_6)_2}$	0.7 : 1.0	0.2 : 1.0–0.3 : 1.0	0.1 : 1.0
$\mathbf{Au_2(L^{Mes})_2(PF_6)_2}$	0.3 : 1.0	0.5 : 1.0	0.5 : 1.0

[a] Reported by Zhong *et al.*[31] n.d. not determined.

already observed for the respective silver complexes, the conformation strongly depends on the wing-tip substituents. For methyl and mesityl-substituted complexes a strong preference for *syn*, *exo* species exists. For isopropyl the preference for a *syn* isomer is less pronounced. These observations are in accord with previously published[31] and recently conducted DFT calculations on methyl- and isopropyl substituted bis(NHC) complexes of Au(I). By comparing the values, it is also evident that they also strongly support the hypothesis of the isomer formation for a particular ligand as a temperature dependent process. For all the tested materials the obtained minor to major product ratios show a steady progress from lower to higher energy. With increased reaction temperature a definitive preference for a *syn* conformation is evident for methyl- and isopropyl-substituted Au–bis(NHC) complexes. In contrast to these observations, the proportion of an *anti* isomer is increased for the mesityl-substituted analogue at higher reaction temperature, but nevertheless a *syn* isomer remains the preferable product.

It is very important to note that the subsequent work-up of crude products severely affects the isomer ratios. For example, the *anti*-isomer of $\mathbf{Au_2(L^{Me})_2(PF_6)_2}$ was seen after repeated fractional precipitation only in traces. On the other hand, for $\mathbf{Au_2(L^{IPr})_2(X)_2}$ (X = PF_6, BPh_4) the same procedure leads to an enrichment of the *anti*, *exo* species. In some cases, due to more elaborate repeated precipitation it was even possible to completely reverse the end-product ratio, *e.g.* for $\mathbf{Au_2(L^{IPr})_2(BPh_4)_2}$, where the *syn* isomer cannot be detected by ^{1}H-NMR spectroscopy afterwards. However, the purification by column chromatography results in a reversed effect, namely in extreme enrichment of *syn* $\mathbf{Au_2(L^{IPr})_2(PF_6)_2}$ rendering the proportion attributed to the *anti* compound almost negligible. Also, the purification of $\mathbf{Au_2(L^{Mes})_2(PF_6)_2}$ by column chromatography or recrystallization yields the pure *syn*, *exo* isomer. Unfortunately, so far the crystallization of the *syn* isomer of the isopropyl-species has remained elusive.

The solid state structures of isopropyl and mesityl substituted Au–bis(NHC) complexes have been further elucidated by SC-XRD, resulting in the confirmation of the NMR experiments. Single crystals of $\mathbf{Au_2(L^{IPr})_2(PF_6)_2}$ and $\mathbf{Au_2(L^{IPr})_2(BPh_4)_2}$ have been grown by slow diffusion of diethyl ether into a saturated solution of the respective purified bulk material in acetonitrile at room temperature. $\mathbf{Au_2(L^{IPr})_2(PF_6)_2}$ crystallizes with one equivalent of diethyl ether in the monoclinic space group $P2_1/c$ as the *anti*, *exo* isomer (Fig. 6). Although the proportion of *syn* species in the bulk material is high, it is not possible to obtain single crystals of it. As expected, since no *syn* isomer was present in the purified $\mathbf{Au_2(L^{IPr})_2(BPh_4)_2}$ sample, the XRD structure shows the *anti*, *exo* isomer in analogy to $\mathbf{Au_2(L^{IPr})_2(PF_6)_2}$ (Fig. S35, ESI†). The isomeric pure sample of $\mathbf{Au_2(L^{Mes})_2(PF_6)_2}$ obtained by recrystallization was crystallized in a mixture of DCM and THF at −4 °C. Its structure is shown in Fig. 7, revealing it to be, as expected, a *syn*, *exo* isomer, crystallizing in the monoclinic space group $P2_1$ with two co-crystalized THF molecules. For comparison of the complexes, all the relevant bond distances and angles are collected in Table 4.

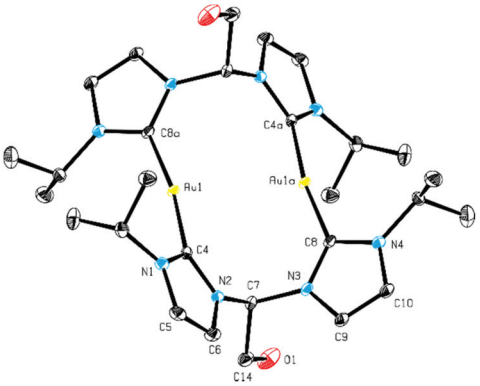

Fig. 6 ORTEP style representation of the cation of $\mathbf{Au_2(L^{IPr})_2(PF_6)_2}$ with ellipsoids at 50% probability. Hydrogen atoms, PF_6^- and co-crystallized diethyl ether molecules are omitted for clarity.

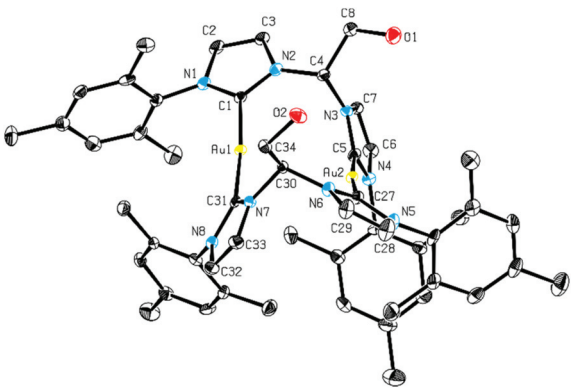

Fig. 7 ORTEP style representation of the cation of $\mathbf{Au_2(L^{Mes})_2(PF_6)_2}$ with ellipsoids at 50% probability. Hydrogen atoms, PF_6^- and co-crystallized tetrahydrofuran molecules are omitted for clarity.

The Au–C_c bond lengths are generally shorter than the distances in the respective Ag complexes. This also reflects the general assumption that bond strengths in coinage metal–NHC complexes are correlated in the order: Au > Cu > Ag.[48] The Au–C_c bond lengths as well as the bond distances in the ligand framework for all Au complexes in this study are comparable and lie within the ranges reported in the literature.[9,18,20,49] The C_c–Au–C_c bond angles (171.0°–175.2°) slightly deviate from linearity, similar to the dications of the silver complexes. Considering intramolecular aurophilicity, the Au···Au separation for the *anti*, *exo* isomers of the methyl and isopropyl analogues is too long for any significant interaction. However, the Au···Au distance of 3.2999(4) Å in $\mathbf{Au_2(L^{Mes})_2(PF_6)_2}$ is smaller than the sum of van der Waals radii of two Au atoms (3.32 Å).[44] This might indicate a weak intramolecular aurophilic interaction for this *syn*, *exo* isomer. Since Au···Au or Ag···Ag interactions are considered responsible for the luminescent properties of the respective coinage metal complexes,[50] the photophysical properties of all the synthesized compounds were investigated at room temperature in the solid state and in acetonitrile solution. The excitation wave-

Table 4 Selected bond lengths (Å) and angles (°) for the reported Au(I)–bis(NHC) complexes

	$Au_2(L^{Me})_2(PF_6)_2$[b,a]	$Au_2(L^{IPr})_2(PF_6)_2$[c]	$Au_2(L^{IPr})_2(BPh_4)_2$[c]	$Au_2(L^{Mes})_2(PF_6)_2$
M···M	3.6401(5)	3.5728(5)	3.6242(3)	3.2999(4)
M–C_C	2.013(9)–2.022(8)	2.020(2)	2.018(3)	2.016(4)–2.021(3)
N–C_C	1.32(1)–1.39(1)	1.345(3)–1.357(3)	1.349(4)–1.356(4)	1.342(5)–1.355(5)
N–C_b	1.46(1)	1.454(3)–1.464(3)	1.460(4)–1.466(4)	1.456(7)–1.471(6)
N–C_C–N	103.8(8)–105.0(7)	104.6(2)–105.0(2)	104.5(3)–105.1(2)	104.9(4)–105.5(4)
N–C_b–N	110.0(6)	110.2(2)	109.5(2)	108.3(4)–108.4(4)
C_C–Ag–C_C	171.0–175.5	171.16(9)	173.0(1)	173.5(2)–175.2(2)

[a] Reported by Zhong *et al.*[31] [b] Contains an intramolecular mirror plane. [c] Contains an intramolecular inversion center; C_c = carbene, C_b = bridge CH.

lengths for all gold complexes reported in this study lie within the UV range (below 400 nm) and can be attributed to π–π* ligand-centred (LC) transitions although they are significantly red-shifted and more intense in comparison with those of the corresponding ligand precursors due to the influence of coordinated Au(I)[51] (see ESI,† UV-vis spectra). Unfortunately, no emission was observed upon excitation of the solution of Au–bis(NHC) complexes in acetonitrile. Also in the solid state no luminescence was observed even for $Au_2(L^{Mes})_2(PF_6)_2$ and $Ag_2(L^{Mes})_2(PF_6)_2$, which show weak intramolecular metallophilic interactions. Tubaro *et al.* previously published a study of a series of Au–bis(NHC) complexes with different metal centre separations, reporting that compounds with shorter Au···Au distance do not necessarily perform better in photoluminescence experiments.[49] Apparently, cation/anion interactions, π–π stacking of the ligand and the nature of wing-tip substituents also play an important role.[7,9,14,49,51] Furthermore, no evidence of π–π stacking was observed in solid-state packing for all compounds in this study.

Antiproliferative effects

Gold(I) complexes have been evaluated for their cytotoxicity against human lung A549 and human liver HepG2 cancer cell lines. The obtained IC_{50} values are summarized in Table 5.

$Au_2(L^{Me})_2(PF_6)_2$ shows only moderate cytotoxic effects against HepG2, while being non-toxic in cancer cells A549. In addition, for both complexes $Au_2(L^{IPr})_2(PF_6)_2$ and $Au_2(L^{IPr})_2(BPh_4)_2$ no antiproliferative effects (IC_{50} > 100 μM) have been observed. However, a dose-dependent inhibition of cell growth is evident in both cell lines for $Au_2(L^{Mes})_2(PF_6)_2$ with a significant increase in cytotoxicity for HepG2. Such differences between the complexes can be related to an effect commonly known for delocalized lipophilic cations.[23,52] An elevated mitochondrial membrane potential in carcinoma cells increases the level of accumulation of large lipophilic cations in mitochondria. Also a possibly easier transportation process into a cell of a complex in a *syn* conformation in comparison with *anti* could play a certain role in increasing the cytotoxic properties, since also $Au_2(L^{Me})_2(PF_6)_2$, as a *syn*, *exo* isomer mainly, shows increased activity in HepG2, thereby seemingly getting somewhat "out of the expectation line". Notably, the corresponding precursors, imidazolium hexafluorophosphates, show no cytotoxicity, suggesting that the growth inhibition of cancer cells is likely the consequence of incorporation of metal cations and is not only due to the application of more lipophilic cations.

Table 5 Cell viability IC_{50} values of screened Au(I)–bis(NHC) complexes, auranofin and cisplatin against human lung (A549) and liver (HepG2) tumor cells incubated for 48 h

	IC_{50} [μM]	
Complex	A549	HepG2
$Au_2(L^{Me})_2(PF_6)_2$[a]	>100	69.4 ± 6.2
$Au_2(L^{IPr})_2(PF_6)_2$[b]	>100	>100
$Au_2(L^{IPr})_2(BPh_4)_2$[c]	>100	>100
$Au_2(L^{Mes})_2(PF_6)_2$[a]	42.2 ± 2.2	14.9 ± 0.9
Auranofin	2.5 ± 0.7	7.08 ± 0.05
Cisplatin	8.1–10.8	8.9–14.4

[a] *syn*, *exo* conformation. [b] A mixture of *anti*/*syn* isomers. [c] Almost exclusively in *anti*, *exo* conformation.

Unfortunately, $Au_2(L^{Mes})_2(PF_6)_2$ shows lower antiproliferative activity in A549 and HepG2 than literature-known, monometallic Au(I)–bis(NHC) complexes (A549, IC_{50} = 3.2–55.6 μM and HepG2, IC_{50} = 3.6–10.52 μM) as well as auranofin and cisplatin.[53–56] The moderate IC_{50}-values of $Au_2(L^{Mes})_2(PF_6)_2$ could be possibly linked to the low solubility of $Au_2(L^{Mes})_2(PF_6)_2$ in aqueous medium. However, the IC_{50}-values of homo-bimetallic Au(I)–bis(NHC) complexes have been previously reported to vary extremely within different cancer cell lines.[19] Therefore, it is conceivable that this complex could show greater potency in other cell types. In addition, the modification of hydrophilicity could be beneficial.

Conclusions

The influence of wing-tip modification and the reaction conditions on the structure and properties of dinuclear 1,1′-(2-hydroxyethane-1,1-diyl)-bridge-functionalized bis(NHC) complexes of silver(I) and gold(I) has been investigated experimentally and by DFT calculations. Evidence for the existence of *anti* and *syn* species for all reported complexes is very strong. For gold complexes the ratio of both isomers strongly depends not only on the used metal, but also on the wing-tip substituents and the reaction temperatures. An application of

sterically hindered mesityl wing-tip substituents shows the best results in a standard MTT assay performed for screening the antiproliferative activity of Au(I)–bis(NHC) complexes against human lung and liver cancer cells. Likely, the fine-tuning of lipophilicity and conformational isomerism are crucial for designing gold–bis(NHC) based anti-cancer drugs. Since isomer formation could be further significantly influenced by purification procedures, an investigation towards the selective application of the different isomers will be conducted. Additionally, experiments towards further functionalization of the OH group in the bridge are ongoing. It might be possible to couple a biological marker and other metals, which are known to inhibit the tumour cell growth, to that functionality. Also, the possibility of inducing stronger aurophilic interactions by further modifying the bridge and wing-tip substituents is currently under investigation in our group. Such a modification could enhance the natural luminescent properties of Au(I)–NHC complexes for visualizing its intracellular distribution.[19]

Experimental

General procedures

All chemicals and solvents were purchased from common commercial suppliers and used without further purification. Acetonitrile was dried *via* an MBraun MB SPS solvent purification system and stored over 4 Å molecular sieves under an argon atmosphere. 1,1′-(2-Hydroxyethane-1,1-diyl)bis(3-methylimidazolium)chloride $\mathbf{H_2L^{Me}(PF_6)_2}$ [32] and the corresponding $\mathbf{Ag_2(L^{Me})_2(PF_6)_2}$ [31] as well as $\mathbf{Au_2(L^{Me})_2(PF_6)_2}$ [31] were synthesized according to the respective literature procedures. ^{1}H- and ^{13}C-NMR spectra were recorded on a Bruker AV400US with a broad band probe and a gradient coil (^{1}H-NMR, 400.13 MHz, ^{13}C-NMR, 100.53 MHz) and a Bruker DRX-400 spectrometer with a broad band probe (^{1}H-NMR, 400.13 MHz, 100.61 MHz). If necessary, 2D-experiments were used for a correct assignment of the signals. Chemical shifts (δ) are reported relative to the residual signal of the deuterated solvent. Elemental analyses were carried out by the microanalytical laboratory at the Technical University of Munich. FAB+ mass spectra were collected on a Finnigan MAT 90. ESI mass spectrometry was performed using a Thermo Scientific LCQ Fleet Spectrometer with a time-of-flight analyser for mass detection. As the eluent a mixture of acetonitrile and formic acid (0.1 vol%) was used. UV-vis spectra were recorded on an Agilent Cary 60 Spectrometer. For luminescence experiments, the samples in solution were placed in fluorimetric 1 cm path quartz cuvettes and the solid state samples (powder) were placed in a covered quartz laboratory dish. Uncorrected emission spectra were obtained with a Hamamatsu C11347 Absolute PL Quantum Yield Spectrometer.

MTT-assay

The assay was performed in 96 well plates. A549/HepG2 cells were grown to 30–40% confluence. The medium was removed and 100 µL medium per well containing 1 µL DMSO compound stock solution were added to the cells and incubated for 48 h. All concentrations as well as the DMSO control were tested in triplicate. 20 µL thiazolyl blue tetrazolium bromide (5 mg mL^{-1} in PBS, Sigma Aldrich) were added to the cells and incubated for 2–4 h until complete consumption was observed. After removal of the medium, the resulting formazan was dissolved in 200 µL DMSO. The optical density was measured at 570 nm (562 nm) and background subtracted at 630 nm (620 nm) using a Tecan Infinite® M200 Pro. For the calculation of IC_{50} values, residual viabilities for the respective compound concentrations were fitted to the equation

$$V = \frac{100}{1 + 10^{(\log(IC_{50}) - \log(c)) \cdot N}}$$

(V: viability [%]; c: inhibitor concentration [M]; N: Hill slope) using GraphPad Prism 6.0.

Single crystal X-ray diffraction

Data were collected using single crystal X-ray diffractometers equipped with a CCD detector (APEX II, κ-CCD), a fine-focus sealed tube and a graphite ($\mathbf{Ag_2(L^{IPr})_2(PF_6)_2}$, $\mathbf{Au_2(L^{IPr})_2(BPh_4)_2}$)/triumph($\mathbf{H_2L^{IPr}(BPh_4)_2}$, $\mathbf{Ag_2(L^{IPr})_2(BPh_4)_2{\cdot}DMSO}$) monochromator or an FR591 rotating anode and a Montel mirror optic ($\mathbf{Ag_2(L^{IPr})_2(BPh_4)_2}$, $\mathbf{Ag_2(L^{Mes})_2(PF_6)_2}$) or a CMOS detector (APEX III, κ-CMOS), an IMS microsource and a Helios optic ($\mathbf{Au_2(L^{IPr})_2(PF_6)_2}$, $\mathbf{Au_2(L^{Mes})_2(PF_6)_2}$) using the APEXII or APEXIII software package.[57,58] For all measurements MoK_α radiation (λ = 0.71073 Å) was used. The crystals were fixed on the top of a glass fibre or kapton microsampler with perfluorinated ether, transferred to the diffractometer and frozen under a stream of cold nitrogen. A matrix scan was used to determine the initial lattice parameters. Reflections were merged and corrected for Lorentz and polarization effects, scan speed, and background using SAINT.[59] Absorption corrections, including odd and even ordered spherical harmonics, were performed using SADABS.[59] Space group assignments were based on systematic absences, E statistics, and successful refinement of the structures. Structures were solved using direct methods (SHELXL-97) or intrinsic phasing (SHELXT) with the aid of successive difference Fourier maps, and were refined against all data using the APEXII or APEX III software package in conjunction with SHELXL-2014 and SHELXLE.[57,58,60–62] Hydrogen atoms were calculated in ideal positions as follows: methyl hydrogen atoms were refined as part of rigid rotating groups, with a C–H distance of 0.98 Å and $U_{iso(H)} = 1.5 \times U_{eq(C)}$. Other H atoms were placed in calculated positions and refined using a riding model, with methylene and aromatic C–H distances of 0.99 Å and 0.95 Å, respectively, other C–H distances of 1.00 Å and $U_{iso(H)} = 1.2 \times U_{eq(C)}$. Non-hydrogen atoms were refined with anisotropic displacement parameters. Full-matrix least-squares refinements were carried out by minimizing $\sum w(F_o^2 - F_c^2)^2$ with the SHELXL-97 weighting scheme.[61] Neutral atom scattering factors for all atoms and anomalous dispersion corrections for the non-hydrogen atoms were taken from the International Tables for Crystallography.[63] A split layer refine-

ment was used to treat with disordered anion/solvent molecules and additional SIMU, DELU and SAME restraints were employed to stabilize the refinement of the layers, if necessary. The unit cell of $\mathbf{Au_2(L^{Mes})_2(PF_6)_2}$ contains two additional molecules of tetrahydrofuran which were treated as a diffuse contribution to the overall scattering without specific atom positions using the PLATON/SQUEEZE procedure.[64] Images were created with PLATON.[65] For more information see the ESI.† Crystallographic data for the structures reported in this paper have also been deposited at the Cambridge Crystallographic Data (CCDC 1511526–1511533).

DFT calculations

All calculations were carried out using the Gaussian 09 package.[66] To ensure comparability to the already published results,[31] the density functional ωB97x-D[67] and the method PM6[68] as well as the basis sets 6-31+g(d), 6-311++g(d,p)[69–71] and LANL2DZ[69,72] (incl. ECP for metals) were employed as implemented.

Suitable input geometries were based on molecular structures obtained using SC-XRD, as available. To achieve atomic coordinates for the remaining isomers, the crystallographic data were slightly modified using GaussView 5. The coordinates were pre-optimized on the PM6 level of theory and then refined employing a double zeta basis set (6-31+g(d) for non-metals and LANL2DZ for metals). All optimized geometries were checked by frequency determination for negative eigenfrequencies, corresponding to the local minima on the potential energy hypersurface. The optimized parameters using the DFT approach have been compared with the mean experimental bonding lengths and are in excellent agreement with them (ESI, Table S1†).

Synthesis procedures and characterization

General procedure for the synthesis of 1,1′-(2-hydroxyethane-1,1-diyl)-bridged bis(imidazolium)salts. The synthesis of this ligand class is based on the preparation of 1,1′-(2-hydroxyethane-1,1-diyl)bis(3-methyl-imidazol-3-ium)chloride.[32] 1.0 equiv. of 2,2-dichloroethanol and 3.0 equiv. of the respective substituted imidazole are placed in an ACE pressure tube and non-dried toluene is added to the mixture. The tube is sealed under air and the reaction mixture is stirred at 135 °C. After the completion of the reaction the hot brown suspension is filtered off and the precipitate was washed with acetonitrile and ether. Subsequently, the obtained bis(imidazolium) chloride is dried under dynamic vacuum. If necessary, 1.0 equiv. of $\mathbf{H_2L^{IPr}Cl_2}$ or $\mathbf{H_2L^{Mes}Cl_2}$ is completely dissolved in water by slightly heating the mixture. A saturated aqueous solution of 2.5 equiv. of either NH_4PF_6 or $NaBPh_4$ is added to this solution. The obtained precipitate is filtered off, washed with water and diethyl ether twice and dried under dynamic vacuum.

1,1′-(2-Hydroxyethane-1,1-diyl)bis(3-methyl-imidazolium) hexafluorophosphate $\mathbf{H_2L^{Me}(PF_6)_2}$. To a suspension of 203.0 mg (0.72 mmol, 1.0 equiv.) of $\mathbf{H_2L^{Me}Cl_2}$ in 5 mL of dry acetonitrile is added a solution of 360.0 g (1.43 mmol, 2.0 equiv.) of $AgPF_6$ in 5 mL of dry acetonitrile. The suspension is stirred at room temperature for 30 min. The precipitate is subsequently separated by centrifugation and washed twice with 2 mL of acetonitrile. The combined organic solutions are filtered through celite and the solvent is removed under reduced pressure. The crude viscous product is purified by repeated fractional precipitation from an acetone/pentane mixture. The compound is obtained as a brown solid. Yield: 30.5 mg (9%).

^{1}H-NMR (400 MHz, DMSO-d_6) δ 9.39 (s, 2H, NC*H*N), 7.95 (virt t, J = 1.9 Hz, 2H, NC*H*CHN), 7.82 (virt t, J = 1.8 Hz, 2H, NCH*CH*N), 6.96 (t, J = 5.1 Hz, 1H, N*CH*(CH_2OH)N), 6.16 (br s, 1H, OH), 4.31 (br s, 2H, NCH(*CH*$_2$OH)N), 3.90 (s, 6H, CH_3). ^{13}C-NMR (101 MHz, DMSO) δ 137.56 (NCHN), 124.33 (NCH*CH*N), 121.07 (N*CH*CHN), 70.15 (N*CH*(CH_2OH)N), 60.08 (NCH(*CH*$_2$OH)N), 36.23 (CH_3). EA Calcd: C, 24.11; H, 3.24; N, 11.25. Found: C, 24.06; H, 3.17; N, 11.07. ESI-MS ([M]+): m/z 1348.51 (15%) [3 × $\mathbf{H_2L^{Me}(PF_6)_2}$ − PF_6^-]$^+$, 850.83 (82%) [2 × $\mathbf{H_2L^{Me}(PF_6)_2}$ − PF_6^-]$^+$, 352.86 (100%) [$\mathbf{H_2L^{Me}(PF_6)_2}$ − PF_6^-]$^+$, 103.97 (43%) [$\mathbf{H_2L^{Me}(PF_6)_2}$ − 2 × PF_6^-]$^{2+}$.

1,1′-(2-Hydroxyethane-1,1-diyl)bis(3-(isopropyl)-imidazolium) chloride $\mathbf{H_2L^{IPr}Cl_2}$. 9.00 g (82.0 mmol, 3.0 equiv.) of 1-(isopropyl)-imidazole and 3.13 g (27.0 mmol, 1.0 equiv.) of 2,2-dichloroethanol are stirred in 15 mL of toluene for 38 days. The compound is obtained as a beige solid. Yield: 4.34 g (48%).

^{1}H-NMR (400 MHz, DMSO-d_6, 300 K) δ 10.13 (virt t, J = 1.6 Hz, 2H, NC*H*N), 8.36 (virt t, J = 1.9 Hz, 2H, NC*H*CHN), 8.08 (virt t, J = 1.7 Hz, 2H, NCH*CH*N), 7.25 (t, J = 5.9 Hz, 1H, N*CH*(CH_2OH)N), 6.46 (t, J = 5.8 Hz, 1H, OH), 4.68 (hept, J = 6.7 Hz, 2H, *CH*(CH_3)$_2$), 4.43 (virt t, J = 5.9 Hz, 2H, CH*CH*$_2$OH), 1.51 (d, J = 6.6 Hz, 12H, (*CH*$_3$)$_2$CH). ^{13}C-NMR (101 MHz, DMSO, 300 K) δ 136.12 (NC*H*N), 121.64 (NC*H*CHN), 121.13 (NCH*CH*N), 69.99 (N*CH*(CH_2OH)N), 59.87 (CH*CH*$_2$OH), 52.93 (*CH*(CH_3)$_2$), 22.14 (CH_3), 22.10 (CH_3). EA Calcd: C, 50.15; H, 7.22; N, 16.71. Found: C, 49.91; H, 7.24; N, 16.43. FAB-MS ([M]+): m/z 299.1 [$\mathbf{H_2L^{IPr}Cl_2}$ − Cl^-]$^+$.

1,1′-(2-Hydroxyethane-1,1-diyl)bis(3-(isopropyl)-imidazolium) hexafluorophosphate $\mathbf{H_2L^{IPr}(PF_6)_2}$. To a solution of 1.00 g (2.89 mmol, 1.0 equiv.) of $\mathbf{H_2L^{IPr}Cl_2}$ in 20 mL of water is added a solution of 1.12 g (6.86 mmol, 2.3 equiv.) of NH_4PF_6 in 10 mL of water. The compound is obtained as a white solid. Yield: 1.15 g (70%).

^{1}H-NMR (400 MHz, DMSO-d_6) δ 9.45 (virt t, J = 2.0 Hz, 2H, NCHN), 8.07 (virt t, J = 1.7 Hz, 2H, NC*H*CHN), 8.03 (virt t, J = 1.7 Hz, 2H, NCH*CH*N), 6.88 (t, J = 5.3 Hz, 1H, *CH*CH_2OH), 6.14 (s, 1H, OH), 4.70 (hept, J = 6.7 Hz, 2H, *CH*(CH_3)$_2$), 4.32 (d, J = 5.2 Hz, 2H, CH*CH*$_2$OH), 1.50 (d, J = 6.5 Hz, 12H, (*CH*$_3$)$_2$CH). ^{13}C-NMR (101 MHz, DMSO, 300 K) δ 135.83 (NC*H*N), 121.47 (NC*H*CHN), 121.26 (NCH*CH*N), 70.41 (N*CH*(CH_2OH)N), 60.11 (CH*CH*$_2$OH), 52.97 (*CH*(CH_3)$_2$), 22.14 (CH_3), 22.06 (CH_3). EA Calcd: C, 30.34; H, 4.36; N, 10.11. Found: C, 30.41; H, 4.57; N, 9.92. FAB-MS ([M]+): m/z 408.9 [$\mathbf{H_2L^{IPr}(PF_6)_2}$ − PF_6^-]$^+$.

1,1′-(2-Hydroxyethane-1,1-diyl)bis(3-(isopropyl)-imidazolium) tetraphenylborate $\mathbf{H_2L^{IPr}(BPh_4)_2}$. To a solution of 1.00 g

(2.98 mmol, 1.0 equiv.) of $\mathbf{H_2L^{IPr}Cl_2}$ in 30 mL of water is added a solution of 2.35 g (6.86 mmol, 2.3 equiv.) of $NaBPh_4$ in 40 mL of water. The compound is obtained as a white solid. Yield: 88%.

^{1}H-NMR (400 MHz, DMSO-d_6) δ 9.47 (virt t, J = 1.6 Hz, 2H, NC*H*N), 8.08 (virt t, J = 1.9 Hz, 2H, NC*H*CHN), 8.03 (virt t, J = 1.9 Hz, 2H, NCH*CH*N), 7.25–7.12 (m, 16H, *ortho*-CH, BPh_4), 6.95–6.87 (m, 17H, N*CH*(CH_2OH)N and *meta*-CH, BPh_4,), 6.83–6.72 (m, 8H, *para*-CH, BPh_4), 6.16 (s, 1H, OH), 4.70 (virt p, J = 6.6 Hz, 2H, *CH*(CH_3)$_2$), 4.32 (d, J = 5.3 Hz, 2H, CHCH_2OH), 1.51 (d, J = 6.7 Hz, 6H, CH(CH_3)$_2$), 1.49 (d, J = 6.7 Hz, 6H, CH(CH_3)$_2$). ^{13}C-NMR (101 MHz, DMSO) δ 163.37 (q, $^1J_{CB}$ = 49.33 Hz, CB, BPh_4), 135.84 (N*C*HN), 135.6–135.5 (m, *ortho*-CH, BPh_4), 125.32 (q, $^3J_{CB}$ = 2.69 Hz, *meta*-CH, BPh_4), 121.54 (s, *para*-CH, BPh_4), 121.49 (N*C*HCHN), 121.24 (NCH*CH*N), 70.37 (N*CH*(CH_2OH)N), 60.09 (CH(CH_2OH)), 52.97 (*CH*(CH_3)$_2$), 22.14 (CH(CH_3)$_2$), 22.07 (CH(CH_3)$_2$). EA Calcd for $\mathbf{H_2L^{IPr}(BPh_4)_2}$ + 1 × acetone: C, 81.25; H, 7.34; N, 5.83. Found: C, 80.94; H, 7.35; N, 5.83. ESI-MS ([M]+): m/z 1485.92 (10%) $[2 \times \mathbf{H_2L^{IPr}(BPh_4)_2} - 3 \times BPh_4^-]^+$, 1256.52 (20%) $[2 \times \mathbf{H_2L^{IPr}(BPh_4)_2} - 2 \times BPh_4^- + 2 \times CHOO^-]^+$, 919.57 (25%) $[2 \times \mathbf{H_2L^{IPr}(BPh_4)_2} - 4 \times BPh_4^- + CH_3CN + CHOO^- - CH_3]^+$, 696.77 (75%) $[2 \times \mathbf{H_2L^{IPr}(BPh_4)_2} - 3 \times BPh_4^- + \text{i-Pr-Im} - H^+]^{2+}$.

1,1′-(2-Hydroxyethane-1,1-diyl)bis(3-mesityl-imidazolium) chloride $\mathbf{H_2L^{Mes}Cl_2}$. 11.02 g (60.0 mmol, 3.0 equiv.) of 1-mesityl-imidazole and 2.27 g (20.0 mmol, 1.0 equiv.) of 2,2-dichloroethanol are stirred in 15 mL of toluene for 42 days. The compound is obtained as a white solid. Yield: 2.47 g (26%).

^{1}H-NMR (400 MHz, DMSO-d_6, 300 K) δ 10.31 (virt t, J = 1.5 Hz, 2H, NC*H*N), 8.63 (virt t, J = 1.7 Hz, 2H, N*CH*CHN), 8.13 (virt t, J = 1.8 Hz, 2H, NCH*CH*N), 7.38 (t, J = 5.7 Hz, 1H, N*CH*(CH_2OH)N), 7.16 (s, 4H, H_{Mes}), 6.55 (t, J = 5.5 Hz, 1H, OH), 4.61 (t, J = 5.6 Hz, 2H, CHCH_2OH), 2.33 (s, 6H, *para*-CH_3), 2.06 (s, 12H, *ortho*-CH_3). ^{13}C-NMR (101 MHz, DMSO, 300 K) δ 140.60 (*C*(*para*-CH_3)), 138.83 (N*C*HN), 134.27 (N*C*C(*ortho*-CH_3)), 130.90 (*C*(*ortho*-CH_3), 129.39 (CH_{Mes}), 124.72 (NCH*CH*N), 122.14 (N*C*HCHN), 70.86 (N*CH*(CH_2OH)N), 59.70 (NCH(CH_2OH)N), 20.65 (*para*-CH_3), 17.05 (*ortho*-CH_3).). EA Calcd: C, 64.06; H, 6.62; N, 11.49. Found: C, 63.60; H, 6.62; N, 11.47. ESI-MS ([M]+): m/z 938.89 (12%) $[2 \times \mathbf{H_2L^{Mes}Cl_2} - Cl^-]^+$, 450.55 (10%) $[\mathbf{H_2L^{Mes}Cl_2} - Cl^-]^+$, 208.26 (100%) $[\mathbf{H_2L^{Mes}Cl_2} - 2 \times Cl^-]^{2+}$.

1,1′-(2-Hydroxyethane-1,1-diyl)bis(3-mesityl-imidazolium) hexafluorophosphate $\mathbf{H_2L^{Mes}(PF_6)_2}$. To a solution of 1.00 g (2.05 mmol, 1.0 equiv.) of $\mathbf{H_2L^{Mes}Cl_2}$ in 100 mL of hot water is added a solution of 836.0 mg (5.13 mmol, 2.5 equiv.) of NH_4PF_6 in 5 mL of water. The compound is obtained as a white solid. Yield: 1.30 g (89%).

^{1}H-NMR (400 MHz, DMSO-d_6, 300 K) δ 9.82 (virt t, J = 1.5 Hz, 2H, NC*H*N), 8.36 (virt t, J = 1.8 Hz, 2H, N*CH*CHN), 8.16 (virt t, J = 1.7 Hz, 2H, NCH*CH*N), 7.18 (s, 4H, H_{Mes}), 7.08 (t, J = 5.1 Hz, 1H, N*CH*(CH_2OH)N), 6.32 (s, 1H, OH), 4.48 (br s, 2H, CHCH_2OH), 2.34 (s, 6H, *para*-CH_3), 2.05 (s, 12H, *ortho*-CH_3). ^{13}C-NMR (101 MHz, DMSO, 300 K) δ 140.65 (*C*(*para*-CH_3)), 138.51 (N*C*HN), 134.22 (N*C*C(*ortho*-CH_3)), 130.85 (*C*(*ortho*-CH_3)), 129.33 (CH_{Mes}), 124.97 (NCH*CH*N), 122.06 (N*C*HCHN), 71.31 (N*CH*(CH_2OH)N), 59.90 (NCH(CH_2OH)N), 20.60 (*para*-CH_3), 16.95 (*ortho*-CH_3). EA Calcd: C, 44.2; H, 4.57; N, 7.93. Found: C, 44.39; H, 4.94; N, 7.91. FAB-MS ([M]+): m/z 560.7 $[\mathbf{H_2L^{Mes}(PF_6)_2} - PF_6^-]^+$.

General procedure for the synthesis of Ag(I)–bis(NHC) complexes

Route 1. This preparation method is based on the synthesis of similar Ag(I) complexes published by Zhong *et al.*[31] In a Schlenk tube 1.0 equiv. of bis(imidazolium)chloride and 3.0 equiv. of Ag_2O are suspended in 3–6 mL of water. The mixture is stirred for 18 h at room temperature under exposure to light. Subsequently, the suspension is centrifuged. The precipitate is washed with water (3 × 5 mL). The combined aqueous solutions are filtered over celite and a saturated aqueous solution of either NH_4PF_6 or $NaBPh_4$ is added to the combined solutions. The obtained suspension is stirred and the precipitate is again separated by centrifugation. The brownish precipitate is washed with water (3 × 5 mL) and dried under dynamic vacuum. Purification is carried out by repeated fractional precipitation from specified solvent mixtures, as brownish, oily, silver containing impurities precipitate before the desired compounds.

Route 2. In a Schlenk tube 1.0 equiv. of bis(imidazolium) hexafluorophosphate and 2.5 equiv. of Ag_2O are suspended in 5 mL of acetonitrile. Then 0.5 mL of water is added. The mixture is stirred for 18 h at room temperature under exposure to light. Subsequently, the suspension is centrifuged and the precipitate is washed with acetonitrile (3 × 5 mL). The combined solutions are filtered over celite and the solvent is removed under vacuum. The crude product is washed with water (3 × 5 mL) and dried again under dynamic vacuum. It is then subsequently dissolved in acetone or dichloromethane and purified repeatedly by fractional precipitation with pentane.

$\mathbf{Ag_2(L^{IPr})_2(PF_6)_2}$. The compound is synthesized according to route 1. 200.0 mg (0.60 mmol, 1.0 equiv.) of $\mathbf{H_2L^{IPr}Cl_2}$ and 346.0 mg (1.49 mmol, 2.5 equiv.) of silver oxide are stirred in 3 mL of water for 66 hours. The crude product is precipitated by adding a saturated solution of NH_4PF_6 in water. $\mathbf{Ag_2(L^{IPr})_2(PF_6)_2}$ is purified by repeated fractional precipitation from wet acetonitrile with diethyl ether. The compound is obtained as a white solid. Yield: 198.6 mg (65%).

^{1}H-NMR (400 MHz, acetonitrile-d_3) δ 7.57 (br s, 4H, N*CH*CHN), 7.38 (d, J = 1.8 Hz, 4H, NCH*CH*N), 7.03 (br s, 2H, N*CH*(CH_2OH)N), 4.67 (virt p, J = 6.8 Hz, 4H, CH_3CHCH_3), 4.39 (d, J = 5.4 Hz, 4H, CH_2OH), 3.90 (s, 2H, OH), 1.48 (d, J = 6.7 Hz, 12H, CH_3), 1.45 (d, J = 6.7 Hz, 12H, CH_3H). DOSY NMR (400 MHz, CD_3CN) D [m^2 s^{-1}] = 8.45 × 10^{-10}. DOSY NMR (400 MHz, DMSO-d_3) D [m^2 s^{-1}] = 1.28 × 10^{-10}. ^{13}C-NMR (101 MHz, CD_3CN) δ 181.32 (d, $^1J_{AgC}$ = 182.60 Hz, NCN), 120.63 (N*CH*CHN), 119.61 (NCH*CH*N), 76.73 (N*CH*(CH_2OH)N), 61.92 (NCH(CH_2OH)N), 55.77 (CH_3CHCH_3), 23.88 (CH_3CHCH_3), 23.50 (CH_3CHCH_3). EA Calcd: C, 32.64; H, 4.30; N, 10.88. Found: C, 32.45; H, 4.27; N, 10.68. ESI-MS ([M]+): m/z 884.92 (100%) $[\mathbf{Ag_2(L^{IPr})_2(PF_6)_2} - PF_6^-]^+$, 370.31 (98%) $[\mathbf{Ag_2(L^{IPr})_2(PF_6)_2} - 2 \times PF_6^-]^{2+}$.

$\mathbf{Ag_2(L^{IPr})_2(BPh_4)_2}$. The complex is synthesized according to route 1. 1.00 g (2.98 mmol, 1.0 equiv.) of $\mathbf{H_2L^{IPr}Cl_2}$ and 1.73 g

(7.46 mmol, 2.5 equiv.) of silver oxide are stirred in 10 mL of water for 13 days. The crude product is precipitated by adding a saturated solution of $NaBPh_4$ in water. $\mathbf{Ag_2(L^{IPr})_2(BPh_4)_2}$ is purified by fractional precipitation from acetone with pentane. The compound is obtained as a white solid containing 0.5 equivalents of acetone. Yield: 881.0 mg (43%).

^{1}H-NMR (400 MHz, acetonitrile-d_3) δ 7.54 (br s, 4H, NC*H*CHN), 7.35 (br s, 4H, NCH*CH*N), 7.27 (m, 16H, *ortho*-CH, BPh_4), 6.99 (t, J = 7.4 Hz, 18H, NC*H*N and *meta*-CH, BPh_4), 6.88–6.79 (m, 8H, *para*-CH, BPh_4), 4.72–4.57 (m, 4H, $CH(CH_3)_2$), 4.38 (t, J = 5.1 Hz, 4H, CH_2OH), 3.80 (s, 2H, OH), 1.47 (d, J = 6.7 Hz, 12H, CH_3), 1.43 (d, J = 6.8 Hz, 12H, CH_3). DOSY NMR (400 MHz, CD_3CN) D [m^2 s^{-1}] = 1.12 × 10^{-9} ($[\mathbf{Ag_2(NHC)_2}]^{2+}$), 1.42 × 10^{-9} (BPh_4^-). DOSY NMR (400 MHz, DMSO-d_3) D [m^2 s^{-1}] = 1.31 × 10^{-10} ($[\mathbf{Ag_2(NHC)_2}]^{2+}$), 2.21 × 10^{-10} (BPh_4^-). ^{13}C-NMR (101 MHz, CD_3CN) δ 189.48 (NCN), 163.78 (q, $^1J_{CB}$ = 48.9 Hz, CB, BPh_4), 135.73 (*ortho*-CH, BPh_4), 125.59 (q, $^3J_{CB}$ = 2.5 Hz, *meta*-CH, BPh_4), 121.77 (*para*-CH, BPh_4), 119.71 (NC*H*CHN), 118.74 (NCH*CH*N), 75.71 (NC*H*N), 60.97 (CH_2OH), 54.83 ($CH(CH_3)_2$), 23.00 (CH_3), 22.62 (CH_3). EA Calcd for $\mathbf{Ag_2(L^{IPr})_2(BPh_4)_2}$ + 0.5 eq. of acetone: C, 66.11; H, 6.23; N, 7.96. Found: C, 65.97; H, 6.18; N, 8.22. ESI-MS ([M]+): m/z 1058.72 (54%) $[\mathbf{Ag_2(L^{IPr})_2(BPh_4)_2} - BPh_4^-]^+$, 370.32 (100%) $[\mathbf{Ag_2(L^{IPr})_2(BPh_4)_2} - 2 \times BPh_4^-]^{2+}$.

$Ag_2(L^{Mes})_2(PF_6)_2$. The complex is synthesized according to route 2. 500.0 mg (0.71 mmol, 1.0 equiv.) of $\mathbf{H_2L^{Mes}(PF_6)_2}$ and 410.0 mg (1.80 mmol, 2.5 equiv.) of silver oxide are stirred in 6 mL of acetonitrile for 5 days. The crude product is purified by repeated fractional precipitation from DCM with pentane. The compound is obtained as a white solid. Yield: 195.4 mg (42%).

^{1}H-NMR (400 MHz, acetonitrile-d_3) δ 7.75 (s, 4H, NC*H*CHN), 7.21 (t, J = 5.9 Hz, 2H, NC*H*(CH_2OH)N), 7.12 (s, 4H. NCH*CH*N), 7.01 (s, 4H, H_{Mes}), 6.95 (s, 4H, H_{Mes}), 4.57 (virt t, J = 5.4 Hz, 4H, $CHCH_2OH$), 3.98 (t, J = 4.8 Hz, 2H, OH), 2.45 (s, 12H, CH_3), 1.66 (s, 12H, CH_3), 1.34 (s, 12H, CH_3).^{13}C-NMR (126 MHz, acetonitrile-d_3) δ 183.23 (dd, $^1J_{^{107}AgC}$ = 181.9 Hz, $^1J_{^{109}AgC}$ = 211.1 Hz, NCN), 140.50 (*ortho*-CH_3CCN), 135.83 (*para*-CH_3C), 135.35 (*ortho*-CH_3CCN), 135.25 (*ortho*-CH_3CCN), 130.28 (s, CH_{Mes}), 125.67 (d, $^3J_{AgC}$ = 6.0 Hz, NC*H*CHN), 120.09 (d, $^3J_{AgC}$ = 5.2 Hz, NCH*CH*N), 76.01 (*CH*CH_2OH), 61.38 (s, $CHCH_2OH$), 21.25 (s, *para*-CH_3), 17.38 (s, *ortho*-CH_3), 17.28 (s, *ortho*-CH_3). EA Calcd: C, 46.79; H, 4.53; N, 8.40. Found: C, 46.73; H, 4.45; N, 8.21. ESI-MS ([M]+): m/z 1189.07 (40%) $[\mathbf{Ag_2(L^{Mes})_2(PF_6)_2} - PF_6^-]^+$, 522.45 (100%) $[\mathbf{Ag_2(L^{Mes})_2(PF_6)_2} - 2 \times PF_6^-]^{2+}$.

General procedure for the synthesis of Au(I)–bis(NHC) complexes

The synthesis of Au(I) complexes is based on the transmetallation reaction *via* the respective Ag(I) complexes published by Zhong *et al.*[31] In a Schlenk tube 1.0 equiv. of the respective Ag(I) complex and 2.1 equiv. of $AuCl(SMe_2)$ or AuCl(THT) (THT = tetrahydrothiophene) are placed. The reaction vessel is evacuated and placed under an argon atmosphere. 3–6 mL of dry acetonitrile are added and the suspension is stirred at the specified temperature and for a specific amount of time (see below). Subsequently, the precipitate is separated by centrifugation and the solid is washed with 1 mL of acetonitrile twice. The combined organic solutions are filtered over celite and the solvent is removed under reduced pressure to yield the crude product. The complexes are purified by ether recrystallization from suitable solvent mixtures, fractional precipitation or chromatography.

Synthesis of $\mathbf{Au_2(L^{IPr})_2(PF_6)_2}$. 100.0 mg (0.10 mmol, 1.0 equiv.) of $\mathbf{Ag_2(L^{IPr})_2(PF_6)_2}$ and 57.2 mg (0.19 mmol, 2.0 equiv.) of $AuCl(SMe_2)$ are stirred at room temperature in 3 mL of acetonitrile for 10 days. The crude product is purified by repeated fractional precipitation from acetone by pentane. The compound is obtained as a white solid containing two conformation isomers in a 4/5 (*anti*/*syn*) ratio. Yield: 94.7 mg (81%).

^{1}H-NMR (400 MHz, acetonitrile-d_3) δ 7.69 (d, J = 2.1 Hz, 4H, *anti*-NC*H*CHN), 7.57 (d, J = 2.2 Hz, 4H, *syn*-NC*H*CHN), 7.45 (d, J = 2.2 Hz, 4H, *anti*-NCH*CH*N), 7.44–7.38 (m, 6H, *syn*-NCH*CH*N and *syn*-NC*H*(CH_2OH)N), 7.35 (t, J = 6.5 Hz, 2H, *anti*-NC*H*(CH_2OH)N), 5.02 (hept, J = 6.85 Hz, 4H, *anti*-*CH*(CH_3)$_2$), 4.89 (hept, J = 6.7 Hz, 4H, *syn*-*CH*(CH_3)$_2$), 4.38 (virt t, J = 5.7 Hz, 4H, *syn*-CH_2OH), 4.32 (virt t, J = 6.1 Hz, 4H, *anti*-CH_2OH), 3.87 (t, J = 5.4 Hz, 2H, *syn*-OH), 3.80 (t, J = 5.7 Hz, 2H, *anti*-OH), 1.57–1.42 (m, 48H, s*yn*&*anti*-CH_3). ^{13}C-NMR (101 MHz, CD_3CN) δ 184.19 (NCN), 121.19 (*anti*-NCH*CH*N), 120.67 (*syn*-NCH*CH*N), 119.99 (*syn*-NC*H*CHN), 119.63 (*anti*-NC*H*CHN), 75.76 (*anti*-NC*H*(CH_2OH)N), 74.89 (*syn*-NC*H*(CH_2OH)N), 62.20 (*anti*-CH_2OH), 61.96 (*syn*-CH_2OH), 55.39 (*syn*-*CH*(CH_3)$_2$), 55.35 (*anti*-*CH*(CH_3)$_2$), 23.78 (*anti*-CH_3), 23.50 (*syn*-CH_3), 23.28 (*syn*-CH_3), 22.91 (*anti*-CH_3). EA Calcd: C, 27.83; H, 3.67; N, 9.27. Found: C, 27.92; H, 3.73; N, 9.22. ESI-MS ([M]+): m/z 1058.72 (32%) $[\mathbf{Au_2(L^{IPr})_2(PF_6)_2} - PF_6^-]^+$, 459.45 (100%) $[\mathbf{Au_2(L^{IPr})_2(PF_6)_2} - 2 \times PF_6^-]^{2+}$.

Synthesis of $\mathbf{Au_2(L^{IPr})_2(BPh_4)_2}$. 200.0 mg (0.15 mmol, 1.0 equiv.) of $\mathbf{Ag_2(L^{IPr})_2(BPh_4)_2}$ and 89.7 mg (0.30 mmol, 2.1 equiv.) of $AuCl(SMe_2)$ are stirred at room temperature in 6 mL of acetonitrile for 4 days. The crude product is purified by repeated recrystallization from an acetone/toluene mixture at −26 °C. The compound is obtained as a white solid with an approximate isomer ratio of *anti*/*syn* of 2 : 1. Yield: 69.5 mg (31%).

^{1}H-NMR (400 MHz, acetonitrile-d_3) δ 7.68 (d, J = 2.2 Hz, 4H, *anti*-NC*H*CHN), 7.56 (d, J = 2.2 Hz, 4H, *syn*-NC*H*CHN), 7.43 (d, J = 2.2 Hz, 4H, *anti*-NCH*CH*N), 7.39 (d, J = 2.2 Hz, 4H, *syn*-NCH*CH*N), 7.35 (t, J = 6.6 Hz, 4H, *syn*&*anti*-NC*H*(CH_2OH)N), 7.30–7.22 (m, 32H, *ortho*-CH, BPh_4), 6.99 (virt t, J = 7.4 Hz, 32H, *meta*-CH, BPh_4), 6.88–6.79 (m, 16H, *para*-CH, BPh_4), 5.01 (virt p, J = 6.8 Hz, 4H, *anti*-*CH*(CH_3)$_2$), 4.90 (virt p, J = 6.7 Hz, 4H, *syn*-*CH*(CH_3)$_2$), 4.35 (d, J = 6.0 Hz, 4H, *syn*-CH_2OH), 4.29 (br s, 4H, *anti*-CH_2OH), 3.79 (br s, 2H, *anti*-OH), 1.54–1.41 (m, 48H, *syn*&*anti* CH(CH_3)$_2$).^{13}C-NMR (101 MHz, CD_3CN) δ 183.99 (NCN), 164.68 (q, $^1J_{CB}$ = 49.2 Hz, CB, BPh_4), 136.67–136.57 (m, *ortho*-CH, BPh_4), 126.51 (q, $^3J_{CB}$ = 2.7 Hz, *meta*-CH, BPh_4), 122.67 (*para*-CH, BPh_4), 121.17 (*anti*-NC*H*CHN), 120.66 (*syn*-NC*H*CHN), 119.91 (*syn*-NCH*CH*N), 119.63 (*anti*-NCH*CH*N), 75.69 (*anti*-NC*H*(CH_2OH)N), 74.92 (*syn*-NC*H*(CH_2OH)N), 62.17 (*anti*-CH_2OH), 61.95 (*syn*-CH_2OH), 55.35 (*syn*-*CH*(CH_3)$_2$), 55.32 (*anti*-*CH*(CH_3)$_2$), 23.78 (*anti*-CH_3), 23.50 (*syn*-CH_3), 23.25 (*syn*-CH'_3), 22.89 (*anti*-CH'_3). EA Calcd: C, 58.62; H, 5.44; N, 7.2. Found: C,

58.13; H, 5.33; N, 7.26. ESI-MS ([M]+): *m*/*z* 1237.20 (48%) $[\mathbf{Au_2(L^{IPr})_2(BPh_4)_2} - BPh_4^-]^+$, 962.83 (6%) $[\mathbf{Au_2(L^{IPr})_2(BPh_4)_2} - 2 \times BPh_4^- + CHOO^-]^+$, 459.51 (100%) $[\mathbf{Au_2(L^{IPr})_2(BPh_4)_2} - 2 \times BPh_4^-]^{2+}$.

Synthesis of $\mathbf{Au_2(L^{Mes})_2(PF_6)_2}$. 200.0 mg (0.5 mmol, 1.0 equiv.) of $\mathbf{Ag_2(L^{Mes})_2(PF_6)_2}$ and 98.3 mg (0.3 mmol, 2.2 equiv.) of $AuCl(SMe_2)$ are stirred in 5 mL acetonitrile at 50 °C for 3 days. The crude product is purified by a double recrystallization from DCM/thf mixture at −26 °C. The compound is obtained as white crystalline solid. Yield: 167.3 mg (72%).

^{1}H-NMR (400 MHz, acetonitrile-d_3) δ 7.78 (d, J = 2.0 Hz, 4H, NC*H*CHN), 7.63 (t, J = 5.6 Hz, 2H, NC*H*(CH_2OH)N), 7.11 (d, J = 2.0 Hz, 4H, NCH*CH*N), 6.99 (br s, 4H, H_{Mes}), 6.93 (br s, 4H, H_{Mes}), 4.55 (virt t, J = 5.6 Hz, 4H, NCH(CH_2OH)N), 3.99 (t, J = 5.4 Hz, 2H, OH), 2.45 (s, 12H, *para*-CH_3), 1.66 (s, 12H, *ortho*-CH_3), 1.37 (s, 12H, *ortho*-CH_3). ^{13}C-NMR (101 MHz, CD_3CN) δ 185.49 (NCN), 140.61 (*ortho*-CH_3CCN), 135.30 (*para*-CH_3C), 135.23 (*ortho*-CH_3CCN), 135.07 (*ortho*-CH_3CCN), 130.22 (CH_{Mes}), 125.73 (NC*H*CHN), 120.31 (NCH*CH*N), 74.03 (*CH*CH_2OH), 61.46 (CHCH_2OH), 21.25 (*para*-CH_3), 17.41 (*ortho*-CH_3), 17.30 (*ortho*-CH_3). EA Calcd: C, 41.28; H, 4.00; N, 7.41. Found: C, 41.24; H, 3.28; N, 7.40. ESI-MS ([M]+): *m*/*z* 1367.00 (20%) $[\mathbf{Au_2(L^{Mes})_2(PF_6)_2} - PF_6^-]^+$, 611.75 (100%) $[\mathbf{Au_2(L^{Mes})_2(PF_6)_2} - 2 \times PF_6^-]^{2+}$.

Acknowledgements

This research was supported by the TUM Institute of Advance Studies, funded by the German Excellence Initiative. J. R., C. J., J. D. and W. H. gratefully acknowledge TUM Graduate School for the support. J. R. thanks Dr Alexander Pöthig and Andrea Schmidt for their valuable insight and expertise and Tim Kratky for experimental support.

References

1 A. J. Arduengo, R. L. Harlow and M. Kline, *J. Am. Chem. Soc.*, 1991, **113**, 361–363.
2 W. A. Herrmann, *Angew. Chem., Int. Ed.*, 2002, **41**, 1290–1309.
3 S. Díez-González, N. Marion and S. P. Nolan, *Chem. Rev.*, 2009, **109**, 3612–3676.
4 *N-Heterocyclic Carbenes: From Laboratory Curiosities to Efficient Synthetic Tools*, ed. S. Díez-González, RCS, Cambridge, 2011.
5 L. Mercs and M. Albrecht, *Chem. Soc. Rev.*, 2010, **39**, 1903–1912.
6 K. M. Hindi, M. J. Panzner, C. A. Tessier, C. L. Cannon and W. J. Youngs, *Chem. Rev.*, 2009, **109**, 3859–3884.
7 L. E. Wedlock, J. B. Aitken, S. J. Berners-Price and P. J. Barnard, *Dalton Trans.*, 2013, **42**, 1259–1266.
8 T. P. Pell, D. J. D. Wilson, B. W. Skelton, J. L. Dutton and P. J. Barnard, *Inorg. Chem.*, 2016, **55**, 6882–6891.
9 M. Monticelli, C. Tubaro, M. Baron, M. Basato, P. Sgarbossa, C. Graiff, G. Accorsi, T. P. Pell, D. J. D. Wilson and P. J. Barnard, *Dalton Trans.*, 2016, **45**, 9540–9552.
10 S. Kobialka, C. Müller-Tautges, M. T. S. Schmidt, G. Schnakenburg, O. Hollóczki, B. Kirchner and M. Engeser, *Inorg. Chem.*, 2015, **54**, 6100–6111.
11 A. Vellé, A. Cebollada, M. Iglesias and P. J. Sanz Miguel, *Inorg. Chem.*, 2014, **53**, 10654–10659.
12 A. Cebollada, A. Velle, M. Iglesias, L. B. Fullmer, S. Goberna-Ferron, M. Nyman and P. J. Sanz Miguel, *Angew. Chem., Int. Ed.*, 2015, **54**, 12762–12766.
13 J. Zheng, Y.-D. Yu, F.-F. Liu, B.-Y. Liu, G. Wei and X.-C. Huang, *Chem. Commun.*, 2014, **50**, 9000–9002.
14 A. Biffis, M. Baron and C. Tubaro, in *Adv. Organomet. Chem*, ed. J. P. Pedro, Academic Press, 2015, vol. 63, pp. 203–288.
15 J. C. Garrison and W. J. Youngs, *Chem. Rev.*, 2005, **105**, 3978–4008.
16 A. Kascatan-Nebioglu, M. J. Panzner, C. A. Tessier, C. L. Cannon and W. J. Youngs, *Coord. Chem. Rev.*, 2007, **251**, 884–895.
17 A. Melaiye, Z. Sun, K. Hindi, A. Milsted, D. Ely, D. H. Reneker, C. A. Tessier and W. J. Youngs, *J. Am. Chem. Soc.*, 2005, **127**, 2285–2291.
18 P. J. Barnard, M. V. Baker, S. J. Berners-Price, B. W. Skelton and A. H. White, *Dalton Trans.*, 2004, 1038–1047.
19 P. J. Barnard, L. E. Wedlock, M. V. Baker, S. J. Berners-Price, D. A. Joyce, B. W. Skelton and J. H. Steer, *Angew. Chem., Int. Ed.*, 2006, **45**, 5966–5970.
20 M. Baron, C. Tubaro, A. Biffis, M. Basato, C. Graiff, A. Poater, L. Cavallo, N. Armaroli and G. Accorsi, *Inorg. Chem.*, 2012, **51**, 1778–1784.
21 N. Marion and S. P. Nolan, *Chem. Soc. Rev.*, 2008, **37**, 1776–1782.
22 S. P. Nolan, *Acc. Chem. Res.*, 2011, **44**, 91–100.
23 P. J. Barnard and S. J. Berners-Price, *Coord. Chem. Rev.*, 2007, **251**, 1889–1902.
24 B. Bertrand and A. Casini, *Dalton Trans.*, 2014, **43**, 4209–4219.
25 S. A. Patil, S. A. Patil, R. Patil, R. S. Keri, S. Budagumpi, G. R. Balakrishna and M. Tacke, *Future Med. Chem.*, 2015, **7**, 1305–1333.
26 A. Meyer, C. P. Bagowski, M. Kokoschka, M. Stefanopoulou, H. Alborzinia, S. Can, D. H. Vlecken, W. S. Sheldrick, S. Wolfl and I. Ott, *Angew. Chem., Int. Ed.*, 2012, **51**, 8895–8899.
27 A. Bindoli, M. P. Rigobello, G. Scutari, C. Gabbiani, A. Casini and L. Messori, *Coord. Chem. Rev.*, 2009, **253**, 1692–1707.
28 S. B. Aher, P. N. Muskawar, K. Thenmozhi and P. R. Bhagat, *Eur. J. Med. Chem.*, 2014, **81**, 408–419.
29 J. L. Hickey, R. A. Ruhayel, P. J. Barnard, M. V. Baker, S. J. Berners-Price and A. Filipovska, *J. Am. Chem. Soc.*, 2008, **130**, 12570–12571.
30 W. Liu and R. Gust, *Chem. Soc. Rev.*, 2013, **42**, 755–773.
31 R. Zhong, A. Pöthig, D. C. Mayer, C. Jandl, P. J. Altmann, W. A. Herrmann and F. E. Kühn, *Organometallics*, 2015, **34**, 2573–2579.
32 R. Zhong, A. Pöthig, S. Haslinger, B. Hofmann, G. Raudaschl-Sieber, E. Herdtweck, W. A. Herrmann and F. E. Kühn, *ChemPlusChem*, 2014, **79**, 1294–1303.

33 J. C. Y. Lin, R. T. W. Huang, C. S. Lee, A. Bhattacharyya, W. S. Hwang and I. J. B. Lin, *Chem. Rev.*, 2009, **109**, 3561–3598.
34 D. T. Weiss, P. J. Altmann, S. Haslinger, C. Jandl, A. Pothig, M. Cokoja and F. E. Kuhn, *Dalton Trans.*, 2015, **44**, 18329–18339.
35 P. J. Altmann, D. T. Weiss, C. Jandl and F. E. Kühn, *Chem. – Asian J.*, 2016, **11**, 1597–1605.
36 I. J. B. Lin and C. S. Vasam, *Coord. Chem. Rev.*, 2007, **251**, 642–670.
37 H. M. J. Wang and I. J. B. Lin, *Organometallics*, 1998, **17**, 972–975.
38 H.-L. Su, L. M. Pérez, S.-J. Lee, J. H. Reibenspies, H. S. Bazzi and D. E. Bergbreiter, *Organometallics*, 2012, **31**, 4063–4071.
39 T. Simler, P. Braunstein and A. A. Danopoulos, *Dalton Trans.*, 2016, **45**, 5122–5139.
40 G. Venkatachalam, M. Heckenroth, A. Neels and M. Albrecht, *Helv. Chim. Acta*, 2009, **92**, 1034–1045.
41 C. A. Quezada, J. C. Garrison, M. J. Panzner, C. A. Tessier and W. J. Youngs, *Organometallics*, 2004, **23**, 4846–4848.
42 Y. Cohen, L. Avram and L. Frish, *Angew. Chem., Int. Ed.*, 2005, **44**, 520–554.
43 D. Li, G. Kagan, R. Hopson and P. G. Williard, *J. Am. Chem. Soc.*, 2009, **131**, 5627–5634.
44 A. Bondi, *J. Phys. Chem.*, 1964, **68**, 441–451.
45 J. Gil-Rubio, V. Cámara, D. Bautista and J. Vicente, *Inorg. Chem.*, 2013, **52**, 4071–4083.
46 A. Biffis, M. Cipani, C. Tubaro, M. Basato, M. Costante, E. Bressan, A. Venzo and C. Graiff, *New J. Chem.*, 2013, **37**, 4176–4184.
47 X. Hu, I. Castro-Rodriguez, K. Olsen and K. Meyer, *Organometallics*, 2004, **23**, 755–764.
48 C. Boehme and G. Frenking, *Organometallics*, 1998, **17**, 5801–5809.
49 C. Tubaro, M. Baron, M. Costante, M. Basato, A. Biffis, A. Gennaro, A. A. Isse, C. Graiff and G. Accorsi, *Dalton Trans.*, 2013, **42**, 10952–10963.
50 P. Pyykkö, *Angew. Chem., Int. Ed.*, 2004, **43**, 4412–4456.
51 F. Jean-Baptiste dit Dominique, H. Gornitzka, A. Sournia-Saquet and C. Hemmert, *Dalton Trans.*, 2009, 340–352.
52 M. V. Baker, P. J. Barnard, S. J. Berners-Price, S. K. Brayshaw, J. L. Hickey, B. W. Skelton and A. H. White, *Dalton Trans.*, 2006, 3708–3715.
53 W. Liu and R. Gust, *Coord. Chem. Rev.*, 2016, **329**, 191–213.
54 J. Turek, Z. Růžičková, E. Tloušťová, H. Mertlíková-Kaiserová, J. Günterová, L. Rulíšek and A. Růžička, *Appl. Organomet. Chem.*, 2016, **30**, 318–322.
55 A. Citta, V. Scalcon, P. Gobel, B. Bertrand, M. Wenzel, A. Folda, M. P. Rigobello, E. Meggers and A. Casini, *RSC Adv.*, 2016, **6**, 79147–79152.
56 A. B. Mullick, Y. M. Chang, I. Ghiviriga, K. A. Abboud, W. Tan and A. S. Veige, *Dalton Trans.*, 2013, **42**, 7440–7446.
57 *APEX suite of crystallographic software, APEX 3 Version 2015-5.2*, Bruker AXS Inc., Bruker, Madison, Wisconsin, USA, 2015.
58 *APEX suite of crystallographic software, APEX 2 Version 2014-9.0*, Bruker AXS Inc., Bruker, Madison, Wisconsin, USA, 2014.
59 *SAINT, Version 8.34A and SADABS, Version 2014/5*, Bruker AXS Inc., Bruker, Madison, Wisconsin, USA, 2014.
60 G. Sheldrick, *Acta Crystallogr., Sect. A: Fundam. Crystallogr.*, 2015, **71**, 3–8.
61 G. Sheldrick, *Acta Crystallogr., Sect. C: Cryst. Struct. Commun.*, 2015, **71**, 3–8.
62 C. B. Hübschle, G. M. Sheldrick and B. Dittrich, *J. Appl. Crystallogr.*, 2011, **44**, 1281–1284.
63 *International Tables for Crystallography, Vol. C, Tables 6.1.1.4 (pp. 500-502), 4.2.6.8 (pp. 219-222), and 4.2.4.2 (pp. 193-199)*, ed. A. J. C. Wilson, Kluwer Academic Publishers, Dordrecht, The Netherlands, 1992.
64 A. Spek, *Acta Crystallogr., Sect. C: Cryst. Struct. Commun.*, 2015, **71**, 9–18.
65 A. Spek, *Acta Crystallogr., Sect. D: Biol. Crystallogr.*, 2009, **65**, 148–155.
66 M. J. Frisch, G. W. Trucks, H. B. Schlegel, G. E. Scuseria, M. A. Robb, J. R. Cheeseman, G. Scalmani, V. Barone, B. Mennucci, G. A. Petersson, H. Nakatsuji, M. Caricato, X. Li, H. P. Hratchian, A. F. Izmaylov, J. Bloino, G. Zheng, J. L. Sonnenberg, M. Hada, M. Ehara, K. Toyota, R. Fukuda, J. Hasegawa, M. Ishida, T. Nakajima, Y. Honda, O. Kitao, H. Nakai, T. Vreven, J. A. Montgomery Jr., J. E. Peralta, F. Ogliaro, M. J. Bearpark, J. Heyd, E. N. Brothers, K. N. Kudin, V. N. Staroverov, R. Kobayashi, J. Normand, K. Raghavachari, A. P. Rendell, J. C. Burant, S. S. Iyengar, J. Tomasi, M. Cossi, N. Rega, N. J. Millam, M. Klene, J. E. Knox, J. B. Cross, V. Bakken, C. Adamo, J. Jaramillo, R. Gomperts, R. E. Stratmann, O. Yazyev, A. J. Austin, R. Cammi, C. Pomelli, J. W. Ochterski, R. L. Martin, K. Morokuma, V. G. Zakrzewski, G. A. Voth, P. Salvador, J. J. Dannenberg, S. Dapprich, A. D. Daniels, Ö. Farkas, J. B. Foresman, J. V. Ortiz, J. Cioslowski and D. J. Fox, *Gaussian 09*, Gaussian Inc, Wallingford, CT, USA, 2009.
67 J.-D. Chai and M. Head-Gordon, *Phys. Chem. Chem. Phys.*, 2008, **10**, 6615–6620.
68 J. J. P. Stewart, *J. Mol. Model.*, 2007, **13**, 1173–1213.
69 T. H. Dunning Jr. and P. J. Hay, *Mod. Theor. Chem.*, 1977, **3**, 1–27.
70 M. M. Francl, W. J. Pietro, W. J. Hehre, J. S. Binkley, M. S. Gordon, D. J. DeFrees and J. A. Pople, *J. Chem. Phys.*, 1982, **77**, 3654–3665.
71 P. C. Hariharan and J. A. Pople, *Theor. Chim. Acta*, 1973, **28**, 213–222.
72 P. J. Hay and W. R. Wadt, *J. Chem. Phys.*, 1985, **82**, 270–283.

Journal of Organometallic Chemistry 866 (2018) 153–164

Contents lists available at ScienceDirect

Journal of Organometallic Chemistry

journal homepage: www.elsevier.com/locate/jorganchem

Medicinal Applications of Gold(I/III)-Based Complexes Bearing *N*-Heterocyclic Carbene and Phosphine Ligands

Bruno Dominelli [a], João D.G. Correia [b, **], Fritz E. Kühn [a, *]

[a] Molecular Catalysis, Department of Chemistry, Catalysis Research Center, Technische Universität München, Lichtenbergstr. 4, 85748, Garching, Germany
[b] Centro de Ciências e Tecnologias Nucleares, Instituto Superior Técnico, Universidade de Lisboa, Campus Tecnológico e Nuclear, Estrada Nacional 10 (km 139,7), 2695-066, Bobadela LRS, Portugal

ARTICLE INFO

Article history:
Received 26 January 2018
Received in revised form
13 April 2018
Accepted 13 April 2018
Available online 14 April 2018

Keywords:
Gold(I/III) complexes
N-Heterocyclic carbenes
Phosphines
Medicinal applications

ABSTRACT

Phosphines are the most studied ligands on gold-based metallodrugs, whereas *N*-heterocyclic carbenes (NHCs) have been emerging in the past years as potential alternative ligands for medicinal applications. Indeed, in both cases, phosphine and NHC allow the preparation of a plethora of transition metal-based complexes with attractive properties for medicinal applications. This review offers an update on phosphine and NHC ligands used in gold complexes with potential anti-cancer, anti-bacterial, anti-parasitic (malaria, leishmaniasis and trypanosomasis) and anti-viral (HIV-1) activity. Structural information about diverse ligands is discussed and the biological activity of the corresponding homo-metallic Au(I), Au(III) and hetero-metallic complexes is summarized in tables and discussed as well. Additionally, these complexes are compared with reference compounds and facts about mechanistic studies and luminescence properties are highlighted. The main target of this review is to find trends in ligand design for medicinal purposes. Particularly, questions about the balance between lipophilicity and hydrophilicity, the presence of functional groups, the utilization of multinuclear complexes and the comparison of neutral versus cationic complexes will be addressed.

1. Introduction

Most of the drugs currently used in clinical settings for treating cancer and bacterial, parasitic or viral infections still present drawbacks that must be overcome in order to develop innovative drugs with higher efficacy and negligible side effects. Current problems include low selectivity between healthy and diseased cells, low drug stability, development of drug resistance, among others, which press for the development of novel compounds [1–3]. Metal-based drugs have been thoroughly exploited aiming to solve some of the mentioned problems. Indeed, a plethora of new metallodrugs have been reported in the last few years, showing very promising biological activity *in vitro*. Since most of them suffer on too low (or even no) activity *in vivo* they do not reach clinical trials. Accordingly, the design of new metal-based drugs is still under active research. One of the main questions to be addressed is the *in vivo* stability of newly designed complexes, which relies on the selection of the most adequate ligands and corresponding metals. This particular question has been discussed in recent reviews by Casini [4], Djuran [5] and Che et al. [6]. The precious element gold became very attractive for biological and medicinal application, since Au(I) allows the selective targeting of several enzymes bearing residual thiol or selenol groups and Au(III) is isoelectronic to Pt (II) known from cisplatin (Fig. 1) [4,5,7,8]. Additionally, in multi-metallic complexes, the nuclei can form aurophilic interactions leading to higher stability and ideally to luminescence properties. Auranofin (Fig. 1) is the leading gold compound that has been studied in clinical phase II against Chronic Lymphocytic Leukemia (CLL, www.clinicaltrials.gov). Phosphine ligands are the most studied ligands in medicinal application of gold. However, similarly to what happened in the catalysis field earlier [9], phosphines are being more and more replaced by the stronger σ-donating NHCs [8]. NHCs are easier and more versatile tunable in their electronic, steric and physical properties. M – C bonds additionally are thermodynamically stronger than M – P bonds [10]. Based on this, NHCs gained increasingly more attention in medicinal chemistry and a number of reviews have been reporting the use of NHCs in this area [8,11,12].

* Corresponding author.
** Corresponding author.
E-mail address: fritz.kuehn@ch.tum.de (F.E. Kühn).

https://doi.org/10.1016/j.jorganchem.2018.04.023
0022-328X/

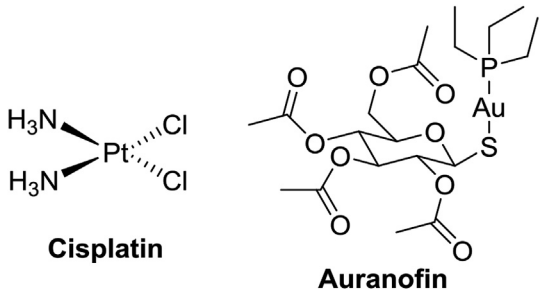

Fig. 1. Structures of cisplatin and auranofin.

In this short review, we aim at comparing the chemical and biological properties of gold complexes stabilized by phosphine and NHC ligands that have been examined for their potential use in the treatment of cancer and bacterial, parasitic or viral infections. It is intended that the comparison of these two ligand systems will contribute to the development of new strategies for the prospective design of metallodrugs.

2. Treatment of cancer

Cisplatin displays low selectivity leading to severe side effects. Additionally, several cancer cell lines show resistance against cisplatin [2]. Consequently, transition metals like titanium, iron, osmium, rhodium, iridium, palladium and the coinage metals have been considered as alternatives to platinum-based metallodrugs due to the cytotoxic properties of some of their compounds [8]. Especially gold in both oxidation states + I and +III recently emerged as suitable anti-cancer active transition metal, due to its more selective mechanism of action, which arises from the high affinity to thiol and selenol groups of cysteine and selenocysteine, respectively. As known from Auranofin, this behavior allows for example the targeting of the cytosolic or mitochondrial enzyme thioredoxin reductase (TrxR), which is more expressed in cancer cells than in healthy cells. The coordination of thiol or selenol groups of TrxR to gold inhibits the enzyme itself to reduce the production of reactive oxygen species (ROS, e.g. H_2O_2). Consequently, the high cellular peroxide concentration leads to cell death *via* oxidative stress [13–15]. Besides the enzymatic targeting, a few gold complexes, for example bearing caffeine-derived NHC ligands apparently interact with the canonical and non-canonical DNA secondary structure (e.g. duplex, mismatched and G-quadruplex DNA, replication forks, etc.) in a coordinative of intercalating pathway leading to anti-cancer activity [16]. As mentioned above, the gold(I)-based drug Auranofin bears a phosphine ligand (PEt_3). Motivated by the success and but also by the disadvantages (low stability *in vivo*) of auranofin, a plethora of new phosphine-based gold complexes were synthesized [7,17]. Fig. 2 and Fig. 3 show different phosphine moieties that have been reported in the past five years as ligands in gold complexes with anti-cancer activity. Some examples of phosphine ligands like **PPh_3** and derivatives, **P_2** and **P_5**, already exhibit cytotoxic activity without coordination to gold. The coumarin-modified phosphine ligand **PPh_2(*p*-cou-Ph)** dissociates *in vivo* in zebrafish larvae and is oxidized to the strongly fluorescent phosphate moiety, which could be externally detected [18]. This phenomenon must be taken into consideration in the case of phosphines being possibly dissociated in the cell. Nevertheless, the corresponding gold(I) complexes have been reported to be stable for 48 h *in vivo* and a high selectivity towards cancer cells with respect to healthy cells was observed.

Banti and Hadjikakou et al. have comparatively examined different cone angles of **PPh_3**, **P(*o*-Me-Ph)$_3$ P(*p*-Me-Ph)$_3$** observing no influence on anti-tumoral activity [19]. Additionally, replacement of the phosphorus atom by arsenic or antimony leads to lower cytotoxic activity. The more lipophilic the phosphine species, the higher cytotoxic is the ligand itself, which could be confirmed by **P_2** and **P_{11}** with varied alkyl chain bridge [20,21]. Consequently, the corresponding gold(I) complexes result to be more cytotoxic as well. However, the degree of lipophilicity of substituent should have a limit. A maximal cytotoxicity could be observed for n = 6, since in the case of **P_{11}** a longer chain leads to higher IC_{50}-values [22]. Narain *et. al.* coupled [Au**PPh_3**]$^+$ to a glycol polymer with one terminal dithiocarbamate side chain and studied the effect of molecule size and weight on anti-cancer activity [23]. The smaller polymer with 10 kDa molecular weight was more active than the heavier polymer with 30 kDa, indicating a limit of size for internalization processes with respect to the membrane potential. Also, modification of 1,3,5-triaza-7-phosphaadamantane phosphine (PTA, **P_3**) with a phenyl substituent to give **$P_{5a,b}$**, which presents an higher degree of lipophilicity, leads to higher cytotoxic activity [24]. Substitution of the phenyl group by a methyl ester (**$P_{5c,d}$**) balances the hydro/lipophilic character, yielding IC_{50}-values in the same range of **$P_{5a,b}$** However, increasing the hydrophilicity with the presence of other functional groups like a carboxylic or a nitrile groups (**$P_{5e,f}$**) does not improve the activity. It was demonstrated that the presence of ester groups, especially activated moieties, enhances the cytotoxicity of the gold complex [25]. The utilization of amino acid functionalized thiol-ligands were reported with the presence of **PPh_3**, whereas the esterificated moieties on C-terminus exhibit the highest cytotoxicity [26]. Thus, the post-modification of functional groups *via* amidation or esterification reactions offers a suitable strategy to balance between hydro- and lipophilicity. Additionally, certain peptide sequences attached on the gold complexes could allow the access to highly selective anti-cancer metal complexes. A gold(I)-complex bearing the two different phosphine ligands **P_{2i}** and **^{t}Bu$_3$P** displays relevant cytotoxicity, with IC_{50}-values in the lower micromolar range [27]. However, this complex [(**P_{2i}**)Au^I(**P^tBu$_3$**)]$^+$ decomposes in solution, yielding two Au(I) complexes [(**P_{2i}**)$_2$Au^I]$^+$ and [(**P^tBu$_3$**)$_2$Au^I]$^+$ bearing the same phosphine ligand. Multidentate phosphine ligands (**P_1**, **P_2**, **P_6**, and **P_{11}**) led to a varied number of multinuclear gold complexes. Another interesting phosphorus-based ligand is the phosphole **P_8**, which increases the thiophilicity of gold complexes and presents promising activity in decreasing the tumor growth in C6 rats with malignant glioblastomas [28].

In some cases, the dinuclear complexes with **P_2**, have presented higher cytotoxicity than the corresponding mononuclear moieties [20,29]. The ligand systems **P_{2j}** and **P_{2k}** lead to the corresponding cyclic tri- and tetranuclear gold(I) complexes, respectively. They exhibit *in vitro* cytotoxicity values near the nanomolar scale and show high selectivity towards tumor cells [30]. In the case of the [2.2]paracyclophane-type ligand systems **P_{13}**, **P_{14}** and **P_{15}**, only the chelating moiety **P_{15}** coordinating on one gold nucleus has shown attractive cytotoxicity *in vivo* in zebrafish larvae in the range of 50–100 μM [31]. The gold complex bearing **P_{15}** seems to bind in a different way to thiol groups avoiding ligand exchange reactions. **P_{16}**, a water-soluble porphyrin-system with terminal diphenylphosphine leads to Au(I)-based theranostics showing luminescence in the near infrared [32]. The mixed Au^I/Au^{III} binuclear gold complex with **PPh_3** and a benzimidazole derivate coordinating in a bridging manner on both nuclei is less active than the mononuclear Au(I) complex [33]. However, Au(III)-based metallodrugs are known to be more active in anti-cancer therapy [34]. Thus, this phenomenon was explained by a possible reduction of gold (III) to gold(I) and, consequently, showing the same reactivity. In contrast, the binuclear Au(III) complex bearing the ligand **P_{2d}** presented higher cytotoxicity than the mononuclear species, the analogue

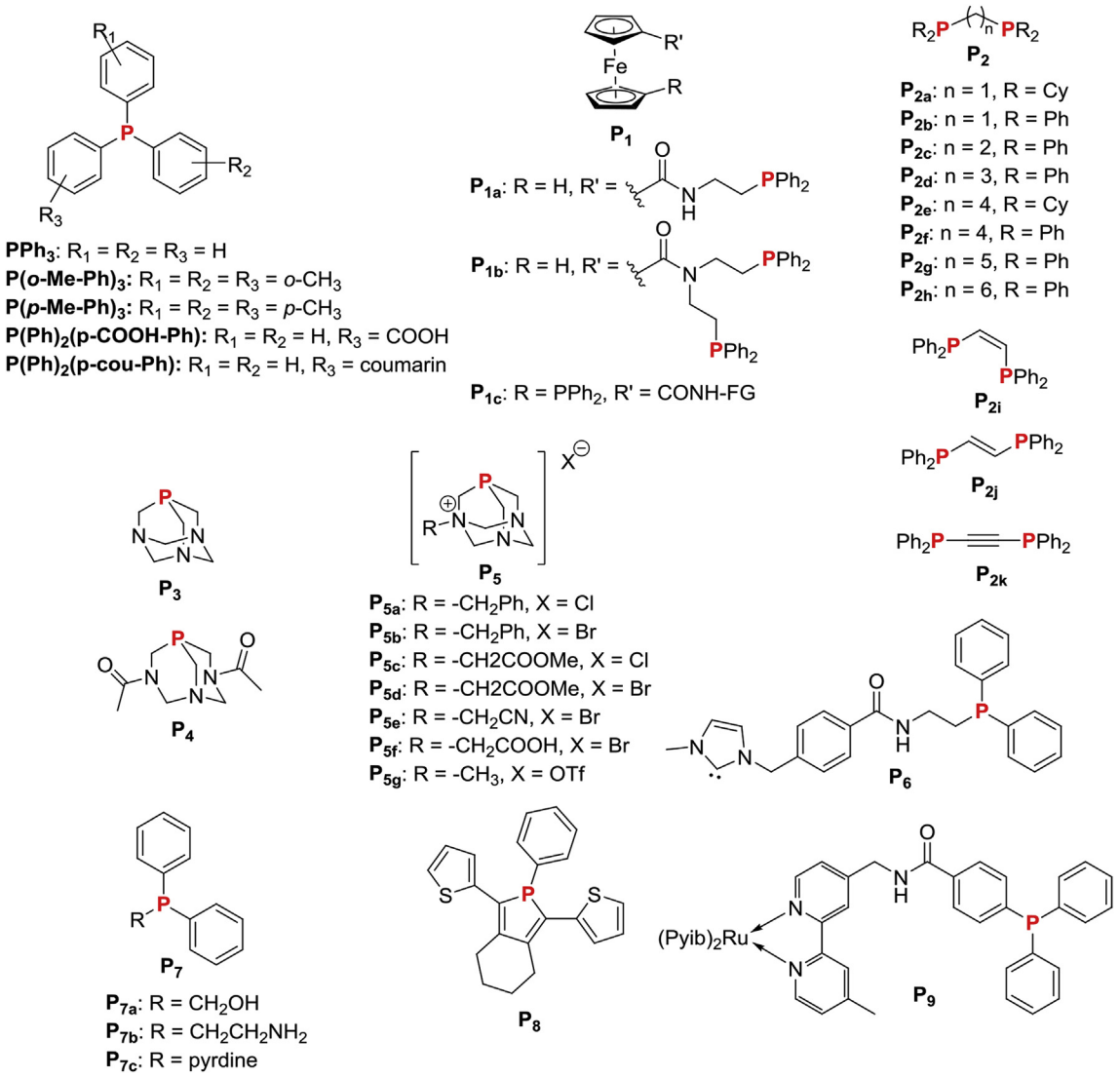

Fig. 2. Phosphine-type ligands being reported from 2013 until 2017 in gold-based complexes with anti-cancer activity (Part I). The phosphorus atoms are highlighted in red. (For interpretation of the references to colour in this figure legend, the reader is referred to the Web version of this article.)

NHC moiety and the binuclear platinum complex. Additionally, promising activity in decreasing the tumor growth has been observed *in vivo*. The synthesis of hetero-metallic complexes combining Au(I) with transition metals such as Fe(II) [35,36], Re(I) [37], Ru(II) [38], Pt (II) [39] or Cu(I) [40] became very attractive leading to complexes with potent anti-cancer activity. In most cases, these hetero-metallic complexes show extremely low IC_{50}-values compared to the mononuclear moiety. Finally, all gold complexes bearing the phosphine type ligands of Figs. 2 and 3 are summarized in Table 1. Fig. 4 displays examples of gold phosphine complexes defining seven different structure types. These structure motifs are abbreviated in superscript form on right-hand side of the chemical formula with T-X (X = I-VII) in all following tables.

Further properties such as cytotoxicity of the pure ligand (a), higher activity than Cisplatin (b) and Auranofin (c), inhibition of enzymes (d), interaction with DNA (e), luminescence (f), *in vivo* (g) and ex vivo studies (h) are additionally indicated by the corresponding letters on the left-hand side of the chemical formula in superscript form. Cytotoxic activities in human cancer cell lines are indicated with the corresponding obtained IC_{50}-values. Beside the IC_{50}-values, the tested human cancer cell line and the incubation time is mentioned.

The development of gold-based NHC complexes as promising anti-cancer agents has strongly increaded in recent decades and a plethora of gold (I/III)-NHC complexes with imidazolydene or triazolydene derivates have been published. Some complexes display very attractive anti-tumoral activity *in vivo* as highlighted in the excellent review of Liu and Gust [8].

In this work the most recently published NHC moieties being reported as ligands for gold complexes (Fig. 5) and their applications as anti-cancer complexes are highlighted. Imidazolium salts are the precursor for NHC ligands and can be modified on both wingtip and backbone positions [10]. Several modification pathways were carried out to increase the lipophilicity and to introduce functional groups for possible water solubility and stability. In the case of **C_{21}**, **C_{23}**, **C_{25}** and **C_{27}**, the replacement of hydrogen atoms by halides, phenyl or triazole groups on the backbone-position enhances the cytotoxicity *in vitro* [53–56]. Increasing the degree of lipophilicity on wingtip-positions delivers the same effect on cytotoxicity, which can be observed on the example of **C_{28}** and **C_{30}** [57–59]. The lone presence of functional groups does not increase the anti-cancer activity *in vitro* without having a certain degree of

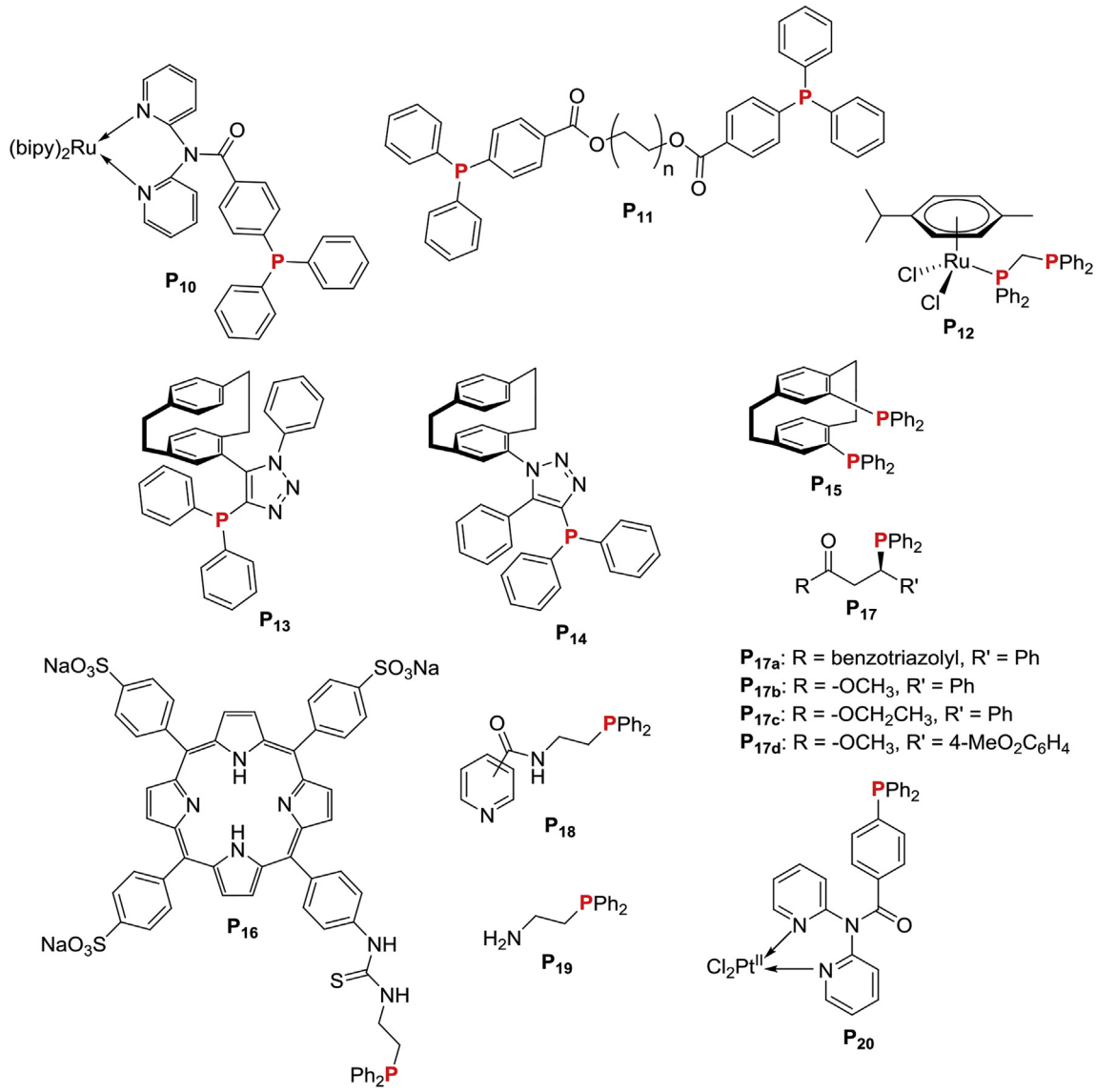

Fig. 3. Phosphine-type ligands being reported from 2013 until 2017 in gold-based complexes with anti-cancer activity (Part II). The phosphorus atoms are highlighted in red. (For interpretation of the references to colour in this figure legend, the reader is referred to the Web version of this article.)

lipophilicity, as seen in **C$_{24}$** [41]. This phenomenon was also observed for some phosphine ligands mentioned above. However, the degree of lipophilicity should not be too strongly increased, otherwise the imidazolium salt exhibits cytotoxicity and the coordination on gold does not have any influence on the cytotoxicity [60]. **C$_{22}$** is a NHC moiety with the backbone being extended with a porphyrin system leading to a gold complex with potential use in photodynamic therapy (PDT), which exhibits light induced Au–S bond break with consequent cytotoxicity [61]. **C$_{36}$** is a NHC ligand fused with the stress inducer naphthoquinone on the backbone-position and the corresponding gold complexes has shown very interesting anti-cancer activity *in vitro* and *in vivo* [62]. The ligand systems **C$_{31}$** and **C$_{32}$** yielded cyclometalated gold (III) complexes with the structure type VII, which allowed a deeper insight into the different targets of intracellular proteins [63]. The photo-activable groups as wingtip-substituent can interact with proteins after light irradiation whereas a terminal alkinyl-groups as second wingtip-substituents can added on a reporter such as for example biotin by a click-reaction. These Au(III) complexes display small drug resistance making the design of metallodrugs with multiple targets more attractive.

This property could also involve the synthesis of hetero-metallic complexes. Indeed, also in the case of NHC, the combination of Au(I) and Ti(IV) delivers hetero-metallic complexes with higher cytotoxicity compared to the homo-metallic complexes [58]. Additionally, the exchange of phosphine by NHC moieties in this hetero-metallic complex has demonstrated to enhance the anti-cancer activity and enforces the thesis mentioned before that NHC can often be used as a better alternative to phopshine-type ligands.

The comparison between neutral and cationic complexes show - similar to the phosphine moieties - no special difference in cytotoxicity. Finally, the corresponding Au-complexes are summarized in Table 2 to allow a comparison to the phosphine-based gold complexes.

3. Treatment of bacterial infections

The use of silver nitrate as anti-bacterial agent has been reported already in the 17th century, and had been used for the treatment of chronic skin ulcers and open wounds [65]. Nowadays,

Table 1
Antiproliferative/viability activity of homo- and heterometallic Au(I/III)-phosphine complexes in selected cell lines.

Complex	Cytotoxicity IC_{50} [μM]			Ref
Au^{I}				
$^{(a,b)}$**Ph_3P**$Au^{I}GP^{(T-I)}$	1,7-4 (MCF-7), 18 h	26-41 (A2780), 18 h	0.67–4 (HEK 293 T), 18 h	[23]
$^{(b)}$**PPh_3**$Au^{I}(SPyCOOH)^{(T-I)}$	15.5 (MCF-7), 24 h	9.2 (MiaPaca2), 24 h	4.6 (Jurkat), 24 h	[26]
$^{(b,d)}$**PPh_3**$Au^{I}(SPyCONH\text{-}AA)^{(T-I)}$ AA = Gly, Ala, Val, Phe, Met, Pro	7.7–30.5 (MCF-7), 24 h	8.1–27.2 (MiaPaca2), 24 h	2.4–7.6 (Jurkat), 24 h	[26,43]
$^{(b,d)}$[(**PPh_3**)$_2Au^{I}_2(\mu_2$-SPyCOOH)](BF$_4$)$^{(T-III)}$	6.9 (MCF-7), 24 h	7.5 (MiaPaca2), 24 h	3.3 (Jurkat), 24 h	[26]
$^{(b)}$[(**PPh_3**)$_2Au^{I}_2(\mu_2$-SPyCONHPro)] (OTf)$^{(T-III)}$	4.1 (MCF-7), 24 h	1.2 (MiaPaca2), 24 h	0.9 (Jurkat), 24 h	[26]
PPh_3 Au^{I}(Flavenoid)$^{(T-I)}$	37.73–43.36 (PC3), 24 h			[44]
PPh_3 $Au^{I}L_x^{(T-I)}$ L_x: pz-dtc, iz-dtz	2.56–2.63 (HeLa), 48 h			[20]
[**PPh_3**Au^{I}NHC](BF$_4$)$^{(T-I)}$	5.2 (A2780), 72 h	11.2 (HEK-293 T), 72 h		[25]
$^{(b)}$**PPh_3**$Au^{I}L_x^{(T-I)}$ L_x: phen-oxadiaz-th	<0.10–1.40 (B16F10), 72 h	<0.10–1.66 (CT26.WT), 72 h		[45]
$^{(b)}$**PPh_3**$Au^{I}L_x^{(T-I)}$ Lx: alkyl-oxadiaz-th Alkyl = C_7, C_9, C_{11}, C_{13}, C_{15}	0.9–4.2 (B16F10), 72 h	3.4–5.9 (CT26.WT), 72 h		[46]
$^{(b)}$**PPh_3**$Au^{I}L_x^{(T-I)}$ Lx: alkyl-oxadiaz-th Alkyl = C_8, C_{10}, C_{12}, C_{14}, C_{16}	1.0–6.6 (B16F10), 72 h	1.4–6.2 (CT26.WT), 72 h		[46]
[**PPh_3**Au^{I}pbiH](PF$_6$)$^{(T-I)}$	1.50 (A2780S), 72 h	6.60 (A2780R), 72 h		[33]
[**PPh_3**Au^{I}pbi](PF$_6$)$^{(T-I)}$	0.6 (A2780S), 72 h	2.0 (A2780R), 72 h		[33]
[(**PPh_3**)$_2Au^{I}_2(\mu_2$-pbi)][PF$_6$]$^{(T-III)}$	0.6 (A2780S), 72 h	3.57 (A2780R), 72 h		[33]
$^{(c,d,e)}$**PPh_3**$Au^{I}L_x^{(T-I)}$ L_x: Alkinyl-chromones, Alkinyl-flavone	10–19.5 (HepG2), 24 h	5.5–13 (MCF-7), 24 h	4.2–49.7 (MDA-MB-231), 24 h	[47]
$^{(a,f,g)}$**PPh_2**(***p*-cou-Ph***)**$Au^{I}L_x^{(T-I)}$ Lx: Cl, tatgp	49.0–50.1 (MCF-7), 48 h	10.1–46.5 (MDA), 48 h	28.4–49.9 (HCT116), 48 h	[18]
PPh_2(***p*-COOH-Ph***)**$Au^{I}L_x^{(T-I)}$ L_x: tatgp	6.9 (A2780)	12.0 (A2780cisR), 72 h	11.7(HEK-293), 72 h	[22]
$^{(b,e)}$**PMe_3**$Au^{I}L_x^{(T-I)}$ L_x: DMDC, DEDC	4.87–6.79 (A549), 72 h	5.77–7.42 (HepG2), 72 h		[48]
$^{(b,e)}$**PEt_3**$Au^{I}L_x^{(T-I)}$ L_x: DMDC, DEDC	6.58–6.64 (A549), 72 h	6.91–8.35 (HepG2), 72 h		[48]
$^{(b)}$**PEt_3**$Au^{I}L_x^{(T-I)}$ L_x: phen-oxadiaz-th	<0.10–0.43 (B16F10), 72 h	<0.10–0.51 (CT26.WT), 72 h		[45]
$^{(b)}$**PEt_3**$Au^{I}L_x^{(T-I)}$ Lx: alkyl-oxadiaz-th Alkyl = C_7, C_9, C_{11}, C_{13}, C_{15}	2.2–4.8 (B16F10), 72 h	2.4–5.4 (CT26.WT), 72 h		[46]
$^{(b)}$**PEt_3**$Au^{I}L_x^{(T-I)}$ Lx: alkyl-oxadiaz-th Alkyl = C_8, C_{10}, C_{12}, C_{14}, C_{16}	0.5–12.3 (B16F10), 72 h	1.4–3.6 (CT26.WT), 72 h		[46]
$^{(b,e)}$**$P^{i}Pr_3$**$Au^{I}L_x^{(T-I)}$ L_x: DMDC	7.71 (A549), 72 h	6.21 (HepG2), 72 h		[48]
$P^{t}Bu_3$ $Au^{I}L_x^{(T-I)}$ L_x: dibenzyldithiocarbamate	96.53 (A549), 24 h	25.90 (HeLa), 24 h	93.7 (HCT15), 24 h	[29]
$^{(b)}$**P_{2b}**$Au^{I}L_x^{(T-I)}$ L_x: dimethyldithiocarbamate Diethyldithiocarbamate Dibenzyldithiocarbamate	5.8–105.3 (A549), 24 h	1.4–93.9 (HeLa), 24 h	9.5–133.1 (HCT15), 24 h	[29]
$^{(a,d)}$**$P_{2a,b,e,f}$**$Au^{I}_2(L_x)^{(T-IV)}_2$ L_x: pyethine	1.1–23.8 (MCF-7)	0.6–15.3 (HT-29)		[21]
$^{(d)}$**$P_{2c,d,h}$**$Au^{I}L_x^{(T-IV)}$ L_x: pz-dtc, iz-dtz	0.51–6.96 (HeLa), 48 h			[20]
$^{(b)}$**P_{2i}**$Au^{I}P^{t}Bu_3Cl^{(T-II)}$	0.29 (HCT 116), 48 h			[27]
$^{(b)}$**P_3**$Au^{I}L_x^{(T-I)}$ L_x: thiosemicarbazones	3.65 (Caco-2/PD7), 72 h	4.53 (Caco-2/TC7), 72 h		[40]
P_3 Au^{I}pbi$^{(T-I)}$	13.3 (A2780S), 72 h	28.8 (A2780R), 72 h		[33]
$^{(d)}$**P_3**Au^{I}(2-py-ethine)$^{(T-I)}$	19.2 (MCF-7), 24 h	51.04 (Caco-2/TC7), 24 h		[49]
$^{(b)}$**P_4**$Au^{I}L_x^{(T-I)}$ L_x: thiosemicarbazones	13.12 (Caco-2/PD7), 72 h	14.91 (Caco-2/TC7), 72 h		[40]
$^{(a,b,c)}$[**$P_{5a\text{-}f}$**Au^{I}Cl](Cl or Br)$^{(T-I)}$	4.4–14.20 (Caco-2/PD7), 72 h	0.93–11.80 (Caco-2/TC7), 72 h		[24]
$^{(a,b)}$[(**$P_{5b,d}$**)$_2Au^{I}$Cl](Br)$^{(T-I)}_2$	5.53–14.74 (Caco-2/PD7), 72 h	8.48–10.17 (Caco-2/TC7), 72 h		[24]
$^{(a,b,c)}$[**$P_{5a,b}$**$Au^{I}L_x$](Cl or Br)$^{(T-I)}$ L_x: Spy, Spyrim, SMepyrim, SMe$_2$pyrim	1.75–6.63 (Caco-2/PD7), 72 h	3.95–7.5 (Caco-2/TC7), 72 h		[24]
$^{(a,b)}$[**$P_{5c,d}$**$Au^{I}L_x$](Cl or Br)$^{(T-I)}$ L_x: Spy, Spyrim, SMepyrim, SMe$_2$pyrim	4.16–9.35 (Caco-2/PD7), 72 h	2.8–7.67 (Caco-2/TC7), 72 h		[24]
μ_2-**P_6**$[Au^{I}Cl]^{(T-III)}_2$	2.2	6.2 (HEK-293 T), 72 h		[25]
$^{(b)}$**P_{7c}**Au^{I}(SPyCONH-Ala)$^{(T-I)}$	15.7 (MCF-7), 24 h	17.4 (MiaPaca2), 24 h	3.8 (Jurkat), 24 h	[26]
$^{(b)}$**P_{7b}**$Au^{I}Cl^{(T-I)}$	38.34 (MCF-7), 24 h	53.97 (A549), 24 h	51.21 (HCT15), 24 h	[50]
[(**P_{7b}**)$_2Au^{I}$](Cl)$^{(T-I)}$	51.73 (MCF-7), 24 h	34.42 (A549), 24 h	34.19 (HCT15), 24 h	[50]
$^{(b,c)}$$\mu_2$-**$P_{11}$**$[Au^{I}(L_x)]^{(T-III)}_2$ L_x: tatgp	0.17–1.5 (A2780), 72 h	0.67–4.7 (A2780cisR), 72 h	1.2–3.3 (HEK-293), 72 h	[22]
$^{(e,g)}$**P_{13}**$Au^{I}Cl^{(T-I)}$	35.5 (MCF-7), 24 h	22.1 (HeLa), 24 h		[31]
$^{(b,e,g)}$**P_{14}**$Au^{I}Cl^{(T-I)}$	10.9 (MCF-7), 24 h	35.9 (HeLa S3), 24 h		[31]
$^{(b,e,g)}$[**P_{15}**Au^{I}tht](ClO$_4$)$^{(T-II)}$	23.9 (MCF-7), 24 h	4.2 (HeLa S3), 24 h		[31]
P_{17} $Au^{I}Cl^{(T-I)}$	0.41–0.58 (A549)			[51]
$^{(b)}$**P_{18}**$Au^{I}Cl^{(T-I)}$	70.3–76.3 (A549), 24 h			[52]
$^{(b)}$**P_{20}**$Au^{I}L_x^{(T-I)}$ L_x: Cl, tatgp	4.2–21.5 (A549), 72 h	1.6–2.9 (A2780R), 72 h	1.2–9.9 (HEK-293 T), 72 h	[39]
$^{(b)}$cyclic[(**P_{2j}**)$_3Au^{I}_3$](X)$^{(T-V)}_3$ X = OTf, PF_6	0.5–1.4 (HeLa), 24 h	0.4–0.8 (MDA-MB-231), 24 h	0.6–4.7 (DU145), 24 h	[30]
$^{(b)}$cyclic[(**P_{2k}**)$_4Au^{I}_4$](X)$^{(T-VI)}_4$ X = OTf, PF_6	2.9–3.1 (HeLa), 24 h	0.9–1.2 (MDA-MB-231), 24 h	2.8–3.9 (DU145), 24 h	[30]
Au^{III}				
$^{(b,d,g,e)}${μ_2-**$P_{2b\text{-}d,\ f\text{-}h}$**$[Au^{III}(L_x)]_2$}(OTf)$^{(T-VII)}_2$ L_x: diphenpy	0.21–5.8 (HepG2), 72 h	0.043–3.2 (HeLa), 72 h	0.17–8.8 (PLC), 72 h	[42]
[(**PPh_3**)Au^{I}(μ_3-pbi)$Au^{III}X_2$](PF$_6$)$^{(T-III+T-VII)}$ X = OAc, Cl	0.6 (A2780S), 72 h	1.25–1.5 (A2780), 72 h		[33]
Hetero-metallic				
P_{1a} $Au^{I}Cl^{(T-I)}$	>100 (A549), 72 h	68 (HepG2), 72 h		[35]
$^{(b,c)}$**P_{1a}**$Au^{I}L_x^{(T-I)}$ L_x: mena, mepu, tcyt, tura	12.6–95.1 (A549), 72 h	7.8–100 (HepG2), 72 h		[35]
P_{1b} $Au^{I}_2Cl^{(T-IV)}_2$	29.9 (A549), 72 h	29.1 (HepG2), 72 h		[35]
$^{(b,c)}$**P_{1b}**$AuI_2(L_x)^{(T-IV)}_2$ L_x: tcyt, tatgp	13.1–14.5 (A549), 72 h	11.1–12.4 (HepG2), 72 h		[35]
$^{(b,c)}$**P_{1c}**$Au^{I}Cl^{(T-I)}$	0.27–3.7 (A2780)	3.1–20.3 (A2780R)	0.94–6.8 (HEK)	[36]
$^{(f)}$[**PPh_3**$Au^{I}L_xRe^{I}$(bipy)$(CO)_3$](OTf)$^{(T-I)}$ L_x: pyethine, Im	4.4–19 (A549), 24 h			[37]
$^{(b,c)}$[(**$P_3Au^{I}L_x$**)$_2Cu^{I}$](PF$_6$)$^{(T-I)}$ L_x: thiosemicarbazones	20 nM (Caco-2/PD7), 72 h	0.03 (Caco-2/TC7), 72 h		[40]
$^{(b,c)}$[(**$P_3Au^{I}L_x$**)$_2Cu^{I}$](PF$_6$)$^{(T-I)}$ L_x: thiosemicarbazones	20 nM(Caco-2/PD7), 72 h	0.03(Caco-2/TC7), 72 h		[40]

(*continued on next page*)

Table 1 (*continued*)

Complex	Cytotoxicity IC_{50} [μM]			Ref
$^{(b,c)}$[(**PPh_3**$Au^I L_x Cu^I$**PPh_3P_3**](**NO_3**)$^{(T-I)}$ L_x: thiosemicarbazones	0.47 (Caco-2/PD7), 72 h	0.6 (Caco-2/TC7), 72 h		[40]
$^{(b,c)}$[(**PPh_3**$Au^I L_x Cu^I$**PPh_3P_4**](**NO_3**)$^{(T-I)}$ L_x: thiosemicarbazones	1.17 (Caco-2/PD7), 72 h	3.4 nM (Caco-2/TC7), 72 h		[40]
$^{(b,f)}$[**P_9**$Au^I L_x$](**Cl_2**)$^{(T-I)}$ L_x: tatgp	26.5 (A549), 72 h	6.4 (A2780R), 72 h	2.7 (A2780S), 72 h	[38]
$^{(b,f)}$[**P_{10}**$Au^I L_x$](**Cl_2**)$^{(T-I)}$ L_x: tatgp	5.7 (A549), 72 h	3.1 (A2780R), 72 h	1.4 (A2780S), 72 h	[38]

a) ligand is cytotoxic; b) more active than cisplatin; c) more active than auranofin; d) enzyme inhibition; e) DNA interaction; f) luminescent; g) *in vivo* studies; h) ex vivo studies. T-X (X = I-VII) indicates the type of structure depicted in Fig. 4. GP = Glyco polymer, bipy = 2,2′-bipyridyl, mena = 2-mercaptonicotinic acid, mepu = 2-mercaptopurine, tcyt = 2-thiocytosine, tura = 2-thiouracil, tatgp = 2,3,4,6-tetra-6-acetyl-1-thiol-β-D-glucopyranosato, pyethine = pyridylethin, Im = imidazole, AA = Amino acid. pz-dtc = pyrazol-1-yl-based dithiocarbamate, iz-dtc = indazol-1-yl-based dithiocarbamate, dmbpy = dimethylbipyridine, tht = tetrahydrothiophen. 3-carboxyph-dmpz = (3-carboxyphenyl)bis(3,5-dimethylpyrazolyl), phen-oxadiaz-th = 5-phenyl-1,3,4-oxadiazole-2-thione, DMDC = Dimethyldithiocarbamate, DEDC = Diethyldithiocarbamate, pbiH = 2-(2′-pyridyl)benzimidazole.

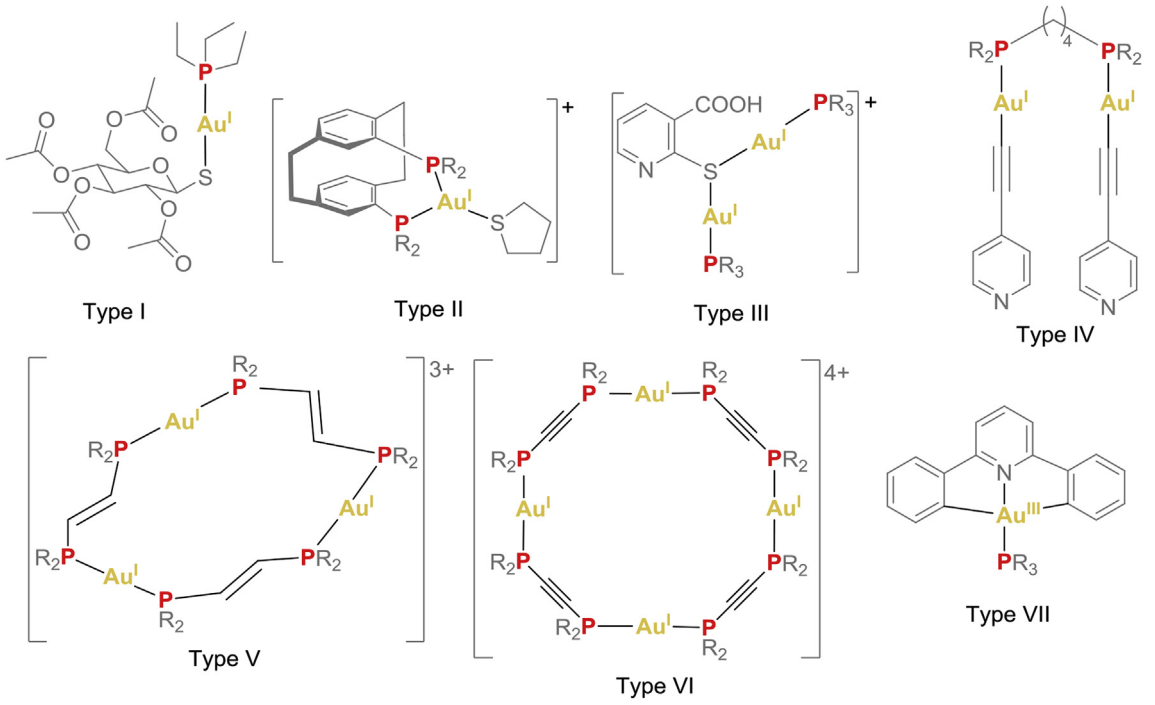

Fig. 4. Some examples of gold phosphine complexes defining seven different structure types: Type I linear, Type II chelating ligand and mononuclear [31], Type III dinuclear with bridging ligand [26], Type IV chelating ligand and dinuclear [21] (with two chelating ligands for example in bis(NHC)-complexes: dinuclear metallacycle) [41], Type V trinuclear metallacycle [30], Type VI tetranuclear metallacycle [30], Type VII Gold (III) square planar [42]. The gold atoms are highlighted in yellow and the phosphorus atoms in red. (For interpretation of the references to colour in this figure legend, the reader is referred to the Web version of this article.)

silver(I)-complexes are the most studied metallodrugs in the treatment of bacterial infections [65–68]. Although a great variety of silver(I)-based anti-bacterial complexes have been reported, bacterial resistance is still a big issue to overcome. Bacterial resistance may have different origins induced by various cellular mechanisms like efflux pumps, target modification, inactivation by enzymes and in the presence of bacterial biofilms [69]. Metallodrugs are known to act as anti-biofilm agents, since metal cations can be incorporated into the matrix of biofilms and consequently hinder their formation.

In the case of gold, $K[Au(CN)_2]$ has been introduced at the end of the 19th century as anti-microbial drug exhibiting activity against *Mycobacterium tuberculosis* [5]. Consequently, gold (I/III)-based metallodrugs with various ligand systems have been reported with potential anti-microbial activity, which have been recently reviewed by Djuran et al. [5] Several gold(I)-phosphine complexes with additional amino-type ligands used as anti-microbial metallodrugs have been patented in 2015 [70]. After 2015, only a few examples of new gold-based phosphine complexes with anti-microbial activity were reported. Sanchez-Puelles et al. have synthesized six auranofin derivatives bearing **PEt_3** and different thiol-containing ligands on *trans*-position replacing the thio-glucopyranosato reaching MIC_{50} (MIC = Minimum inhibitory Concentration) of 0.12–0.42 μM in *Staphylococcus pneumonia* D39 [71]. De Almeida et al. have combined **PEt_3** with 1,3,4-oxadiazol-2-thione and 1,3-thiazolidine-2-thione moieties with different alkyl chain lengths (from *n*-heptyl to *n*-hexadecyl) [46]. The high lipophilicity of these gold(I) complexes led to anti-microbial activity with MIC_{50}-values amounting to 0.2–23.1 μM (*Staphylococcus aureus*), 0.1–23.1 μM (*Staphylococcus epidermidis*) and 7.8–26.8 μM (*Escherichia coli*). These MIC-values are higher than the metal-free antibiotic Chloramphenicol. The linear gold(I) complex bearing **PPh_3** moieties delivered MIC_{50}-values of 2.6–19.1 μM (*Staphylococcus aureus*) and 2.6–19.1 (*Staphylococcus epidermidis*) showing higher activity than the antibiotic as well. Further gold(I)-**PPh_3** complexes with alkynyl-chromone and alkynyl-flavone ligands on *trans*-position have been published with MIC_{50}-values in the range of 4–32 μM in *Staphylococcus aureus* [47].

In the case of NHC ligands, gold(I)-based metallodrugs with anti-bacterial activity have been reported in the last 3 years (Fig. 6).

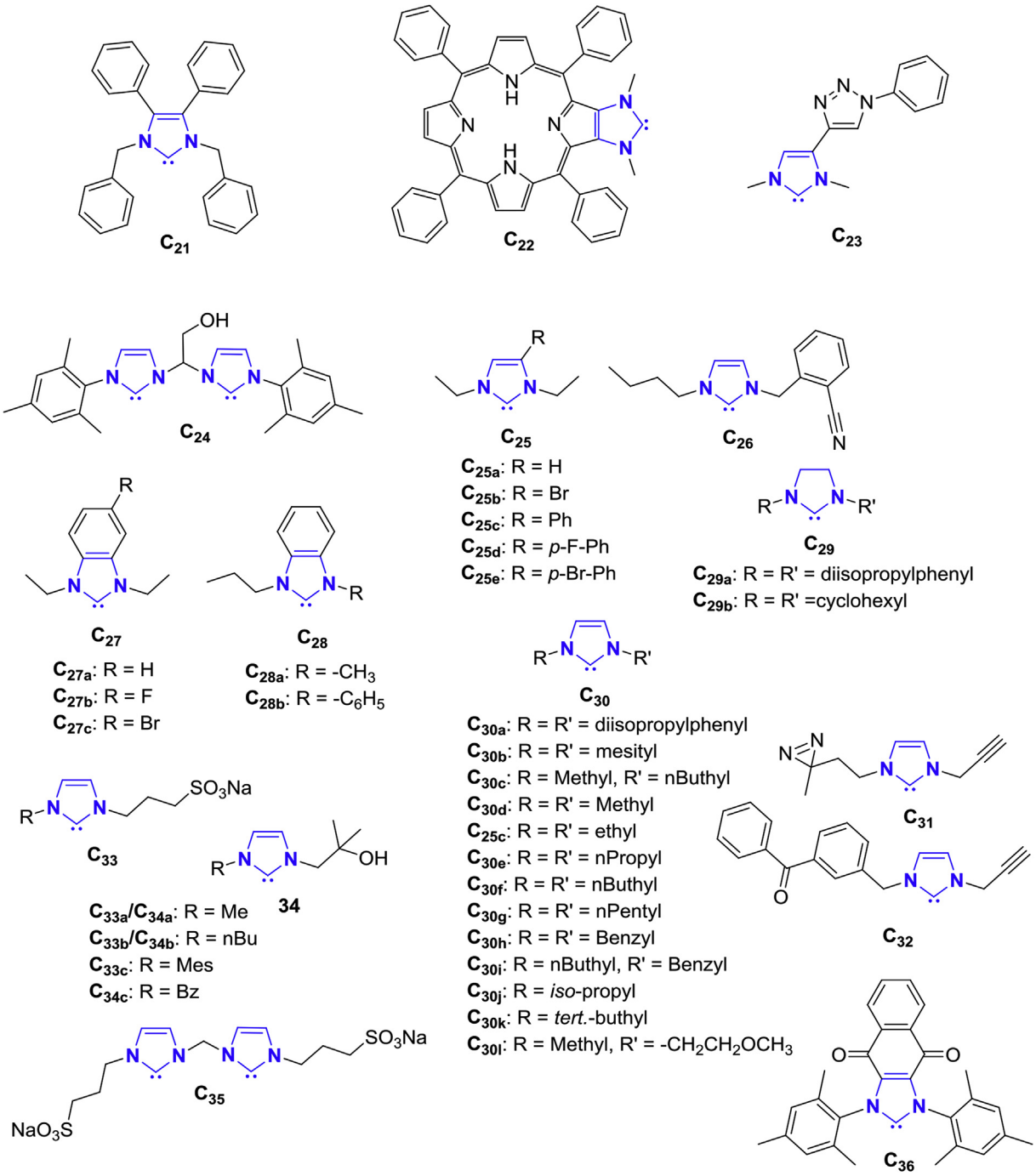

Fig. 5. NHC ligands being reported 2016 and 2017 in gold-based complexes with anti-cancer activity. NHCs are highlighted in blue. (For interpretation of the references to colour in this figure legend, the reader is referred to the Web version of this article.)

The corresponding anti-bacterial activity is shown in Table 3. The series of ligand **C_{30}** being active against *Helicobacter pylori* with MIC-values in the range between 2.0 μM and 15.3 μM [72]. The two most active gold(I) NHC complexes against *Helicobacter pylori* bear the NHC moieties **C_{30k}** and the caffeine derivative **C_{37}**. No higher activity was observed by changing the chloro with the thio-glucopyranosato on *trans*-position.

By replacing the chloro-ligand with hormone derivatives (ethynylestradiol, ethiosterone) the anti-bacterial activity against *S. aureus* and *E. coli* could be drastically enhanced and additionally relevant results *in vivo* could be obtained [73]. Schmidt et al. have varied the lipophilicity of the NHC ligands **C_{25}** on the backbone-position and **C_{25c}** with a phenyl-group resulted to be the most active complex [55]. The introduction of halide substituted phenyl-groups decreased the activity. The benzimidazolydene moieties **C_{27}** have confirmed this observation, since the non-modified species have been the most active [56]. However, the corresponding cation complexes additionally exhibit very promising cytotoxic activities. All gold complexes bearing the NHC moieties (s. Fig. 6) are summarized in Table 3 with their activity against diverse bacteria. Also in this table, additional information such as the comparison with reference compounds, *in vivo* tests and cytotoxicity in human cells are highlighted with letters on the chemical structures.

Table 2
Antiproliferative/viability of homo- and heterometallic Au(I/III)-NHC complexes in selected cell lines.

Complex	Cytotoxicity IC_{50} [μM]			Ref
Au^{I}				
C_{21} $Au^{I}L_x^{(T-I)}$ L_x: Cyclohexanethiolate, Thiocyanate, Azide	0.47–1.74 m (MCF-7)	0.37–1.82 (SN12C)	0.29–1.95 (COLO 205)	[53]
C_{23} $Au^{I}Cl^{(T-I)}$	6.4 (HCT116)	7 (MCF-7)	6 (PC3)	[54]
$[(\mathbf{C_{24}})_2Au^{I}_2](PF_6)_2^{(T-IV)}$	42.2 (A549)	14.9 (HepG2)		[41]
$^{(c,d)}[(\mathbf{C_{25a\text{-}c,e}})_2Au^{I}](I)^{(T-I)}$	0.14–5.54 (HT-29)	0.06–4.20 (MCF-7)	0.05–3.44 (RC-124)	[55]
$^{(c,d)}$**$C_{25a\text{-}e}$**$Au^{I}Cl^{(T-I)}$	6.14–16.97 (HT-29)	4.73–11.25 (MCF-7)	4.46–10.58 (RC-124)	[55,56]
$^{(c,d)}$**C_{27a}**$Au^{I}Cl^{(T-I)}$	11.15–11.71 (HT-29)	6.68–9.05 (MCF-7)	5.07–11.48 (RC-124)	[56]
$^{(a)}[(\mathbf{C_{28a,b}})_2Au^{I}]Cl^{(T-I)}$	23.4–49.9(HCT 116), 72 h	7.3–7.6 (MCF-7), 72 h	5.6–126.3(PC3), 72 h	[57]
$C_{29a,b}$ Au^{I}(Hmba)$^{(T-I)}$	65.1–66.3 (PC3), 72 h	59.9–74.8 (DU145), 72 h	81.4–88.9 (Caki-1), 72 h	[58]
$C_{30a,b}Au^{I}$(Hmba)$^{(T-I)}$	57.1–70.4 (PC3), 72 h	60.9–67.6 (DU145), 72 h	79.2–97.2 (Caki-1), 72 h	[58]
$^{(b,c,h)}$**C_{30c}**$Au^{I}L_x^{(T-I)}$	0.8–6 (MCF-7), 72 h			[59]
L_x: Cl, tatgp, ^{t}Bu-ethinyl				
$^{(b,c,h)}[(\mathbf{C_{30c}})_2Au^{I}](PF_6)^{(T-I)}$	2 (MCF-7), 72 h			[59]
$^{(a)}$**C_{36}**$Au^{I}Cl^{(T-I)}$	12.1 (A549)			[62]
$^{(a,c)}[(\mathbf{C_{36}})2Au^{I}](Cl)^{(T-I)}$	75 nM (A549)			[62]
$^{(a,c,e)}[(\mathbf{C_{36}})2Au^{I}](AgCl_2)^{(T-I)}$	73 nM (A549)	26 nM (A2780)	96 nM (PC3)	[62]
AuIII				
C_{26} $Au^{III}Cl_3^{(T-VII)}$	50 nM (HCT 116), 72 h	0.3 nM (MCF-7), 72 h	0.3 nM (PC3), 72 h	[57]
$^{(b,e)}$**[$C_{25a,\ 30d\text{-}i}$**Au^{III}(diphenpy)](OTf)$^{(T-VII)}$	0.36–2.04 (HeLa), 72 h	0.20–4.4 (HCT 116), 72 h		[63]
$^{(b,e)}$**[C_{31}**Au^{III}(diphenpy)](OTf)$^{(T-VII)}$	0.19 (HeLa), 72 h	0.43 (HCT 116), 72 h		[63]
$^{(b,e)}$**[C_{32}**Au^{III}(diphenpy)](OTf)$^{(T-VII)}$	0.67 (HeLa), 72 h	0.68 (HCT 116), 72 h		[63]
Hetero-metallic				
$^{(d)}$**$C_{29a,b}$**Au^{I}(mba)$Ti^{IV}MeCp_2^{(T-I)}$	9.8–11.8 (PC3), 72 h	11.8–16.7 (DU145), 72 h	21.0–42.9 (Caki-1), 72 h	[58]
$^{(d)}$**$C_{30a,b}$**Au^{I}(mba)$Ti^{IV}MeCp_2^{(T-I)}$	10.3–17.1 (PC3), 72 h	13.8–18.9 (DU145), 72 h	29.1–51.5 (Caki-1), 72 h	[58]
$[(\mathbf{C_{38}})_2Au^{I}](BF_4)^{(T-I)}$	0.14 (Hela), 72 h			[64]
$[(\mathbf{C_{38}})_2Au^{I}](BF_4)^{(T-I)}$	0.23 (Hela), 72 h			[64]

a) ligand is cytotoxic, b) more active than cisplatin, c) more active than auranofin, d) enzyme inhibition, e) DNA interaction, f) luminescent, g) *in vivo* studies, h) ex vivo studies. T-X (X = I-VII) indicates the type of structure depicted in Fig. 4. Hmba = 4-mercaptobenzoic acid (as thiolate), mba = 4-mercaptobenzoic acid (as thiolate and carboxylate).

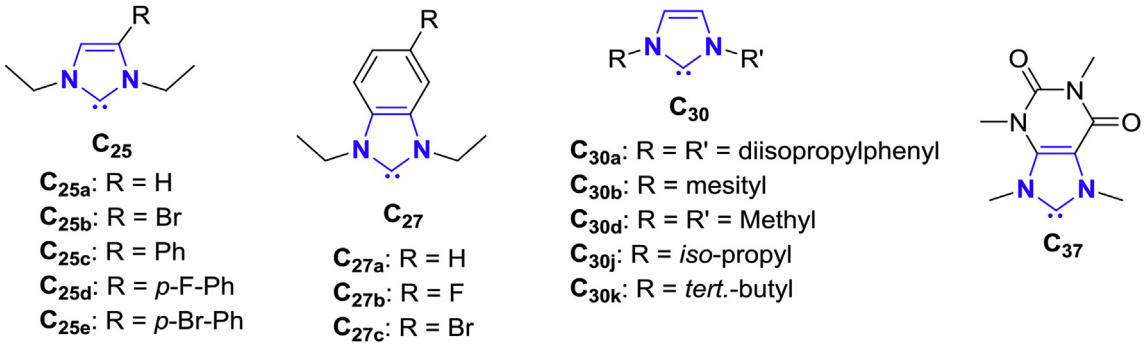

Fig. 6. NHC ligands being reported from 2015 until 2017 in gold-based complexes with anti-bacterial activity. NHCs are highlighted in blue. (For interpretation of the references to colour in this figure legend, the reader is referred to the Web version of this article.)

Table 3
Anti-bacterial activity of some homo-metallic Au(I)-NHC complexes.

Complex	Minimum Inhibitory Concentration MIC_{50} [μM]			IC_{50} [μM]	Ref
C_{30a} $Au^{I}Cl^{(T-I)}$	15.3 (*H. pylori*)			40.7 (HEK 293 T)	[72]
C_{30b} $Au^{I}L_x^{(T-I)}$ L_x: Cl, tatgp	4.6–6.0 (*H. pylori*)			26.4–36.1 (HEK 293 T)	[72]
C_{30j} $Au^{I}L_x^{(T-I)}$ L_x: Cl, tatgp	4.5–4.6 (*H. pylori*)			29.2–37.4 (HEK 293 T)	[72]
C_{30k} $Au^{I}L_x^{(T-I)}$ L_x: Cl, tatgp	2.0 (*H. pylori*)			20.7–50.2 (HEK 293 T)	[72]
C_{37} $Au^{I}L_x^{(T-I)}$ L_x: Cl, tatgp	2.0 (*H. pylori*)			30.2–58.0 (HEK 293 T)	[72]
$^{(b)}[(\mathbf{C_{25a\text{-}c,\ e}})_2Au^{I}](I)^{(T-I)}$	2.3–16.6 (*MRSA RKI*)	1.7–79 (*MRSA DSM*)	8.7–70 (*E. faecium*)		[55]
$^{(a,b)}$**$C_{25a\text{-}e}$**$Au^{I}Cl^{(T-I)}$	0.64–6.28 (*MRSA RKI*)	0.64–7.3 (*MRSA RKI*)	2.97–12.51 (*E. faecium*)		[56]
$^{(a,b)}$**$C_{27a\text{-}c}$**$Au^{I}Cl^{(T-I)}$	1.03–3.13 (*MRSA RKI*)	1.94–4.16, (*MRSA RKI*)	4.8–8.34 m (*E. faecium*)		[56]
$^{(c)}$**C_{30d}**$Au^{I}L_x^{(T-I)}$ Lx: Cl, ethinylestradiolm Ethisterone	7.02–115 (*S. aureus*)	1.17–75 (*E. coli*)			[73]
$^{(c)}$**C_{30d}**$Au^{I}L_x^{(T-I)}$ Lx: Cl, ethinylestradiol ethister one	7.02–129 (*S. aureus*)	4.68–9.37 (*E. coli*)			[73]

Additional information are labelled with following letters: (a) more toxic than auranofin, (b) more toxic than metal-free antibiotic, (c) *in vivo* tests. T-X (X = I-VII) indicates the type of structure depicted in Fig. 4. MRSA RKI and MRSA DSM = methicillin resistant *Staphylococcus aureus*, E. faecium = Enterococcus faecium.

4. Treatment of parasitic infections

Parasitic infections are classified to be within the top diseases worldwide, especially in tropical countries [74]. Thereby, malaria, trypanosomiasis and leishmaniasis represent the three major lethal protozoa illnesses. Similar to anti-bacterial compounds, issues such as drug resistance and low effectiveness are currently hindering the development of highly active anti-parasitic compounds. Although

the enhancement of activity *via* metal-drug synergism is well known, the field of metal-based anti-parasitic drugs has been poorly explored. Nowadays, metal salts based on antimony (leishmaniasis) and bismuth (malaria) were still used as clinical anti-parasitic drugs. Very promising metallodrugs are ferrocene derivates such as ferroquine and ferrocifen, being both in clinical phase II and preclinical studies, respectively [75]. Also gold has attracted the attention of several research groups and various gold-based complexes have been introduced [5,76]. Gold is presumed to have a similar mechanism of action as antimony (III/V) acting as trypanothione reductases inhibitor (TyrR) of *Leishmania* parasites, which in mammals is not present as selenol-proteins as in TrxR in cancer cell, but consist of several cysteine residues [45]. In this work it is intended to update a review by Djuran et al., summarizing all phosphine- and NHC-based gold complexes used as anti-malaria, anti-leishmanial and anti-trypanosomial compounds [5]. In the last three years, only a limited number of phosphine gold complexes has been newly reported. Chaves et al. reported **PEt_3**Au(I) and **PPh_3**Au(I) derivates with 5-phenyl-1,3,4-oxadiazole-2-thione on *trans*-position being tested against *Leishmania infantum* and *Leishmania braziliensis*, showing IC_{50} values in the range of 2.7–6.9 μM and 5.7–10.6 μM, respectively. The *para*-position of the phenyl ring was modified with different functional groups whereas the unsubstituted moiety exhibited the best results. The Au(I) complexes with **PEt_3** as phosphine ligand displays higher activity than those with **PPh_3**. Nevertheless, all these complexes are less active than the metal-free based amphotericin B [45].

Also in the field of anti-parasitic agents, more examples with NHC moieties have been reported in the past years, which are depicted in Fig. 7. Hemmert et al. have introduced several mono- and dinuclear cationic gold(I) and gold (III) complexes bearing the ligand systems **C_{40}**, **C_{41}**, **C_{42}** and **C_{44}** with anti-malarial activity against chloroquine resistant *Plasmodium falciparum* [77]. The activity seems to be independent of the oxidation state and of the number of gold nuclei. The presence of phenyl- and pyridine-groups and quinoline deliver the best activities. Thus, also in the field of anti-malarial metallodrugs lipophilicity plays a decisive role. However, it has to be taken into consideration that the corresponding imidazolium salts are toxic themselves. The same group has described neutral and cationic gold(I) complexes with **C_{41}** and **C_{42}** and tested them against *Leishmania infantum* [78]. Thereby, the neutral complex with a low degree of lipophilicity has shown the most attractive activity. Nolan et al. have synthesized 10 neutral gold(I) complexes bearing the NHC moieties **C_{43}**. This group varied different ligands on *trans*-position and different substituent on both, the wingtip- and backbone-positions, reaching activities in the range of 5.3 μM–17.3 μM [79]. These concentration values were lower than metal-free antibiotics used against the parasite *Leishmania major*. Higher activities (4.6 μM-5.2 μM) were obtained by testing the imidazolium salt of **C_{25a}** with $[Au^{I}Cl_2]^-$ and $[Au^{III}Cl_4]^-$ as counter-anions. The best results (3.1 μM) were obtained after using the dinuclear Au(I) complex with both nuclei bearing the NHC ligand **C_{25a}** and being connected by a hydroxy-bridge.

The hetero-metallic gold(I)-iron (II) complex with **C_{38}** and the homo-metallic gold(I) complexes with **C_{39}** lead to anti-trypanocidal activities in the lower nanomolar range [64]. The corresponding Au-complexes of all NHC moieties depicted in Fig. 7 and their anti-parasitic activities are summarized in Table 4.

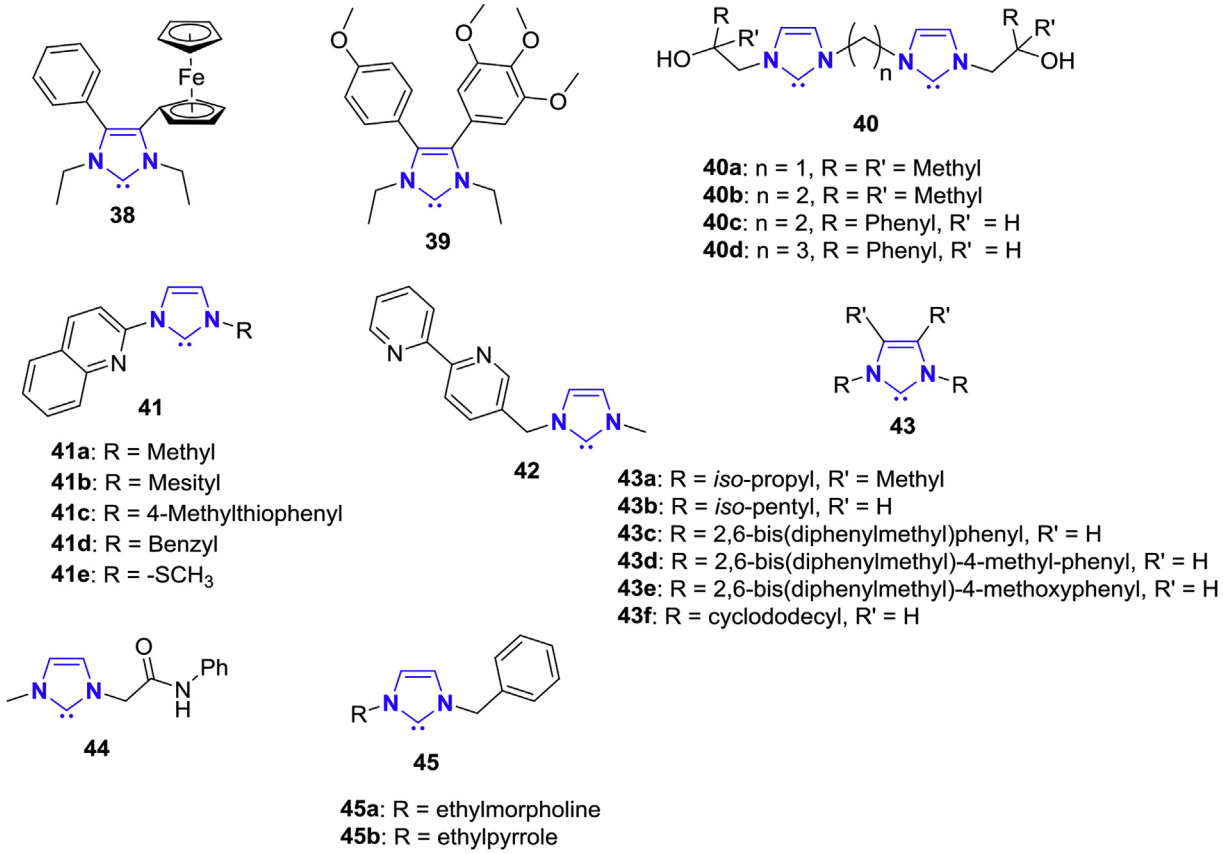

Fig. 7. NHC ligands being reported from 2015 until 2017 in gold-based complexes with anti-parasitic activity. NHCs are highlighted in blue. (For interpretation of the references to colour in this figure legend, the reader is referred to the Web version of this article.)

Table 4
Anti-parasitic activity of relevant homo- and hetero-metallic Au(I/III)-NHC complexes.

Complex	IC_{50}-values[μM]		Ref
Anti-Malaria			
[a][(**C40a,b**)$_2$Au$^I_2$](PF$_6$)$_2^{(T-IV)}$	>39 μM *P. falciparum*		[77]
[a][(**C40c**)$_2$Au$^I_2$](PF$_6$)$_2^{(T-IV)}$	15 μMP. *falciparum*		[77]
[a][(**C40d**)$_2$Au$^I_2$](PF$_6$)$_2^{(T-IV)}$	>33 μM *P. falciparum*		[77]
[a][(**C40a**)$_2$(Au^{III}Br$_2$)$_2$](PF$_6$)$^{(T-IV)}$	30 μM *P. falciparum*		[77]
[a][(**C40c**)$_2$(Au^{III}Br$_2$)$_2$](PF$_6$)$^{(T-IV)}$	9 μM *P. falciparum*		[77]
[a][(**C40d**)$_2$(Au^{III}Br$_2$)$_2$](PF$_6$)$^{(T-IV)}$	13 μM *P. falciparum*		[77]
[(**C44**)$_2$Au^I](Cl)$^{(T-I)}$	>15 μM *P. falciparum*		[77]
[(**C41a**)$_2$Au^I](PF$_6$)$^{(T-I)}$	1.1 μM *P. falciparum*		[77]
[(**C42**)$_2$Au^I](PF$_6$)$^{(T-I)}$	0.33 μM *P. falciparum*		[77]
Anti-leishmaniasis			
[a,c]**C41a**Au^{I}Cl$^{(T-I)}$	0.39 μM$^{(d)}$ *L. infantum*$^{(Pro)}$	0.40 μM$^{(d)}$ *L. infantum*$^{(Ama)}$	[78]
[a,c][(**C41a**)$_2$Au^I](PF$_6$)$^{(T-I)}$	1.53 μM$^{(d)}$ *L. infantum*$^{(Pro)}$	0.96 μM$^{(d)}$ *L. infantum*$^{(Ama)}$	[78]
[a,c][(**C41b**)$_2$Au^I](PF$_6$)$^{(T-I)}$	0.42 μM *L. infantum*$^{(Pro)}$	- *L. infantum*$^{(Ama)}$	[78]
[a,c][(**C41c**)$_2$Au^I](PF$_6$)$^{(T-I)}$	0.43 μM$^{(d)}$ L. infantum$^{(Pro)}$	0.24 μM$^{(d)}$ *L. infantum*$^{(Ama)}$	[78]
[c][(**C42**)$_2$Au^I](PF$_6$)$^{(T-I)}$	1.86 μM$^{(d)}$ *L. infantum*$^{(Pro)}$	- *L. infantum*$^{(Ama)}$	[78]
[c]**C25a**Au^{I}L$_x^{(T-I)}$ L$_x$: Cl, OH, OAc, CH_2COCH_3	5.4–8.9 μM *L. major*		[80]
C43c Au^{I}Cl$^{(T-I)}$	17.25 μM *L. major*		[80]
[c]**C30k**Au^{I}Cl$^{(T-I)}$	8.38 μM *L. major*		[80]
[(**C25a**)Au$^I_2$(μ$_2$-OH)](BF$_4$)$^{(T-III)}$	3.29 μM *L. major*		[80]
[c][**H-C25a**][Au^{I}Cl$_2$]	5.19 μM *L. major*		[80]
[c][**H-C25a**][Au^{III}Cl$_4$]	4.60 μM *L. major*		[80]
[c]**C41b**Au^{I}Cl$^{(T-I)}$	4.68 μM *L. infantum*$^{(Pro)}$	0.68 μM$^{(d)}$ *L. infantum*$^{(Ama)}$	[81]
[c]**C41d**Au^{I}Cl$^{(T-I)}$	11.16 μM *L. infantum*$^{(Pro)}$	1.17 μM$^{(d)}$ *L. infantum*$^{(Ama)}$	[81]
[c]**C41e**Au^{I}Cl$^{(T-I)}$	8.27 μM *L. infantum*$^{(Pro)}$	0.73 μM$^{(d)}$ *L. infantum*$^{(Ama)}$	[81]
[c]**C45a**Au^{I}Cl$^{(T-I)}$	57.03 μM *L. infantum*$^{(Pro)}$	11.07 μM$^{(d)}$ *L. infantum*$^{(Ama)}$	[81]
[c]**C45b**Au^{I}Cl$^{(T-I)}$	10.32 μM *L. infantum*$^{(Pro)}$	2.17 μM$^{(d)}$ *L. infantum*$^{(Ama)}$	[81]
Anti-tryposomasis			
[(**C38**)$_2$Au^I](BF$_4$)$^{(T-I)}$	0.93 nM$^{(d)}$ *T. brucei*, 72 h		[64]
[(**C39**)$_2$Au^I](BF$_4$)$^{(T-I)}$	3.01 nM$^{(d)}$ *T. brucei*, 72 h		[64]

(a) ligand is toxic, (b) more toxic than metal-free reference compounds Artemisinin and chloroquine (c) Amphotericin B, Miltefosine and Pentamidine, (d) selectivity index between cytotoxicity and anti-parasitic <1.0. T-X (X = I-VII) indicates the type of structure depicted in Fig. 4. Pro = Promastigotes, Ama = Amastigotes, T. brucei = Trypanosoma brucei.

5. Treatment of viral infections

Gold-based complexes have also been explored as inhibitors of human immunodeficiency virus (HIV)-related enzymes [82,83]. Fig. 8 shows different phosphine- and NHC-type ligands used in gold complexes, which were tested as anti-HIV agents.

Meyer et al. reported new [**PR$_3$**Au^{I}Cl] complexes (PR$_3$ = **P46**, **P47**, **P48**, and **P50c**) that inhibit HIV-1 reverse transcriptase (RT) in the range of 50–96% at a concentration between 25 μM and 250 μM [82]. The complexes with **P49**, **P50a** and **P50b** exhibit similar inhibition potential at lower concentration of 6.25 μM. This enzyme is only present in viruses and is used to convert RNA strains into DNA. Additional inhibition of HIV-1 PR (protease) is observed for complexes [**P49**Au^{I}Cl], [(**P50a**)$_2$Au^I](Cl), [**P4**Au^I(tatgp)] and [(**P5g**Au^I-tatgp)] in the range of 50% and 75%. The pure ligand systems are not active confirming the anti-viral activity of gold [82]. Farrell et al. evaluated the replacement of zinc(II) in HIV-1 NCP7 zinc finger by gold(I) using [**PPh$_3$**Au^{I}L$_x$] moieties with amino-based ligands on *trans*-position. HIV-1 NCP7 zinc finger produces nucleocapsid proteins, which envelope the virus in order to interact with the cell and finally to help to invade the host cell. Using mass spectrometry and ^{31}P NMR spectroscopy the formation of both species, [**PPh$_3$**Au^I(NCP7)] and [Au^I(NCP7)], could be confirmed, showing long life stability. As the thiol-groups of the cysteine residues of this zinc finger are extremely nucleophilic, this enzyme could be a very attractive target for gold-based anti-HIV metallodrugs [84]. Thereby, the main focus was set on using weaker binding ancillary ligands than phosphines. The same group investigated in more more detail the mode of action and the influence of both the cone angle of phosphines and the selection of ancillary ligand on *trans*-position [85]. Several phosphine-based complexes [**PEt$_3$**Au^{I}Cl], [**PEt$_3$**Au^I(dmap)] (dmap = dimethylpyrolydine) and analogue complexes with **PCy$_3$** (Cy = Cyclohexyl) were used showing that in the case of **PCy$_3$** with a high cone angle (170°) the intramolecular interaction processes of the biomolecule are hindered. The cleaved ancillary ligand shows interaction with tryptophan residues of the protein *via* π-π-stacking processes. The dinuclear gold(I) complex [**C51**(Au^{I}Cl)$_2$] of type IV, stabilized by the bidentate chelating NHC ligand **C51**, was reported to inhibit (ca. 80%) HIV-1 infected MTC4 cells *via* interaction with enveloping HIV-1 proteins [86].

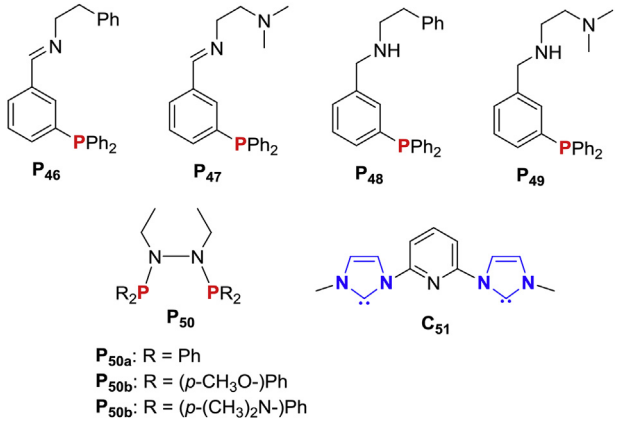

Fig. 8. Phosphine and NHC ligands being reported in gold-based complexes with anti-HIV-1 activity. Phosphorus atoms are highlighted in red and NHCs in blue. (For interpretation of the references to colour in this figure legend, the reader is referred to the Web version of this article.)

6. Conclusion and outlook

This review presents an update on phosphine- and NHC-based gold complexes potentially useful as anti-cancer, anti-bacterial, anti-parasitic and anti-viral metallodrugs. Thus, complexes being published within the last five years or after the last reviews were organized according to their corresponding activities and compared with metal-based or non-metal-containing reference compounds. Additionally, information about mechanism of action, luminescence properties and biological activity are highlighted. It is still difficult to establish a direct correlation between structural parameters of the complexes and their biological activity, for example in cancer cells. Nevertheless, upon comparison among the different ligand moieties used to prepare metal complexes potentially useful as anti-cancer, some trend could be recognized from repeated observations, which might be applicable for both phosphines and NHCs.

(i) A certain balance between hydrophilic and lipophilic character is demanded. However, the lipophilicity is more pivotal than the presence of functional groups. Phenyl, mesityl, pyridine-groups or derivatives on wingtip- or backbone-position of NHC ligands or as additional ligands in the first coordination sphere of gold are very attractive. However, the size of lipophilic substituents is limited, otherwise the ligand itself exhibits cytotoxicity and no influence of the gold nucleus is observed. This concerns more directly NHC ligands, since several examples of phosphine ligands are already known to be cytotoxic. Good balances could be reached by attachment of lipophilic substituents on functional groups like amines, alcohols- or carboxy groups *via* esterification or amidation. However, it should be taken into consideration that ester bonds are hydrolyzed by esterases present in biological systems. Therefore, amidation is more adequate and some post-modification such as the coupling of certain target-specific peptide sequences could be planned for higher selectivity by targeting highly expressed receptors on tumor cells.

(ii) Multidentate ligands present promising results *in vitro* and *in vivo*. The resulting mono- or multinuclear complexes appear to be more stable and in some cases a different coordination of thiol-containing molecules has been observed without dissociation of the ligand. The extension of the bridging alkyl-chain improves the activity of gold complexes bearing phosphine moieties. For both ligand systems, aromatic bridging compounds (like cyclophane) positively affect the cytotoxicity and selectivity. In the most cases, chelating ligand moieties deliver stable metallacycles with high cytotoxicity and even more interesting with high selectivity towards cancer cells.

(iii) The number of gold nuclei seems to have a small but significant effect on the cytotoxicity and a higher number of gold atoms seems to be more favorable. However, it should be taken into consideration that the activity is not proportionally increasing with the increasing number of gold nuclei.

(iv) Both neutral or cationic complexes are equally active and no trend can be pointed out so far.

(v) The synthesis of hetero-metallic complexes is extremely advantageous, since a synergism between both anti-cancer metals leads to multiple targeting metallodrugs with very low drug resistance. Additionally, some examples of hetero-metallic complexes have shown to be much more cytotoxic in human cancer cells compared to the homo-metallic analogues reaching IC_{50}-values in the nanomolar range.

The low number of examples of gold complexes published in the field of anti-bacterial and anti-parasitic metallodrugs does not yet allow to find a trend in ligand design. It seems, however, that high lipophilicity is advantageous.

More interesting is the utilization of gold complexes as anti-viral drug with inhibition activity against the HIV-1 virus. Since gold exhibits a high affinity towards thiol (cysteine) or selenol groups (selenocysteine), this behavior is very useful for targeting certain enzymes of this virus. The very small number of examples available so far have shown that phosphine ligands with big cone angles are favored, since after the intercalation of the drug several intramolecular interactions within the proteins can be interrupted. Additionally, the presence of highly lipophilic groups enables better interaction of the drug with proteins. In the case of NHC ligands, the pyridine-bridged bidentate ligand leads to a gold(I) complex in a metallacycle fashion with good inhibition activity of enveloping viral proteins. The very successful use of cyclic compounds against HIV-1 is literature-known [87].

Acknowledgments

B. Dominelli acknowledges financial support by the TUM Graduate School. J. D. G. Correia gratefully acknowledges support from the Fundação para a Ciência e a Tecnologia through the UID/Multi/04349/2013 project as well as from the Technische Universität München through an August-Wilhelm Scheer Visiting Professorship.

References

[1] Z.H. Siddik, Oncogene 22 (2003) 7265–7279.
[2] L. Kelland, Nat. Rev. Canc. 7 (2007) 573–584.
[3] R.A. Sanchez-Delgado, A. Anzellotti, Mini rev. Med. Chem. 4 (2004) 23–30.
[4] B. Bertrand, A. Casini, Dalton Trans. 43 (2014) 4209–4219.
[5] B.D. Glisic, M.I. Djuran, Dalton Trans. 43 (2014) 5950–5969.
[6] T. Zou, C.T. Lum, C.-N. Lok, J.-J. Zhang, C.-M. Che, Chem. Soc. Rev. 44 (2015) 8786–8801.
[7] E.R.T. Tiekink, Crit. Rev. Oncol.-Hematol. 42 (2002) 225–248.
[8] W.K. Liu, R. Gust, Coord. Chem. Rev. 329 (2016) 191–213.
[9] W.A. Herrmann, Angew. Chem. Int. Ed. 41 (2002) 1290–1309.
[10] M.N. Hopkinson, C. Richter, M. Schedler, F. Glorius, Nature 510 (2014) 485–496.
[11] I. Ott, R. Gust, Arch. Pharm. (Weinheim) 340 (2007) 117–126.
[12] W.K. Liu, R. Gust, Chem. Soc. Rev. 42 (2013) 755–773.
[13] A. Bindoli, M.P. Rigobello, G. Scutari, C. Gabbiani, A. Casini, L. Messori, Coord. Chem. Rev. 253 (2009) 1692–1707.
[14] V. Gandin, A.P. Fernandes, M.P. Rigobello, B. Dani, F. Sorrentino, F. Tisato, M. Bjornstedt, A. Bindoli, A. Sturaro, R. Rella, C. Marzano, Biochem. Pharmacol. 79 (2010) 90–101.
[15] E. Schuh, C. Pfluger, A. Citta, A. Folda, M.P. Rigobello, A. Bindoli, A. Casini, F. Mohr, J. Med. Chem. 55 (2012) 5518–5528.
[16] Ö. Karaca, S.M. Meier-Menches, A. Casini, F.E. Kühn, Chem. Commun. (J. Chem. Soc. Sect. D) 53 (2017) 8249–8260.
[17] J.C. Lima, L. Rodriguez, Anti Canc. Agents Med. Chem. 11 (2011) 921–928.
[18] M. Ali, L. Dondaine, A. Adolle, C. Sampaio, F. Chotard, P. Richard, F. Denat, A. Bettaieb, P. Le Gendre, V. Laurens, C. Goze, C. Paul, E. Bodio, J. Med. Chem. 58 (2015) 4521–4528.
[19] C.N. Banti, C. Papatriantafyllopoulou, M. Manoli, A.J. Tasiopoulos, S.K. Hadjikakou, Inorg. Chem. 55 (2016) 8681–8696.
[20] F.K. Keter, I.A. Guzei, M. Nell, W.E. van Zyl, J. Darkwa, Inorg. Chem. 53 (2014) 2058–2067.
[21] A. Meyer, A. Gutierrez, I. Ott, L. Rodriguez, Inorg. Chim. Acta. 398 (2013) 72–76.
[22] L.K. Batchelor, E. Paunescu, M. Soudani, R. Scopelliti, P.J. Dyson, Inorg. Chem. 56 (2017) 9617–9633.
[23] M. Ahmed, S. Mamba, X.H. Yang, J. Darkwa, P. Kumar, R. Narain, Bioconjugate Chem. 24 (2013) 979–986.
[24] E. Garcia-Moreno, S. Gascon, E. Atrian-Blasco, M.J. Rodriguez-Yoldi, E. Cerrada, M. Laguna, Eur. J. Med. Chem. 79 (2014) 164–172.
[25] B. Bertrand, E. Bodio, P. Richard, M. Picquet, P. Le Gendre, A. Casini, J. Organomet. Chem. 775 (2015) 124–129.
[26] A. Gutierrez, L. Gracia-Fleta, I. Marzo, C. Cativiela, A. Laguna, M.C. Gimeno, Dalton Trans. 43 (2014) 17054–17066.
[27] G. Lupidi, L. Avenali, M. Bramucci, L. Quassinti, R. Pettinari, H.K. Khalife, H. Gali-Muhtasib, F. Marchetti, C. Pettinari, J. Inorg. Biochem. 124 (2013)

78–87.
[28] E. Jortzik, M. Farhadi, R. Ahmadi, K. Toth, J. Lohr, B.M. Helmke, S. Kehr, A. Unterberg, I. Ott, R. Gust, V. Deborde, E. Davioud-Charvet, R. Reau, K. Becker, C. Herold-Mende, Biochim. Biophys. Acta Protein Proteonomics 1844 (2014) 1415–1426.
[29] M. Altaf, M. Monim-ul-Mehboob, A.A. Isab, V. Dhuna, G. Bhatia, K. Dhuna, S. Altuwaijri, New J. Chem. 39 (2015) 377–385.
[30] T.S. Reddy, S.H. Priver, N. Mirzadeh, S.K. Bhargava, J. Inorg. Biochem. 175 (2017) 1–8.
[31] S. Bestgen, C. Seidl, T. Wiesner, A. Zimmer, M. Falk, B. Koberle, M. Austeri, J. Paradies, S. Brase, U. Schepers, P.W. Roesky, Chem. Eur J. 23 (2017) 6315–6322.
[32] S. Tasan, C. Licona, P.E. Doulain, C. Michelin, C.P. Gros, P. Le Gendre, P.D. Harvey, C. Paul, C. Gaiddon, E. Bodio, J. Biol. Inorg. Chem. 20 (2015) 143–154.
[33] M. Serratrice, M.A. Cinellu, L. Maiore, M. Pilo, A. Zucca, C. Gabbiani, A. Guerri, I. Landini, S. Nobili, E. Mini, L. Messori, Inorg. Chem. 51 (2012) 3161–3171.
[34] R.V. Parish, Met.-Based Drugs 6 (1999) 271–276.
[35] H. Goitia, Y. Nieto, M.D. Villacampa, C. Kasper, A. Laguna, M.C. Gimeno, Organometallics 32 (2013) 6069–6078.
[36] J. Schulz, J. Tauchman, I. Cisarova, T. Riedel, P.J. Dyson, P. Stepnicka, J. Organomet. Chem. 751 (2014) 604–609.
[37] V. Fernandez-Moreira, I. Marzo, M.C. Gimeno, Chem. Sci. 5 (2014) 4434–4446.
[38] M. Wenzel, A. de Almeida, E. Bigaeva, P. Kavanagh, M. Picquet, P. Le Gendre, E. Bodio, A. Casini, Inorg. Chem. 55 (2016) 2544–2557.
[39] M. Wenzel, E. Bigaeva, P. Richard, P. Le Gendre, M. Picquet, A. Casini, E. Bodio, J. Inorg. Biochem. 141 (2014) 10–16.
[40] E. García-Moreno, S. Gascón, M.J. Rodriguez-Yoldi, E. Cerrada, M. Laguna, Organometallics 32 (2013) 3710–3720.
[41] J. Rieb, B. Dominelli, D. Mayer, C. Jandl, J. Drechsel, W. Heydenreuter, S.A. Sieber, F.E. Kühn, Dalton Trans. 46 (2017) 2722–2735.
[42] R.W.Y. Sun, C.N. Lok, T.T.H. Fong, C.K.L. Li, Z.F. Yang, T.T. Zou, A.F.M. Siu, C.M. Che, Chem. Sci. 4 (2013) 1979–1988.
[43] A. Gutierrez, I. Marzo, C. Cativiela, A. Laguna, M.C. Gimeno, Chem. Eur J. 21 (2015) 11088–11095.
[44] N. Mirzadeh, S.H. Priver, A. Abraham, R. Shukla, V. Bansal, S.K. Bhargava, Eur. J. Inorg. Chem. (2015) 4275–4279.
[45] J.D.S. Chaves, L.G. Tunes, C. Franco, T.M. Francisco, C.C. Correa, S.M.F. Murta, R.L. Monte-Neto, H. Silva, A.P.S. Fontes, M.V. de Almeida, Eur. J. Med. Chem. 127 (2017) 727–739.
[46] A.M. de Almeida, B.A. de Oliveira, P.P. de Castro, C.C. de Mendonca, R.A. Furtado, H.D. Nicolella, V.L. da Silva, C.G. Diniz, D.C. Tavares, H. Silva, M.V. de Almeida, Biometals 30 (2017) 841–857.
[47] P. Hikisz, Ł. Szczupak, A. Koceva-Chyła, A. Guśpiel, L. Oehninger, I. Ott, B. Therrien, J. Solecka, K. Kowalski, Molecules 20 (2015) 19647.
[48] S.S. Al-Jaroudi, M. Altaf, A.A. Seliman, S. Yadav, F. Arjmand, A. Alhoshani, H.M. Korashy, S. Ahmad, A.A. Isab, Inorg. Chim. Acta. 464 (2017) 37–48.
[49] I. Marmol, M. Virumbrales-Munoz, J. Quero, C. Sanchez-De-Diego, L. Fernandez, I. Ochoa, E. Cerrada, M.J.R. Yoldi, J. Inorg. Biochem. 176 (2017) 123–133.
[50] A.A.A. Sulaiman, M. Altaf, A.A. Isab, A. Alawad, S. Altuwaijri, S. Ahmad, Z. Anorg, Allg. Chem. 642 (2016) 1454–1459.
[51] R.J. Chew, K. Sepp, B.-B. Li, Y. Li, P.-C. Zhu, N.S. Tan, P.-H. Leung, Adv. Synth. Catal. 357 (2015) 3297–3302.
[52] A. Luengo, V. Fernández-Moreira, I. Marzo, M.C. Gimeno, Inorg. Chem. 56 (2017) 15159–15170.
[53] O. Dada, D. Curran, C. O'Beirne, H. Muller-Bunz, X.M. Zhu, M. Tacke, J. Organomet. Chem. 840 (2017) 30–37.
[54] M. Monticelli, S. Bellemin-Laponnaz, C. Tubaro, M. Rancan, Eur. J. Inorg. Chem. (2017) 2488–2495.
[55] C. Schmidt, B. Karge, R. Misgeld, A. Prokop, M. Bronstrup, I. Ott, Medchemcomm 8 (2017) 1681–1689.
[56] C. Schmidt, B. Karge, R. Misgeld, A. Prokop, R. Franke, M. Bronstrup, I. Ott, Chem. Eur J. 23 (2017) 1869–1880.
[57] R.A. Haque, M.Z. Ghdhayeb, S. Budagumpi, M.B.K. Ahamed, A. Majid, RSC Adv. 6 (2016) 60407–60421.
[58] Y.F. Mui, J. Fernandez-Gallardo, B.T. Elie, A. Gubran, I. Maluenda, M. Sanau, O. Navarro, M. Contel, Organometallics 35 (2016) 1218–1227.
[59] N. Estrada-Ortiz, F. Guarra, I.A.M. de Graaf, L. Marchetti, M.H. de Jager, G.M.M. Groothuis, C. Gabbiani, A. Casini, ChemMedChem 12 (2017) 1429–1435.
[60] J. Arcau, V. Andermark, M. Rodrigues, I. Giannicchi, L. Pérez-Garcia, I. Ott, L. Rodríguez, Eur. J. Inorg. Chem. 2014 (2014) 6117–6125.
[61] J.F. Longevial, K. El Cheikh, D. Aggad, A. Lebrun, A. van der Lee, F. Tielens, S. Clement, A. Morere, M. Garcia, M. Gary-Bobo, S. Richeter, Chem. Eur J. 23 (2017) 14017–14026.
[62] R. McCall, M. Miles, P. Lascuna, B. Burney, Z. Patel, K.J. Sidoran, V. Sittaramane, J. Kocerha, D.A. Grossie, J.L. Sessler, K. Arumugam, J.F. Arambula, Chem. Sci. 8 (2017) 5918–5929.
[63] S.K. Fung, T. Zou, B. Cao, P.-Y. Lee, Y.M.E. Fung, D. Hu, C.-N. Lok, C.-M. Che, Angew. Chem. Int. Ed. 56 (2017) 3892–3896.
[64] I. Winter, J. Lockhauserbaumer, G. Lallinger-Kube, R. Schobert, K. Ersfeld, B. Biersack, Mol. Biochem. Parasitol. 214 (2017) 112–120.
[65] K.M. Hindi, M.J. Panzner, C.A. Tessier, C.L. Cannon, W.J. Youngs, Chem. Rev. 109 (2009) 3859–3884.
[66] N.A. Johnson, M.R. Southerland, W.J. Youngs, Molecules 22 (2017).
[67] N. Kaloglu, M. Kaloglu, I. Ozdemir, S. Gunal, I. Ozdemir, J. Chin. Chem. Soc. 64 (2017) 420–426.
[68] P.N. Muskawar, P. Karthikeyan, S.A. Aswar, P.R. Bhagat, S.S. Kumar, Arab. J. Chem. 9 (2016) S1765–S1778.
[69] T. Bernardi, S. Badel, P. Mayer, J. Groelly, P. de Fremont, B. Jacques, P. Braunstein, M.L. Teyssot, C. Gaulier, F. Cisnetti, A. Gautier, S. Roland, ChemMedChem 9 (2014) 1140–1144.
[70] I. Holmes, A. Naylor, G. Negoita-Giras, J. Powell, I. Charles, D. Alber, Auspherix Limited, UK, 2015, p. 64.
[71] L. Aguinagalde, R. Díez-Martínez, J. Yuste, I. Royo, C. Gil, Í. Lasa, M. Martín-Fontecha, N.I. Marín-Ramos, C. Ardanuy, J. Liñares, P. García, E. García, J.M. Sánchez-Puelles, J. Antimicrob. Chemother. 70 (2015) 2608–2617.
[72] J.P. Owings, N.N. McNair, Y.F. Mui, T.N. Gustafsson, A. Holmgren, M. Contel, J.B. Goldberg, J.R. Mead, FEMS Microbiol. Lett. 363 (2016).
[73] A. Velle, R. Maguire, K. Kavanagh, P.J.S. Miguel, D. Montagner, ChemMedChem 12 (2017) 841–844.
[74] M. Navarro, C. Gabbiani, L. Messori, D. Gambino, Drug Discov. Today 15 (2010) 1070–1078.
[75] M. Patra, G. Gasser, Nature Reviews Chemistry 1 (2017).
[76] M. Navarro, Coord. Chem. Rev. 253 (2009) 1619–1626.
[77] C. Hemmert, A. Fabie, A. Fabre, F. Benoit-Vical, H. Gornitzka, Eur. J. Med. Chem. 60 (2013) 64–75.
[78] L. Paloque, C. Hemmert, A. Valentin, H. Gornitzka, Eur. J. Med. Chem. 94 (2015) 22–29.
[79] A.M. Al-Majid, S. Yousuf, M.I. Choudhary, F. Nahra, S.P. Nolan, Chemistry 1 (2016) 76–80.
[80] A.M. Al-Majid, M.I. Choudhary, S. Yousuf, A. Jabeen, R. Imad, K. Javeed, N.N. Shaikh, A. Collado, E. Sioriki, F. Nahra, S.P. Nolan, Chemistry 2 (2017) 5316–5320.
[81] C. Zhang, S. Bourgeade Delmas, A. Fernandez Alvarez, A. Valentin, C. Hemmert, H. Gornitzka, Eur. J. Med. Chem. 143 (2018) 1635–1643.
[82] P. Fonteh, D. Meyer, Metall 1 (2009) 427–433.
[83] M. Mphahlele, M. Papathanasopoulos, M.A. Cinellu, M. Coyanis, S. Mosebi, T. Traut, R. Modise, J. Coates, R. Hewer, Bioorg. Med. Chem. 20 (2012) 401–407.
[84] C. Abbehausen, E.J. Peterson, R.E.F. de Paiva, P.P. Corbi, A.L.B. Formiga, Y. Qu, N.P. Farrell, Inorg. Chem. 52 (2013) 11280–11287.
[85] R.E.F. de Paiva, Z. Du, E.J. Peterson, P.P. Corbi, N.P. Farrell, Inorg. Chem. 56 (2017) 12308–12318.
[86] O. Sanchez, S. Gonzalez, A.R. Higuera-Padilla, Y. Leon, D. Coll, M. Fernandez, P. Taylor, I. Urdanibia, H.R. Rangel, J.T. Ortega, W. Castro, M.C. Goite, Polyhedron 110 (2016) 14–23.
[87] L. Ronconi, P.J. Sadler, Coord. Chem. Rev. 251 (2007) 1633–1648.

Dalton Transactions

PAPER

View Article Online
View Journal | View Issue

Cite this: *Dalton Trans.*, 2019, **48**, 14036

Dinuclear zwitterionic silver(I) and gold(I) complexes bearing 2,2-acetate-bridged bisimidazolylidene ligands†

Bruno Dominelli,[a] Gerri M. Roberts,[a] Christian Jandl,[a] Pauline J. Fischer,[a] Robert M. Reich,[a] Alexander Pöthig,[a] João D. G. Correia[b] and Fritz E. Kühn*[a]

Received 24th July 2019,
Accepted 24th August 2019

DOI: 10.1039/c9dt03035b

rsc.li/dalton

Four novel dinuclear Ag(I) and Au(I) NHC complexes bearing two 2,2-acetate-bridged bisimidazolylidene ligands (R = Me and iPr) of zwitterionic and metallacyclic forms are reported. The functionalized methylene bridge of the ligands leads to water soluble complexes, which have been characterized by NMR and IR spectroscopy, elemental analysis and single crystal X-ray diffraction in the case of $\mathbf{L_a\text{-}H_2\text{-}PF_6}$, $\mathbf{Ag_2(L_a)_2}$, $\mathbf{Ag_2(L_b)_2}$ and $\mathbf{Au_2(L_a)_2}$. Dimerization processes caused by hydrogen bonding or Ag(I)-carboxylate interactions in the solid state were observed for $\mathbf{L_a\text{-}H_2\text{-}PF_6}$ and $\mathbf{Ag_2(L_a)_2}$. DOSY NMR experiments confirmed that both bisimidazolium salts appear as dimers in aqueous solutions, in contrast to the corresponding monomeric Ag(I) and Au(I) complexes. Both gold(I) complexes form *syn*- and *anti*-isomers analogous to the reference coinage metal-based complexes. Protonation studies of the *syn*-isomer gold(I) complex $\mathbf{Au_2(L_a)_2}$ were successful, whereas post-modification esterification or amidation reactions were not feasible. Additionally, decarboxylation reactions (thermally induced Krapcho- or oxidative Hunsdiecker-type) of the bisimidazolium salts were observed. Thus, the proximity of the carboxyl moiety to imidazolium/imidazolylidene rings seems to negatively affect stability and reactivity.

Introduction

N-Heterocyclic carbene (NHC) ligands are highly relevant in the design of organometallic compounds for catalysis or medicinal chemistry.[1–3] NHCs are – at least in part – replacing the well-established phosphine-type ligands due to stronger bonding to transition metals, higher versatility and lower toxicity.[4–6] In particular, multidentate NHC ligands give very stable transition metal complexes due to their chelating effect.[7] For example, gold(I), bidentate scaffolds tend to form stable multinuclear complexes in a metallacyclic fashion attributed to the favored linear coordination geometry of coinage metals.[8,9] The historical development and current progress of this class of coinage metal-based complexes were extensively discussed in a recent review.[9] The stability of these gold(I)-based macrocycles allows in some cases to moderate the reactivity towards thiol groups ensuring a cytotoxic effect without decomposition by blood transport systems (*e.g.* glutathione, serum albumin).[10,11] Another relevant aspect relates to the formation of aurophilic interactions resulting in luminescence properties.[12–14] The proximity of the gold nuclei can be synthetically regulated depending on the type of *N*-substituent, bridging molecules or on the environment (*e.g.* counteranion). Additionally, the coordination sphere of both gold(I) nuclei can be extended under oxidizing conditions ($SOCl_2$, Br_2 or I_2) by forming for example metallacycles containing Au(I)/Au(III) or even Au(II)/Au(II) with additional coordination of halides.[15,16] Besides the variation of backbone- and *N*-substituents or tuning the flexibility of the bridge, the functionalization of the bridging unit plays an increasingly important role in the design of bidentate NHC moieties.[17] However, the number of bridged-functionalized bidentate NHC ligands and corresponding metal complexes is still limited.[7,17–23] One of the first examples was a palladium(II) complex bearing a 2-hydroxyethane-1,1-diyl-bridged bisimidazolylidene ligand, which has been successfully anchored on styrene functionalized silica and applied in cross coupling catalysis.[17] The presence of a hydroxyl substituent on the

[a]*Catalysis Research Center, Molecular Catalysis, Technische Universität München, Ernst-Otto-Fischer-Straße 1, D-85748 Garching bei München, Germany. E-mail: fritz.kuehn@ch.tum.de; Fax: +4989 289 13473; Tel: +49 89 289 13096*
[b]*Centro de Ciências e Tecnologias Nucleares, Departamento de Engenharia e Ciências Nucleares, Instituto Superior Técnico, Universidade de Lisboa, Campus Tecnológico e Nuclear, Estrada Nacional N° 10 (km 139, 7), 2695-066 Bobadela LRS, Portugal*

†Electronic supplementary information (ESI) available. CCDC 1942899–1942902. For ESI and crystallographic data in CIF or other electronic format see DOI: 10.1039/c9dt03035b

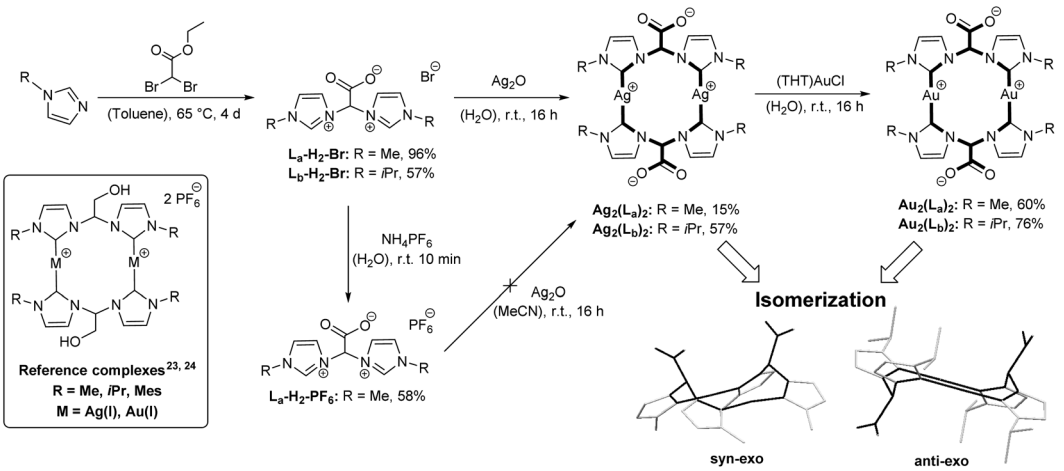

Scheme 1 Synthesis procedure for the bisimidazolium salts $L_{a/b}$-H_2-Br/PF_6, silver(I) complexes $Ag_2(L_{a/b})_2$ and the gold(I) complexes $Au_2(L_{a/b})_2$. Additionally, the reference Au(I) complex is depicted.[23,24] Me = methyl, iPr = isopropyl, Mes = mesityl or 2,4,6-trimethylphenyl, THT = tetrahydrothiophen. Both isomer-types, *syn*- and *anti-exo*, are given in the ORTEP-style view of $Ag_2(L_a)_2$ and $Ag_2(L_b)_2$ using capped sticks. ((Ortep-style (Oak Ridge thermal ellipsoid plot)).

bridge allows both immobilization and maintenance of the electronic and steric properties given by the backbone and wingtip positions. Dinuclear Cu(I), Ag(I) and Au(I) NHC complexes with the same ligand system have been reported as well. In this family of complexes, the formation of *syn*- and *anti*-isomers, in relation to the methylene bridge, has been observed depending on the metal.[23] More recently, the lipophilic character of the complexes was increased by varying the *N*-substituents. Such a modification led to complexes with moderate antiproliferative activity in the human cancer cell lines HepG2 and A549 (reference complex, Scheme 1).[24] Additionally, the variation of wingtips led to isomer mixtures.

Considering the first results of bridge-functionalized NHC complexes as antiproliferative agents towards cancer cell lines, the abovementioned successive work prompted us to design novel Ag(I) and Au(I) complexes bearing 2,2-acetate bridged bisimidazolylidene for bioconjugation purposes and biological applications.[22,25]

Results and discussion

Synthesis and characterization of ligand precursors

The bisimidazolium salts L_a-H_2-Br and L_b-H_2-Br were synthesized following literature described procedures (Scheme 1).[22,25] The expected ethyl ester group in the bridge could not be obtained due to hydrolysis in the presence of the counter-anion bromide, as reported previously.[22] L_b-H_2-Br requires an additional filtration step over basic aluminium oxide, since it appears in a mixture of carboxylate and carboxylic acid. Another undesired side product identified in the reaction mixture results from the decarboxylation process on the bridge promoted by high temperature. The formation of impurities can be followed by variable temperature ^{1}H-NMR spectroscopy (VT(^{1}H)-NMR, r.t. to 90 °C) as exemplified with L_a-H_2-Br in DMSO-d_6 (Fig. 1). Therefore, to avoid thermal induced decarboxylation on the bridge in solution, the reaction temperature was reduced to 65 °C. Interestingly, when the same experiment was conducted in D_2O no decarboxylation was observed. From a mechanistic point of view, a thermally induced Krapcho-type decarboxylation reaction takes places, since the C_α bears electron-withdrawing imidazolium rings.[26] These withdrawing properties additionally explain the isolation of the bisimidazolium salt in the form of carboxylate. Better σ-donating *N*-substituents like isopropyl groups might reduce this effect and indeed, in the case of L_b-H_2-Br, a mixture of carboxylic acid and carboxylate was obtained. Consequently, bisimidazolium derivatives with sterically more demanding *N*-substituents (*e.g.* mesityl, pyridyl, benzyl or *n*-butyl) could not be obtained, since higher reaction temperatures are required. This decarboxylation process could not be

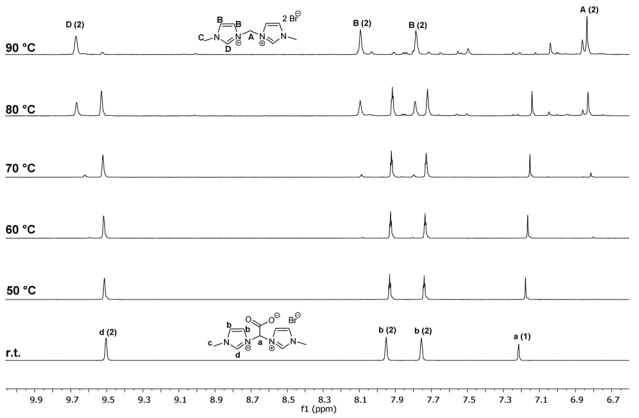

Fig. 1 VT(^{1}H)-NMR (section between 6.5 ppm and 10 ppm) of L_a-H_2-Br in DMSO-d_6 between room temperature (r.t.) and 90 °C. The chemical shifts are assigned with letters and the corresponding integral in brackets.

even suppressed by increasing the pressure of a Fischer–Porter bottle with 10 bar CO_2 or the addition of small amounts of water to the aprotic solvents to stabilize the carboxylate group. One of the ways to avoid that process could be, for instance, the elongation of the bridging unit (*e.g.* C_3 or longer) in order to allow the combination of sterically more hindered (more lipophilic) *N*-substituents and a carboxyl group.[25] With the aim of enhancing the solubility in organic solvents, the counter-anion was successfully exchanged in the case of **L_a-H_2-Br** by adding ammonium hexafluorophosphate (2.5 equivalents) to an aqueous solution of the imidazolium salt. Treatment of the resulting **L_a-H_2-PF_6** with Ag_2O in acetonitrile leads exclusively to the decarboxylated silver(I) complex. Thus, the bromide salt **L_a-H_2-Br** has proven to be a more suitable ligand precursor than **L_a-H_2-PF_6** for the synthesis of **$Ag_2(L_a)_2$**, as it displays better water solubility and avoids oxidative decarboxylation.[27]

The imidazolium salts have been characterized by FTIR and multinuclear NMR spectroscopy, elemental analysis and single crystal X-ray diffraction analysis in the case of **L_a-H_2-PF_6**. Suitable crystals of **L_a-H_2-PF_6** were obtained *via* slow diffusion of diethyl ether into a solution of the bisimidazolium salt in acetonitrile. A summary of the crystal data, structure solution, and refinement parameters are given in the ESI† (Table 1). An ORTEP-style view of the zwitterionic molecular structure of **L_a-H_2-PF_6**, together with selected bond lengths and angles are given in Fig. 2.

L_a-H_2-PF_6 crystallizes in the monoclinic space group $P2_1/n$ with three co-crystallized water molecules. No significant differences in bond lengths and angles are observed when comparing this ligand precursor with the previously published hydroxyethyl-2,2-bridged bisimidazolium salt.[17] Five water molecules form a ring by hydrogen bond interactions and consequently connect two bisimidazolium salts in the solid state in the form of a pseudo-dimerization *via* interaction with the carboxylate group. This structural feature could also be confirmed in the FTIR spectrum of **L_a-H_2-Br**, where two very close peaks assigned to the OH bond stretching and carbonyl stretching were observed.

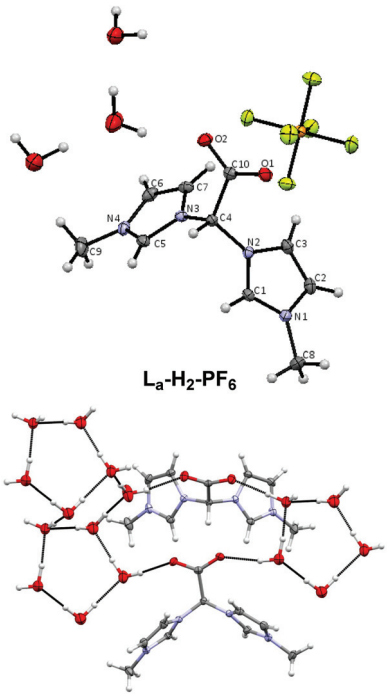

Fig. 2 ORTEP-style view of the zwitterionic molecular structure of **L_a-H_2-PF_6** with three co-crystallized water molecules (top) and dimerization (bottom). All atoms are shown using ellipsoids at a probability level of 50%. Relevant bond lengths [Å] and angles [°]: N1–C1 1.320(2), N2–C1 1.337(2) N3–C5 1.342(2), N4–C5 1.322(2), N2–C4 1.458(2), N3–C4 1.462(2), C4–C10 1.558(2), C10–O1 1.242(2), C10–O2 1.249(2); N1–C1–N2 108.42(16), N3–C5–N4 108.10(16), N2–C4–N3 111.21(14), C10–C4–N3 112.98(14), C10–C4–N2 112.81(14). O–O distances between carboxylate and water 2.80 Å and the water molecules themselves 2.75 Å (averaged).

Synthesis and characterization of Ag(I)-complexes

The zwitterionic Ag(I)-complexes **$Ag_2(L_a)_2$** and **$Ag_2(L_b)_2$** were synthesized upon treatment of the respective bisimidazolium salt with Ag_2O in an aqueous solution at room temperature (Scheme 1).[23,24] The water soluble Ag(I)-complexes were characterized by multinuclear NMR and FTIR spectroscopy, elemental analysis and single crystal X-ray diffraction analysis.

Water was observed to co-crystallize in nearly all compounds reported in this work, thus affecting the corresponding elemental analysis by an increased hydrogen content. The functionalization of the bridge with carboxyl groups successfully enhanced the solubility in water introducing four new complexes in the short list reported so far for water-soluble Ag(I)- and Au(I) NHC complexes.[28–35] ORTEP style views of **$Ag_2(L_a)_2$** and **$Ag_2(L_b)_2$**, including selected bond lengths and angles, are shown in Fig. 3 and 4, respectively. Single crystals of **$Ag_2(L_a)_2$** were obtained *via* slow diffusion of acetone into a solution of the complex in water, crystallizing in the triclinic space group $P\bar{1}$ with 16 co-crystallized water molecules. Suitable crystals of **$Ag_2(L_b)_2$** were analogously obtained by the slow diffusion of diethyl ether in an ethanol solution and this complex also crystallizes in the triclinic space group $P\bar{1}$ with co-crystallized ethanol molecules. In both cases, all bond lengths and bond angles are similar to the silver reference complex with a hydroxymethyl-functionalized methylene bridge.[24] In particular, the Ag–C bonds are within the range and all C–Ag–C angles are close to the linearity as known for dinuclear, metallacycled Ag(I) NHC complexes of this structure motif. Interestingly, the C–Ag–C angles of **$Ag_2(L_b)_2$** have a higher linearity when compared to **$Ag_2(L_b)_2$**. In the case of **$Ag_2(L_a)_2$** and **$Ag_2(L_b)_2$**, the distances between both Ag(I) nuclei are 3.60 Å and 3.94 Å, respectively, being not in the range for argentophilic interactions. Such distances are longer than the sum of van der Waals radii (3.4 Å).[36] Accordingly, in comparison with the reference Au(I) complex, the methyl-*N*-substituents lead to a *syn-exo*-isomer (Fig. 3), whereas the isopropyl-wingtips form the anti-*exo* complex (Fig. 4).[24] Interestingly, **$Ag_2(L_b)_2$** crystallizes in an *anti*-fashion, although this complex was synthesized in aqueous solution and water was expected to regulate the formation of the *syn*-conformation by forming H-bond interactions as observed in complexes of the same type.[23,24]

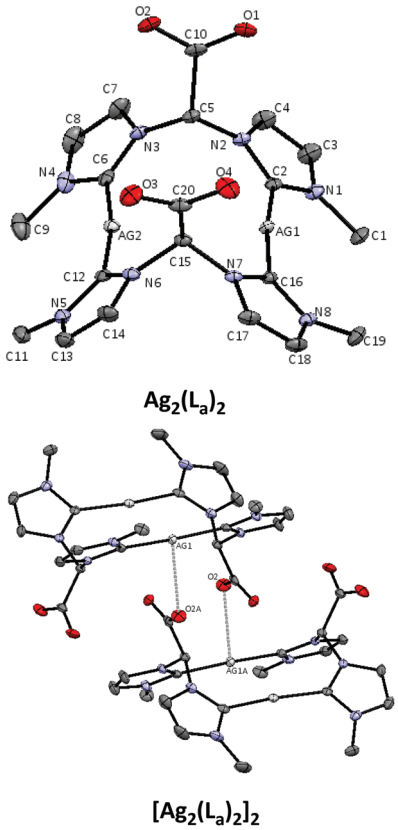

Fig. 3 ORTEP-style presentation of the zwitterionic molecular structure of $Ag_2(L_a)_2$ (top) and intermolecular interactions of $[Ag_2(L_a)_2]_2$ (bottom). All atoms are shown using ellipsoids at a probability level of 50%. H-Atoms and co-crystallized solvents were omitted for clarity. Relevant bond lengths [Å] and angles [°]: Ag1–C2 2.097(2), Ag1–C16 2.102(2), Ag2–C6 2.082(2), Ag2–C12 2.086(2); C2–Ag1–C16 172.01(10), C6–Ag2–C12 171.15(9). Both interactions [Å]: Ag1···O2 2.808(2). Symmetry code to create equivalent atoms: *–x*, *–y*, *–z*.

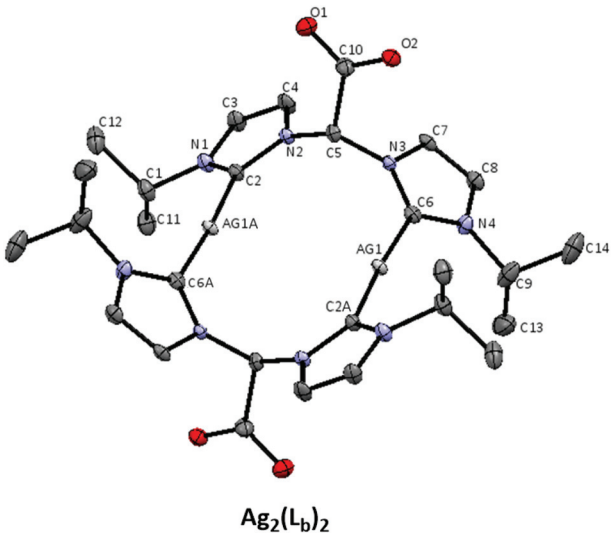

Fig. 4 ORTEP-style representation of the zwitterionic molecular structure of $Ag_2(L_b)_2$. All atoms are shown using ellipsoids with a probability level of 50%. H-Atoms and co-crystallized solvents were omitted for clarity. Relevant bond lengths [Å] and angles [°]: Ag1–C6 2.086(2), Ag1–C2A 2.087(2), Ag1A–C2 2.087(2), Ag1A–C6A 2.087(2), C6–Ag1–C2A 175.65(9), C2–Ag1A–C6A 175.65(9). Symmetry code to create equivalent atoms: *–x*, *–y*, *–z*.

Intermolecular interactions between the carboxylate group and the Ag(I) nucleus in a T-shape coordination geometry are observed in the case of $Ag_2(L_a)_2$ (Fig. 3).

Synthesis and characterization of Au(I)-complexes

The gold(I) complexes $Au_2(L_a)_2$ and $Au_2(L_b)_2$ have been synthesized by transmetallation from the corresponding Ag(I) complexes to (THT)AuCl (THT = tetrahydrothiophene) in the aqueous solution.[37] Both water soluble complexes were characterized by multinuclear NMR, FTIR spectroscopy, elemental analysis, and single crystal X-ray diffraction analysis in the case of $Au_2(L_a)_2$ (Fig. 5). Suitable crystals were obtained *via* slow diffusion of acetone into a solution of $Au_2(L_a)_2$ in water/DMSO (1/1). The complex crystallizes in a monoclinic unit cell of *C*2/*m* symmetry. Despite the poor quality, additional co-crystallized acetone and water molecules were detected and water was observed to form hydrogen bond interactions with the carboxylate group probably supporting the formation of the *syn*-isomer. All bond lengths and bond angles, especially the Au–C bonds and the linear C–Au–C angle, are similar to

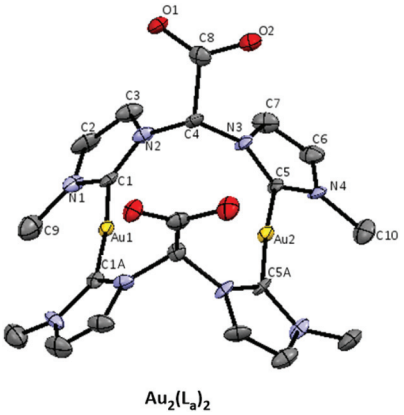

Fig. 5 ORTEP-style plot of the zwitterionic molecular structure of $Au_2(L_a)_2$. All atoms are shown with thermal ellipsoids of a 50% probability level. H-Atoms and co-crystallized solvents were omitted for clarity. Relevant bond lengths [Å] and angles [°]: Au1–C1 2.013(5), Au1–C1A 2.013(5), Au2–C5 2.012(5), Au2–C5A 2.012(5), C1–Au1–C1A 173.6(3), C5–Au2–C5A 175.1(3). Symmetry code to create equivalent atoms: *x*, 1 – *y*, *z*.

the reference gold complex (Scheme 1).[24] The distance between both Au(I) nuclei (3.77 Å) is not in the range of aurophilic interactions being longer than the sum of van der Waals radii (3.32 Å).[36] Also here, the *syn-exo* isomer was obtained, similarly to the case of the analogue $Ag_2(L_a)_2$ complex.

The *syn-exo* species precipitates in an isomerically pure manner after the concentration of the aqueous solution. Unlike $Au_2(L_a)_2$, $Au_2(L_b)_2$ could not be isolated as a single

crystal and thus no XRD structure was obtained. The proton NMR spectrum of $\mathbf{Au_2(L_b)_2}$ shows an isomer mixture, displaying an analogue behavior as observed for the hydroxyethyl-2,2-diyl-bridged bismidazolydene gold(I) complex with isopropyl *N*-substituents.

DOSY NMR experiment

In the case of $\mathbf{L_a\text{-}H_2\text{-}PF_6}$ and $\mathbf{Ag_2(L_a)_2}$, a dimerization was observed in the solid state. Consequently, DOSY NMR experiments in D_2O at room temperature were conducted for all bisimidazolium salts reported herein and the corresponding Ag(I) and Au(I) complexes to analyze the structural behavior in solution. All obtained diffusion coefficients and calculated hydrodynamic radii (Stokes equation) are summarized in Table 1.

Table 1 Diffusion coefficient and calculated hydrodynamic radii of $\mathbf{L_a\text{-}H_2\text{-}Br}$, $\mathbf{L_b\text{-}H_2\text{-}Br}$, $\mathbf{Ag_2(L_a)_2}$, $\mathbf{Ag_2(L_a)_2}$, $\mathbf{Ag_2(L_a)_2}$ and $\mathbf{Ag_2(L_a)_2}$. Stokes equation: $R_0 = (k_b{\cdot}T)/(6\pi{\cdot}\eta{\cdot}D)$. $k_B = 1.38 \times 10^{-23}$ J K^{-1}, $T = 298$ K, $\eta(D_2O) = 0.891 \times 10^{-3}$ Pa s

	Diffusion coefficient D [cm^2 S^{-1}]	Hydrodynamic radius R_0 [Å]
$\mathbf{L_a\text{-}H_2\text{-}Br}$	4.60×10^{-6}	5.32
$\mathbf{L_b\text{-}H_2\text{-}Br}$	4.74×10^{-6}	5.17
$\mathbf{Ag_2(L_a)_2}$	4.13×10^{-6}	5.93
$\mathbf{Ag_2(L_b)_2}$	4.40×10^{-6}	5.56
$\mathbf{Au_2(L_a)_2}$	4.26×10^{-6}	5.75
$\mathbf{Au_2(L_b)_2}$	4.00×10^{-6}	6.12

Collectively the results obtained demonstrate that also in solution both ligand precursors exist as dimers, since the hydrodynamic radii are in the range of those of the complexes. Comparing the latter value with the profile distances in all three axis *x*, *y* and *z* of the single crystal structure of $\mathbf{Ag_2(L_a)_2}$, it is confirmed that no dimerization is observed in the aqueous solution in the case of all four complexes. In the case of $\mathbf{Au_2(L_b)_2}$, the DOSY experiment was conducted with the isomer mixtures and both isomers exhibit the same coefficient showing no specific difference in their size in solution.

Reactivity studies

First post-modifications *via* esterification and amidation reactions were conducted on $\mathbf{L_a\text{-}H_2\text{-}Br}$ and on $\mathbf{Au_2(L_a)_2}$ in order to find a suitable coupling method of the carboxylate for bioconjugation. A summary of all attempted methods are given in the ESI† (Scheme 1).[38] Unfortunately, neither the activation of the carboxylate (acyl chloride or mixed anhydride) nor the use of coupling reagents led to a successful post-modification. Thereby, isopentylamine or 9-(hydroxymethyl)anthracene was chosen as the coupling reagent to increase the degree of lipophilicity and to insert chromophoric systems. Thus, in addition to being sensitive to decarboxylation, the proximity of the carboxylate group to the imidazolium or imidazolylidene moiety leads to lower reactivity.

Next, the zwitterionic $\mathbf{Au_2(L_a)_2}$ and $\mathbf{Au_2(L_b)_2}$ were treated with 10 w% of aqueous hydrobromic acid and trifluoro acetic or 2.1

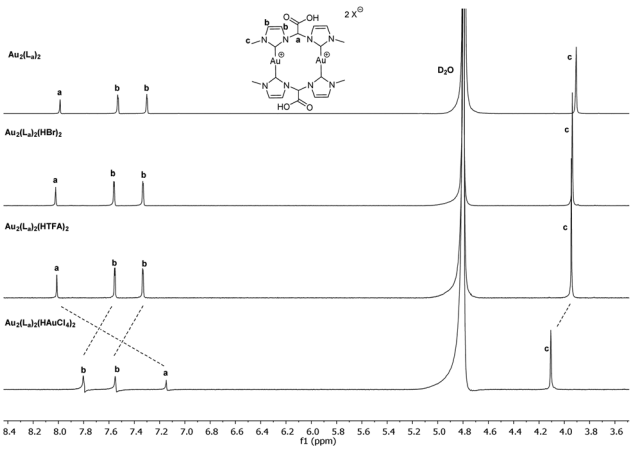

Fig. 6 Stacked ^{1}H NMR spectra in the section of 3.5 ppm and 8.5 ppm of $\mathbf{Au_2(L_a)_2}$, $\mathbf{Au_2(L_a)_2(HBr)_2}$, $\mathbf{Au_2(L_a)_2(HTFA)_2}$ and $\mathbf{Au_2(L_a)_2(HAuCl_4)_2}$ in D_2O at room temperature.

equivalents of tetrachloroauric(III) acid. Thereby, the influence of counter-anions on the structure of the complexes, particularly with the additional presence of carboxylic acids, was studied. The approximation of two Au(I) nuclei until aurophilic interactions in similar metallacyclic systems have been reported after re-salination to bromide.[13] In the case of $\mathbf{Au_2(L_a)_2}$, all protonated products, $\mathbf{Au_2(L_a)_2(HBr)_2}$, $\mathbf{Au_2(L_a)_2(HTFA)_2}$ and $\mathbf{Au_2(L_a)_2(HAuCl_4)_2}$ precipitated in the aqueous solution after the addition of the corresponding acidic solution and could be characterized by NMR spectroscopy and elemental analysis. In the proton spectra (Fig. 6), no changing chemical shift patterns are observed for $\mathbf{Au_2(L_a)_2(HBr)_2}$ and $\mathbf{Au_2(L_a)_2(HTFA)_2}$ when compared to the starting zwitterionic $\mathbf{Au_2(L_a)_2}$ indicating no structural diversity of the protonated products.

Interestingly, the resonance pattern of $\mathbf{Au_2(L_a)_2(HAuCl_4)_2}$ changed, since the proton of the methylene bridge is shifted to a high field (~1 ppm). A direct interaction of a halide with the methylene-H-atom should lead to a downfield shift, as previously reported.[13] Thus, the interaction presumably occurs between the carboxylic acid and the tetrachloroaurate(III) counter-anion, which formally discharges the bridging proton causing the highfield shift. Additionally, the CH_3-group shifts downfield indicating a possible enhancement of strain in the metallacycle. Nevertheless, related to the elemental analysis a mixed-valent tetranuclear gold(I/III) complex could be isolated after the use of a metal-based acid.

In the case of $\mathbf{Au_2(L_b)_2}$, which is expected to crystallize in analogy to the reference complex as the *anti-exo* isomer (Scheme 1), it immediately decomposes after the addition of each of the three acids, indicating the lower stability of the *anti*-isomer compared to the *syn*-species.

Conclusions

The 2,2-acetate-bridged bisimidazolium salts $\mathbf{L_a\text{-}H_2\text{-}Br/PF_6}$ and $\mathbf{L_b\text{-}H_2\text{-}Br}$,[22,25] allow the preparation of the zwitterionic com-

plexes $Ag_2(L_a)_2$, $Ag_2(L_b)_2$, $Au_2(L_a)_2$ and $Au_2(L_b)_2$. The obtained compounds have been characterized by NMR and FTIR spectroscopy, elemental analysis and single crystal X-ray diffraction in the case of L_a-H_2-PF_6, $Ag_2(L_a)_2$, $Ag_2(L_b)_2$ and $Au_2(L_a)_2$. Hydrogen bond interactions between the carboxylate group and co-crystallized water molecules were observed in the single crystal structure of L_a-H_2-PF_6, indicating a pseudo-dimerization process in the solid state caused by the five-membered ring of water molecules. DOSY experiments of L_a-H_a-**Br** and L_b-H_2-**Br** allowed the determination of the respective diffusion coefficients, which are similar to those of the corresponding Ag(I) and Au(I) complexes. Consequently, both ligand precursors are expected to behave as dimers in solution. $Ag_2(L_a)_2$ crystallizes in the *syn*-form, whereas $Ag_2(L_b)_2$ crystallizes as the *anti*-isomer, being similar to the analogous reference system.[24] $Ag_2(L_a)_2$ shows intermolecular coordinative interactions in a T-shape between the carboxylate group and one of the Ag(I) atoms of a neighboring complex, leading again to a dimer in the solid state. DOSY experiments on the complexes reveal hydrodynamic radii in the same range as observed for the monomeric structure. The presence of a carboxyl group at the bridging unit promotes water solubility. The proximity of the carboxylate group to imidazolium/imidazolylidene rings leads to thermally induced Krapcho-type or oxidative Hunsdiecker-type decarboxylation. Performing the synthesis in water suppresses the undesired decarboxylation. Additionally, the carboxylate group is unreactive towards esterification or amidation routes complicating the post-modification for bio-conjugation. The complex $Au_2(L_a)_2$ was successfully protonated with various acids leading to the products $Au_2(L_a)_2(HBr)_2$, $Au_2(L_a)_2(HTFA)_2$ and $Au_2(L_a)_2(HAuCl_4)_2$. $Au_2(L_b)_2$, expected to crystallize in the *anti*-form decomposes under acidic conditions. In the case of $Au_2(L_a)_2(HAuCl_4)_2$, the resonance pattern in the ^{1}H NMR spectrum extremely differs when compared to $Au_2(L_a)_2$, which is explained by interactions with the counter-anion and enhanced ring tension of the metallacycle. This protonation method allows access to mixed-valent Au(I/III) complexes consisting of cationic and anionic components. $Au_2(L_b)_2$ immediately decomposes under acidic conditions showing a higher stability of the *syn-exo* isomer than the *anti-exo* species.

Experimental

Synthesis of bisimdazolium salts

L_a-H_2-Br: 2,2-Dibromo acetate ethyl ester (5.26 mL, 10.0 g, 40.7 mmol, 1.0 eq.) and 1-methylimidazole (13.0 mL, 13.4 g, 162.7 mmol, 4.0 eq.) are dissolved in toluene (15 mL and stirred for 4 days at 65 °C. The brown precipitate is separated by vacuum filtration and washed 3× with toluene (5 mL), 3× with acetonitrile (5 mL) and finally 3× with diethyl ether (5 mL). The white solid is dissolved in methanol, stirred in basic aluminium oxide for 30 min and after filtration re-precipitated with diethyl ether. After drying under dynamic vacuum, 11.8 g of **L_a-H_2-Br** as a white powder is obtained. Yield: 96%.

^{1}H NMR (400 MHz, DMSO-d_6, 300 K): δ 9.53–9.44 (m, 2H, NC***H***N), 7.92 (t, 2H, J_{HH} = 1.8 Hz, NC***H***CHN), 7.74 (t, 2H, J_{HH} = 1.8 Hz, NCHC***H***N), 7.16 (s, 1H, NC***H***(COO)N), 3.89 (s, 6H, C***H***$_3$). ^{1}H NMR (400 MHz, D_2O, 300 K): δ 7.73 W(t, 2H, J_{HH} = 1.8 Hz, NC***H***CHN), 7.56 (t, 2H, J_{HH} = 1.8 Hz, NCHC***H***N), 3.94 (m, 6H, C***H***$_3$).^{13}C NMR (101 MHz, DMSO-d_6, 300 K): δ 159.35 (CH***C***OO), 137.82 (N***C***HN), 123.44 (N***C***HCHN), 121.92 (NCH***C***HN), 70.41 (N***C***H(COO)N), 36.06 (***C***H$_3$). EA calcd: C 35.62, H 5.08, N 16.62. Found: C 35.56, H 4.89, N 16.32. **FT-IR** (cm^{-1}): 3384 (OH), 3444 (OH), 1662 (C═O), 1678 (C═O).

L_b-H_2-Br: The same procedure as that of **L_a-H_2-Br** using 2,2-dibromo acetate ethyl ester (5.26 mL, 10.0 g, 40.7 mmol, 1.0 eq.) and 1-isopropylimidazole (18.5 mL, 17.9 g, 162.7 mmol, 4.0 eq.) in toluene (15 mL). 8.3 g of the desired product as a white powder is obtained. Yield: 57%.

^{1}H NMR (400 MHz, DMSO-d_6, 300 K): δ 9.62 (d, 2H, J_{HH} = 1.9 Hz NC***H***N), 8.04–8.01 (m, 2H, NC***H***CHN), 7.99–7.97 (m, 2H, NCHC***H***N), 7.13 (s, 1H, NC***H***(COO)N), 4.70 (p, 2H, J_{HH} = 6.7 Hz, C***H***(CH$_3$)$_2$), 1.49 (dd, 12H, J_{HH} = 6.5 Hz, J_{HH} = 3.2 Hz, ***C***H$_3$). ^{1}H NMR (400 MHz, D_2O, 300 K): δ 7.81 (dd, 2H, J_{HH} = 2.1 Hz, 1.0 Hz, NC***H***CHN), 7.76 (d, 2H, J_{HH} = 2.2 Hz, NCHC***H***N), 4.73 (h, 2H, J_{HH} = 6.7 Hz, C***H***(CH$_3$)$_2$), 1.59 (d, 12H, J_{HH} = 6.7 Hz, C***H***$_3$). ^{13}C NMR (101 MHz, DMSO-d_6, 300 K): δ 159.40 (CH***C***OO), 136.19 (N***C***HN), 122.38 (N***C***HCHN), 120.33 (NCH***C***HN), 70.52 (N***C***H(COO)N),52.64 (***C***H(CH$_3$)$_2$), 22.17 (***C***H$_3$), 22.05 (***C***H$_3$). FT-IR (cm^{-1}), 3436 (OH), 1674 (C═O).

Synthesis of silver(I)-bis(NHC) complexes

$Ag_2(L_a)_2$: L_a-H_2-Br (1.0 g, 3.3 mmol, 1.0 eq.) and Ag_2O (1.9 g, 8.3 mmol, 2.5 eq.) are suspended in water (50 mL) and stirred at room temperature for 16 h under exclusion of light. The brown suspension is centrifuged and filtered over Celite®. The resulting colourless solution is concentrated *in vacuo* and $Ag_2(L_a)_2$ is obtained as a white solid *via* repeated fractional precipitation with acetone. The precipitate is washed 3× with acetone (5 mL) and diethyl ether, respectively. 155 mg of $Ag_2(L_a)_2$ is obtained. Yield: 15%.

^{1}H NMR (400 MHz, D_2O, 300 K): δ 7.51 (d, 4H, J_{HH} = 1.9 Hz, NC***H***CHN), 7.48 (s, 2H, NC***H***(COO)N), 7.28 (d, 4H, J_{HH} = 1.9 Hz, NCHC***H***N), 3.86 (s, 12H, C***H***$_3$). ^{13}C NMR (101 MHz, D_2O, 300 K): δ 183.09 (N***C***N), 169.70 (***C***OO), 124.75 (N***C***HCHN), 120.99 (NCH***C***HN), 39.28 (***C***H$_3$), N***C***H(COO)N not visible. EA calcd with 1.15 H_2O: C 35.59, H 3.63, N 16.60. Found: C 35.08, H 3.34, N 15.85. **FT-IR** (cm^{-1}): 1636 (C═O).

$Ag_2(L_b)_2$: The same procedure as that of $Ag_2(L_a)_2$ using **L_b-H_2-Br** (1.0 g, 2.8 mmol, 1.0 eq.) and Ag_2O (1.62 g, 7.0 mmol, 2.5 eq.) in water (50 mL). 0.70 g of the desired product as a white powder is obtained. Yield: 57%.

^{1}H NMR (400 MHz, D_2O, 300 K): δ 7.57 (d, 4H, J_{HH} = 2.3 Hz, NC***H***CHN), 7.54 (s, 2H, NC***H***(COO)N), 7.41 (d, 4H, J_{HH} = 2.0 Hz, NCHC***H***N), 4.64 (p, 4H, J_{HH} = 6.7 Hz, C***H***(CH$_3$)$_2$), 1.42 (d, 12H, J_{HH} = 6.7 Hz, C***H***$_3$), 1.28–1.21 (m, 12H, J_{HH} = 6.7 Hz, C***H***$_3$). ^{13}C NMR (101 MHz, D_2O, 300 K): δ 168.58 (***C***OO), 119.67 (NCH***C***HN), 54.48 (***C***H(CH$_3$)$_2$) 22.88 (***C***H$_3$) 22.65 (***C***H$_3$), N***C***N, N***C***HCHN and N***C***H(COO)N not visible. EA calcd with 2 H_2O: C

41.91, H 5.28, N 13.96. Found: C 41.20, H 5.43, N 13.54. **FT-IR** (cm^{-1}): 3405 (OH), 1651 (C═O).

Synthesis of gold(I)-bis(NHC) complexes

$Au_2(L_a)_2$: **$Ag_2(L_b)_2$** (0.12 g, 0.19 mmol, 1.0 eq.) and (tetrahydrothiophene)gold(I)chloride (0.13 g, 0.39 mmol, 2.1 eq.) are suspended in water (50 mL) and stirred at room temperature for 16 h under exclusion of light. The suspension is centrifuged and vacuum-filtered. The resulting colourless solution is concentrated *in vacuo* and **$Au_2(L_a)_2$** crystallizes as a white powder after storage at 4 °C. The precipitate is washed 3× with acetone (5 mL) and diethyl ether, respectively and dried under dynamic vacuum. 90 mg of **$Au_2(L_a)_2$** is obtained. Yield: 60%.

^{1}H NMR (400 MHz, D_2O, 300 K): *syn*-isomer δ 7.99 (s, 2H, NC***H***(COO)N), 7.53 (d, 4H, J_{HH} = 2.1 Hz, NC***H***CHN), 7.30 (d, 4H, J_{HH} = 2.1 Hz, NCHC***H***N), 3.91 (s, 12H, CH_3). ^{13}C Cryo NMR (101 MHz, D_2O, 300 K): δ 185.01 (N***C***N), 167.87 (***C***OO), 124.33 (N***C***HCHN), 119.70 (NCH***C***HN), 74.54 (N***C***H(COO)N), 37.59 (***C***H_3). EA calcd with 1 H_2O: C 28.25, H 2.84, N 13.18. Found: C 28.27, H 2.76, N 13.15. **FT-IR** (cm^{-1}): 1651 (C═O).

$Au_2(L_b)_2$: The same procedure as that of **$Au_2(L_a)_2$** using **$Ag_2(L_b)_2$** (0.05 g, 0.07 mmol, 1.0 eq.) and (tetrahydrothiophene) gold(I)-chloride (0.044 g, 0.14 mmol, 2.1 eq.) suspended in water (10 mL) and stirred at room temperature for 16 h under exclusion of light. The suspension is centrifuged, vacuum-filtered and water is completely removed *in vacuo*. The desired product is obtained after repeated fractional precipitation with ethanol and diethyl ether in the second fraction. The precipitate is washed 3× with diethyl ether (5 mL) and dried under dynamic vacuum. 0.05 g is obtained as a white powder. Yield: 76%.

^{1}H NMR (400 MHz, D_2O, 300 K): *anti*-isomer δ 7.90 (s, 2H, NC***H***(COO)N), 7.53 (d, 4H, J_{HH} = 2.5 Hz, NC***H***CHN), 7.43 (d, 4H, J_{HH} = 1.9 Hz, NCHC***H***N), 4.89–4.82 (m, 4H, C***H***$(CH_3)_2$), 1.46–1.42 (m, 12H, C***H***$_3$), 1.28 (dd, 12H, J_{HH} = 6.4 Hz, 2.2 Hz, C***H***$_3$). ^{13}C NMR (101 MHz, D_2O, 300 K): δ 183.36 (N***C***N), 167.65 (***C***OO), 120.08 (N***C***HCHN), 119.61 (NCH***C***HN), 75.37 (N***C***H(COO)N) 53.99 (***C***H$(CH_3)_2$), 22.66 (***C***H_3), 22.09 (***C***H_3). EA calcd with 2 H_2O: C 34.30, H 4.32, N 11.43. Found: C 33.22, H 4.24, N 10.90. **FT-IR** (cm^{-1}): 3384 (OH), 1664 (C═O).

Decarboxylation studies

In a NMR scale experiment, 5 mg of the analyzed compound is dissolved in 0.45 mL of the corresponding deuterated solvent and after being heated for 10 min proton NMR is measured at the adjusted temperature (r.t. until 90 °C).

Protonation studies

$Au_2(L_a)_2(HBr)_2$: To a solution of **$Au_2(L_a)_2$** (10.0 mg, 12.0 μmol, 1.0 eq.) in water (3.5 mL) is added a 10 w% aqueous hydro bromic acid solution (0.50 mL) and stirred for 10 min at room temperature. The white precipitate is isolated by centrifugation, washed 3× with water (0.50 mL) and dried under dynamic vacuum. 4 mg of **$Au_2(L_a)_2(HBr)_2$** is obtained as a white powder. Yield: 33%.

^{1}H NMR (400 MHz, D_2O, 300 K): δ 8.01 (s, 2H, NC***H***(COO)N), 7.55 (d, 4H, J_{HH} = 2.1 Hz, NC***H***CHN), 7.32 (d, 4H, J_{HH} = 2.1 Hz, NCHC***H***N), 3.93 (s, 12H, CH_3). EA calcd: C 24.16, H 2.43, N 11.27. Found: C 23.15, H 2.57, N 10.64.

$Au_2(L_a)_2(HTFA)_2$: The same procedure as that of **$Au_2(L_a)_2(HBr)_2$**. Yield: 7%.

^{1}H NMR (400 MHz, D_2O, 300 K): δ 8.01 (s, 2H, NC***H***(COO)N), 7.55 (d, 4H, J_{HH} = 2.1 Hz, NC***H***CHN), 7.32 (d, 4H, J_{HH} = 2.1 Hz, NCHC***H***N), 3.94 (s, 12H, CH_3). EA calcd: C 27.08, H 2.91, N 10.53. Found: C 26.45, H 3.23, N 8.42.

$Au_2(L_a)_2(HAuCl_4)_2$: To a solution of **$Au_2(L_a)_2$** (10.0 mg, 12.0 μmol, 1.0 eq.) in water (3.5 mL) is added tetrachloroauric acid (8.57 mg, 25.2 μmol, 2.1 eq.) in water (2 mL) and an analogue procedure to that of **$Au_2(L_a)_2(HBr)_2$** is adopted. Yield: 47%.

^{1}H NMR (400 MHz, D_2O, 300 K): δ 7.79 (d, 4H, J_{HH} = 2.0 Hz, NC***H***CHN), 7.54 (d, 4H, J_{HH} = 2.0 Hz, NCHC***H***N), 7.13 (s, 2H, NC***H***(COO)N), 4.10 (s, 12H, CH_3). EA calcd: C 15.89, H 1.60, N 7.41. Found: C 14.81, H 1.76, N 6.82.

Conflicts of interest

There are no conflicts to declare.

Acknowledgements

BD, CJ, and PJF acknowledge the TUM Graduate School for financial support. GMR was supported by a Fulbright grant from the German-American Fulbright Commission. JDGC gratefully acknowledges the Fundação para a Ciência e a Tecnologia, Portugal, for financial support through projects UID/Multi/04349/2019 and PTDC/QUI-NUC/30147/2017. BD thanks Waldemar Schmidt, David Mayer and Tobias Muschialik for experimental support.

References

1 M. N. Hopkinson, C. Richter, M. Schedler and F. Glorius, *Nature*, 2014, **510**, 485–496.
2 J. A. M. Lummiss, C. S. Higman, D. L. Fyson, R. McDonald and D. E. Fogg, *Chem. Sci.*, 2015, **6**, 6739–6746.
3 W. K. Liu and R. Gust, *Coord. Chem. Rev.*, 2016, **329**, 191–213.
4 B. Dominelli, J. D. G. Correia and F. E. Kühn, *J. Organomet. Chem.*, 2018, **866**, 153–164.
5 M. Mora, M. C. Gimeno and R. Visbal, *Chem. Soc. Rev.*, 2019, **48**, 447–462.
6 P. F. Ai, C. Gourlaouen, A. A. Danopoulos and P. Braunstein, *Inorg. Chem.*, 2016, **55**, 1219–1229.
7 A. C. Lindhorst, M. Kaspar, P. J. Altmann, A. Pöthig and F. E. Kühn, *Dalton Trans.*, 2018, **47**, 1857–1867.
8 M. Porchia, M. Pellei, M. Marinelli, F. Tisato, F. Del Bello and C. Santini, *Eur. J. Med. Chem.*, 2018, **146**, 709–746.

9 M. M. Gan, J. Q. Liu, L. Zhan, Y. Y. Wang, F. E. Hahn and Y. F. Han, *Chem. Rev.*, 2018, **118**, 9587–9641.
10 T. Zou, C.-N. Lok, P.-K. Wan, Z.-F. Zhang, S.-K. Fung and C.-M. Che, *Curr. Opin. Chem. Biol.*, 2018, **43**, 30–36.
11 T. Zou, C. T. Lum, C. N. Lok, W. P. To, K. H. Low and C. M. Che, *Angew. Chem., Int. Ed.*, 2014, **53**, 5810–5814.
12 C. Hemmert, R. Poteau, F. Dominique, P. Ceroni, G. Bergamini and H. Gornitzka, *Eur. J. Inorg. Chem.*, 2012, 3892–3898.
13 A. A. Penney, V. V. Sizov, E. V. Grachova, D. V. Krupenya, V. V. Gurzhiy, G. L. Starova and S. P. Tunik, *Inorg. Chem.*, 2016, **55**, 4720–4732.
14 T. P. Pell, B. D. Stringer, C. Tubaro, C. F. Hogan, D. J. D. Wilson and P. J. Barnard, *Eur. J. Inorg. Chem.*, 2017, 3661–3674.
15 M. Baron, M. Dalla Tiezza, A. Carlotto, C. Tubaro, C. Graiff and L. Orian, *J. Organomet. Chem.*, 2018, **866**, 144–152.
16 A. H. Mageed, B. W. Skelton, A. N. Sobolev and M. V. Baker, *Eur. J. Inorg. Chem.*, 2018, 109–120.
17 R. Zhong, A. Pöthig, S. Haslinger, B. Hofmann, G. Raudaschl-Sieber, E. Herdtweck, W. A. Herrmann and F. E. Kühn, *ChemPlusChem*, 2014, **79**, 1294–1303.
18 O. Kühl, *Germany Pat*, WO2012034880A1, 2012.
19 E. Mas-Marzá, M. Poyatos, M. Sanaú and E. Peris, *Organometallics*, 2004, **23**, 323–325.
20 E. Mas-Marzá, M. Sanaú and E. Peris, *J. Organomet. Chem.*, 2005, **690**, 5576–5580.
21 M. Viciano, E. Mas-Marzá, M. Poyatos, M. Sanaú, R. H. Crabtree and E. Peris, *Angew. Chem., Int. Ed.*, 2005, **44**, 444–447.
22 R. Puerta-Oteo, M. Hölscher, M. V. Jiménez, W. Leitner, V. Passarelli and J. J. Pérez-Torrente, *Organometallics*, 2018, **37**, 684–696.
23 R. Zhong, A. Pöthig, D. C. Mayer, C. Jandl, P. J. Altmann, W. A. Herrmann and F. E. Kühn, *Organometallics*, 2015, **34**, 2573–2579.
24 J. Rieb, B. Dominelli, D. Mayer, C. Jandl, J. Drechsel, W. Heydenreuter, S. A. Sieber and F. E. Kühn, *Dalton Trans.*, 2017, **46**, 2722–2735.
25 Y. Li, B. Dominelli, R. M. Reich, B. Liu and F. E. Kühn, *Catal. Commun.*, 2019, **124**, 118–122.
26 A. P. Krapcho, J. F. Weimaster, J. M. Eldridge, E. G. E. Jahngen, A. J. Lovey and W. P. Stephens, *J. Org. Chem.*, 1978, **43**, 138–147.
27 R. G. Johnson and R. K. Ingham, *Chem. Rev.*, 1956, **56**, 219–269.
28 C. E. Czegeni, G. Papp, A. Katho and F. Joo, *J. Mol. Catal. A: Chem.*, 2011, **340**, 1–8.
29 E. Tomas-Mendivil, P. Y. Toullec, J. Borge, S. Conejero, V. Michelet and V. Cadierno, *ACS Catal.*, 2013, **3**, 3086–3098.
30 H. Ibrahim, P. de Fremont, P. Braunstein, V. Thery, L. Nauton, F. Cisnetti and A. Gautier, *Adv. Synth. Catal.*, 2015, **357**, 3893–3900.
31 G. A. Fernandez, A. B. Chopa and G. F. Silbestri, *Catal. Sci. Technol.*, 2016, **6**, 1921–1929.
32 Ö. Karaca, V. Scalcon, S. M. Meier-Menches, R. Bonsignore, J. Brouwer, F. Tonolo, A. Folda, M. P. Rigobello, F. E. Kühn and A. Casini, *Inorg. Chem.*, 2017, **56**, 14237–14250.
33 M. Pellei, V. Gandin, M. Marinelli, C. Marzano, M. Yousufuddin, H. V. R. Dias and C. Santini, *Inorg. Chem.*, 2012, **51**, 9873–9882.
34 P. C. Kunz, C. Wetzel, S. Kogel, M. U. Kassack and B. Spingler, *Dalton Trans.*, 2011, **40**, 35–37.
35 G. A. Fernandez, A. S. Picco, M. R. Ceolin, A. B. Chopa and G. F. Silbestri, *Organometallics*, 2013, **32**, 6315–6323.
36 A. Bondi, *J. Phys. Chem.*, 1964, **68**, 441–451.
37 J. Cure, R. Poteau, I. C. Gerber, H. Gornitzka and C. Hemmert, *Organometallics*, 2012, **31**, 619–626.
38 C. Montalbetti and V. Falque, *Tetrahedron*, 2005, **61**, 10827–10852.